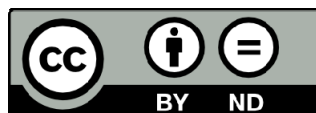




UNIVERSITAT_{DE}
BARCELONA

**Influence of Mesozoic structural inheritance
on fault reactivation in the central Catalan Coastal
Ranges (Catalan Margin, NW Mediterranean).
Paleogene and Neogene tectonostratigraphic evolution**

Miquel À. Marín Pérez



Aquesta tesi doctoral està subjecta a la llicència **Reconeixement- SenseObraDerivada 4.0.
Espanya de Creative Commons.**

Esta tesis doctoral está sujeta a la licencia **Reconocimiento - SinObraDerivada 4.0.
España de Creative Commons.**

This doctoral thesis is licensed under the **Creative Commons Attribution-NoDerivatives 4.0.
Spain License.**

Influence of Mesozoic structural inheritance on fault reactivation in the central Catalan Coastal Ranges (Catalan Margin, NW Mediterranean). Paleogene and Neogene tectonostratigraphic evolution



Miquel À. Marín Pérez
Ph.D. Thesis Dissertation
April 2025

Supervisors:
Lluís Cabrera
Oriol Ferrer

Institut de Reserca Geomodels
Grup de Geodinàmica i Anàlisi de Conques
Departament de Dinàmica de la Terra i de l'Oceà
Facultat de Ciències de la Terra
Universitat de Barcelona

*Institut de Recerca Geomodels
Departament de Dinàmica de la Terra i de l'Oceà
Grup de Recerca de Geodinàmica i Anàlisi de Conques
Universitat de Barcelona*

**Influence of Mesozoic structural inheritance on fault
reactivation in the central Catalan Coastal Ranges (Catalan
Margin, NW Mediterranean). Paleogene and Neogene
tectonostratigraphic evolution.**

Dissertation submitted by **Miquel À. Marín Pérez** for the degree of
Doctor of Philosophy (PhD) in Earth Sciences

This dissertation has been prepared within the framework of the *Programa de Doctorat de
Ciències de la Terra (HDK09)* of the University of Barcelona under the advice of
Dr. Lluís Cabrera and **Dr. Josep Oriol Ferrer**

Miquel À. Marín Pérez
Barcelona, April 2025

Dr. Lluís Cabrera (Tutor and co-supervisor, Universitat de Barcelona)

Dr. Josep Oriol Ferrer (co-supervisor, Universitat de Barcelona)

*Institut de Recerca Geomodels
Departament de Dinàmica de la Terra i de l'Oceà
Grup de Recerca de Geodinàmica i Anàlisi de Conques
Universitat de Barcelona*

**Influència de l'herència estructural mesozoica en la reactivació
de falles a la Cadenes Costaneres Catalanes (Marge Català,
Mediterrània Occidental). Evolució tectonoestratigràfica
paleògena i neògena.**

Memòria sotmesa per **Miquel À. Marín Pérez** per obtenir el grau de
Doctor en Ciències Geològiques

Aquesta memòria ha estat preparada dins el marc del Programa de Doctorat de Ciències de la
Terra (HDK09) de la Universitat de Barcelona sota la supervisió de
Dr. Lluís Cabrera i Dr. Josep Oriol Ferrer

Miquel À. Marín Pérez
Barcelona, Abril 2025

Dr. Lluís Cabrera (Tutor i co-supervisor, Universitat de Barcelona)

Dr. Josep Oriol Ferrer (co-supervisor, Universitat de Barcelona)

This PhD thesis has been done within the Grup de Recerca de Geodinàmica i Anàlisi de Conques (2014SGR467; 2021SGR76), funded by the Secretaria d'Universitats i Recerca del Departament d'Economia i Coneixement de la Generalitat de Catalunya and the Agència de Gestió d'Ajuts Universitaris i de Recerca) and the Institut de Recerca Geomodels. The work as PhD student has been carried out at the Departament de Dinàmica de la Terra i de l'Oceà (section Departament d'Estratigrafia, Paleontologia i Geociències Marines) of the Universitat de Barcelona. From August 2005 to July 2009, during the first period of work related to this PhD thesis, Miquel A. Marín benefited from a predoctoral FPI (Formación de Personal Investigador - BES-2005-10178) studentship associated to the research project MARES 3D (Modelización 3D de análogos de reservorios sedimentarios - CGL2004-05816-C02-02) from the former Ministerio de Educación y Ciencia of Spain. During this period, between 2007 and 2010, the research was also funded by the REMOS 3D/4D (Reconstrucción y modelización 3D y 4D de sistemas sedimentarios - CGL2007-66431-C02-02BTE) project. Two scientific visits at the Université de Lorraine in Nancy (France) were funded by two travel grants associated to the predoctoral FPI studentship. From October 2016 to January 2025, the second phase of the research received the support from collaborations with different research groups from the Universitat de Barcelona and the Consejo Superior de Investigaciones Científicas (CSIC), which allowed the multidisciplinary approach of the publications included in this dissertation. In this regard, the Grup Consolidat de Recerca Geologia Sedimentaria and the Grup d'Exploració Electromagnètica i Sísmica (EXES) from the Universitat de Barcelona, alongside the Paleomagnetic Laboratory CCiT UB - GEO3BCN-CSIC, are acknowledged for their collaboration. During this period, financial support was provided by projects SALTCONBELT (CGL2017-85532-P AEI/FEDER, UE) from the Spanish Ministerio de Economía y Competitividad; IMPACSYS (PID2019-106440GB-C21) from the European Regional Development Fund (ERDF); SABREM (PID2020-117598GB-I00) funded by MCIN/ AEI /10.13039/501100011033; and ORRI (Diagénesis controlada por pliegues y fallas en sistemas orogénicos y de rifting: implicaciones en los recursos geotérmicos y almacenaje de CO₂ - PID2021-122467NB-C22) from the Ministerio de Ciencia, Innovación y Universidades/Agencia Estatal de Investigación/Fondo Europeo de Desarrollo Regional. Additional support was also received from Project FBG 310505 "Caracterització litostratigràfica i estructural i cartografia geològica del Paleogen dels fulls 758 de Sarrià (67-31) i Montblanc (67-32) del Mapa Geològic de Catalunya 1:25000" funded by the Institut Cartogràfic i Geològic de Catalunya. The research has also been benefited from the use of academic software licenses for Move[®] and Dynel2D[®] respectively provided by Petroleum Experts and SLB.

À Claire et à nos enfants Mathéo et Maud

A mis padres y mis hermanas.

Als meus amics. A mis amigos. To my friends. À mes amis.

Acknowledgements - Remerciements - Agraïments

This is the part of writing a dissertation where one must express and acknowledge all the people who have contributed, in one way or another, for the finalization of this work. My path as a PhD student has been long and transformative. During this period, I have had the privilege of crossing many people with whom I spent time and space, in and out the university. Their technical guidance, motivation and, in many cases, friendship have been priceless in helping me bringing this to an end. This journey has often had its ups and downs, with moments of low motivation. Without the support and encouragement of these people, the completion of this dissertation would not have been possible. I am deeply grateful, and I aim to acknowledge all of you through this piece of text. My research has taken place during two very different periods with a long break in between. For this reason, the acknowledgements here are split also addressing different locations. During the first period, spanning between 2006 and 2010, the research mainly took place in Barcelona as a PhD student at the university department, also including two research visits to France. The second period, from 2017 to the submission of this document, the context was more challenging since it was done as part-time PhD student in parallel to my job in the industry, living abroad between Belgium, Germany and the United Kingdom. Without further ado, I will proceed to list everyone and apologize if I missed anyone.

First, I would like to express my gratitude to Lluís Cabrera and Eduard Roca, my supervisors during the initial phase of this thesis. Thank you both for giving me the opportunity to embark on my doctorate and for supporting me with an FPI (Formación de Personal Investigador) pre-doctoral studentship. Your mentorship and constructive feedback have been key in shaping me as geologist during these early years. A special acknowledgment goes to Eduard for your (sometimes exhausting!) detailed corrections you did for the publications included in this dissertation. I appreciate your implication. The laughs we have shared at the department, during lunch breaks in Farmàcia or out in the field, have left me with many unforgettable souvenirs. I highly value your support and motivation, particularly in these final months. Beyond the names included on the cover of this dissertation, you know you have played a key role throughout the entire journey. Moltes gràcies per tot Eduard.

The second phase of my research, up to January 2025 (!), has been a complicated ride alongside unpredictable family and professional responsibilities, and including the Covid-19 pandemic, which delayed the world and my thesis for several months. During these years, I am deeply grateful to Oriol Ferrer, who, together with Lluís, was my co-supervisor. Lluís, it seems we've finally reached the finish line. I know the way wasn't always clear, and I sincerely appreciate your dedicated support throughout the two periods of my thesis. On the other hand, Oriol, you've been both a mentor and a friend. Balancing family, work, and this thesis has often been overwhelming, and your support made all the difference. Thanks for smoothing out the many challenges that arose during these years despite your always packed schedule with lectures, research, and laboratory duties. You were always reachable when needed. Your quick feedback and encouragement ensured that I never reached the point of making

that so-expected call to say “Uri, plego!”. Thanks for all the calls, conversations, jokes, dinners, and mushroom and fossil pictures. Gràcies amic.

I would also like to extend my appreciation to all the colleagues I met and work with in the Facultat de Ciències de la Terra (former Facultat de Geologia) during this long journey. Long list coming below!

A first and very special mention to Patricia Cabello (Pati) and Telm Bover. I am immensely thankful to both of you for your constant support, calls, and the friendship we've built together. If I finished this is thanks to you and your continuous encouragement. I truly believe there will be many other things we will be able to do together in the future. Moltíssimes gracies!

To the people from the former Structural Geology Department and the Geomodels Research Institute, some of them already left the department, some still continue: Joana Mencos, Marc Rubinat, David Garcia, Oscar Gratacós, Oriol Falivene, Oscar Fernández, Pau Arbués, Giorgi Khazaradze, Ylenia Almar, Hector Perea, Jordi Bausà, Mireia Butillé, Stefano Tavani, Daniel Bello, Bahman Soleimany, Eloi Carola, Ana Carmona, Diego Iaffa, Nuria Carrera, Marco Snidero, Bet and Teresa Beamud, Pablo Granado, Josep Anton Muñoz, Joan Guimerà, Francesc Sàbat, Josep Maria Casas, Eulalia Masana, and many others that stayed for a shorter period. Countless hours spent together guys, in and out of the university walls. I miss our calçotades and barbacoas varies. To the geophysicists of the department: Àlex Marcuello, Pilar Queralt, Anna Martí, Bea Benjumea, Juanjo Ledo, Emma Surinyach and Ignasi Vilajosana.

A very special thanks to Oskar Vidal and Oriol Rosell, essential half of the Guateconchudos Group alongside Oriol Ferrer. For being good friends and for continuing to keep the spirit alive to this day. Piolo, happy to have shared with you long drives and long days digging holes in places I would never have imagined could hold an MT site during several data acquisition campaigns.

To my colleagues from the Sedimentary Geology research group: Anna Travé, Irene Cantarero and, specially, to Vinyet Baqués with whom I spent good times measuring fractures in the Montmell limestones. Special thanks also to Ramon Salas for sharing his passion and for helping out with the Mesozoic sequences in El Garraf and Montmell areas during the early days of my thesis. Thanks for your personal advice and for supporting my research.

Special thanks also to Miguel López-Blanco, for our conversations about music, your assistance with the not-really-my-strength geological mapping, the conglomerates here and unconformities there, for helping me exploring different perspectives and for being always reachable via email, call or messaging.

To my mates in Room 336 during those first four years: Ruben Calvo, Camino Liqueste, Xènia Valois, for many hours together, and specially Elisenda Costa, with whom I shared countless hours in the field, meaningful discussions, and mutual support.

To Miguel Garcés and Alberto Sáez for the given motivation and our conversations. To Mariano Marzo for his last-minute corrections of my Permian and Triassic stratigraphic descriptions.

To the GRC Geociències Marines ("els marinos"), with whom we shared the same side of the third floor: David Amblàs, Roger Urgeles, Ben de Mol, Olaia Iglesias, Jaume Frigola, Galderich Lastras, Sara Lafuerza, Toni Calafat, Anna Sànchez, among others. Thank you for sharing your passion for the sea and your sailing adventures.

À toutes les personnes qui m'ont accueilli lors de mes deux séjours à Nancy où j'ai visité l'Institut National Polytechnique de Lorraine de l'Université de Lorraine pendant la première période de mon doctorat, en 2007 et en 2008. À Mary Ford pour avoir accepté ma candidature. Aux membres, professeurs et étudiants de l'ancien laboratoire du LIAD : Guillaume Caumon et Pauline Collon pour m'avoir accueilli et intégré comme un membre à part entière de leur équipe ; à mon bon ami Marc-Olivier Titeux, à Pauline Durand-Riard et Florent Lallier, ainsi qu'aux autres doctorants. Je garde un excellent souvenir de ces mois passés en France, et c'est là que j'ai rencontré celle qui est maintenant ma compagne et la mère de mes enfants. À tous les autres amis que je me suis fait durant cette période.

To my colleagues and friends in SLB, previously known as Schlumberger, during these last and critical years and months: Russell Davies (my mentor), Teodoro Cassola, Sami Sheyh Husein, Jean-Pierre Joonnekindt, Oliver Schenk, Barbara Claussmann and Daniel Palmowski. Thank you for the geological discussions and for your support. For helping, offering ideas, and encouraging me to finish the work.

Als meus amics, molts de vosaltres casi familia. Alfons, Mireia, Mar, Kiku, Carlos, Vàngelis, Àlex, Alba, Joan, Josep, Suso, Dani, malgrat el temps, la distancia i les circumstàncies personals de cadascú, tots vosaltres heu viscut també d'alguna manera aquest procés en les seves diferents fases i formes.

A mis hermanas Silvia y Fanny y, sobretodo, a mis padres, Miguel y Paula. Llegar hasta aquí ha sido un largo camino lleno de momentos de incertidumbre y estrés. Fanny, gracias por el dibujo de la portada! Este logro no habría sido posible sin vosotros. Gracias, de corazón, por vuestro apoyo incondicional durante todos estos años, a pesar de la distancia. Este momento es también vuestro. Os quiero un montón.

Et, pour terminer, à ma bulle de protection, Claire, Mathéo et Maud, pour votre patience, soutien et résilience. Pour vos rires, les jeux, les aventures, et l'apprentissage que nous avons fait ensemble. À toi, Claire, merci beaucoup pour les acrobaties que tu as réalisées pour concilier un travail exigeant, l'attention nécessaire à deux enfants en pleine croissance et, en plus, le poids de ma thèse, surtout durant ces derniers mois difficiles. Je vous aime infiniment.

A tots vosaltres.

Òxford, Gener de 2025

Index

List of figures	i
Resum i paraules clau	xiii
Abstract	xix
Resumen	xxiii
Chapter 1: General introduction	1
1.1. Motivation and objectives	3
1.2. Structure and coherency of the memoir	8
1.3. Overview of inversion tectonics	11
1.3.1. Definition and concept of inversion tectonics	11
1.3.2. Positive inversion	13
1.3.3. Negative inversion	17
1.3.4. Main controls on tectonic inversion and fault reactivation	18
1.4. Geological introduction to NE Iberia and the Catalan Coastal Ranges	28
1.4.1. Location and overview on the tectonic framework	28
1.4.2. Overview on the stratigraphy	35
1.4.3. Final remarks	46
1.5. Problem approach and methodologies	47
1.5.1. Problem approach	47
1.5.2. Methodology and applied techniques	48
1.5.3. Concluding remarks on the applied techniques	55
Chapter 2: First Publication	57
Structure and Mesozoic structural inheritance in the Gaià-Montmell High	59
Chapter 3: Second Publication	75
Paleogene compression reconstruction in the central Catalan Coastal Ranges	79
Chapter 4: Third Publication	105
Fault zone characterization and structural inheritance along of the Montmell-Vallès Fault System	107
Chapter 5: General discussion	123
5.1. Introduction to the summary and integration of the discussions	125
5.2. Mesozoic configuration of the central Catalan Coastal Ranges	126
5.2.1. Geometrical reconstruction of the Mesozoic structures	126
5.2.2. Late Jurassic (Oxfordian) - Early Cretaceous (Albian) rift basin-fill	130
5.2.3. Post-rift phase reconstruction	131
5.2.4. Relative position of the Montmell-Garraf and Barcelona basins in the Alpine Tethys rifting margin	132

5.3. Paleogene compression and tectonic inversion in the central Catalan Coastal Ranges	134
5.3.1. Regional context and pre-compressional stage in the Gaià-Montmell High	134
5.3.2. Paleogene compressional evolution in the Gaià-Montmell High: positive inversion of the Montmell Fault and emplacement of the Gaià-El Camp Thrust	136
5.3.3. Paleogene compression and inversion along the Montmell-Vallès Fault System	139
5.3.4. Comparison between the Paleogene compression in the southern and northern sectors of the central Catalan Coastal Ranges	142
5.4. Neogene extension and negative inversion	145
3.4.1. Neogene extension in the Gaià-Montmell High	145
3.4.2. Mesozoic structural inheritance and Neogene fault zone characterization along the Montmell-Vallès Fault System	147
3.4.3. Controls on the Montmell-Vallès Fault System extensional reactivation during the Neogene	150
Chapter 6: Summary of the conclusions	153
6.1. Tectonic evolution and structural inheritance in the Gaià-Montmell High	155
6.2. Structural inheritance and control factors of the reactivation along the MVFS	158
References	161
List of acronyms	181

List of figures

List of figures

CHAPTER 1: General Introduction

1.1. Motivation and objectives of the research

- | | | |
|-----------------|--|---------------|
| Fig. 1.1 | Geologic map of NE Iberia showing the major Cenozoic structural units including the three orogenic belts bounding the Ebro Basin: the Pyrenees, the Iberian Range, and the Catalan Coastal Ranges. Cenozoic foreland basin-fill is highlighted in orange. Coordinates in geographical system. Labels A, B and C respectively correspond to The Montserrat-Sant Llorenç del Munt, Pontils-Cabra del Camp and Montsant areas. Labels PH, GMH and GH respectively correspond to the Prades Block, the Gaià-Montmell High and the Garraf High. | Page 4 |
| Fig. 1.2 | A) Geological map of the Pontils-Cabra del Camp area showing the distribution of the Sant Miquel del Montclar conglomerates. B) Geological cross-section showing a composite progressive unconformity involving Paleogene (mainly Eocene) strata in the forelimb of the Cabra-Carme Anticline (redrawn from Anadón <i>et al.</i> , 1986). | Page 5 |
| Fig. 1.3 | Map illustrating Cretaceous outcrops in the central and southern Catalan Coastal Ranges classified by their thicknesses. The map also shows the main inferred structural lineaments (redrawn from Esteban and Robles, 1976). | Page 6 |

1.3. Overview of inversion tectonics

- | | | |
|-----------------|---|----------------|
| Fig. 1.4 | Synoptic examples of positive and negative inversion tectonics in the evolution from a rifted margin to a fold-and-thrust belt, including thin- and thick-skinned deformation examples. A) Rift basin underneath continental margin; B) Thin-skinned fold-and-thrust belt without significant inversion; C) Hybrid Thin- and thick-skinned fold-and-thrust belt with positive inversion; D) Post-orogenic extension with negative inversion (modified from Granado <i>et al.</i> , 2017). | Page 12 |
| Fig. 1.5 | Schematic example of an inverted half-graben related to a listric fault showing the tectono-sequences associated to each tectonic phase. The positive inversion causes the contractional reactivation of the inherited listric fault that propagates upward into the undeformed post-rift units, the uplift of the basin-fill, and the development of a footwall short-cut. A) End of the post-rift phase; B) end of the inversion phase (modified after Cooper <i>et al.</i> , 1989). | Page 13 |
| Fig. 1.6 | Conceptual sections illustrating the inversion ratio showing the degree of inversion of an inverted fault using the null point position. A) Extensional graben with no inversion; B) Minor inversion of the extensional graben; C) Major inversion; D) Complete inversion (modified from Williams <i>et al.</i> , 1989). | Page 14 |
| Fig. 1.7 | Inversion structures: A) Extensional half-graben; B) Arrowhead or harpoon structure developed as the result of an inverted half-graben; C) By-pass thrusts and buttressing; D) Complex combination including back-thrusts, buttressing, pop-up structure and footwall short-cut (adapted from Granado and Ruh, 2019). | Page 15 |

Fig. 1.8	Cartoon summary of geometries associated to negative inversion tectonics. Note the short-cut extensional fault developed within the hangingwall of the partially inverted pre-existing thrust, which develops a half-graben with growth strata. The tectono-sequences associated to the tectonic phases are also indicated (modified from Tari <i>et al.</i> , 2023).	Page 18
Fig. 1.9	Main types of normal faults: A) Listric fault; B) Planar fault with a horizontal detachment at depth; C) Planar rotational or domino-style faults (compiled from Gillcrust <i>et al.</i> , 1987, McClay 1992 and Buchanan and McClay, 1992).	Page 19
Fig. 1.10	Models of inversion for simple extensional systems, based on analogue sandbox models (modified from McClay <i>et al.</i> , 1992). A) Inversion of a concave upwards simple listric fault; B) Inversion of a planar fault with a deep horizontal detachment; C) Inversion of a domino-style fault system.	Page 21
Fig. 1.11	Analogue sandbox model cross-sections illustrating the structural styles of inversion of complex fault geometries. A) Ramp-flat listric fault; B) Kinked planar fault (redrawn after Ferrer <i>et al.</i> , 2016).	Page 22
Fig. 1.12	Subdivision of inversion into two modes of inversion. A) Mode I inversion when the post-rift succession is thinner than the syn-rift succession in the pre-existing extensional basin; B) Mode II inversion when the post-rift succession is thicker than the syn-rift one (modified from Tari <i>et al.</i> , 2020).	Page 23
Fig. 1.13	Idealized depth-dependent strength profiles for dry and wet lithosphere to stresses (tension and compression) and their corresponding thermal gradients. The graph assumes a quartz/diorite/olivine rheology corresponding to the upper crust, lower crust, and lithospheric mantle. A) Normal lithosphere profile (i.e., unstretched or cratonic scenarios) with 30 km thick crust and 70 km thick lithospheric mantle. B) Stretched lithosphere profile (i.e., rifted, stretched scenarios) and thermally unstable lithosphere thinned to 20 km thick crust and 45 km lithospheric mantle (modified from Ziegler <i>et al.</i> , 2001).	Page 25
Fig. 1.14	Mohr circle and Mohr envelope for brittle behaviour, showing how cohesion and friction influence fault behaviour under compressive stress. A) The envelope for rock with cohesion C_0 and an internal friction angle ϕ , showing the typical strength of intact rock. B) The envelope for a pre-existing fault, with lower cohesion C_0' and a sliding friction angle ϕ' .	Page 26

1.4 Geological introduction to the Catalan Coastal Ranges

Fig. 1.15	Shaded relief map of NE of the Iberian Peninsula with the location of the three main alpine mountain belts: the Pyrenees, the Iberian Range, and the Catalan Coastal Ranges, which bound the Ebro Foreland Basin to the north, southwest and southeast respectively. Red square indicates the central domain of the Catalan Coastal Ranges area in which this thesis is focussed. A-A' line indicates the location of the regional section shown in Figure 1.16. Base map made with GeoMapApp (https://www.geomapapp.org/) / CC BY / CC BY, Ryan <i>et al.</i> , 2009).	Page 28
Fig. 1.16	Depth section through the Catalan margin showing the SE-NW increase of the crustal thickness between the Valencia Trough and the Iberian Plate (modified from Gaspar-Escribano <i>et al.</i> , 2003).	Page 29
Fig. 1.17	Schematic geological map of NE Iberia showing the three major structural units bounding the Ebro Basin: the Pyrenees to the North, the Iberian Range to the SW, and the Catalan Coastal Ranges (CCR) to the SE. The limits of the southern, central, and northern domains of the CCR are indicated in orange dashed lines. The trace of the Montmell-Vallès	Page 30

Fault System the tectonic evolution of which is presented in this Thesis is highlighted with a thick blue line in the central domain of the CCR (modified from Garcés *et al.*, 2020).

- Fig. 1.18** Reconstruction of the Iberia-Eurasia margin and surrounding areas in the mid-Cretaceous times. Major basins, transform faults, and crustal domains are indicated. PB: Parentis basin; LP: Landes plateau; BCB: Basque-Cantabrian basin; CB: Cameros basin; FNB: Flysch Noir basin; OB: Organyà basin; MsB: Maestrat basin; VB: Vocontian basin; DI: Durance isthmus; SPB: South Provence basin; FMB: Figueres-Montgrí basin; PrB: Perelló basin; MGB: Montmell-Garraf Basin; BB: Barcelona basin. Red square indicates the area of study (modified from Tavani *et al.*, 2018). **Page 31**
- Fig. 1.19** Present-day structural maps of the CCR showing the main onshore structures active during the two Cenozoic tectonic phases that affected the area. A) Main structures active during Paleogene compression. 1: Pla de Barcelona Thrust; 2: Vallès-Penedès Thrust; 3: Miramar-Gaià Thrust; 4: Gandesia-Ulledemolins Thrust; 5: Portarubio-Vandellòs-Tarragona Thrust. B) Main structures active during latest Oligocene to Miocene extension. A: Pla de Barcelona Fault; B: Vallès-Penedès Fault; C: El Camp Fault; D: Baix Ebre Fault. VPB: Vallès-Penedès Basin; ECB: El Camp Basin; GMH: Gaià-Montmell High; PH: Prades High; GMtH: Garraf-Montnegre High (modified from Roca *et al.*, 2004). **Page 33**
- Fig. 1.20** Geological map of the Gaià-Montmell High, the transfer zone of the two major Neogene extensional faults: the Vallès-Penedès and El Camp Neogene faults. The two main domains characterizing the Gaià-Montmell High are indicated: the Miramar-Gaià and the Montmell domains. Label "M" and the thick dashed line indicates the approximate location of the Mesozoic type-succession (Salas, 1987). The red square indicates the area between Vallespinosa and Cabra del Camp in the Ebro Basin margin, the tectonostratigraphy of which was studied in detail in this thesis. **Page 34**
- Fig. 1.21** Chronostratigraphic chart of the study and the adjoining areas. Main tectonic events are indicated. Major unconformities are labelled as follows: MU: Messinian Unconformity; MAU: Middle Albian Unconformity; VU: Variscan Unconformity. Lithostratigraphy has been compiled from Ortí (1974), Anadón *et al.* (1978), Colombo (1986), Lanaja (1987), Salas (1987), Casas and Permanyer (1991), Calvet and Marzo (1994), Cabrera and Calvet (1996), Salas *et al.* (2001), Mercedes-Martín *et al.* (2014), Ortí *et al.* (2017) and Escudero-Mozo *et al.* (2017). **Page 35**
- Fig. 1.22** Detail of the central Catalan Coastal Ranges highlighting the structural units, basins, sectors, and domains present in the study area. MR: Miramar Range; ECB: El Camp Basin; GMH: Gaià-Montmell High; BPB: Baix Penedès Basin; PB: Penedès Basin; VP: Vallès Basin; GH: Garraf High; BP: Barcelona Plain; CMH: Collserola-Montnegre High; MH: Montseny High; BF: Barcelona Fault; BMB: Barcelona-Maresme Basin; MAZ: Marmellar Accommodation Zone. **Page 36**
- Fig. 1.23** Paleozoic outcrops in the Miramar Range (see Figure 1.22 for its location). A) Highly deformed Silurian black-grey slates with quartzitic levels showing folds and cleavage/foliations. B) Carboniferous slates and red sandstones with cleavage/foliations. **Page 37**
- Fig. 1.24** A) Permian-Mesozoic thicknesses across the Ebro Basin and the central Catalan Coastal Ranges. Upper reference datum corresponds to the base of the Tertiary. Mesozoic thicknesses based on Salas (1987), Lanaja (1987) and ICGC (2005); Permian based on Marzo (1980), Marzo and Calvet (1985) and López-Gómez (2002). Horizontally not-to-scale. B) Tectonostratigraphic map of the central Catalan Coastal Ranges at the end **Page 38**

of the late Jurassic - early Cretaceous extensional phase. St-1: Senant-1 well; StS-1: Sant Sadurní-1 well.

- Fig. 1.25** Triassic outcrops in the Gaià-Montmell High. S_0 indicates bedding orientation A) Quartz clast-rich conglomerates and red lutites Lower Buntsandstein facies; B) Quartz clast-rich Lower Buntsandstein conglomerate facies; C) Fine laminated Lower Muschelkalk (Mu1) marine carbonate facies; D) Deformed (see folds in the upper left corner of the image) Middle Muschelkalk (Mu2) red-beds and evaporitic facies; E) Foliated and faulted Upper Muschelkalk (Mu3) marine carbonate facies; F) Keuper fine detrital and evaporite facies. **Page 39**
- Fig. 1.26** Chrono-lithostratigraphic diagram showing the Upper Jurassic-Lower Cretaceous succession recognized in the Montmell-Garraf Basin compiled from Salas *et al.* (2001), Moreno-Bedmar *et al.* (2017) and Martín-Closas *et al.* (2021). **Page 40**
- Fig. 1.27** Not-to-scale schematic chrono-lithostratigraphic panel for the Paleocene-Eocene units outcropping between Vallespinosa and Cabra del Camp towns (see Figure 1.20 for location). Numbers in the panel indicate the four major lithostratigraphic assemblages defined in the area by Colldeforns *et al.* (1994a and b): 1) basal continental unit (Mediona Fm.) and a lower marine unit (Orpí Fm.); 2) Pontils-Cornudella Group; 3) Santa Maria Group, and 4) Barberà-Anoia Group. **Page 42**
- Fig. 1.28** Paleogene outcrops of the central southeastern margin of the Ebro Basin in the Cabra-Vallespinosa area. A) Mediona and Orpí formations (marine carbonatic basal succession) on top of Upper Triassic Keuper; B) Mediona Fm., continental unit constituted by alluvial mudstones affected by intense pedogenic processes; C) Lacustrine limestones alternating with versicoloured mudstones of the Santa Cándia Fm.; D) Red mudstones with minor sandstone and carbonate bed intercalations of the Carme Fm.; E) Sulphate evaporites and lacustrine carbonates of the Valdeperes Fm.; F) Lacustrine and palustrine limestones with interbedded marls and cherts bearing beds of the Bosc d'en Borràs Fm.; G) Shallow marine fine-grained sandstones of the Vallespinosa Fm.; H) Red beds of the Montblanc Fm.; I) Cabra del Camp Mb. verticalized bed (Montblanc Fm.); J) Inverted beds of the Cabra del Camp Mb. (Montblanc Fm.); K) Sant Miquel del Montclar massive conglomerates with centimetric to decimetric carbonate clasts. **Page 43**

1.5. Problem approach and methodology

- Fig. 1.29** Flow diagram showing the three phases that covers the performed research. **Page 47**
- Fig. 1.30** Simplified geological map of the central Catalan Coastal Ranges indicating the areas where has been performed the stratigraphic recognition and characterization of specific stratigraphic successions and the gathering of structural data: 1) Triassic successions in Querol in the centre of the Miramar-Gaià Domain (1') and the Miramar Range (1''); 2) Lower Cretaceous successions in Coll de Santa Cristina - La Rubiola at the Montmell Domain; 3) Upper Jurassic-Lower Cretaceous (Early Valanginian) successions; 4) Upper Jurassic-Lower Cretaceous successions nearby la Juncosa del Montmell town; 5) Paleogene units preserved both in the southeastern margin of the Ebro Basin between Vallespinosa and Cabra del Camp. **Page 48**
- Fig. 1.31** Geological map of the Gaià-Montmell High and surrounding areas (modified from ICC, 2017). The map includes the location of the constructed sections: A) Gaià-Montmell Section; B) Marmellar Section **Page 51**

and C) Cabra Section. The map also shows the acquired parametric MT soundings along the Gaià-Montmell Section.

- Fig. 1.32** Senant-1, Sant Sadurní-1 and Martorell-1 boreholes (St-1, SS-1 and Ma-1 respectively in the map) used during the construction of the structural sections and tectonostratigraphic maps (modified from Lanaja, 1987). PH: Prades High; MR: Miramar Range; ECB: El Camp Basin; ECF: El Camp Fault; GMH: Gaià-Montmell High; VPB: Vallès-Penedès Basin; VPF: Vallès-Penedès Fault; GMtH: Garraf-Montnegre High; BF: Barcelona Fault; BB: Barcelona Basin. **Page 52**

- Fig. 1.33** A) Cabra de Camp Mb. (Montblanc Fm.) verticalized conglomerate bar; B) Example of yellowish centimetric Mesozoic bioclastic clast sampled from the Cabra del Camp Mb.; C) Example of Mesozoic reddish centimetric bioclastic clast sampled from the Cabra del Camp Mb.; D) Paleochannel bottom outcrop in conglomerates of the Cabra del Camp Mb. used for paleocurrent measurements; E) Ripples at the bed top of marine-continental transitional facies. Dashed white arrow indicates the paleocurrent direction. **Page 55**

CHAPTER 2: First Publication

Mesozoic structural inheritance in the Cenozoic evolution of the central Catalan Coastal Ranges (western Mediterranean): Structural and magnetotelluric analysis in the Gaià-Montmell High. (Marín *et al.*, 2021).

- Fig. 1** Schematic structural map of the Catalan Margin (Western Mediterranean). ECB: El Camp Basin; ECF: El Camp Fault; GMtH: Garraf-Montnegre High; GMH: Gaià-Montmell High; MR: Miramar Range; PH: Prades High; VPB: Vallès-Penedès Basin; VPF: Vallès-Penedès Fault; MH: Montseny High; BF: Barcelona Fault; BB: Barcelona Basin; GUT: Gandesa-Ulldemolins Thrust; PVT: Portlucet-Vandellòs Thrust; PeB: Perelló Mesozoic Basin; EMB: Eastern Maestrat Mesozoic Basin; St-1: Senant-1 well. Red stars in the Prades High indicate the location of the two MT soundings recorded on top of Paleozoic rocks. (For interpretation of the references to colour in this figure legend, the reader is referred to the web version of this article.) **Page 60**
(2 of 15)
- Fig. 2** Geological map of the Gaià-Montmell High and surrounding areas. The map includes the location the Gaià-Montmell and the Marmellar cross-sections (Figs. 5 and 6 respectively) and the acquired parametric MT soundings along the Gaià-Montmell Section. M-labelled thick dashed line indicates the approximate location of the Mesozoic succession-type described by Salas (1987) in the Marmellar area. Black dots are village locations used in the text to facilitate the explanations. See Fig. 1 for the exact location of the Senant-1 well. **Page 61**
(3 of 15)
- Fig. 3** Chronostratigraphic chart of the study and the adjoining areas. Main tectonic events are indicated. Major unconformities are labelled as follows. MU: Messinian Unconformity; MAU: Middle Albian Unconformity; VU: Variscan Unconformity. Lithostratigraphy has been compiled from Ortí (1974), Anadón *et al.* (1978), Colombo (1986), Lanaja (1987), Salas (1987), Casas and Permanyer (1991), Calvet and Marzo (1994), Cabrera and Calvet (1996), Salas *et al.* (2001), Mercedes-Martín *et al.* (2014), Ortí *et al.* (2017) and Escudero-Mozo *et al.* (2017). **Page 62**
(4 of 15)

Fig. 4	Gaià-Montmell Section showing the Alpine structure at the linkage zone between the Neogene Vallès-Penedès and El Camp faults in the central Catalan Coastal Ranges. See location of the section in Fig. 3. The hatched area labelled with “T” indicates the zone of distributed shear at the upper tip of the Gaià-El Camp Thrust. B) Detail of the structure of the L'Arboçar deformation strip.	Page 64 (6 of 15)
Fig. 5	A) Riera del Marmellar outcrop exemplifying collected structural data and stereographic plots (lower hemisphere) with measured fault planes and slip directions in the present-day and their orientations after unfolding the bedding. B) Marmellar Section showing the structure at the NE sector of the Montmell Domain and adjoining Miramar-Gaià Domain areas. Location of the Riera del Marmellar and Guardiola de Font-Rubí outcrops are indicated with a red star. See Fig. 3 for the location of the section and the outcrop in map view. (For interpretation of the references to color in this figure legend, the reader is referred to the web version of this article.)	Page 65 (7 of 15)
Fig. 6	A) Final magnetotelluric 2D model of the Gaià-Montmell Section showing the differentiated conductive (C labels) and resistive (R labels) bodies. B) The model with the interpreted stratigraphic boundaries (black lines), faults (red lines) and the top of the Variscan basement (dashed white line). White stars indicate the location of the MT soundings (see Fig. 3 for their location). (For interpretation of the references to color in this figure legend, the reader is referred to the web version of this article.)	Page 67 (9 of 15)
Fig. 7	Sequential structural restoration of the Gaià-Montmell Section applying flexural slip and bed length preservation. A) Present-day after the latest Oligocene- Neogene extension. B) Early Oligocene (end of the Paleogene compression). C) Late Cenomanian (end of the Late Jurassic-Early Cretaceous extension). No vertical exaggeration.	Page 69 (11 of 15)
Fig. 8	Schematic geological map of the Gaià-Montmell High showing the major Neogene extensional faults and their related relay ramps.	Page 70 (12 of 15)

CHAPTER 3: Second Publication

Paleogene kinematics of the central Catalan Coastal Ranges: temporal constraints from magneto-chronology and provenance analysis in synorogenic deposits in the SE margin of the Ebro Basin (NE Spain). (Marín *et al.*, 2025)

Fig. 1	Schematic diagram of a thick-skinned fold-and-thrust belt, which includes an inverted extensional basin and its related foreland basin. T _i to T _v stand for relative timing of deformation. End-member thrusting sequences (forward-breaking and break-back) are also specified. Other combinations of relative timing imply out-of-sequence thrusting.	Page 80 (1 of 25)
Fig. 2	A) Geologic map of NE Iberia showing the major Cenozoic structural units including its three bounding orogenic belts: the Pyrenees and the intraplate Iberian and Catalan ranges. Cenozoic foreland basin-fill is highlighted in orange. Coordinates in geographical system. Labels 1 and 2 respectively correspond to the Prades Block and the Montserrat-Sant Llorenç del Munt areas referred in the text. B) Geological map of the Gaià-Montmell High in the central Catalan Coastal Ranges and adjoining areas. The area corresponds to the linkage zone between the Neogene Montmell-Vallès Fault System and El Camp Fault. Coordinates in UTM kms. C) Cross-section across the Gaià-Montmell High and its neighbouring areas. The hatched area labelled with “T” indicates the zone	Page 81 (2 of 25)

of distributed shear at the tip of the Gaià-El Camp Thrust (modified from Marín *et al.*, 2021). Legend for B and C is the same.

- Fig. 3** A) Mesozoic thicknesses across the central Catalan Coastal Ranges and the present-day offshore Barcelona-Maresme Basin. Upper reference datum corresponds to the base of the Tertiary. Mesozoic thicknesses based on Salas (1987), Lanaja (1987) and ICGC (2005). B) Tectonostratigraphic map of the central Catalan Coastal Ranges and offshore areas at the end of the late Jurassic - early Cretaceous extensional phase. Bcn E-1: Barcelona Marina E-1 well; StS-1: Sant Sadurní-1 well. **Page 83**
(5 of 25)
- Fig. 4** A) Geological map of the SE margin of the Ebro Basin between Cabra del Camp and Vallespinosa locations based on Carrera *et al.* (2020) and extended towards the northeast using the map from Colldeforns (unpublished). Labels i, i', i'' stand for the Pontils magnetostratigraphic logs from Beamud *et al.*, (2012). The basal portion of the magnetostratigraphic log corresponding to the Carme Fm. present in Figure 8, is located in the map shown in Figure 1 of the supplementary material. Label j indicates the location of the Rocafort de Queralt magnetostratigraphic log from Barberà *et al.* (1999, 2001). The location of the cross-section in Figure 5 is shown. The map uses UTM projection for zone 31N (ETR96 datum) and the coordinates are in meters. B) Not-to-scale schematic lithostratigraphic panel for the Eocene units. Numbers in the panel indicate the four major lithostratigraphic units defined in the area by Colldeforns *et al.* (1994a and b): 1) basal continental unit (Mediona Fm.) and a lower marine unit (Orpí Fm.); 2) Pontils-Cornudella Group; 3) Santa Maria Group, and 4) Barberà-Anoia Group. **Page 84**
(6 of 25)
- Fig. 5** A) Geological cross-section of the SE margin of the Ebro Basin across the locality of Cabra del Camp. The section includes the NW frontal structure of the Catalan Coastal Ranges (Cabra-Carme Monocline). B) Field image of the limit between the Triassic and the succession of the foreland. See map in Figure 2 for location at regional scale and map in Figure 4 for a detail section location in the study area. **Page 85**
(7 of 25)
- Fig. 6** A) Paleochannel bottom outcrop in conglomerates of the Cabra del Camp Mb. used for paleocurrent measurements. B) Ripples at the bed top of marine-continental transitional facies. Dashed white arrow indicates the paleocurrent direction. C) Stereographic plot of paleocurrent measurements in the Cabra Fm. around the Cabra del Camp (n = number of measurements). See map in Figure 4 for location. D) Restored paleocurrent directions showing the predominant direction of the sediment supply. **Page 88**
(10 of 25)
- Fig. 7** Clast microfacies. A) Photomicrograph of a grainstone texture from the Ypresian Orpí Fm. showing two *Alveolina* tests (left) and one of *Opertorbitolites* (upper right). Sampling site 1. B) Detail of a pebble-sized clast with ostracods giving rise to a wackestone texture. Santa Cándia Fm. (late Ypresian-Bartonian?). Sampling site 1. C) Close-up view of a packstone clast (centre to right) with small foraminifera and a section of a bivalve. Basal part of the Orpí Fm. (Ypresian). Sampling site 1. D) Sand-sized clast exhibiting a grainstone texture with ooids perhaps eroded from the Cenomanian Can Xuech Fm. Note the presence of an orbitolinid within the conglomerate matrix (right). Sampling site 1. E) Close-up view of a dolomitized miliolid and peloidal grainstone of Barremian-Aptian age. Sampling site 2. F) Photomicrograph of a recrystallized limestone exhibiting abundant sections of calcareous green algae. Cretaceous? Sampling site 2. G) Detail of an orbitolinid grainstone of Barremian-Aptian age. Sampling site 3. H) Pebble-sized clast of Aptian age showing a "bacinellid" fabric. Sampling site 3. I) Barremian-Aptian grainstone texture exhibiting a section of a belemnite rostrum (centre) under cross **Page 89**
(11 of 25)

polarized light. Note the presence of an orbitolinid in the lower left part of the image. Sampling site 4.

Fig. 8	Magnetostratigraphy of the Pontils section. A) Magnetostratigraphic section and correlation to the GPTS (Gradstein <i>et al.</i> , 2020). PO and RO correspond to Pontils and Rocafort de Queralt fossil sites, respectively, with their attribution to Mammal Paleogene Reference Levels in brackets. White squares in the VGP graph represent type 3 directions, discarded to build the local magnetostratigraphy. B.A. Gp., B.B. and R.B-M stand for Barberà-Anoia Group, Bosc d'en Borràs and Riu de Boix-Montblanc formations in the stratigraphic column. B) Sedimentation rates values and evolution for the Pontils section. Blue arrow: Bartonian transgressive event at the base of Santa Maria Group. Orange arrow: time of disconnection from the ocean of the Ebro Basin.	Page 90 (12 of 25)
Fig. 9	Source area age attribution of the upper Eocene clasts in the central SE margin of the Ebro Basin. Clast type classification: A: Ypresian wackestones-packstones. B: Alveolina limestone. C: Cenomanian ooidal grainstones. D: Lacustrine limestones (Barremian-Aptian, Upper Cretaceous, Ypresian. E: Barremian-Aptian: orbitolinid limestone. F: Barremian Aptian grainstones. G: Undifferentiated Cretaceous limestone. H: Undifferentiated Cretaceous or Early Eocene dolostones.	Page 91 (13 of 25)
Fig. 10	Schematic sequential structural restoration of the Gaià-Montmell Section applying flexural slip and bed length preservation. A) late Lutetian pre-compressional stage. B) late Lutetian – middle Bartonian syn-compressional stage. C) middle Bartonian to late Priabonian latest stages of the compressional stage. No vertical exaggeration.	Page 94 (16 of 25)
Fig. 11	Geological cross-section of the SE margin of the Ebro Basin across the locality of Cabra del Camp showing the tectono-sequences differentiated by the tectono-stratigraphic analysis. See Figure 4 for section location.	Page 95 (17 of 25)

CHAPTER 4: Third Publication

Fluid-rock interaction control on fault reactivation: A review of the Montmell-Vallès Fault System, central Catalan Coastal Ranges (NE Iberia). (Marín *et al.*, 2023)

Fig. 1	A) Schematic geological map of NE Iberia showing the three major structural units bounding the Ebro Basin: the Pyrenees to the North, the Iberian Range to the SW, and the Catalan Coastal Ranges (CCR) to the SE. The trace of the Montmell-Vallès Fault System (MVFS) is highlighted with a thick blue line. The limits of the southern, central, and northern domains of the CCR are indicated in orange (names and dashed lines). Black squares indicate the location of Figs. 2, 5 and 6. The map in geographical coordinates. B) Detail of the central Catalan Coastal Ranges highlighting the three sectors of the Montmell-Vallès Fault System indicated in the text. The location of the structural sections and seismic profile shown in Fig. 3 is also indicated. BF: Barcelona Fault; BP: Barcelona Plain; VP: Vallès Basin; PB: Penedès Basin; GH: Garraf High; GMH: Gaià-Montmell High; MH: Montseny High; CMH: Collserola-Montnegre High; PeB: Perelló Basin; MAZ: Marmellar Accommodation Zone. (For interpretation of the references to colour in this figure legend, the reader is referred to the web version of this article.)	Page 108 (2 of 16)
Fig. 2	Simplified geological map of the central Catalan Coastal Ranges highlighting the major Cenozoic faults and the sectors of the Montmell-Vallès Fault System indicated in the text. Star symbols indicate the	Page 109

	location of fluid flow analysis in fault planes performed by (1) Travé <i>et al.</i> , 1998, (2) Belaid <i>et al.</i> , 2008, (3) Baqués <i>et al.</i> , 2010, (4) Baqués <i>et al.</i> , 2012, (5) Baqués <i>et al.</i> , 2014, (6) Cantarero <i>et al.</i> , 2014a, (7) Marcén <i>et al.</i> (2018), (8) Travé and Calvet (2001), (9) and Cantarero <i>et al.</i> (2014c). The location of the structural sections and the seismic profile shown in Fig. 3 is also indicated. VB: Vallès Basin; PB: Penedès Basin; BPB: Baix Penedès Basin; ECB: El Camp Basin; MAZ: Marmellar Accommodation Zone (Marín <i>et al.</i> , 2021); Ma-1: Martorell-1 borehole; SS-1: San Sadurní-1 borehole. Paleogene alluvial and fan-delta systems: SLM: Sant Llorenç del Munt alluvial fan and fan delta; Mr: Montserrat fan delta; SMM: Sant Miquel del Montclar alluvial fan.	(3 of 16)
Fig. 3	Structural sections across the central Catalan Coastal Ranges: i: Llobregat section based on surface structural, fission track and Martorell-1 oil exploratory well data, i(s): PV-2 seismic profile with the interpretation of the Vallès-Penedès Fault with the base of the Vallès-Penedès Basin infill and intrabasinal lower to middle Miocene reflectors (modified from Bartrina <i>et al.</i> , 1992; see location in Fig. 1B); ii: Gaià-Montmell Section (modified after Marín <i>et al.</i> , 2021). See location of the sections in Fig. 2.	Page 111 (5 of 16)
Fig. 4	Tectonostratigraphic maps and conceptual cross-sections showing the Late Jurassic (A) to late Miocene (C) evolution of the central Catalan Coastal Ranges. Map A includes sketched stratigraphic columns of the Mesozoic. On each map and cross-section active faults are shown with thick colored traces and lines, and previous inactive faults with thinner black lines.	Page 112 (6 of 16)
Fig. 5	Schematic map of the Montmell-Vallès Fault System showing fault damage zone characteristics of three sectors (A, B and C) during the different Late Jurassic- Early Cretaceous, Paleogene and late Oligocene-Neogene tectonic deformational stages. Fluid and petrological descriptions compiled after Travé and Calvet (2001), Baqués <i>et al.</i> (2008), Baqués <i>et al.</i> (2010), Baqués <i>et al.</i> (2012), Baqués <i>et al.</i> (2014) and Cantarero <i>et al.</i> (2014a, 2014c). Llobregat Relay Ramp from Belenguer <i>et al.</i> (2012). Magnetotelluric data (MT) from Marín <i>et al.</i> (2021).	Page 113 (7 of 16)
Fig. 6	A: Geological section of the Vallès-Penedès Fault in the northern sector of the Montmell Vallès Fault System showing the characteristics of the fault zone. Zoomed area: sketch of the Colònia Sedó outcrop highlighting Neogene fractures related to the hangingwall damage zone. B: Geological section across the Montmell Fault in the Marmellar Accommodation Zone area in the southern sector of the Montmell Vallès Fault System (modified from Marín <i>et al.</i> , 2021). Zoomed area: sketch of the Riera de Marmellar outcrop highlighting Mesozoic, Paleogene and Neogene fractures related to the hangingwall damage zone (modified from Baqués <i>et al.</i> , 2012). Fracture types are not to scale. A and B sections located in Fig. 3.	Page 114 (8 of 16)
Table 1	Characteristics of the northern sector (Vallès area) of the Montmell-Vallès Fault System. Compiled from Anadón <i>et al.</i> (1985), Julià and Santanach (1984, 1998), Camps and Morera (2014) and Cantarero <i>et al.</i> (2014a).	Page 115 (9 of 16)
Table 2	Characteristics of the central sector (Penedès area) of the Montmell-Vallès Fault System. Compiled from Amigó (1984) and Baqués <i>et al.</i> (2012).	Page 117 (11 of 16)
Table 3	Characteristics of the southern sector (Montmell area) of the Montmell-Vallès Fault System. Compiled from Belaid <i>et al.</i> (2008), Baqués <i>et al.</i> (2010, 2012, 2014) and Marín <i>et al.</i> (2021).	Page 117 (11 of 16)

CHAPTER 5: Discussion

5.2. Mesozoic configuration of the central Catalan Coastal Ranges

- Fig. 5.1** Simplified geological map of the central Catalan Coastal Ranges highlighting the major Cenozoic faults and the sectors of the Montmell-Vallès Fault System. The location of the Gaià-Montmell Section as well as the three main sectors of the Montmell-Vallès Fault System are also indicated. VB: Vallès Basin; PB: Penedès Basin; BPB: Baix Penedès Basin; ECB: El Camp Basin; MAZ: Marmellar Accommodation Zone; Ma-1: Martorell-1 borehole; SS-1: San Sadurní-1 borehole. Paleogene alluvial and fan-delta systems: SLM: Sant Llorenç del Munt alluvial fan and fan delta; Mr: Montserrat fan delta; SMM: Sant Miquel del Montclar alluvial fan. The subsurface distribution of the Jurassic-Cretaceous is based on Lanaja (1987) and Bartrina *et al.* (1992). **Page 127**
- Fig. 5.2** Sequential structural restoration of the Gaià-Montmell Section. A) Present-day after the latest Oligocene-Neogene extension. B) Early Oligocene (end of the Paleogene compression). C) Late Cenomanian (end of the Late Jurassic-Early Cretaceous extension). Restoration performed with the software Dynel 2D[®]. No vertical exaggeration. **Page 128**
- Fig. 5.3** A) 3D schematic view of the base of the Late Jurassic-Early Cretaceous rift basin system developed in the central CCR. Sn-1: Senant-1 well; SS-1: Sant Sadurní-1 well; Ma-1: Martorell-1 well; Bc E-1: Barcelona E-1 well. B) Schematic cross-sections across the rift basin system (see location in Figure 5.3A) showing the main basins and sub-basins and the corresponding extensional faults. Orange portion in section i-i' corresponds to the present-day location of the GMH. **Page 130**
- Fig. 5.4** A) Schematic cross section highlighting the primary morphology of magma-poor rifted margins showing the main tectonic domains (modified from Chenin *et al.*, 2017); B) Reconstruction of a synthetic crustal section across the Alpine-European margin and the former Alpine Tethys rift system. Abbreviations: hyperext.: hyperextended; dom.: domain; C) Reconstruction of a synthetic crustal section showing the proximal domain of the Iberian/Ebro margin across the central Catalan Coastal Ranges; D) Schematic map showing the succession of rifting events and in Western Europe and the location of sections i-i' and ii-ii' (modified from Chenin *et al.*, 2022). **Page 132**

5.3. Paleogene compression and tectonic inversion in the central Catalan Coastal Ranges

- Fig. 5.5** Schematic sequential structural restoration of the Gaià-Montmell Section applying flexural slip and bed length preservation. A) late Lutetian pre-compressional stage. B) late Lutetian – middle Bartonian syn-compressional stage. C) middle Bartonian to late Priabonian latest stages of the compressional stage. The images include the location of the later compressional structures. See approximate location of the reconstructed section in Figure 5.1. No vertical exaggeration. **Page 135**
- Fig. 5.6** Geological cross-section of the SE margin of the Ebro Basin across the locality of Cabra del Camp (Cabra Section in Figure 5.1). The section includes the NW frontal structure of the Catalan Coastal Ranges (Cabra-Carme Monocline) as well as the location of the Cabra del Camp Mb. (Montblanc Fm.) sampling sites referred in the text. **Page 136**

Fig. 5.7	Magnetostratigraphy of the Pontils section. A) Magnetostratigraphic section and correlation to the GPTS (Gradstein <i>et al.</i> , 2020). PO and RO correspond to Pontils and Rocafort de Queralt fossil sites, respectively, with their attribution to Mammal Paleogene Reference Levels in brackets. White squares in the VGP graph represent type 3 directions, discarded to build the local magnetostratigraphy. B.A. Gp., B.B. and R.B-M stand for Barberà-Anoia Group, Bosc d'en Borràs and Riu de Boix-Montblanc formations in the stratigraphic column. B) Sedimentation rate values and evolution for the Pontils section. Blue arrow: Bartonian transgressive event at the base of Santa Maria Group. Orange arrow: time of disconnection from the ocean of the Ebro Basin.	Page 138
Fig. 5.8	Tectonostratigraphic map showing the end of the positive inversion of the Mesozoic faults and contractional footwall short-cuts in the central Catalan Coastal Ranges at late Oligocene (approximately 28My). The location of the Gaià-Montmell Section and the section in Figure 10 are also indicated.	Page 140
Fig. 5.9	Schematic map of the Montmell-Vallès Fault System showing fault damage zone characteristics of three sectors (A, B and C) during the Paleogene compressional phase. Fluid and petrological descriptions compiled after Travé and Calvet (2001), Baqués <i>et al.</i> (2008, 2010, 2012, and 2014), and Cantarero <i>et al.</i> (2014a and 2014c).	Page 141
Fig. 5.10	Structural reconstruction of the northern sector of the central Catalan Coastal Ranges and the Valencia Trough domain at the end of the compressional stage (late Oligocene - Chattian, approximately 28Ma). An estimate location of the limit of the Late Jurassic-Early Cretaceous rift basin is shown with red dashed-lines. Depth of the basal detachment corresponding to the top of the reflective crust based on Fernández and Banda (1990), Sàbat <i>et al.</i> (1997) and Roca <i>et al.</i> (2004) (modified from Gaspar-Escribano <i>et al.</i> , 2004).	Page 143
Fig. 5.11	Time chart showing the periods of tectonic activity of each individual major fault in the southern and northern sectors of the Central Catalan Coastal Ranges during the Pyrenean Orogeny (see the location of the sectors in Figure 5.1). Ages for the southern sector are based on the results of this research. Ages for the northern sector are based on previous publications (e.g., López-Blanco <i>et al.</i> , 2000a; López-Blanco, 2002; Parcerisa <i>et al.</i> , 2007; Gaspar-Escribano <i>et al.</i> , 2004).	Page 144

5.4. Neogene extension and negative inversion in the central Catalan Coastal Ranges

Fig. 5.12	Schematic geological map of the Gaià-Montmell High pointing out the major Neogene extensional faults. Up to three relay ramps linking extensional faults are present in the area.	Page 145
Fig. 3.13	Structural cross-section across the Gaià-Montmell High illustrating the age of the different faults that are present in the area as well as their reactivation during the Cenozoic.	Page 146
Fig. 5.14	Tectonostratigraphic map showing the end of the extensional motion of the Vallès-Penedès, El Camp and Baix Penedès faults and related extensional short-cuts in central Catalan Coastal Ranges at late Tortonian (approximately 7My). The locations of the Gaià-Montmell Section (Figure 5.13) and the Llobregat Section (Figure 5.15) are indicated.	Page 148
Fig. 5.15	Llobregat section across the northern sector of the MVFS (Vallès area) (modified from Bartrina <i>et al.</i> , 1992). See location in Figure 5.14.	Page 148

Schematic map of the Montmell-Vallès Fault System showing fault damage zone characteristics of three sectors (A, B and C) developed during the latest Oligocene-Neogene extensional phase. Fluid and petrological descriptions compiled after Travé and Calvet (2001), Baqués *et al.* (2008), Baqués *et al.* (2010), Baqués *et al.* (2012), Baqués *et al.* (2014) and Cantarero *et al.* (2014a and 2014c). Magnetotelluric data (MT) from Marín *et al.* (2021) included in Chapter 2.

RESUM

Les Serralades Costaneres Catalanes (CCR en les seves sigles en anglès), localitzades al NE de la Península Ibèrica, corresponen a una de les unitats estructurals alpines que limiten la Conca de l'Ebre i en constitueixen el seu límit SE. Aquesta unitat és també la porció emergida del marge continental que delimita la Fossa de València al NO. Actualment, aquesta es caracteritza per una configuració de tipus *basin-and-range* amb orientació NE-SO que consisteix en una sèrie de blocs amb direcció ENE a NE, limitats per falles regionals que mostren un patró escalonat a la dreta. L'evolució geològica alpina de les CCR és complexa i inclou fins a tres fases tectòniques principals que donen lloc a la seva configuració actual: (1) una fase extensiva multiepisòdica des del Permià superior fins a l'Aptià, (2) una fase compressiva durant el Paleogen, i (3) una fase extensiva de l'Oligocè superior al Miocè mitjà.

En aquest context de fases tectòniques superposades, la herència estructural s'ha postulat com un factor clau en el control de l'evolució tectònica de l'àrea. Aquesta herència s'ha basat en dos aspectes fonamentals: 1) la idea general del control exercit per la configuració de les conques mesozoïques sobre l'evolució tectònica cenozoica de l'àrea (és a dir, els límits de la conca mesozoica es troben alineats amb les tendències estructurals paleògenes i neògenes posteriors), i 2) la proposta d'inversió negativa de les estructures contractives del Paleogen durant el Neogen, fets que explicarien la configuració actual de les CCR. Tanmateix, les particularitats i l'abast d'aquesta herència estructural, inclosos els mecanismes que impulsen la deformació cortical tant durant la contracció com la formació de conques, segueixen sent objecte de discussió. Es creu que aquests mecanismes són claus per comprendre una àrea amb possibles múltiples reactivacions de falles. Mentre que la majoria dels estudis recents ofereixen interpretacions fragmentades, aquesta tesi doctoral cobreix la totalitat del domini central de les CCR (des de la Conca d'El Camp al sud a l'extrem nord-est de la Conca del Vallès-Penedès) y proporciona una reconstrucció integral de la seva evolució tectònica des del Mesozoic fins a l'actualitat mitjançant un enfoc multidisciplinari. Aquest estudi presta especial atenció a l'Alt Gaià-Montmell (GMH) per tres raons principals. Primer, la successió mesozoica en aquest alt es troba ben preservada, particularment les unitats juràssiques i cretàiques. Segon, l'àrea correspondria també amb l'àrea font de les successions sinorogèniques preservades a la part central del marge sud-est de la Conca de l'Ebre, la interpretació prèvia de la qual suggeria la presència d'una discordança progressiva que enregistra l'evolució tectònica paleògena de les CCR. I tercer, el GMH correspon a la zona de relleu entre dues estructures neògenes majors, el Sistema de Falles Montmell-Vallès (MVFS en les seves sigles en anglès) i la Falla d'El Camp. Aquesta tesi doctoral es basa en anàlisis geològics i geofísics jut a la revisió i integració de tots els estudis sobre interaccions fluids-roca disponibles per aquesta regió, contribuint així a un model geodinàmic refinat de la zona.

Les investigacions realitzades inclouen l'anàlisi de dades de camp procedents de cartografia geològica, la recopilació de dades estructurals i estratigràfiques, la recollida de mostres per a anàlisis

magnetoestratigràfiques i de procedència, l'adquisició de dades magnetotellúriques (MT) i la caracterització de zones de falles al llarg dels diferents sectors del MVFS. Les dades estructurals i estratigràfiques (p.e., inclinació i orientació d'estrats i falles) es van utilitzar per a la construcció de tres seccions estructurals en localitzacions clau: les seccions de Gaià-Montmell, Marmellar i Cabra. Les dades de MT adquirides al llarg de la secció Gaià-Montmell, junt amb les dades de pous d'exploració petrolífera disponibles, han permès delimitar i caracteritzar els estils estructurals presents en l'escorça superior. Aquesta secció geològica va ésser balancejada per mitjà de tècniques de restitució estructural, els resultats de la qual mostren l'evolució tectònica de l'àrea en dos moments clau: el final de l'extensió del mesozoica i el final de la compressió paleògena. A més a més, l'estudi magnetoestratigràfic i de procedència realitzats al marge sud-est de la Conca de l'Ebre permeten un refinament precís de les edats de les formacions paleògenes estudiades, restringint el moment de la sedimentació sinorogènica, així com la caracterització de les àrees font. En conseqüència, aquests resultats han permès realitzar una precisa reconstrucció de la deformació compressiva paleògena.

L'evolució tectonoestratigràfica durant el Cenozoic de l'àrea central de les CCR va estar altament controlada per la seva herència estructural mesozoica. Durant el Mesozoic, el MVFS va constituir el límit nord-oest de la Conca del Montmell-Garraf d'edat Juràssic tardà-Cretaci inferior. El límit nord-est d'aquesta conca estaria situat diversos quilòmetres al nord de l'actual riu Llobregat, tal com suggereixen els sediments detrítics paleògens sintectònics en aquesta part del marge de la Conca de l'Ebre. A més, aquesta conca mesozoica hauria format part d'un sistema més ampli que incloïa una altra falla de basament (Falla de Barcelona), també amb rumb ENE i cabussament SE. Les conques del Montmell-Garraf i de Barcelona conformarien el domini proximal o l'inici del domini d'aprimament del marge continental que separava el Bloc de l'Ebre del Tetis occidental.

Dos episodis successius d'inversió tectònica van caracteritzar l'evolució cenozoica del sector central de les CCR. El primer, relacionat amb la convergència entre Iberia i Euràsia durant el Paleogen, va reactivar el MVFS. Com a resultat, es van desenvolupar importants *short-cuts* de bloc inferior dirigits cap al NO, entre els quals s'inclou el encavalcament de Gaià-El Camp. L'edat precisa de la inversió tectònica i l'emplaçament dels encavalcaments durant aquest període s'ha proporcionat mitjançant anàlisis tectonoestratigràfiques que inclouen anàlisis de procedència i magnetostatigrafia en sediments sinorogènics dipositats al marge SE de la Conca de l'Ebre. Els resultats revelen que la inversió del MVFS va començar al Bartonian i va continuar fins al Priabonian tardà, mentre que l'emplaçament de l'encavalcament de Gaià-El Camp va tenir lloc al Priabonian. Aquest segon període compressiu es va caracteritzar per un ràpid augment de les taxes de sedimentació, seguit d'una disminució durant el Priabonian tardà, interpretada com el preludi del final de la fase compressiva paleògena a l'àrea d'estudi.

El segon episodi d'inversió tectònica es va produir quan les estructures compressives paleògenes van ser reactivades en extensió durant el Neogen. Al GMH, aquesta fase es va caracteritzar per una

reactivació aparentment restringida de la Falla de Montmell i la transmissió de l'extensió amb la formació d'una nova falla de major cabussament al bloc superior de la falla: la Falla del Baix Penedès. La reactivació extensiva de l'encavalcament de Gaià-El Camp es manifesta també amb el desenvolupament d'un conjunt de falles extensives al flanc posterior de l'Anticlinal de Carme-Cabra, que corresponen i coincideixen amb l'extrem NE de la Falla d'El Camp. Aquest episodi d'inversió tectònica negativa va donar lloc al desenvolupament de diferents zones d'acomodació entre les falles principals, que es caracteritzen per la presència de rampes de relleu amb estructures tipus *breaching-faults*.

La reactivació del MVFS mostrarà diferències al llarg del seu rumb durant ambdues fases d'inversió tectònica. Aquestes diferències semblen estar relacionades amb el desacoblament de la deformació entre les parts més superficials i profundes del pla de falla a causa de la seva geometria interpretada com a tipus *kinked-planar* (formada per diversos panells planars amb diferents inclinacions) i el corresponent canvi d'inclinació de $>60^\circ$ en superfície a 30° en profunditat. Els panells més profunds i de menor inclinació es van reactivar de manera contractiva durant el Paleogen i com extensiva durant el Neogen, mentre que les parts més someres amb major inclinació només van mostrar reactivacions localitzades. La capacitat de les falles mesozoiques per reactivar-se i la distribució espacial de la deformació semblen, no obstant això, estar també influenciades per les diferències presents a les diferents zones de falla heretades. Les observacions de les interaccions fluid-roca indiquen que, a més de la geometria de la falla, les diferències litològiques de la roca hoste (granits i metasediments siliciclàstics al sector nord del MVFS davant de roques carbonatades als sectors central i sud) van controlar el tipus de precipitació mineral i ciments associats a la circulació de fluids. Aquests canvis van donar lloc a variacions en les propietats mecàniques de les roques de falla resultants (bretxes cimentades davant farina de falla) al llarg de la falla, fet que va controlar significativament la seva reactivació. La inversió tectònica va ser efectiva en àrees amb predominança de farina de falla no cohesiva a la zona de falla preexistent (formada a àrees amb granits paleozoics i metasediments siliciclàstics caracteritzant la roca hoste), mentre que la reactivació de la falla va ser limitada o fins i tot nul·la en àrees on la zona deformada preexistent estava formada per bretxes altament cimentades i cohesionades (àrees amb potents successions de carbonats mesozoics).

Els resultats d'aquest treball i l'enfocament multidisciplinari adoptat ofereixen un marc tectonoestratigràfic refinat per al sector central de les CCR des del Mesozoic fins a l'actualitat. Així mateix, els resultats assolits proporcionen una interpretació detallada de la influència de l'herència estructural mesozoica. D'aquesta herència, destacaria la importància de les geometries de falla i l'efecte de les heterogeneïtats litològiques sobre les propietats mecàniques resultants de les zones de falla heretades en els diversos sectors com a factors clau en la reactivació de falles i la transmissió d'esforços tectònics a l'àrea estudiada.

PARAULES CLAU

Paraules clau de la tesis i codis UNESCO

- Ciències de la terra i l'espai (250000)
- Geologia (250600)
- Geologia estructural (250620)
- Tectònica (250707)
- Geologia regional (250601)
- Paleomagnetisme (250704)
- Paleogeografia (550508)

ABSTRACT

The Catalan Coastal Ranges (CCR), located at the NE of the Iberian Peninsula is one of the alpine structural units that limit the Ebro Basin and it constitutes its southeastern boundary. Moreover, this unit is also the onshore portion of the continental margin that bounds the Valencia Trough to the NW. It is nowadays characterized by a NE-SW trending basin-and-range configuration that consists in series of ENE- to NE-striking blocks bounded by major faults displaying a right-stepping en-echelon pattern. The Alpine geological evolution of the CCR is complex and includes up to three main tectonic phases that shaped its distinguishing present-day configuration: (1) a multiepisodic extensional phase from the late Permian to the Aptian, (2) a compressional phase during the Paleogene, and (3) a latest Oligocene-middle Miocene extension.

Within this scenario of superimposed tectonic phases, structural inheritance has been previously postulated as a key factor of control on the tectonic evolution of the area. This inheritance has often been related to two main aspects: the general idea of the control exerted by the Mesozoic basin configuration on the Cenozoic tectonic evolution of the area (i.e., the limits of the Mesozoic basin appear aligned to subsequent Paleogene and Neogene structural trends), alongside the proposed negative inversion of Paleogene contractional structures during the Neogene, facts that would explain the present-day configuration of the CCR. However, the particularities and extent of this structural inheritance including the mechanisms driving crustal deformation during contraction and basin formation were still under discussion. These mechanisms are believed to be key in the understanding of an area with potential multiple fault reactivations. While most of the recent studies offer fragmented interpretations, the present Ph.D. thesis covers the central domain of the CCR, between the El Camp Basin in the south to the northeast end of the Vallès-Penedès Basin, aiming to provide a comprehensive reconstruction of its tectonic evolution from the Mesozoic to the present-day using a multidisciplinary approach. Special attention was paid to the Gaià-Montmell High for three main reasons. First, this area is characterized by its preserved Mesozoic succession, particularly the presence Jurassic and Cretaceous strata; second, the area would also correspond to the source of sediments of the well-preserved synorogenic successions deposited in the central part of the southeast margin of the Ebro Basin, the previous interpretation of which suggested the presence of a progressive unconformity that recorded the Paleogene tectonic evolution of the CCR; and third, the Gaià-Montmell High corresponds to the relay between two major Neogene structures, the Montmell-Vallès Fault System (MVFS) and the El Camp Fault. These three factors make this area of the CCR an appropriate candidate for the proposed objectives. The research involved geological and geophysical analysis together with the review and integration of the available fluid-rock interactions studies in the region, thereby contributing to a refined geodynamic model of the region.

The performed investigations comprised the analysis of field data from geological mapping, the collection of structural and stratigraphic data, gathering samples for magnetostratigraphic and provenance analysis, the acquisition of magnetotelluric (MT) data as well as the characterization of fault zones in the different sectors along MVFS. Structural and stratigraphic data (e.g., dip and orientation of bedding and faults) were used for the construction of three structural cross-sections at key locations: the Gaià-Montmell, the Marmellar, and the Cabra sections. MT data acquired along the Gaià-Montmell Section, alongside data from available exploratory wells, allowed the constraint and characterization of the structural styles present in the upper crust. This geological section was balanced via structural restoration techniques, the results of which illustrate the tectonic evolution of the area at two key time-steps: the end of the Late Jurassic-Early Cretaceous extension and the end of the Paleogene compression. Moreover, the magnetostratigraphic and provenance analysis performed in the southeast margin of the Ebro Basin allowed an accurate refinement of the ages of the studied Paleogene formations, hence allowing to constrain the timing of the synorogenic sedimentation and the identification of the source areas. Accordingly, these results made possible a precise reconstruction of the Paleogene compressional deformation.

The Cenozoic tectonostratigraphic evolution of the central CCR was highly controlled by its Mesozoic structural inheritance. During the Mesozoic, the MVFS constituted the northwest limit of the Late Jurassic-Early Cretaceous Montmell-Garraf Basin. The northeastern limit of this basin would be located several kilometres north of the present-day Llobregat River valley as suggested by syn-tectonic Paleogene detrital sediments in the Ebro Basin margin next to this area. Moreover, this basin belonged to a larger basin system that included another ENE-trending, SE-dipping basement fault displaying a right-stepped en-echelon arrangement: the Barcelona Fault. Together, the Montmell-Garraf and the Barcelona basins conformed the proximal to, perhaps, the initial necking domain of the continental margin that separated the Ebro Block from the Alpine-Ligurian Tethys.

Two successive episodes of tectonic inversion characterized the Cenozoic evolution of central CCR. The first one, related to the convergence between Iberia and Eurasia during the Paleogene, reactivated the MVFS as compressional. As a result, major NW-directed basement footwall shortcuts including the Gaià-El Camp Thrust developed. The precise timing of inversion and thrust emplacement during this period has been provided by the tectono-stratigraphic analysis involving provenance analysis and magnetostratigraphic dating performed in synorogenic sediments deposited in the SE margin of the Ebro Basin. These analyses reveal that the inversion of the Montmell-Vallès Faults System started in the Bartonian and continued up to the late Priabonian, and that the emplacement of the Gaià-El Camp Thrust took place from early to late Priabonian. A rapid increase of the sedimentation rates characterized this second contractional pulse, followed by a decrease during late Priabonian, which can be interpreted as the prelude of the end of the Paleogene compressional phase in the area.

The second episode of tectonic inversion occurred when the previously formed compressional structure during the Paleogene became reactivated as extensional during the Neogene. In the Gaià-Montmell High, this phase was characterized by a limited reactivation of the Montmell Fault and the transmission of the extension to the formation of a hangingwall short-cut: the Baix Penedès Fault. The reactivation of the Gaià-El Camp Thrust was also attested by the development of an array of extensional faults in the backlimb of the Carme-Cabra Anticline that corresponds to the NE-end of El Camp Fault. This episode of negative inversion resulted in the development of accommodation zones between the major faults characterized by the presence of relay ramps with breaching faults.

The reactivation of the MVFS showed differences along strike during both phases of tectonic inversion. These differences appeared to be related to the decoupling of the deformation from surface to depth due to its interpreted kinked-planar geometry and the change of fault dip from $>60^\circ$ at surface to 30° at depth. The deeper and less dipping panels of the fault system were reactivated (as contractional during the Paleogene and as extensional during the Neogene), whereas the highly dipping shallower parts of the fault system only show localized reactivations. The ability of the Mesozoic faults to be reactivated and the spatial distribution of the deformation appear also influenced by differences the inherited fault rocks. The observations from fluid-rock interactions denote that, alongside the fault geometries, different rock-host lithologies (granites and siliciclastic metasediments in the north of the MVFS versus carbonate rocks in the central and southern sectors) controlled the type of mineral precipitation and cementation product of fluid circulation. These resulted in changes in the mechanical properties of the resulting fault rocks (gouge versus cemented breccias) along the fault trend, significantly controlling its reactivation. Tectonic inversion was effective in areas with non-cohesive fault gouge in the pre-existent fault core (areas with Paleozoic granites and siliciclastic metasediments characterized as host-rock), whereas fault reactivation appeared limited or even precluded in areas where the pre-existent damage zone was formed by highly cemented and cohesive breccias (areas with thick Mesozoic carbonate successions).

The results of the present research and the multidisciplinary approach adopted herein offer a refined tectono-stratigraphic framework for the central Catalan Coastal Ranges from the Mesozoic to the present-day and provide a detailed interpretation of the influence of the Mesozoic structural inheritance. It emphasizes the importance of fault geometries and the effect of the lithological heterogeneities on the resulting mechanical properties of the inherited fault zones as key factors on fault reactivation and the transmission of the tectonic stresses in the studied area.

RESUMEN

Las Cordilleras Costeras Catalanas (CCR en sus siglas en inglés), ubicadas en el NE de la Península Ibérica, corresponden a una de las tres unidades estructurales alpinas que delimitan la Cuenca del Ebro y constituyen su límite sureste. Esta unidad es también la porción emergida del margen continental que limita la Surco de Valencia al NO. Actualmente, dicha unidad estructural se caracteriza por una configuración de tipo *basin-and-range* con una orientación NE-SO, compuesta por una serie de bloques con dirección ENE a NE delimitados por fallas regionales que presentan un patrón escalonado hacia la derecha. La evolución geológica alpina de las CCR es compleja e incluye hasta tres fases tectónicas principales que han dado lugar a su configuración actual: (1) una fase extensiva multiepisódica desde el Pérmico tardío hasta el Aptiense, (2) una fase compresiva durante el Paleógeno, y (3) una fase extensiva desde el Oligoceno tardío hasta el Mioceno medio.

En este escenario de fases tectónicas superpuestas, la herencia estructural se ha postulado como un factor clave en el control de la evolución tectónica del área. Esta herencia se ha basado en dos aspectos principales: 1) la idea general del control ejercido por la configuración de las cuencas mesozoicas sobre la evolución tectónica cenozoica del área (es decir, los límites de la cuenca mesozoica aparecen alineados con las tendencias estructurales paleógenas y neógenas posteriores), y 2) la propuesta de inversión negativa de las estructuras contractivas paleógenas durante el Neógeno, hechos que explicarían la configuración actual de las CCR. Sin embargo, las particularidades y el alcance de esta herencia estructural, incluidos los mecanismos que impulsan la deformación de la corteza terrestre tanto durante la deformación contractiva y la formación de cuencas, siguen siendo objeto de discusión. Se cree que estos mecanismos son clave para comprender un área con posibles múltiples reactivaciones de fallas. Mientras que la mayoría de los estudios recientes ofrecen interpretaciones fragmentadas, esta tesis doctoral cubre el dominio central de las CCR en su totalidad (desde la Cuenca de El Camp al sur hasta el extremo NE de la Cuenca del Vallès-Penedès) y proporciona una reconstrucción integral de su evolución tectónica desde el Mesozoico hasta la actualidad mediante un enfoque multidisciplinar. Este estudio presta especial atención al Alto del Gaià-Montmell (GMH) por tres razones principales. Primero, la sucesión mesozoica en este alto se encuentra bien preservada, particularmente las unidades jurásicas y cretácicas. Segundo, el área se correspondería también con el área fuente de las sucesiones sinorogénicas preservadas en la parte central del margen sureste de la Cuenca del Ebro, cuya interpretación previa en el área de estudio sugería la presencia de una discordancia progresiva que registra parte de la evolución tectónica paleógena de las CCR. Y tercero, el GMH se corresponde con la zona de relevo entre dos estructuras neógenas mayores, el Sistema de Fallas Montmell-Vallès (MVFS en sus siglas en inglés) y la Falla de El Camp. La tesis doctoral se basa en análisis geológicos y geofísicos junto con la revisión e integración de todos los estudios sobre interacciones fluido-roca disponibles para esta región, contribuyendo así a un modelo geodinámico refinado de la zona.

Las investigaciones realizadas incluyen el análisis de datos de campo procedentes de cartografía geológica, la recopilación de datos estructurales y estratigráficos, la recogida de muestras para análisis magnetoestratigráficos y de procedencia, la adquisición de datos magnetotelúricos (MT), así como la caracterización de zonas de fallas en diferentes sectores a lo largo del MVFS. Los datos estructurales y estratigráficos se utilizaron para la construcción de tres secciones estructurales en ubicaciones clave: las secciones de Gaià-Montmell, la de Marmellar y la de Cabra. Los datos de MT adquiridos a lo largo de la sección Gaià-Montmell, junto con datos de pozos de exploración petrolera disponibles, permitieron delimitar y caracterizar los estilos estructurales presentes en la corteza superior. Esta sección geológica fue balanceada mediante técnicas de restitución estructural, cuyos resultados ilustran la evolución tectónica del área en dos momentos clave: el final de la extensión del Jurásico tardío-Cretácico temprano y el final de la compresión paleógena. Además, el estudio magnetoestratigráfico y de procedencia realizados en el margen sureste de la Cuenca del Ebro permiten un refinamiento más preciso de las edades de las formaciones paleógenas estudiadas, restringiendo el momento de la sedimentación sinorogénica, así como la caracterización de las áreas fuente. En consecuencia, estos resultados han permitido realizar una reconstrucción precisa de la deformación compresiva paleógena.

La evolución durante el Cenozoico del área central de las CCR estuvo altamente controlada por su herencia estructural mesozoica. Durante el Mesozoico, el MVFS constituyó el límite NW de la Cuenca del Montmell-Garraf de edad Jurásico tardío-Cretácico temprano. El límite NE de esta cuenca estaría ubicado varios kilómetros al norte del actual valle del río Llobregat, tal y como sugieren los sedimentos detríticos paleógenos sintectónicos en esta parte del margen de la Cuenca del Ebro. Además, esta cuenca mesozoica formaba parte de un sistema más amplio que incluía otra falla de basamento (Falla de Barcelona) con rumbo ENE y buzamiento SE. Las cuencas del Montmell-Garraf y de Barcelona conformarían el dominio proximal o el inicio del dominio de adelgazamiento del margen continental que separaba el Bloque del Ebro del Tethys occidental.

Dos episodios sucesivos de inversión tectónica caracterizaron la evolución cenozoica del sector central de las CCR. El primero, relacionado con la convergencia entre Iberia y Eurasia durante el Paleógeno reactivó el MVFS. Como resultado, se desarrollaron importantes *short-cuts* de bloque inferior dirigidas hacia el NO, entre las que se incluye el cabalgamiento de Gaià-El Camp. La edad precisa de la inversión tectónica y el emplazamiento de cabalgamientos durante este periodo ha sido proporcionada mediante los análisis tectonoestratigráficos que incluyen análisis de procedencia y magnetoestratigrafía en sedimentos sinorogénicos depositados en el margen SE de la Cuenca del Ebro. Los resultados revelan que la inversión del MVFS comenzó en el Bartonense y continuó hasta el Priabonense tardío, mientras que el emplazamiento del cabalgamiento del Gaià-El Camp tuvo lugar en el Priabonense. Este segundo periodo estuvo marcado por un rápido aumento de las tasas de sedimentación, seguido por una disminución durante el Priabonense tardío, interpretada como el preludio del final de la fase compresiva paleógena en el área de estudio.

El segundo episodio de inversión tectónica se produjo cuando las estructuras compresivas paleógenas fueron reactivadas extensivamente durante el Neógeno. En el GMH, esta fase estuvo caracterizada por una reactivación aparentemente restringida de la Falla de Montmell y la transmisión de la extensión con la formación de una nueva falla de mayor buzamiento en el bloque superior de la falla: la Falla del Baix Penedès. La reactivación extensiva del cabalgamiento Gaià-El Camp se evidencia con el desarrollo de un conjunto de fallas extensivas en el flanco posterior del Anticlinal de Carme-Cabra, que corresponden y coinciden con el extremo NE de la Falla de El Camp. Este episodio de inversión tectónica negativa resultó en el desarrollo de diferentes zonas de acomodación entre las fallas principales, que se caracterizan por la presencia de rampas de relevo con estructuras tipo *breaching-faults*.

La reactivación del MVFS mostró diferencias a lo largo de su rumbo durante ambas fases de inversión tectónica. Estas diferencias parecen estar relacionadas con el desacople de la deformación entre las partes más superficiales y profundas del plano de falla debido a su geometría interpretada como de tipo *kinked-planar* (formada por varios paneles planares con diferentes buzamientos) y su correspondiente cambio de buzamiento de $>60^\circ$ en superficie a 30° en profundidad. Los paneles más profundos y de menor buzamiento se reactivaron contractivamente durante el Paleógeno y extensivamente durante el Neógeno, mientras que las partes más someras con mayor inclinación solo mostraron reactivaciones localizadas. La capacidad de las fallas mesozoicas para reactivarse y la distribución espacial de la deformación parecen no obstante estar también influenciadas por las diferencias presentes en las zonas de falla heredadas. Las observaciones de las interacciones fluido-roca denotan que, además de la geometría de falla, las diferencias litológicas de la roca huésped (granitos y metasedimentos siliciclásticos en el norte del MVFS contra rocas carbonatadas en los sectores central y sur) controlaron el tipo de precipitación mineral y cementos asociados a la circulación de fluidos. Estos cambios resultaron en variaciones en las propiedades mecánicas de las rocas de falla resultantes (brechas cementadas contra polvo de falla) a lo largo de la dirección de la falla, lo que controló significativamente su reactivación. La inversión tectónica fue efectiva en áreas con harina de falla no cohesiva en la falla preexistente (formada en las áreas con granitos paleozoicos y metasedimentos siliciclásticos caracterizando la roca huésped), mientras que la reactivación de la falla fue limitada o incluso nula en áreas donde la zona deformada preexistente estaba formada por brechas altamente cementadas y cohesivas (generadas en áreas con potentes sucesiones de carbonatos mesozoicos).

Los resultados de este trabajo y el enfoque multidisciplinar adoptado ofrecen un marco tectonoestratigráfico refinado para el sector central de las CCR desde el Mesozoico hasta la actualidad. Asimismo, los resultados alcanzados proporcionan una interpretación detallada de la influencia de la herencia estructural mesozoica. De esa herencia destacaría la importancia de las geometrías de falla y el efecto de las heterogeneidades litológicas sobre las propiedades mecánicas resultantes de las zonas de falla heredadas en los diversos sectores como factores clave en la reactivación de fallas y la transmisión de esfuerzos tectónicos en el área estudiada.

CHAPTER 1

GENERAL INTRODUCTION

1.1. Motivation and objectives

1.2. Structure and coherency of the memoir

1.3. Overview of inversion tectonics

1.4. Geological introduction to NE Iberia and the Catalan Coastal Ranges

1.5. Problem approach and methodologies

1.1. Motivation and objectives of the research

In basin analysis, tectonostratigraphy is a discipline that analyses the effects of tectonics on lithostratigraphy (Berthelsen, 1978) and integrates both tectonic and stratigraphic data analysis in order to understand the geological evolution of an area. This type of analysis allows interpreting the relationship between tectonic activity (e.g., faulting and folding) and changes in the depositional patterns of sedimentary layers. Therefore, tectonostratigraphic analysis helps in identifying how sedimentary basins form, evolve, and are structured due to tectonic forces through time. These studies can also comprise the reconstruction of paleoenvironments by interpreting how deformation influenced sedimentation types and patterns (e.g., depositional systems, environments as well as thickness and lateral distribution of their deposits), which in turn are closely controlled by specific tectonic settings (e.g., rift, passive margin, foreland, etc.).

The reconstruction of the evolution of a basin and its dynamics is often critical for natural resource exploration such as oil, gas, or minerals as well as the assessment of geohazards (Allen and Allen, 1990; Hantschel and Kauerauf, 2009). Most of oil and gas traps are associated with tectonic structures such as folds and faults, being their distribution subject to the type of tectonic setting. Tectonostratigraphic analysis helps identify these reservoirs by understanding where and how sediments accumulated and were furtherly deformed in specific areas or regions. Additionally, stratigraphic traps, unconformities and source-to-sink relationships (showing how sediments are transported and deposited) are controlled by tectonics, which may have an impact on exploration success.

Dating the ongoing processes plays a critical role in tectonostratigraphy because it allows to accurately relate specific tectonic events to the deposition of sedimentary layers over geological time. Understanding when tectonic events, such as faulting or folding, occurred helps in deciphering the sequences of deposition, erosion and deformation. This temporal framework is key for reconstructing basin evolution because allows identifying periods of tectonic activity or quiescence. Specifically, in resource exploration, timing control is fundamental, for instance, for predicting critical moments between the maturation, migration and trapping of hydrocarbons (Magoon, 1987; 2009; Makeen *et al.*, 2016). Thus, accurate dating ensures linking tectonic events to the stratigraphic record, offering insights for making informed decisions. In this scenario, the geometrical and genetic analysis of syn-tectonic strata and growth geometries (Riba, 1976; Suppe *et al.*, 1992) has been broadly used to understand the kinematics of individual structures (e.g., Vergés and Muñoz, 1990; Suppe *et al.*, 1992; Burbank *et al.*, 1992; Hardy *et al.*, 1996; Ford *et al.*, 1997; Vergés *et al.*, 2002; Salvini and Storti, 2002; Fernández *et al.*, 2004).

When paying attention on the tectonic evolution of NE Iberia we observe that the Ebro Basin is surrounded by three orogenic belts that developed heterochronously from the Late Cretaceous to the

Paleogene: the Pyrenees to the north, the Iberian Range to the southwest, and the Catalan Coastal Ranges (CCR) to the southeast (Figure 1.1).

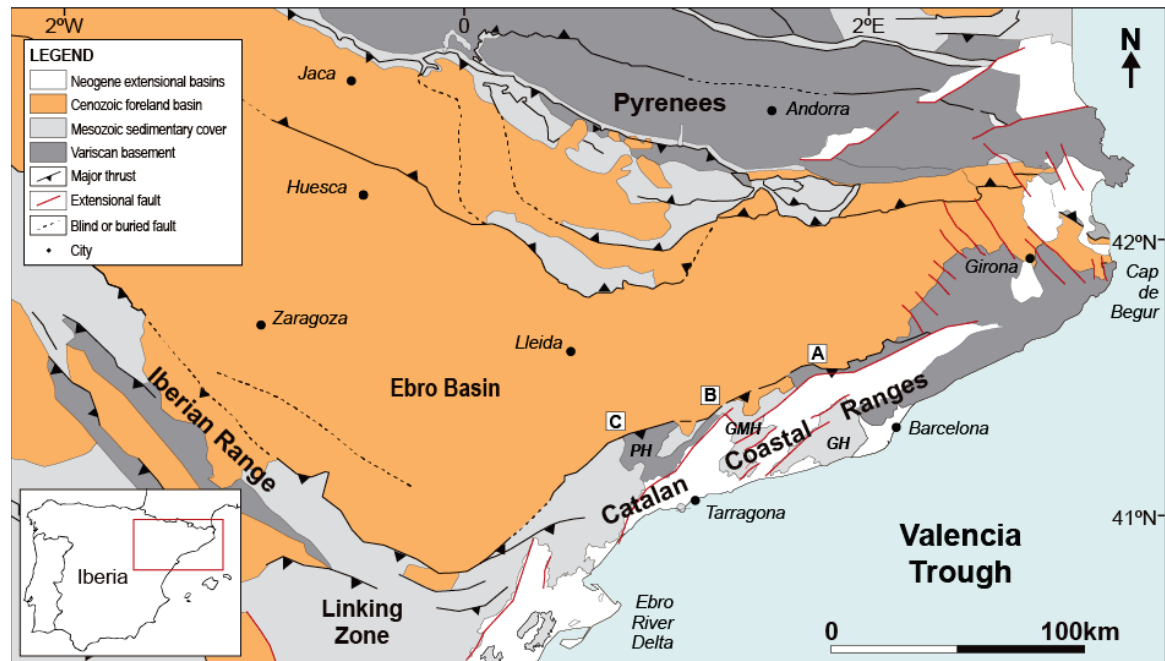


Figure 1.1. Geologic map of NE Iberia showing the major Cenozoic structural units including the three orogenic belts bounding the Ebro Basin: the Pyrenees, the Iberian Range, and the Catalan Coastal Ranges. Cenozoic foreland basin-fill is highlighted in orange. Coordinates in geographical system. Labels A, B and C respectively correspond to Montserrat-Sant Llorenç del Munt, Pontils-Cabra del Camp and Montsant areas. Labels PH, GMH and GH respectively correspond to the Prades Block, the Gaià-Montmell High and the Garraf High.

The Ebro Basin-fill records the evolution of these three structural units as it is illustrated by many studies of world-class examples of growth strata documented along the three margins (e.g., Riba, 1973,1976; Anadón, 1978; Anadón *et al.*, 1985, 1986; Vergés and Muñoz, 1990; Suppe *et al.*, 1992, 1997; Colombo, 1994; Ford *et al.*, 1997; López-Blanco, 2002; Gómez-Paccard *et al.*, 2011). Given this scenario, sedimentation in the southeastern margin of the Ebro Basin records the Paleogene tectonic evolution of the Catalan Coastal Ranges. Growth strata geometries have been here documented at different locations in the central part of the margin (e.g., Montserrat-Sant Llorenç del Munt, Pontils-Cabra del Camp, Montsant; Figure 1.1). Tectonostratigraphic analysis in these areas reveal the interactions between the Paleogene compression and the related response of the sedimentary systems (Anadón, 1978; Anadón *et al.*, 1985, 1986; Colombo, 1994; López-Blanco *et al.*, 2000a, b; López-Blanco, 2002; Gómez-Paccard *et al.*, 2011). Precisely, the work performed by Anadón *et al.* (1986) in the Pontils-Cabra del Camp area suggested the presence of a composite progressive unconformity in this part of the Ebro Basin margin (Figure 1.2), the genetic and structural characteristics of which are re-visited in this work.

Clast composition and paleocurrent indicators found in Paleogene alluvial fan and fan-delta conglomerates deposited along the SE margin of the Ebro Basin suggest that their source areas corresponded to the adjacent emerged regions of the Catalan Coastal Ranges during the Paleogene. (Anadón *et al.*, 1986; Colombo, 1994; López-Blanco, 2002). The tectonic evolution of the Catalan Coastal Ranges plays then a key role on the observed patterns in the sedimentary successions deposited along the southeast Ebro Basin margin and their potential progressive incorporation in the orogenic wedge. Hence, their genetic and structural analysis helps decipher the coeval tectonic evolution of its source area.

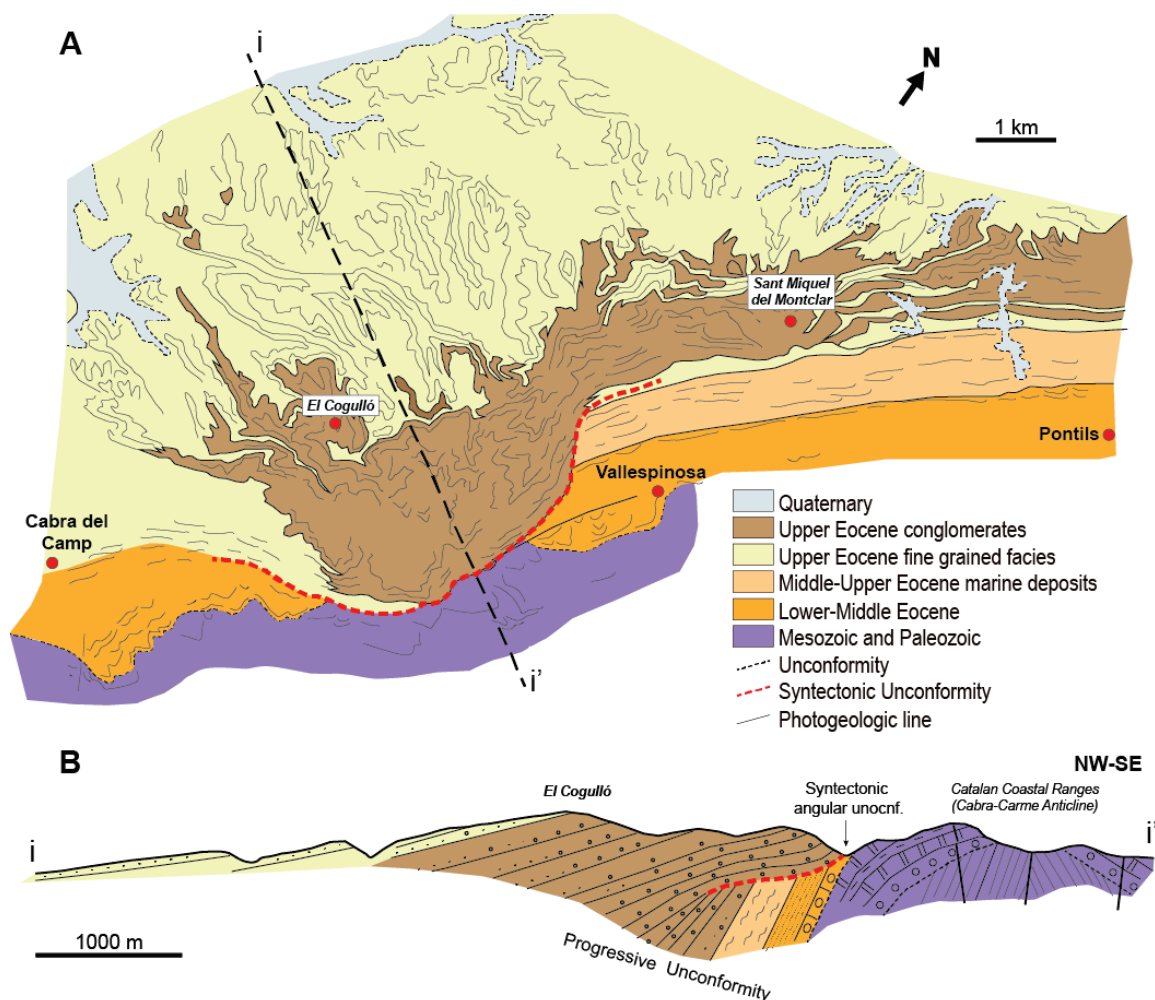


Figure 1.2. A) Geological map of the Pontils-Cabra del Camp area showing the distribution of the Sant Miquel del Montclar conglomerates. **B)** Geological cross-section showing a composite progressive unconformity involving Paleogene (mainly Eocene) strata in the forelimb of the Cabra-Carme Anticline (redrawn from Anadón *et al.*, 1986).

The geology of the Catalan Coastal Ranges is complex due to a multi-episodic tectonic history that involved multiple periods of extension and compression since, at least, late Paleozoic times (Fontboté, 1954). Fault reactivation and tectonic inversion has been appointed in several works to describe its

evolution, most of them appointing to the extensional reactivation of Paleogene contractional faults during Neogene times (e.g., Fontboté, 1954; Gaspar-Escribano *et al.*, 2004; López-Blanco *et al.*, 2000; Marcén *et al.*, 2018). The control played by pre-Cenozoic structures has commonly been poorly constrained although previously presumed by regional observations. These assumptions were mostly supported by significant changes in the Mesozoic stratigraphic thicknesses and sedimentary environments hence implying a sort of structural control (Esteban and Robles, 1976; Salas and Casas, 1993; Salas *et al.*, 2001). Esteban and Robles (1976) justified these stratigraphic observations with the potential presence of basement faults that would have controlled the differential subsidence, the limits of which coincided with the direction and trend of the main longitudinal and transversal fractures (i.e., regional faults) in the Catalan Coastal Ranges. The delineation of several sectors and domains with distinct subsidence outlined the limits of a preliminary Mesozoic basin system configuration and, to some extent, the structural control on these depocentres (Figure 1.3).

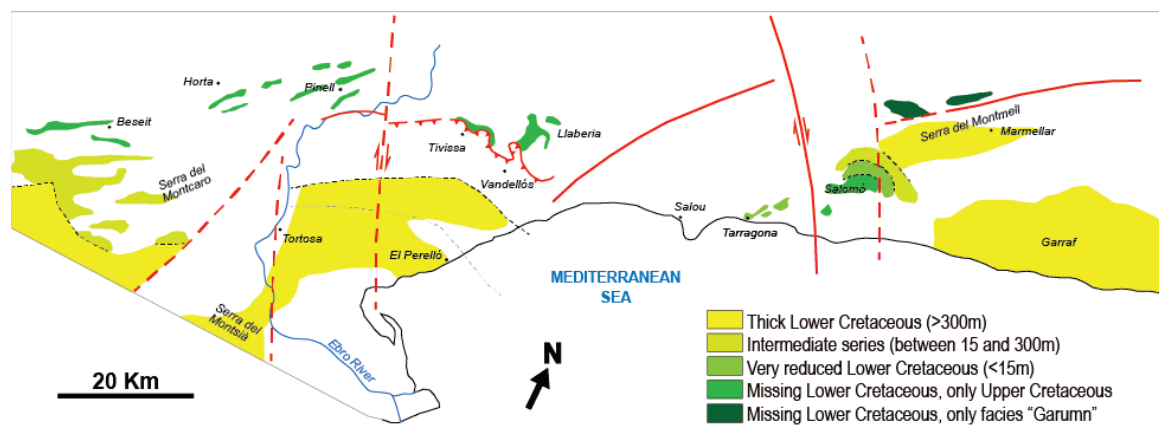


Figure 1.3. Map illustrating Cretaceous outcrops in the central and southern Catalan Coastal Ranges classified by their thicknesses. The map also shows the main inferred structural lineaments (redrawn from Esteban and Robles, 1976).

Other studies suggested the Cenozoic reactivation of Mesozoic extensional faults (Roca and Guimerà, 1992; Gómez and Guimerà, 1999) as well as the control the Mesozoic succession had on the growth of Paleogene contractional structures (Anadón *et al.*, 1985; Guimerà and Alvaro, 1990). Moreover, works based on geochemical investigations in crustal-scale fault damage zones (i.e., fluid circulation, mineral neoformation) disclosed multiple reactivations in response to the tectonic evolutionary stages affecting the Iberian Peninsula since the Mesozoic (e.g., Baqués *et al.*, 2013; Cantarero *et al.*, 2014). Nevertheless, before this research, the timing of the potential reactivation and the formation of the contractional structures responsible for the build-up of the Catalan Coastal Ranges during the Paleogene remained uncertain because of the following reasons: 1) the lack of preserved syn-kinematic strata at key locations; 2) the fact that the Neogene extensional phase dismantled the previously formed Paleogene contractional structure and its direct observation and interpretation is only possible in the

preserved structural highs, and 3) the lack of subsurface data coverage in the region, thus being the interpretation of the deep structure mostly inferred from surface geology.

Within this context, several questions can be addressed in order to fill the understanding gaps and drive the activities performed in this thesis. Each of the below questions are considered as the main objectives of the research, which have been resolved by the research papers included in this dissertation:

1. How is the structure of the preserved source areas of the synorogenic strata, which were deposited and preserved in the central southeast margin of the Ebro Basin during the Paleogene compressional phase? What was the tectonic evolution of this area since the Mesozoic to the present-day?
2. How are the fault zones of the major structures involved in the Paleogene deformation (i.e., Montmell-Vallès Fault System) characterized along-strike and which were the processes controlling the main differences observed during its reactivation/inversion?
3. What are the tectonostratigraphic relationships between the observed compressional structures in the source area and the geometries and sedimentary environments displayed in the basin margin? When did the reactivation start?

To address the above-mentioned three points a fit-for-purpose technical approach has been planned and implemented. This approach includes: 1) field work in both the source area (Gaià-Montmell High, Figure 1.1), the adjoining Neogene basins and the adjacent Ebro Basin margin; 2) the acquisition, processing, and interpretation of magnetotelluric data along a 2D profile in the Gaià-Montmell High; 3) the construction and structural restoration of a 2D crustal-scale geological section across the Gaià-Montmell High; 4) the review of all the fluid-rock interaction works published in the area of interest; 5) a provenance analysis involving the study of clasts from synorogenic strata and paleotransport directions; and 6) the acquisition and analysis of a new magnetostratigraphic section of well-exposed synorogenic strata in the central southeastern Ebro Basin margin. A detailed explanation of all these methodologies and techniques is provided in section 1.5.

The current research work aims to provide a comprehensive reconstruction of the tectonostratigraphic evolution of the central Catalan Coastal Ranges highlighting the role of the Mesozoic structural inheritance and inversion tectonics, to bridge the conceptual gaps left by early studies and contribute to a more refined understanding of the processes driving the formation of this orogenic belt.

1.2. Structure and coherency of the memoir

This memoir is structured into a preface section and four main chapters, each contributing to the key research objectives and reflecting the format of a dissertation based on a compilation of papers published in peer-reviewed international research journals and special volumes. This organization aims at providing a comprehensive narrative that bridges the general concepts and the individual studies while offering a broader context and discussion of their impact.

Chapter 1 starts with setting the stage for the dissertation by outlining the motivation behind the research (section 1.1). It discusses the broader significance of the study, explaining why the topics of tectonic inversion and synorogenic sedimentation are important and how these fit into the larger field of structural geology. This section reflects on the academic interests of this research and provides a rationale for why the particular steps of the study were undertaken. Further on, the structure and organization of the dissertation is presented offering a roadmap for readers to understand how the document is arranged (section 1.2). It briefly describes the content of each chapter, highlighting how they contribute to the overall research objectives. This overview helps readers navigate the dissertation and understand the logical flow of the research. The section concludes by explaining the coherence and relationships between the three papers included in the dissertation. It outlines how the papers are interrelated, emphasizing their individual contributions and how they collectively form a unified study that addresses the research gaps and objectives.

The chapter continues with the foundation for the dissertation by introducing the main research problem and situating it within the context of existing literature on tectonic inversion. It begins with a detailed literature review (section 1.3) covering key theoretical frameworks and concepts related to tectonic inversion processes. This section includes and summarizes the key studies that have contributed to the current understanding of the field. The review pretends to identify potential knowledge gaps and justifies the need for further research, which the subsequent papers aim to address. Following the literature review, an overview of the geological setting of the study area is presented to provide the essential context for the research (section 1.4). This section describes the regional tectonic evolution, and the main stratigraphic units present in the study area, which are essential for understanding the results of the papers. The setting is presented in terms of its relevance to tectonic inversion processes and how this context influences the evolution of the studied area. Lastly, section 1.5 outlines the problem approach and the methodology and instrumental techniques used across the three peer-review publications included in this dissertation. This section describes the data collection and analysis techniques, including fieldwork, geophysical and laboratory methods, as well as any modelling approaches employed. The methodology is explained in detail to provide a clear understanding of the tools and instrumental approaches that support the results of the published

papers. It also highlights how these methods are suited to answering the research questions stated in the motivation and objectives section.

Chapters 2, 3 and 4 include the results obtained from the three peer-reviewed research papers that form the core of this dissertation. Each publication addresses specific aspects of the research questions stated in the motivation section, with a focus on distinct but interrelated topics. A direct reproduction of the SCI publications alongside the information of the journal, their quality indexes and DOI are included in each chapter. The complete references of the three papers included in this dissertation are the following:

- **Publication 1:** Marín, M., Roca, E., Marcuello, A., Cabrera, L., Ferrer, O., 2021. Mesozoic structural inheritance in the Cenozoic evolution of the central Catalan Coastal Ranges (western Mediterranean): Structural and magnetotelluric analysis in the Gaià-Montmell High. *Tectonophysics*, 814, 228970.
<https://doi.org/10.1016/j.tecto.2021.228970>
- **Publication 2:** Marín, M., Carola, E., Beamud, B., Bover-Arnal, T., López-Blanco, M., Garcés, M., Roca, E., Costa, E., Ferrer, O., Cabrera, L., 2025. Paleogene kinematics of the central Catalan Coastal Ranges: temporal constraints from magneto-chronology and provenance analysis in synorogenic deposits in the SE margin of the Ebro Basin (NE Spain). *Geologica Acta* 23.2, 1-25.
<https://doi.org/10.1344/GeologicaActa2025.23.2>
- **Publication 3:** Marín, M., Roca, E., Baqués, V., Cantarero, I., Cabrera, L., Ferrer, O., Travé, A., 2023. Fluid-rock interaction control on fault reactivation: A review of the Montmell-Vallès Fault System, central Catalan Coastal Ranges (NE Iberia). *Global and Planetary Change*, 220, 104011.
<https://doi.org/10.1016/j.gloplacha.2022.104011>

While each paper is presented as a standalone study, these chapters emphasize how their results contribute to the overall objective of the investigation. Key points of convergence are noted as well as any divergences in methodology or findings, thus setting the stage for the later integration and discussion in the following chapter.

Chapter 5 corresponds to the critical linking section of the dissertation, synthesizing the findings from the three research papers and discussing their regional implications. This chapter plays a key role in unifying the distinct, yet interconnected, studies offering a comprehensive view of how each paper contributes to the research objectives. This section goes beyond the individual results presented in chapter 2 to engage in a deeper discussion of how the presented conclusions relate to the regional understanding. Therefore, chapter 3 bridges some gaps between the studies, creating an interrelated description that connects the methodologies, and outcomes. Moreover, chapter 3 incorporates bits of

the theoretical frameworks supporting each study, and how they collectively enhance the answers to the research questions. In addition to the thematic links, this chapter reflects on the limitations of the methodologies used in the studies. A comparative analysis is done to assess the strength of the research design, providing a view of how the different methods employed contribute to the outcomes. Finally, the chapter includes some theoretical implications of the results and connects the research to the literature. By presenting the research as an interconnected body of work, this chapter highlights the significance of the dissertation as a coherent whole.

The final **Chapter 6** provides a concise summary of the conclusions drawn from the dissertation. It revisits the key outcomes from the research papers and their synthesis, addressing the practical implications of the research. Additionally, it offers considerations for future research, identifying potential areas of further investigation that could build on top of the findings presented in this dissertation.

This dissertation ends with the list of references cited in the text, followed by the annexes and data repositories, which contain the detailed supplementary material that has been used in the research (e.g., field, magnetotelluric and magnetostratigraphic data), enabling validation of the findings presented in this dissertation.

1.3. Overview of inversion tectonics

This section aims to explain essential concepts and terminology relevant to the research presented in the papers included in chapter 2 of this dissertation, laying the groundwork for the general discussion in chapter 3. This review establishes a coherent framework of the main principles in inversion tectonics, with a particular focus on the associated geometries, kinematic aspects, and the main control factors of fault reactivation. The concepts explained here are intended to guide the reader through the theory of inversion tectonics, ensuring coherency and consistency of key concepts. Hence, this section provides the context for the obtained results and frames the discussions incorporated in the dissertation.

Most of the concepts about inversion tectonics here explained have been previously reviewed by Cooper and Williams (1989), Coward (1994), Buchanan and Buchanan (1995) and, more recently, Cooper and Warren (2020) and Tari *et al.* (2020). These works mainly focus on positive inversion. Tari *et al.* (2023), however, have recently done a deep analysis focussed on negative inversion.

1.3.1. Definition and concept of inversion tectonics

The concept of inversion tectonics and structural inheritance was originally proposed from the 1970s, when it was recognized the influence of pre-existing geological features on subsequent tectonic deformation (e.g., Ziegler, 1974; Kent, 1975; Bally, 1984). These works introduce the idea that ancient rift-related fault systems and pre-orogenic features may control how orogenic belts later develop and evolve. However, at that time, the mechanisms behind structural inheritance were not fully understood and its role in later structural evolution remained speculative. The analytical tools and geophysical techniques available then were limited, and the different levels of structural complexities of reactivated inherited structures were not fully comprehended.

Numerous authors have proposed definitions for tectonic inversion. Here we summarize some of the most relevant. Bally (1984) described inversion as inverted extensional features in which basins, half-grabens, or graben systems are compressed and turned inside out reactivating pre-existing normal faults in a contractional regime (Figure 1.4). Williams *et al.* (1989) defined the inversion of a fault-controlled sedimentary basin as the uplift and partial or complete extrusion of its sedimentary fill when subjected to contraction or transpression. This definition specifically addresses cases where faults controlling a basin formation undergo reversal under a contractional regime, transforming depocenters into positive structures and leading eventually to exhumation. In the same year, looking at it from a more regional perspective, Cooper *et al.* (1989) suggested that tectonic inversion could also be defined as a change in the structural elevation of a regional level during a subsequent deformation phase. On the other hand, Allaby (2013) defines inversion tectonics as the process by which a pre-existing fault is reactivated in either compression or extension. Compression leads to positive inversion of pre-existing extensional faults, resulting in uplift, whereas negative inversion caused by extension leads to subsidence and

faulting. This is perhaps a first key definition in which the distinction between two main types of tectonic inversion, positive and negative, is emphasized. More recently, Zwaan *et al.* (2022) define basin inversion as the reversal of subsidence in a (rift) basin due to compressional tectonics, resulting in the uplift and/or exhumation of the basin's sedimentary infill, with or without reactivation of previously established normal faults.

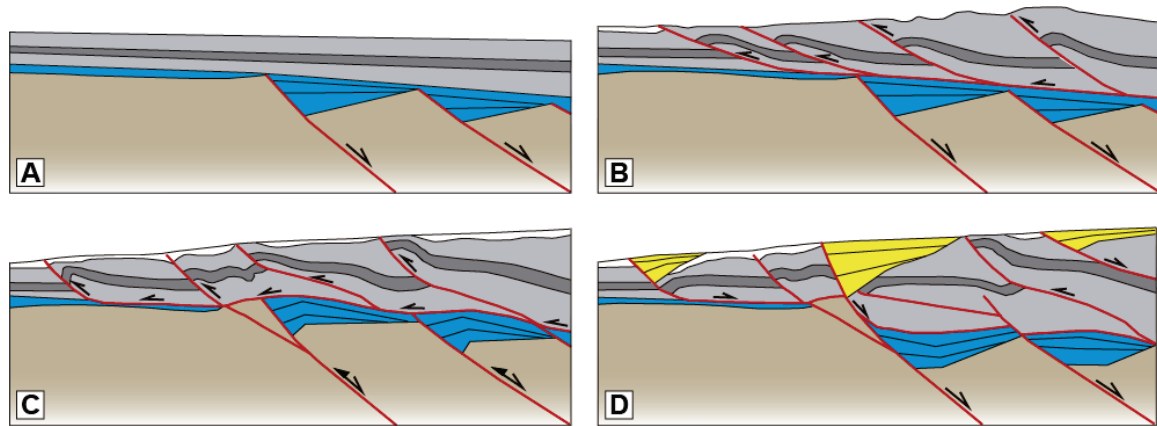


Figure 1.4. Synoptic examples of positive and negative inversion tectonics in the evolution from a rifted margin to a fold-and-thrust belt, including thin- and thick-skinned deformation examples. **A)** Rift basin underneath continental margin; **B)** Thin-skinned fold-and-thrust belt without significant inversion; **C)** Hybrid Thin- and thick-skinned fold-and-thrust belt with positive inversion; **D)** Post-orogenic extension with negative inversion (modified from Granado *et al.*, 2017).

Positive inversion has been recognised in basins at different scales and within different tectonic settings such as orogens like the Pyrenees (e.g., Bon and McClay, 1995; Lopez-Mir *et al.*, 2015) or the Atlas (e.g., Perez *et al.*, 2019); passive margins like the North Atlantic (e.g., García-Senz *et al.*, 2020; Stephenson *et al.*, 2020); strike-slip systems like Sumatra (e.g., Schlüter *et al.*, 2002); delta systems developed in subduction related settings like Barram Delta in Brunei (e.g., Morley *et al.*, 2003). On the other hand, negative inversion has been also documented in different tectonic scenarios such as collapsed orogens like the Devonian basins in Norway (e.g., Osmundsen *et al.*, 1998); extension within fold-thrust belts like the Rocky Mountains in Alberta (e.g., Power and Williams 1989); or in strike-slip systems like the San Andreas fault system in California (e.g., Wakabayashi *et al.*, 2004).

Tectonic inversion must be differentiated from fault reactivation. Tectonic inversion involves a change in the direction of the fault motion, whereas fault reactivation refers to the renewed movement along an existing fault plane. Fault reactivation may refer either to the same direction as the original fault movement or to a different direction depending on the stress conditions. Accordingly, tectonic inversion can be considered as a specific type of fault reactivation in which the motion direction changes over geological time.

From a chronostratigraphic perspective, assessing any case of tectonic inversion requires identifying the sedimentary sequences associated with each tectonic phase. Ideally, pre-rift, syn-rift, post-rift and, if preserved, syn-inversion sequences should be recognized within any inverted basin (Figure 1.5). This approach essentially enables the deciphering of the tectonic evolution of a basin or a specific structure.

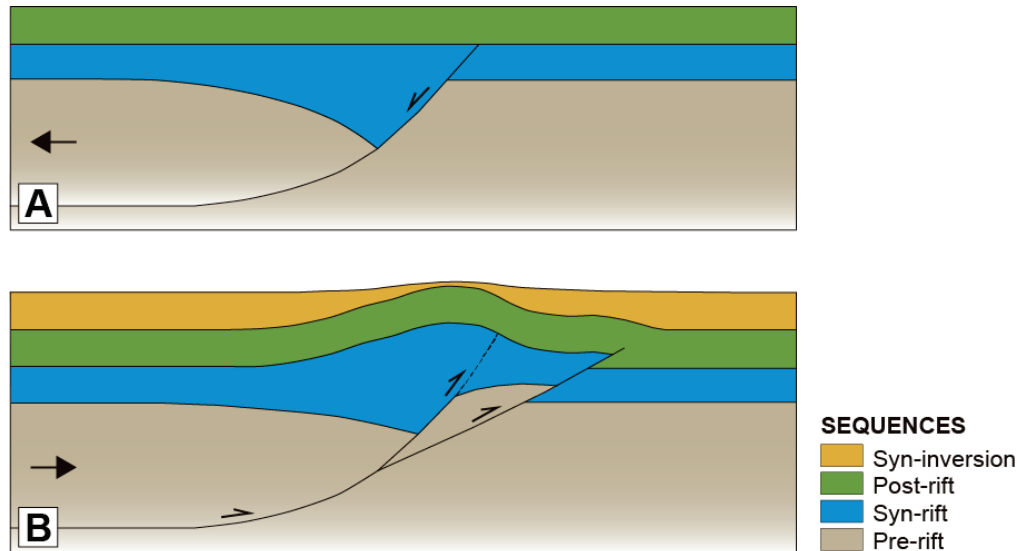


Figure 1.5. Schematic example of an inverted half-graben related to a listric fault showing the tectono-sequences associated to each tectonic phase. The positive inversion causes the contractional reactivation of the inherited listric fault that propagates upward into the undeformed post-rift units, the uplift of the basin-fill, and the development of a footwall short-cut. **A)** End of the post-rift phase; **B)** end of the inversion phase (modified after Cooper *et al.*, 1989).

1.3.2. Positive inversion

1.3.2.1. General concept

Positive inversion involves the reactivation of an extensional fault or a fault system under compressional regimes (Bally 1984). The process develops characteristic features depending on fault orientation, the extent of sediment infill, and the defined as inversion ratio (see below), among several other control factors. Bally (1984) accounts to the amount of recovery of the pre-existent extensional displacement of the fault during the inversion. Upon a compressional regime, pre-existing faults that developed growth sedimentation during the extension may exhibit mixed normal and reverse offsets depending on the level of inversion. This concept is generally known as "inversion ratio", which quantifies this shift as the proportion of contractional displacement relative to the syn-rift thickness, allowing assessment of whether inversion is "partial" or "complete" (De Paor and Eisenstadt, 1987; Williams *et al.*, 1989) (Figure 1.6). Intermediate cases of inversion are illustrated by a pre-rift sequence still showing a net extensional pattern (Figure 1.6B and C), whereas the post-rift sequence may present shortening and structural features related to the compression/inversion (Figure 1.6A). Accordingly, the

amount of (positive) inversion can be assessed using a conceptual "null point" ("null line" in three dimensions) (De Paor and Eisenstadt, 1987; Gibbs, 1987; Williams *et al.*, 1989), which separates the net contraction from the net extension along a fault. The "null point" migrates down the fault plane during progressive migration until reach the stage of total inversion when it will cease to exist, and no extensional offset is present across the fault for the pre-rift sequence (Figure 1.6D).

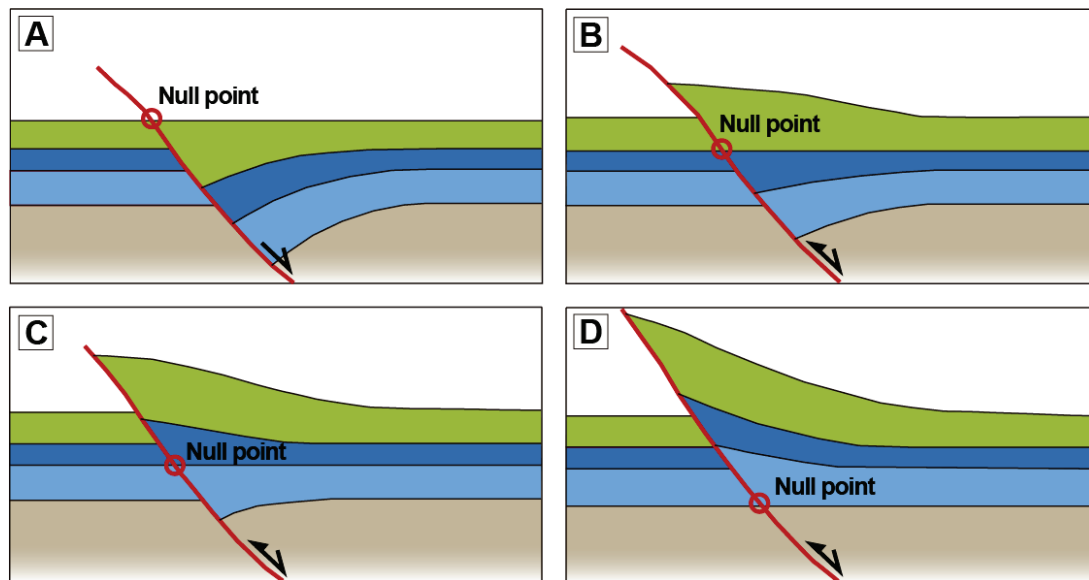


Figure 1.6. Conceptual sections illustrating the inversion ratio showing the degree of inversion of an inverted fault using the null point position. **A)** Extensional graben with no inversion; **B)** Minor inversion of the extensional graben; **C)** Major inversion; **D)** Complete inversion (modified from Williams *et al.*, 1989).

Different degrees of inversion may occur across a basin-system but also within a single inverted depocentre. Hence, basins may exhibit varying structural styles across domains or sectors, some also experiencing multiple phases of extension and inversion (De Paor and Eisenstadt, 1987; Cooper *et al.*, 1989). The incorporation of a rift basin into the structural framework of a fold-and-thrust belt would represent an end-member case. In these cases, traces of their extensional past may still be preserved and revealed through fault displacements and stratigraphic records along and across the inherited fault systems (MacGregor, 1995). The controlling factors of these potential differences are described later in the section. Nevertheless, the analysis and assessment of the tectonic inversion also depend on their depth. For example, a case near the surface would perform differently than an inverted fault beneath a thick foreland sedimentary sequence. This positioning has implications for their analysis depending on the data and technique used of their study (e.g., seismic imaging), because it may or may not allow the recognition of changes in the sedimentary depocentres or the determination of the relative timing of inversion from cross-cutting relationships. In some cases, methods like analogue sandbox modelling (e.g., Buchanan and McClay, 1991; Nalpas *et al.*, 1995; McClay, 1995; Amilibia *et al.*, 2005; Jagger and McClay, 2006; Bonini *et al.*, 2012; Moragas *et al.*, 2017; Roma *et al.*, 2018a and b; Zwaan *et al.*, 2020; Dooley and Hudec, 2020; Ferrer *et al.*, 2016, 2023; Miró *et al.*, 2023; Wilson *et al.*, 2023; Krzywiec *et al.*,

2024) or numerical models (e.g., Gerya and Yuen, 2007; Ruh, 2017; Ruh and Vergés, 2018; Granado *et al.*, 2021) are used to overcome these limitations and therefore better predict subsurface geometries allowing the observation of the fault systems, their related folding and the deformation patterns under controlled conditions that mimic natural cases.

1.3.2.2. Geometries associated to positive tectonic inversion

Tectonic inversion can be identified by the geometries that develop during the inversion process. These associated geometries commonly include, but are not limited to, those listed in this section. Given the thick-skinned character of the Paleogene compressive tectonics in the Catalan Coastal Ranges, the descriptions of the geometries in this section exclude the ones related to or resulting from the presence of salt and/or regional detachments and, therefore, it focusses on thick-skinned tectonics. Figure 1.7 illustrates a generalized summary of the geometries associated to positive tectonic inversion.

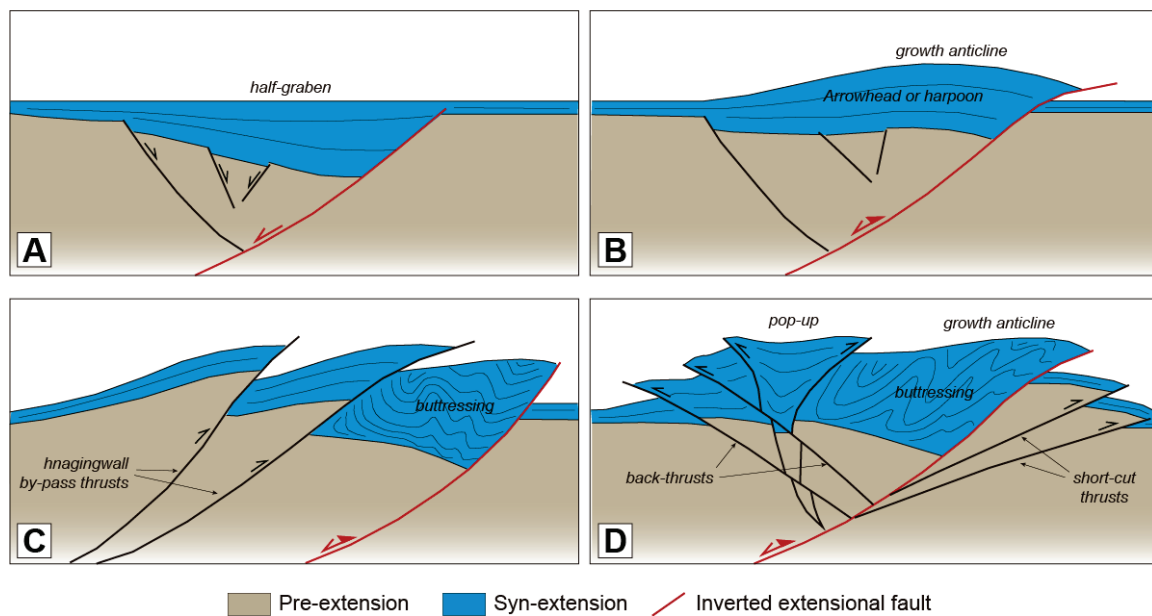


Figure 1.7. Inversion structures: **A)** Extensional half-graben; **B)** Arrowhead or harpoon structure developed as the result of an inverted half-graben; **C)** By-pass thrusts and buttressing; **D)** Complex combination including back-thrusts, buttressing, pop-up structure and footwall short-cut (adapted from Granado and Ruh, 2019).

- **Arrowhead or harpoon structures:** these structures are probably the most classic geometric feature used for the recognition of an inverted semi-graben and form for partial inversion of the extensional growth strata of a single half graben (arrowhead) or a set of them (harpoon) (Figure 1.7B). They typically develop in response to low-angle fault reactivation and are commonly recognized in seismic data (e.g., Goudswaard and Jenyon, 1988; McClay, 1995).
- **Footwall short-cut thrusts:** developed due to the contractional reactivation of extensional faults, these are new reverse faults that cut through the footwall to accommodate compressional deformation (Huyghe, and Mugnier, 1992) (Figure 1.7D).

- **Growth anticlines:** contractional reactivation causes the uplift of the extensional basin, forming anticlines in the hanging wall of the reactivated faults (Figure 1.7D). These structures frequently exhibit significant thickening of syn-extensional sequences towards the anticline crest, which correspond to the maximum depth of the extensional depocenter. Arrowheads and harpoons structures are formed by the uplifted extensional growth strata defining a growth anticline. When inversion occurs asymmetrically across a half-graben, it can produce monoclines within the inverted half-graben close or above the inverted fault. The resulting anticlines are asymmetric, with a steeper forelimb (eventually overturned) and a gently dipping backlimb away from the reactivated fault (Withjack *et al.*, 1995).
- **Hangingwall buttressing and back-thrusting:** when a previously extensional fault is reactivated under compression, its hangingwall may experience restricted movement or "buttressing" against the footwall block. This process may result in the internal deformation of the hangingwall strata the associated geometries of which may help on the recognition and characterization of the tectonic inversion. Common buttressing geometries concentrated in the inverted fault hangingwall are: 1) a sudden increase of folded layers and tilted blocks due to resistance at the fault plane; 2) the presence of foreland-facing folds often with steeply dipping or overturned forelimbs adjacent to the main fault; 3) back thrusts dipping opposite to the primary inverted fault may develop as a response to the stress redistribution in the hangingwall layers (Figure 1.7C and D), and to relieve stress by allowing additional shortening. Mechanical contrasts within hangingwall layered sediments can influence on the presence and pattern of these structures in less competent strata (Cooper and Warren, 2020 and references therein).

Deformation and shortening within the hanging wall via buttressing and the formation back thrusts (hangingwall-vergent thrusts) may be significant before the reactivation of the master extensional fault (Colpron *et al.*, 1998). Buttressing effect may also increase as the fault planes steepen, especially near the fault tip where compression concentrates. Additionally, hangingwall buttressing is important in determining the strain distribution in inverted structures. The above listed complexities can help distinguish between an inverted structure from a standard compressive feature during interpretation.

- **Forced Folds:** they form above reactivated faults as a reaction to the compressive stress into the overlying sedimentary layers. To some extent, they can be considered within the buttressing category since they form as hanging walls and are uplifted and compressed against reactivated faults. In inversion, forced folds often show asymmetry with steeply dipping forelimbs and gentler back limbs. In sandbox analogue models, forced folding is influenced by the angle and depth of the reactivated faults and the competency of the layers involved (Ferrer *et al.*, 2023).
- **Pop-up structures:** these structures are thrust faults that propagate outward from a graben structure due to the contraction and inversion of a pre-existing extensional feature (Buchanan and

McClay, 1992). The referred works exemplify these geometries like a pop-up or pseudo-flower structure bounded by high-angle inverse faults and rooted at the main inverted fault plane (Figure 1.7D).

- **Hangingwall bypass thrusts:** develop within the hangingwall of the inverted fault along the trajectory of the ramp section of the main detachment and propagate upwards (Figure 1.7C), thrusting the extensional ramp syncline over the inverted rollover anticline (Ferrer *et al.*, 2016). In areas where the pre-existing extensional faults display little or no reactivation, bypass thrusts are often present, the geometry of which are strongly controlled by the extensional fault architecture with thrust ramps located at pre-existing extensional fault steps (Butler, 1989).

1.3.3. Negative inversion

1.3.3.1. General concept

Negative inversion refers to the reactivation of pre-existing compressional structures, such as thrust faults, in an extensional context. This process is essentially the opposite of positive inversion, where extensional structures are reactivated in a compressional regime. Negative inversion is seen less frequently than positive inversion and may have special importance in areas with a history of subsequent compressional and extensional tectonic regimes (Tari *et al.*, 2023). Accordingly, the geometries associated to negative tectonic inversion can also be used to provide insights into the geological evolution of an area, such as a change of regime in an area previously dominated by compression to the development of extensional features such as normal faults and vice-versa.

Negative inversion has recently been documented in several regions like the Rocky Mountains (Bally and Snelson., 1980), Arctic Canada (Connors and Houseknecht, 2022), the Betic Chain in Spain (García- Dueñas *et al.*, 1992) and the Apennines in Italy (Tavani *et al.*, 2023). The Rockies and Canadian Arctic cases exemplify how the post-orogenic reactivation of pre-existing thrust planes as normal faults formed structural traps and influenced on hydrocarbon migration. On the other hand, in the Mediterranean region, negative inversion has been related to post-orogenic slab rollback and crustal stretching associated with back-arc basin formation (e.g., Apennines, Tavani *et al.*, 2023; Catalan Coastal Ranges, Fontboté *et al.*, 1990; Roca and Guimerà, 1992). A comprehensive compilation of negative inversion cases has been recently published by Tari *et al.* (2023).

1.3.3.2. Geometries associated to negative inversion

Negative inversion displays kinematic patterns that include specific structures consequence of the extensional reactivation of pre-existing compressional faults. The resulting geometries are often more difficult to identify than those associated with positive inversion. However, these structures show

perhaps less complexities than its positive counterpart. The geometries are briefly described below and illustrated in the Figure 1.8.

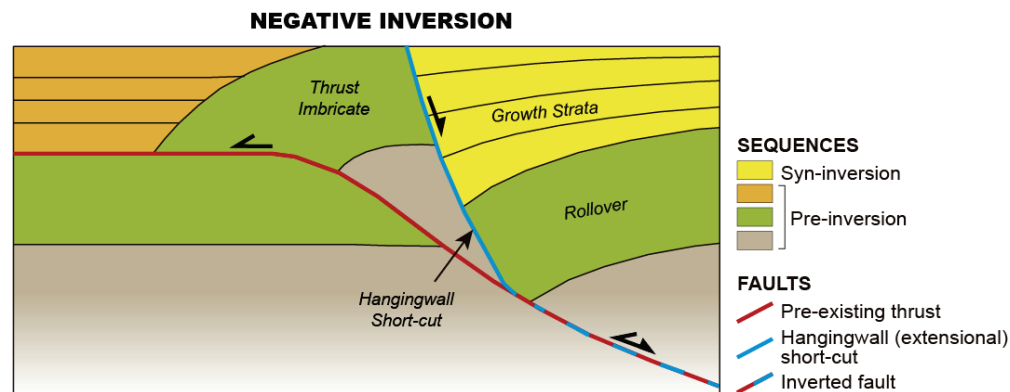


Figure 1.8. Cartoon summary of geometries associated to negative inversion tectonics. Note the short-cut extensional fault developed within the hangingwall of the partially inverted pre-existing thrust, which develops a half-graben with growth strata. The tectono-sequences associated to the tectonic phases are also indicated (modified from Tari *et al.*, 2023).

- Hangingwall short-cut faults:** these structures occur during inversions when a normal fault is created within the hangingwall of the pre-existing compressional fault or thrust sheet reactivated in its deeper part and abandoned in its shallower part (Huyghe, and Mugnier, 1992) (Figure 1.8). They are formed to accommodate the new stress direction. This type of structure contrasts with its counterpart positive inversion in two different aspects: positive inversion short-cuts involve low-angle thrusts developed in the footwall of the extensional fault (structure 2 in Figure 1.7) (McClay, 1995), whereas steep short-cut extensional faults developed in the hangingwall generally characterize negative inversion (Figure 1.8) (Tari *et al.*, 2023). Extensional short-cut faults are normally detached at a ramp segment of the original thrust plane, where the extensional forces are most likely to nucleate. Unlike positive inversion, negative inversion frequently includes the formation of hangingwall short-cuts with independency of the inversion degree. In some cases, negative inversion exhibits listric (curved) faulting patterns, where extensional forces reactivate the lower-angle segments of thrust planes. Half-grabens may develop above these structures as seen, for instance, in the Apennines (Tavani *et al.*, 2023).
- Extensional growth strata patterns:** negative inversion may develop growth strata arrangements within the previously mentioned half-grabens above the hangingwall short-cuts. These geometries are characterized by a progressively thickening of the sedimentary packages against the inverted fault, which may be a key indicator seen in seismic profiles (Figure 1.8).

1.3.4. Main controls on tectonic inversion and fault reactivation

Inversion structures exhibit diverse geometries and complexities. This section outlines the first-order controls that determine whether a basin undergoes inversion and how structures develop during this

inversion. In general, pre-existing faults are expected to represent areas of weakness within the surrounding undeformed rock, such as the development of fault gouge that may reduce the cohesive strength compared to the unaltered rock from which it originates (Sibson, 1977; Sibson, 1985). Hence, once formed, faults are likely to reactivate under new or renewed stress fields. However, several factors such as the geometry of the pre-existing fault (e.g., McClay, 1990; Buchanan and McClay, 1992), the effect of the sedimentary successions (e.g., Tari *et al.*, 2020) or the rheology of the crust (e.g., Ziegler *et al.*, 2001) control the type and extent of the inversion processes and resulting geometries. These factors have mostly been studied based on positive inversion tectonic case studies, although they must also be considered in negative inversion cases. Additionally, some of the controls can be co-dependent, having their interplay a notable significance. These interactions would highly influence the degree of inversion, the resulting structural style, and the distribution of deformation and strain within the resulting inverted basin. This fact highlights that inversion dynamics cannot be attributed to isolated factors but rather to a combination of controls that shape the overall structural and mechanical response of an inverted basin.

1.3.4.1. Geometrical aspects

The geometrical characteristics of the pre-existing extensional fault or fault system mostly refers to the dip of the fault plane and its orientation relative to the regional stress. These are crucial in determining whether or how the faults will be reactivated during inversion. Commonly, one would assume in terms of fault dip geometry that steeply dipping faults will generally require higher compressional stresses to reactivate rather than low-dipping faults. Therefore, fault dip differences will influence the resulting structural style during and after fault reactivation and inversion. Extensional fault systems show a wide variety of fault geometries (McClay, 1990) (Figure 1.9).

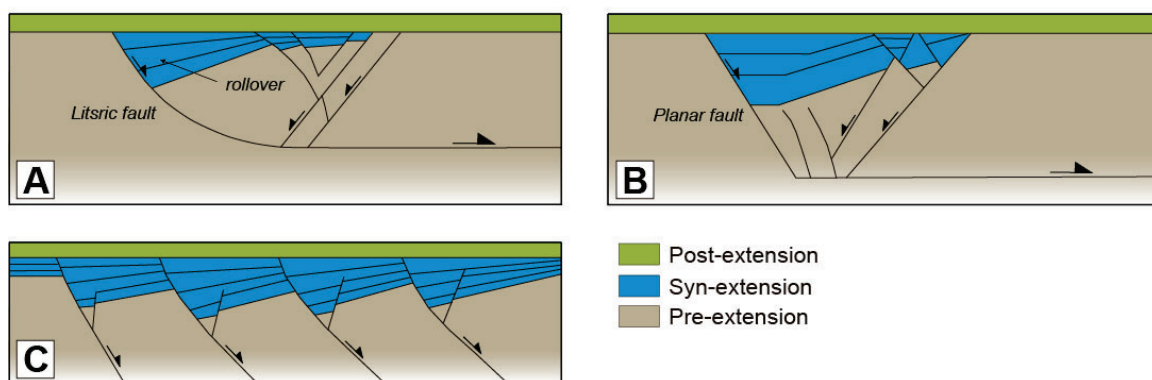


Figure 1.9. Main types of normal faults: **A)** Listric fault; **B)** Planar fault with a horizontal detachment at depth; **C)** Planar rotational or domino-style faults (compiled from Gillcrst *et al.*, 1987, McClay 1992 and Buchanan and McClay, 1992).

The 2D geometric classification of extensional faults proposed by Wernicke and Burchfield (1982) include two main categories of normal faults: 1) listric faults that tend to be curved and sole out into a

basal horizontal detachment at depth with a rollover anticline at its hangingwall (e.g., Gibbs, 1984); and 2) planar extensional faults differentiating non rotational faults (e.g., Anderson, 1951; Sibson, 1985) and rotational or domino-style faults (e.g., Buchanan and McClay, 1992; Jagger and McClay, 2018). Further complexities and combinations of these endmember 2D fault geometries as well as dip variations of the detachment at depth should also be considered (e.g., Ferrer *et al.*, 2016).

Listric extensional faults curve and flatten at depth, developing fault-bend fold anticlines in the hangingwall known as a rollover (Gibbs, 1984; Figure 1.9A). When inverted, this extensional rollover fold becomes accentuated, uplifting the sedimentary fill in the hangingwall with a thrust that cuts through the post-rift sequence (Figure 1.10A). The reactivation is more pronounced in gently dipping areas, with displacement decreasing as the fault dip increases. Depending on the intensity of inversion and the dip of the extensional fault, different structures may form, ranging from gentle anticlines in mild inversion to complex systems including hangingwall imbricated thrusts, backthrusting, and footwall short-cut thrusts, in cases of highly inverted faults with steep upper parts that would not reactivate (Figure 1.10A, see description of the different type of resulting structures in section 1.3.2.2.).

As shown by experimental sandbox analogue models (e.g., Dooley *et al.*, 2005; Withjack and Schlische, 2006; Ferrer *et al.*, 2014, 2016), non-rotational planar extensional faults with a horizontal detachment at depth are characterized by planar or gently kinked rollover anticlines (Figure 1.9B). These works show that hanging-wall rollover geometries are controlled by the amount of extension, by the dips of the bounding faults and by the kink-band bend in the fault surface. Geometries depend on the dip of the planar fault. For instance, experiments with low-dipping (20°) fault, develop small antithetic faults near the detachment breakaway, whereas higher dipping faults (60°) develop narrow rollover with closely spaced antithetic faults that bound a deep, flat half-graben basin (Ferrer *et al.*, 2016). During inversion non-rotational planar faults reactivate the main detachment, causing a gentle uplift of the hanging wall, forming a small frontal inversion anticline, creating a broad zone of uplift in the syn-extensional strata above their regional level and developing a short-cut structure in case of low-dipping (20°) (Ferrer *et al.*, 2016; Buchanan and McClay, 1991, 1992). In contrast, 60°-dipping planar faults, shaped well-developed asymmetric hanging-wall inversion anticlines with moderately dipping frontal limbs and gently dipping back limbs (Figure 1.10B). Footwall short-cuts thrusts in front of the inversion anticline, buttressing against the footwall produced new hanging-wall back-thrusts, and small crestal-collapse graben developed on the outer arc of the asymmetrical inversion anticlines are present in these models (Figure 1.10B).

Extensional domains governed by hard or soft domino-styles with planar or sigmoidal fault geometries respectively (e.g., Axen, 1988; Buchanan and McClay, 1992; Figure 1.9C) involve both extension and rotation with the faults operating together and the development of a series of half-graben basins formed as fault blocks rotated synchronously (McClay, 1990). Rotational faults display a parallel pattern and

show the same displacement along the fault plane during extension and rotation. This allows the development of half-graben basins with layers thickening toward fault planes, forming wedge geometries (Figure 1.9C). Minor antithetic faults might develop, increasing in size with distance from the basin-bounding fault. During inversion, domino-style faults reactivate with reverse displacement. This uplifts the syn-rift and post-rift units although no major deformation is observed within the half-grabens (Jagger and McClay, 2018) (Figure 1.10C). Depending on the inversion degree, reactivation may produce null points along the fault planes, marking zones where the net displacement across the fault is zero, separating areas of net contraction above from areas of net extension below. Footwall short-cut thrusts, creating fan-like or horsetail structures, appear in response to the shortening strain (Jagger and McClay, 2018). Moreover, distinctive growth anticlines or forced folds, arrowhead structures will develop in the reactivated syn-extensional sequence (Figures 1.7 and 1.10C).

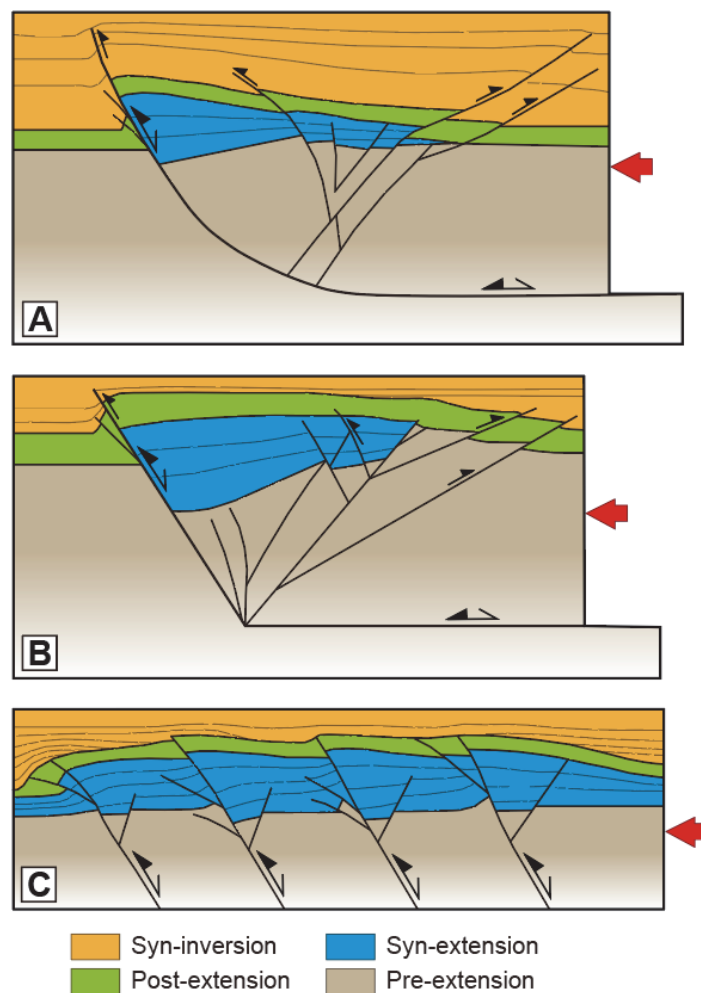


Figure 1.10. Models of inversion for simple extensional systems, based on analogue sandbox models (modified from McClay *et al.*, 1992). **A)** Inversion of a concave upwards simple listric fault; **B)** Inversion of a planar fault with a deep horizontal detachment; **C)** Inversion of a domino-style fault system.

Beyond the inversion of the simple extensional faults explained above, rift basin systems may present complex patterns of the inherited extensional basin configuration, which will produce a wide range of

geometries. Complex pre-existing faults geometries, such as ramp-flat listric or kinked planar faults, will introduce notable geometry complexities after inversion due to variations in dip of the different fault panels and shape along the fault plane at depth. For instance, in the case of a ramp-flat listric fault (Figure 1.11A), inversion produces an asymmetric frontal anticline with steeper front-limb and footwall short-cut thrusts (Buchanan and McClay, 1992; McClay, 1995; Ferrer *et al.*, 2016). This inversion geometry reflects the interaction of pre-existing listric segments, leading to displacement along footwall-vergent bypass thrusts developed or rooted at the end of the lower ramp (Buchanan and McClay, 1992; McClay, 1995; Ferrer *et al.*, 2016). Similarly, the kinked planar fault with two panels of varying dip (Figure 1.11B) generates an even more complex inversion structure. Here, inversion introduces asymmetric folding in the hanging wall, along with additional back-thrusts that arise from buttressing effects along the steeper upper fault segment (Ferrer *et al.*, 2016). Crestal-collapse graben formations develop in the inversion anticline's outer arc. These features highlight the role of the complex fault geometry in producing distinctive and compartmentalized inversion structures that differ substantially from the simpler arrowhead-like inversion geometries seen in planar or single-listric faults.

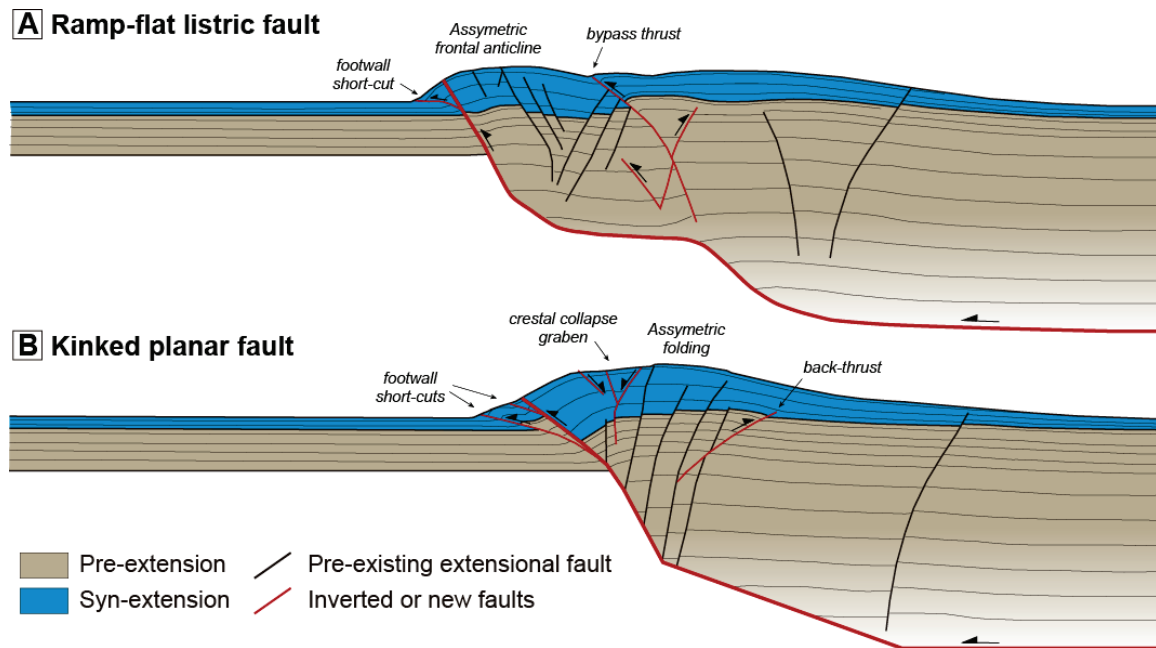


Figure 1.11. Analogue sandbox model cross-sections illustrating the structural styles of inversion of complex fault geometries. **A)** Ramp-flat listric fault; **B)** Kinked planar fault (redrawn after Ferrer *et al.*, 2016).

Fault orientation or strike relative to the compression or stress direction has also an impact on the inversion of pre-existing fault systems. In general terms, faults that are aligned perpendicular to the direction of maximum compressive stress are the most likely to be reactivated (i.e., optimal fault orientation). In these cases, compressive forces act directly along the fault plane, making it easier for the fault to slip or for stress to be accommodated by fault reactivation. Experimental sandbox models by Buchanan and McClay (1992) demonstrated that faults oriented perpendicular to the applied

shortening direction exhibit the highest degree of reactivation. In contrast, experiments with fault orientations that are oblique or parallel to the compression direction show that these faults require greater stress to reactivate, leading to selective inversion within the fault systems. The alignment of fault strike relative to the compression direction also influences the inversion geometry. Optimally oriented faults typically produce more direct and continuous reactivation, often resulting in broad uplifted structures or symmetric anticlines in the hanging wall. Conversely, faults oriented at an angle to the compression direction can create complex deformation patterns, including asymmetric folds, local uplifting, or wrenching movements along strike-slip components. This orientation-dependent behaviour is therefore essential for understanding the development of inversion in regions where multiple fault systems with varied strikes are present.

1.3.4.2. Syn- vs. post-rift sequence thicknesses

It has been documented that the thickness of syn- and post-rift sequences also plays a significant role in influencing structural styles during tectonic inversion, shaping the type and behaviour of inversion structures. Two primary inversion modes (I and II, Figure 1.12) differentiate the influenced by the relative thicknesses of these two kinds of sequences (Tari *et al.*, 2020).

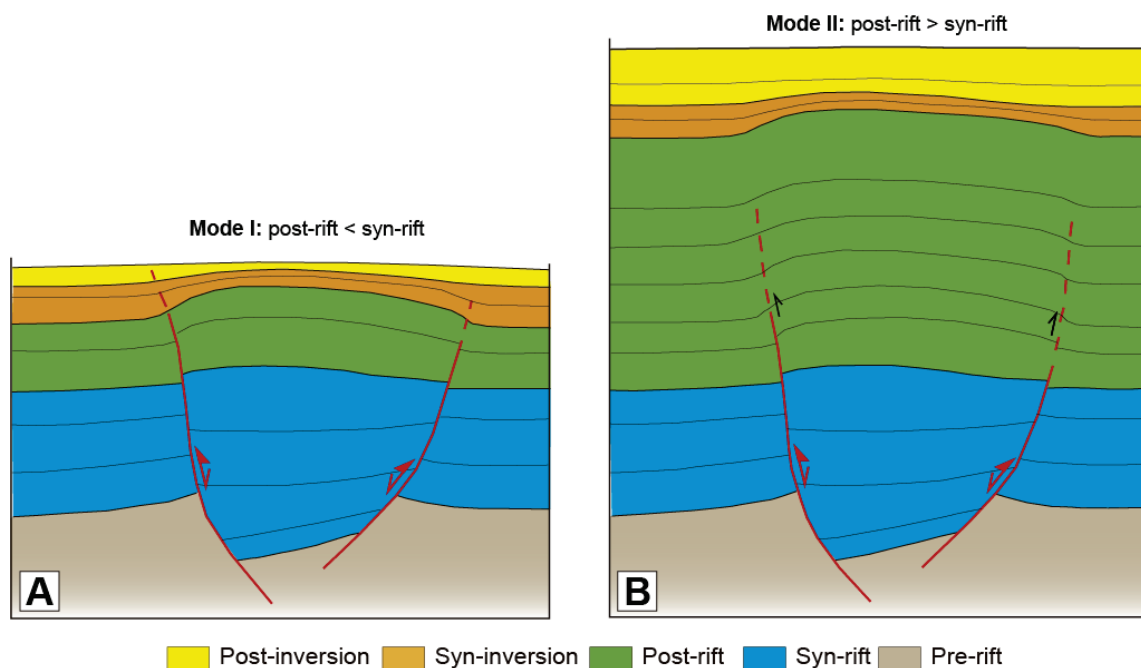


Figure 1.12. Subdivision of inversion into two modes of inversion. **A)** Mode I inversion when the post-rift succession is thinner than the syn-rift succession in the pre-existing extensional basin; **B)** Mode II inversion when the post-rift succession is thicker than the syn-rift one (modified from Tari *et al.*, 2020).

It occurs when the syn-rift succession is thicker than the post-rift cover. During tectonic inversion, reverse-fault-bounded structures develop. These structures often experience significant displacement along faults, creating steeper anticlines and more intense fault reactivation. On the other hand, in Mode

If the post-rift cover is thicker than the syn-rift deposits. In these cases, inversion typically results in gentler, open forced folds rather than steep, fault-bounded structures, characterized by less structural deformation.

Experimental studies such as sandbox analogue models (e.g., Tamas *et al.*, 2023) validate these structural styles under different thickness scenarios of syn- and post-rift sequences. These models demonstrate that in basins with a thin post-rift sequence, fault inversion is more pronounced, producing reverse faults extending into the post-rift cover, while in thicker post-rift sequences, fault propagation is restricted, favouring the development of open folds rather than fault-dominated structures. Therefore, the post-rift sequence thickness directly affects the propagation of inherited faults.

1.3.4.3. Lithosphere's integrated strength

In a simplified lithosphere model where quartz controls the rheology of the upper crust, diorite the lower crust and olivine the upper mantle (e.g., Kirby and Kronenberg, 1987; Roure *et al.*, 2006), a strength profile can be made (Figure 1.13). This profile shows an upper crust that exhibits brittle behaviour, and the strength increasing with depth due to rising confining pressure. However, as depth increases, the combination of higher temperatures and pressures that reduces rock strength promotes a limit into ductile deformation at the base of the upper crust. This brittle-ductile transition occurs at depths around 15 km and temperatures of around 250°C. Low-strength regions likely exist at the base of the crust, resulting from the rheological contrast between quartz and olivine, a limit known as Moho discontinuity.

The strength of the lithosphere is strongly influenced by crustal thickness but also by the time elapsed since stretching. Different stretching models (e.g., McKenzie, 1978; Wernicke, 1981) would therefore display different strength profiles. A rapid and homogeneously stretching crust as the one defined by McKenzie (1978) will show that the stretched lithosphere's overall strength (Figure 1.13B) is lower than that of the unstretched lithosphere (Figure 1.13A). However, after stretching (i.e., rifting) the lithosphere tends to cool until it re-establishes its original geothermal gradient, with the strength curve adjusting accordingly. On the other hand, in Wernicke's asymmetric stretching model (Wernicke, 1981), extension in the upper crust is laterally transmitted to the lower crust and mantle. Under the fault, the crustal strength curve would not change significantly, whereas in areas where the lithospheric mantle thins, the geothermal gradient increases, causing a decrease in strength.

The variation of the lithosphere strength through time is therefore strongly dependent on its composition and thermal history. Hence, in tectonic inversion, these factors should be considered as a function of the time span between the end of the rifting and the onset of the later contractional and shortening phase (Ziegler *et al.*, 2001).

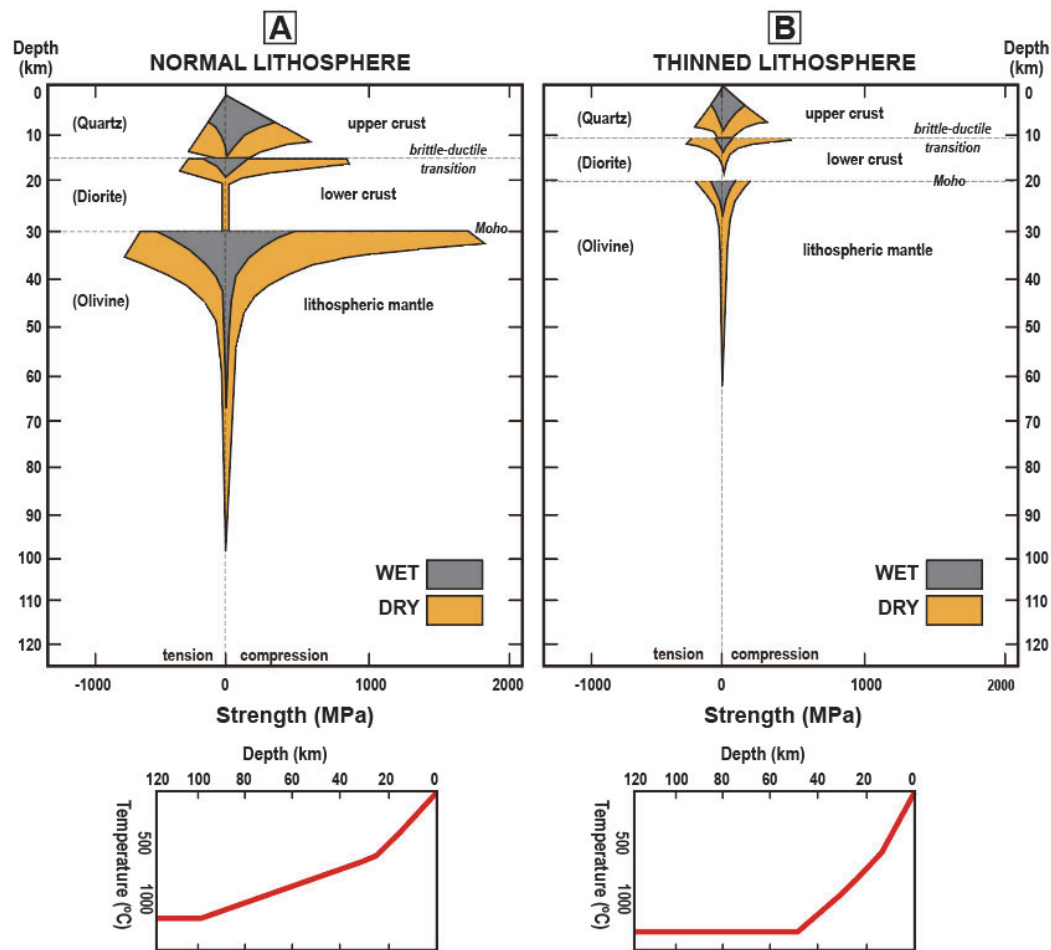


Figure 1.13. Idealized depth-dependent strength profiles for dry and wet lithosphere to stresses (tension and compression) and their corresponding thermal gradients. The graph assumes a quartz/diorite/olivine rheology corresponding to the upper crust, lower crust, and lithospheric mantle. **A)** Normal lithosphere profile (i.e., unstretched or cratonic scenarios) with 30 km thick crust and 70 km thick lithospheric mantle. **B)** Stretched lithosphere profile (i.e., rifted, stretched scenarios) and thermally unstable lithosphere thinned to 20 km thick crust and 45 km lithospheric mantle (modified from Ziegler *et al.*, 2001).

1.3.4.4. Mechanical properties of the fault zone

If fault reactivation occurs under conditions where the rock behaves in a brittle domain, such as the upper crust, the Navier-Coulomb criterion can be applied and can be represented with a Mohr diagram (Figure 1.14). In this context, the capacity of a fault to reactivate depends on several key parameters such as: cohesion, friction coefficient, orientation, and fluid pressure (Sibson, 1985). Under brittle conditions, these parameters can influence whether a fault will slip again when subjected to a change or reactivation of the stress field. Therefore, through Mohr's circle diagrams one can show how faults might respond under different stress conditions (Jaeger and Cook, 1979).

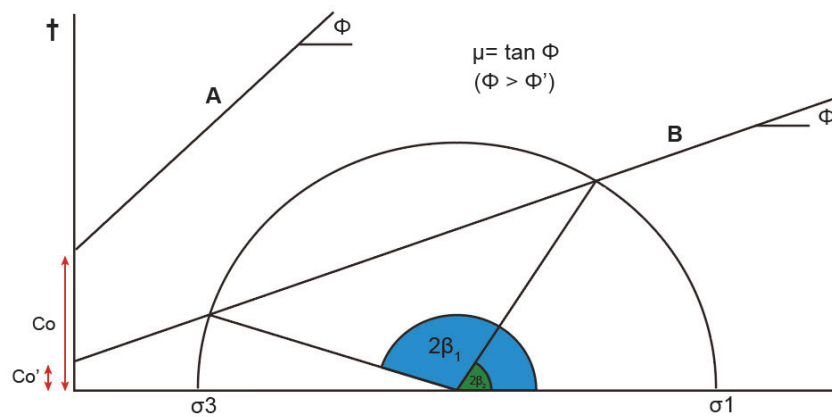


Figure 1.14. Mohr circle and Mohr envelope for brittle behaviour, showing how cohesion and friction influence fault behaviour under compressive stress. **A)** The envelope for rock with cohesion Co and an internal friction angle Φ , showing the typical strength of intact rock. **B)** The envelope for a pre-existing fault, with lower cohesion Co' and a sliding friction angle Φ' .

Of all those parameters, cohesion and friction coefficient are critical to influence fault reactivation. Cohesion reflects the fault's inherent resistance, and lower cohesion typically makes reactivation easier, especially for pre-existing faults. Friction, specifically the internal friction angle and the friction coefficient, also plays a significant role in fault reactivation (Sibson, 1985). Faults with lower friction coefficients are more prone to reactivation than those with higher values, particularly as stress changes. On the other hand, the orientation of the fault plane relative to the direction of compressive forces is also critical. Faults positioned at angles closer to the ideal rupture angle will reorient and reactivate more easily under compression (Sibson, 1985). This orientation factor means that faults already aligned with principal stress directions tend to reactivate before new fractures form.

1.3.4.5. Burial, pressure, fluids, and temperature conditions

The control of burial, pressure, and temperature on tectonic inversion is complex, governed by the interplay of stress conditions, fluid presence, and depth-dependent deformation mechanisms (Hubbert and Rubery 1959; Sibson, 1985). These factors can have an important influence on the mechanical properties of faults; hence, this section is highly interconnected to the previous one. Increased burial, fluid pressure, and geothermal gradients within fault zones may alter the stresses, enabling or inhibiting fault reactivation, influencing both fault strength and the mode of deformation.

As burial depth increases, so do pressure and temperature, shifting the deformation mechanisms from brittle to ductile. However, in shallow crustal levels, brittle deformation and frictional slip typically dominates. Lafosse *et al.* (2016) show that increasing burial depth and temperature gradient decreases the effectiveness of frictional strength along inherited faults, leading to more distributed deformation and vertical extrusion of basins rather than fault reactivation. However, increased fluid pressure can

substantially reduce the effective stress within fault zones, by lowering the normal stress on fault planes. High fluid pressure makes therefore reactivation easier, particularly in faults favourably oriented to the compressive forces. In conditions where fluid pressures are high, faults with lower cohesion and friction values may reactivate under compression. Faults misaligned with the primary stress field or with steeper dips, however, would demand higher fluid pressures for reactivation (Donath and Crandwell, 1981). Sibson (1985) further emphasizes the role of fluids in facilitating inversion by reducing the effective stress along faults.

Additionally, fluid circulation and temperature regime may facilitate the crystallization of minerals or the development of cements within the fault zones (e.g., De Brit 1989; Muchez *et al.*, 1995; Travé *et al.*, 1998; Travé and Calvet 2001; Labaume *et al.*, 2007; Micarelli *et al.*, 2005; Benedicto *et al.*, 2008; Vilasi *et al.*, 2009; André *et al.*, 2010; Baqués *et al.*, 2012). This would have a direct impact since newly formed minerals and rock types with different friction values along the faults will control inversion/reactivation. Logan *et al.* (1981) demonstrated that montmorillonite fault gouge could withstand higher shear stresses, indicating that pre-existing faults are not always the first to reactivate under deformation.

1.4 Geological introduction to NE Iberia and the Catalan Coastal Ranges

This section presents an introduction to the geological setting of the Catalan Coastal Ranges, mainly focussing on its central part where the study area is located. The section is structured in three main blocks: (1) overview of the tectonic framework, (2) overview of the main stratigraphic assemblages and (3) concluding remarks

1.4.1 Location and overview of the tectonic framework

The Catalan Coastal Ranges (hereinafter CCR) are located at the NE of the Iberian Peninsula and are one of the three alpine structural units that limit the Ebro Basin (Figure 1.15). The Ebro Basin is the late southern foreland basin of the Pyrenean orogen that developed during the convergence between Iberian plate and Eurasian plates from Late Cretaceous to middle Miocene times (Srivastava *et al.*, 1990; Muñoz, 1992; 2001; Rosenbaum *et al.*, 2002; Mouthereau *et al.*, 2014). To the southwest and southeast, the Ebro Basin is bounded by two intraplate fold-and-thrust belts: the Iberian Range, and the CCR respectively (Figure 1.15). These three major alpine structural units display overall similarities in terms of tectonic evolution, such as the presence of pre-existent Mesozoic rift basin systems, which were tectonically inverted during the Late Cretaceous-Cenozoic compression that affected the western Tethyan regions (Rosenbaum *et al.*, 2002; Mouthereau *et al.*, 2014).

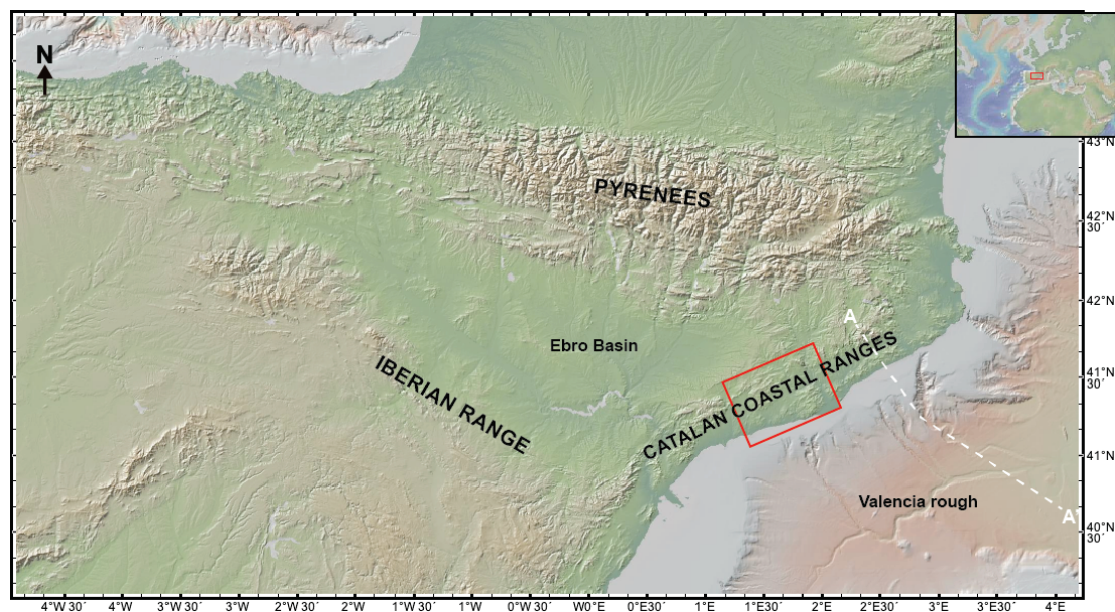


Figure 1.15. Shaded relief map of NE of the Iberian Peninsula with the location of the three main alpine mountain belts: the Pyrenees, the Iberian Range, and the Catalan Coastal Ranges, which bound the Ebro Foreland Basin to the north, southwest and southeast respectively. Red square indicates the central domain of the Catalan Coastal Ranges area in which this thesis is focussed. A-A' line indicates the location of the regional section shown in Figure 1.16. Base map made with GeoMapApp (<https://www.geomapapp.org>) / CC BY / CC BY, Ryan *et al.*, 2009).

The CCR constitute the current onshore expression of the northeastern part of the extensional continental margin that separates the thinned crust of the Valencia Trough from the thicker crust of the Iberian Plate (Dañobeitia *et al.*, 1992; Roca and Guimerà, 1992; Vidal *et al.*, 1998; Gaspar-Escribano *et al.*, 2003) (Figure 1.16). The CCR extend for over 250 km parallel to the Mediterranean coastline and are characterized by a NE-SW-oriented basin-and-range configuration that consists in series of ENE- to NE-striking blocks bounded by faults ranging from 50 to 150 km in length (Figure 1.17). Onshore, these major faults display a right-stepping en-echelon pattern (Ashauer and Teichmüller, 1935; Llopis-Lladó, 1947; Anadón *et al.*, 1985; Guimerà, 2004). Major faults generally dip towards the southeast and show a combination of normal, reverse, and limited left-lateral strike-slip motions (Guimerà, 1988, 2004; Roca, 1996). The central domain of the CCR is comprised between the El Camp Basin in the south to the northeastern tip of the Vallès-Penedès Basin to the north (Figure 1.17).

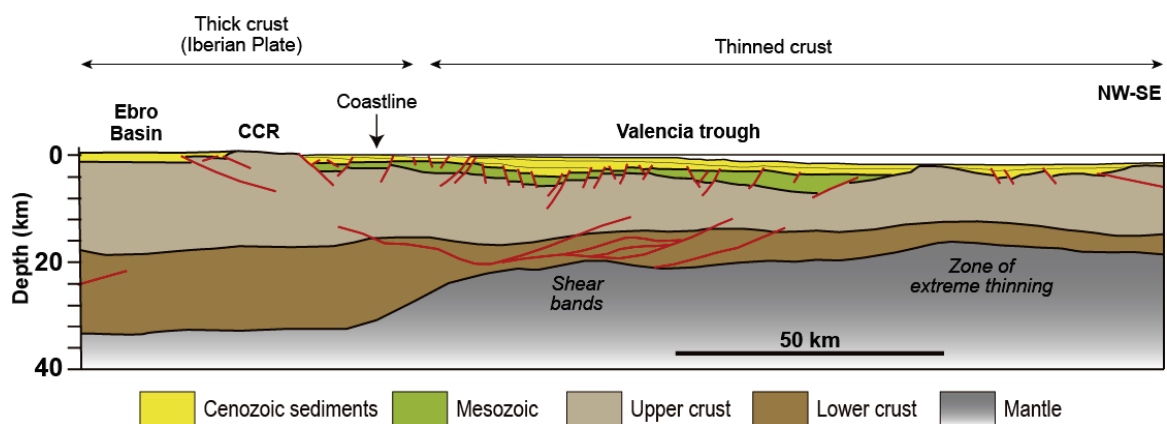


Figure 1.16. Depth section through the Catalan margin showing the SE-NW increase of the crustal thickness between the Valencia Trough and the Iberian Plate (modified from Gaspar-Escribano *et al.*, 2003).

The tectonic evolution of the CCR can be outlined in three major tectonic phases that are the responsible of its present-day configuration: (1) a multiepisodic extensional phase from the late Permian to the Aptian, (2) a compressional phase during the Paleogene, and (3) a latest Oligocene-middle Miocene extension (Llopis-Lladó, 1947; Anadón *et al.*, 1979; Roca and Guimerà, 1992; Bartrina *et al.*, 1992; López-Blanco *et al.*, 2000a, b; Baqués *et al.*, 2012; Cantarero *et al.*, 2014a, b; Marín *et al.*, 2021). Each of these three main tectonic phases are described in detail below.

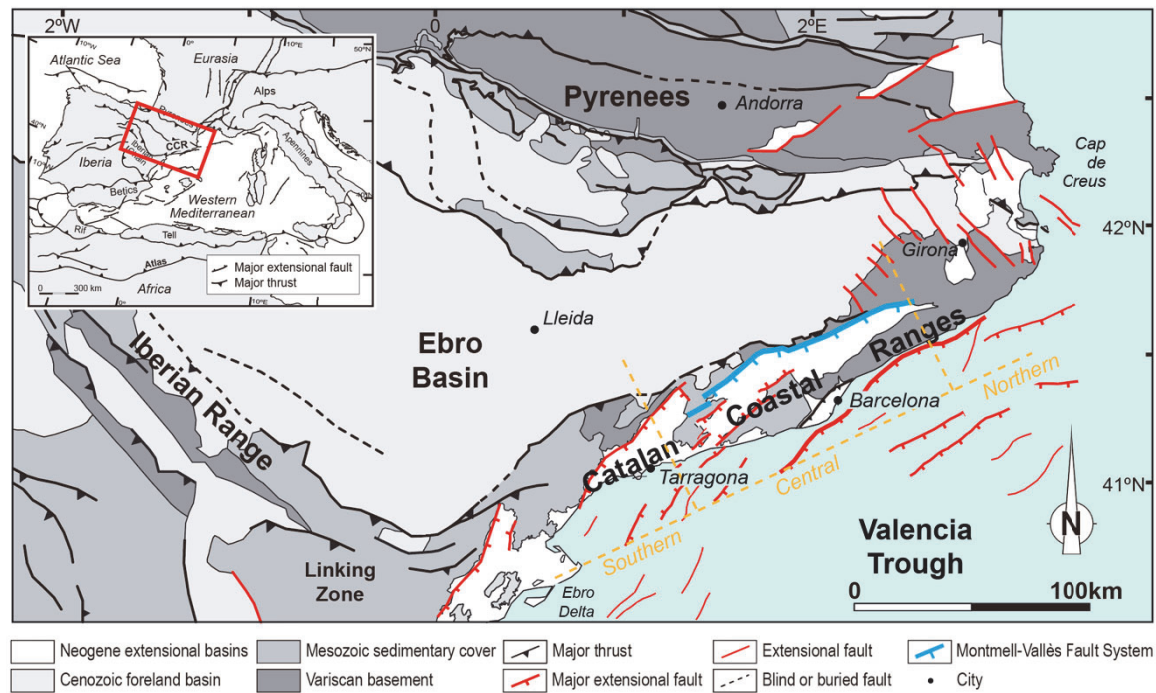


Figure 1.17. Schematic geological map of NE Iberia showing the three major structural units bounding the Ebro Basin: the Pyrenees to the north, the Iberian Range to the SW, and the Catalan Coastal Ranges (CCR) to the SE. The limits of the southern, central, and northern domains of the CCR are indicated in orange dashed lines. The trace of the Montmell-Vallès Fault System the tectonic evolution of which is presented in this Thesis is highlighted with a thick blue line in the central domain of the CCR (modified from Garcés *et al.*, 2020).

1.4.1.1. Late Permian - Mesozoic extensional phase

The first extensional period occurred from the Late Permian to the Triassic, related to the opening of the Neotethys Ocean (López-Gómez *et al.*, 2002). This period is characterized by the development of a basin system that started its development during the Middle-Late Permian due to widespread extension (Galán-Abellán *et al.*, 2013) and evolved as a NE-SW-oriented rift basin with conjugate NW-SE fault systems that controlled the development of the Permo-Triassic depocenters. The second rifting event, from the Late Jurassic to the Early Cretaceous (i.e., latest Oxfordian to Aptian), was coeval with the opening of the North Central Atlantic and the Bay of Biscay, which led to the uncoupling of the Iberian Plate from Eurasia in northern part of Iberia (Srivastava *et al.*, 1990; Salas and Casas, 1993; Salas *et al.*, 2001; Sibuet *et al.*, 2004). During this phase, several basins heterochronously developed south and east of the Ebro Block including the Cameros, Columbrets, Maestrat, Perelló, Montmell-Garraf, and Barcelona basins as result of the divergent processes both in the Atlantic-Biscay domain in the north and the continuing opening of the Tethys in the east (Salas, 1987; Salas and Casas, 1993; Salas *et al.*, 2001; Tavani *et al.*, 2018) (Figure 1.18). The major extensional faults that delimited the basin development during these two periods, controlled the subsidence and basin-fill in these areas and were involved in the later inversion of the extensional basins.

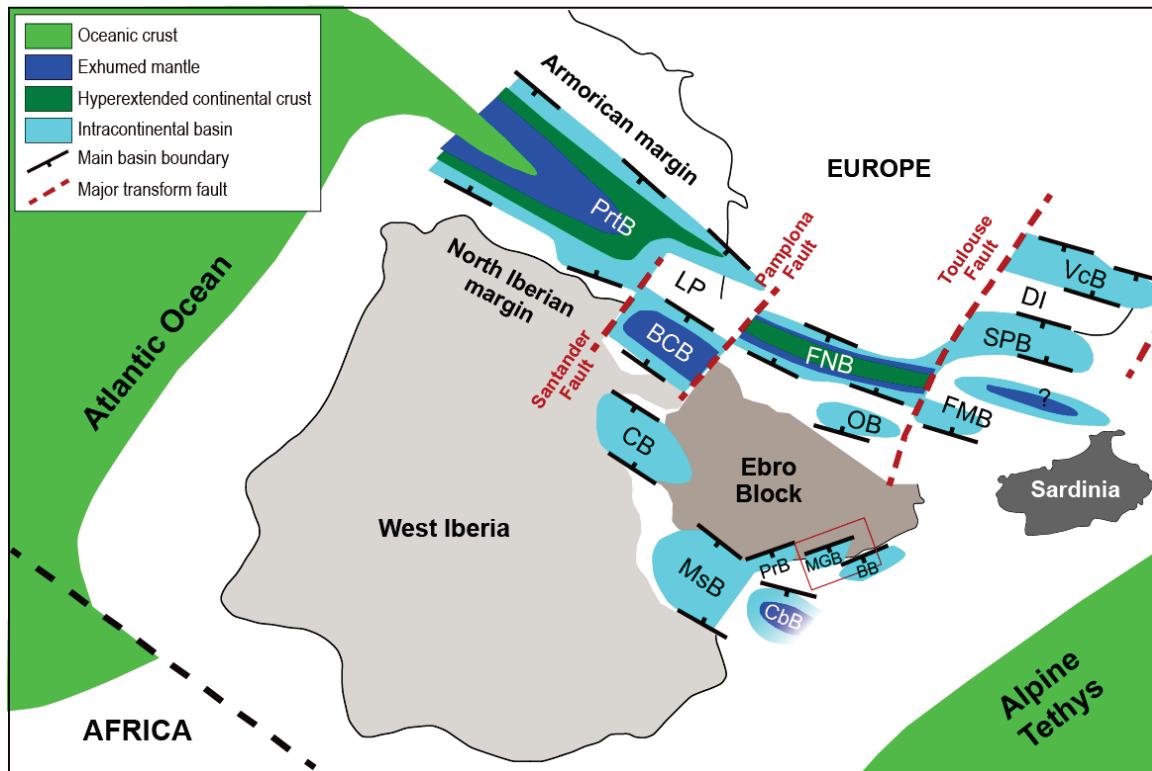


Figure 1.18. Reconstruction of the Iberia-Eurasia margin and surrounding areas in the mid-Cretaceous times. Major basins, transform faults, and crustal domains are indicated. **PrtB**: Parentis Basin; **LP**: Landes Plateau; **BCB**: Basque-Cantabrian Basin; **CB**: Camaros Basin; **FNB**: Flysch Noir Basin; **OB**: Organyà Basin; **MsB**: Maestrat Basin; **VcB**: Vocontian Basin; **DI**: Durance Isthmus; **SPB**: South Provence Basin; **FMB**: Figueres-Montgrí Basin; **PrB**: Perelló Basin; **MGB**: Montmell-Garraf Basin; **BB**: Barcelona Basin. The red square indicates the area of study (modified from Tavani *et al.*, 2018).

Despite its diachronic character and the eastward propagation of the basin system development in the Atlantic-Biscay-Pyrenees domain (Tavani *et al.*, 2018 and references therein) and the Iberian domain (Álvaro *et al.*, 2019; Salas and Casas, 1993; Salas *et al.*, 2001) the extensional phase predominantly ends during the Aptian. However, minor tectonic activity has been also identified up to the mid-Albian (Salas *et al.*, 2001). From this moment on, the entrance of siliciclastic sedimentation from late Albian to Cenomanian characterizes the beginning of a post-rift phase controlled by the thermal relaxation and a generalized eustatic rising of the sea-level (Haq *et al.*, 1988; Alonso *et al.*, 1993; Salas *et al.*, 2001). The post-Cenomanian evolution is, however, difficult to be established due to the lack of preserved sedimentary record in the study area. Two main hypotheses may explain this time span: 1) the no deposition of post-Cenomanian sedimentary successions in the central CCR north of the Perelló Basin (i.e., Serra de Lloveria in Gil *et al.*, 2004; Segura *et al.*, 2004) (Figure 1.18), underscoring a period of tectonic quiescence in the area, and 2) sedimentation occurred but was followed by uplift and erosion. The causes of this uplift and the associated exhumation and erosion can be related to a post-rift isostatic uplift (e.g., Burov *et al.*, 1997) or, otherwise, an uplift related to the compression related to the Pyrenean Orogeny affecting the western Tethys (Srivastava *et al.*, 1990; Rosenbaum *et al.*, 2002).

1.4.1.2. Paleogene (Paleocene-late Oligocene) contractional phase

From the Paleocene to the latest Oligocene, the CCR experienced a contractional phase due to the northward drift of Africa and the collision of the uncoupled Iberian and Eurasian plates (Srivastava *et al.*, 1990; Rosenbaum *et al.*, 2002). This drastic change in the relative motion of Iberia generated the Pyrenean fold-and-thrust belt from the inversion of the Mesozoic rift-system (Muñoz, 1992; Vergés *et al.*, 2002; Roca *et al.*, 2011; Muñoz, 2017; García-Senz *et al.*, 2019). The contractional deformation progressed southwards leading to the inversion of the Mesozoic rift basins developed in the Iberian Plate and forming the Iberian Range and, in the current position of the CCR, the Catalan Intraplate Chain (CIC). The preserved structure of the CIC consists of major NNW-directed thick- and thin-skinned thrusts as well as strike-slip faults with an ENE- to NE trend (Anadón *et al.*, 1985; Guimerà and Álvaro, 1990). The main Paleogene compressional structures present in the CCR and related to the build-up of the CIC are shown in the map of Figure 1.19A. According to studies performed in preserved growth strata, the development of the CIC started during the early Eocene at its NE end and progressed towards the southwest up to the latest Oligocene (Guimerà and Santanach, 1978; Guimerà, 1984; Anadón *et al.*, 1985; Anadón, 1986; Barberà *et al.*, 2001; López-Blanco, 2002; Jones *et al.*, 2004; Garcés *et al.*, 2020). The earliest synorogenic sediments recorded along the SE Ebro Basin margin are the early Eocene Cairat Fm. (Ypresian-early Cuisian in age), which were deposited northeast of the study area in the Montserrat-Sant Llorenç del Munt area (Anadón, 1978; López-Blanco, 2002).

1.4.1.3. Latest Oligocene-Miocene extensional phase

An extensional tectonic stage took place from latest Oligocene and extended through the Neogene up to late Miocene (Bartrina *et al.*, 1992; Roca, 1994; van Hinsbergen *et al.*, 2014). Subduction of the Tethyan Maghrebien Ocean beneath the Iberian Plate induced back-arc processes and stretching in the eastern Iberian Plate from the rollback of the subducting plate (Horvath and Berckhemer, 1982; Fontboté *et al.*, 1990; Roca and Guimerà, 1992; Roca, 1994; Carminati *et al.*, 1998; Roca *et al.*, 2004; Van Hinsbergen *et al.*, 2014, 2020). During this period, Paleogene thrust faults were reactivated as normal faults (Roca, 2001; Gaspar-Escribano *et al.*, 2004; Marín *et al.*, 2021; Baqués *et al.*, 2012). The region was divided into a series of tilted fault blocks, forming the system of horsts and half-grabens bounded by crustal-scale SE- to SSE-dipping extensional faults with kilometeric displacements (Roca and Guimerà, 1992; Bartrina *et al.*, 1992) that characterizes the current configuration of the CCR (Figure 1.19B). In the central CCR, the Vallès-Penedès and El Camp faults were active during this phase, controlling the development of the El Camp and the Vallès-Penedès basins respectively, which, at specific locations, accumulated over 4 km of latest Oligocene to Recent sediments (Roca, 1994; Gaspar-Escribano *et al.*, 2004). This period induced the isostatic uplift of the major footwall blocks of up to 1.2 km (Juez-Larré, 2003; Gaspar-Escribano *et al.*, 2004).

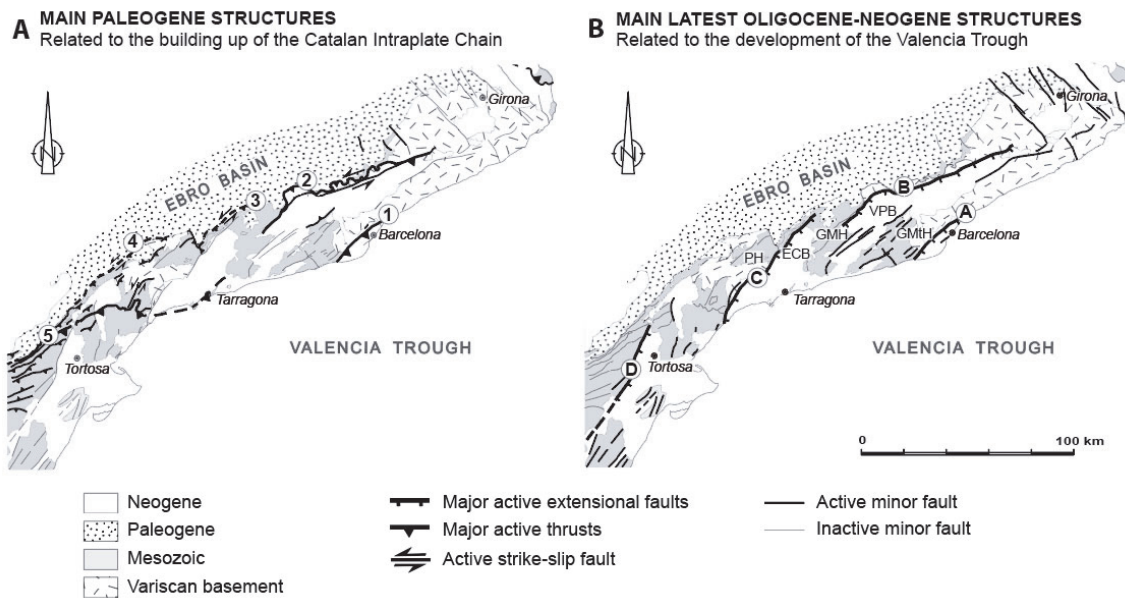


Figure 1.19. Present-day structural maps of the CCR showing the main onshore structures active during the two Cenozoic tectonic phases that affected the area. **A)** Main structures active during Paleogene compression. 1: Pla de Barcelona Thrust; 2: Vallès-Penedès Thrust; 3: Miramar-Gaià Thrust; 4: Ganesa-Ulldemolins Thrust; 5: Portlirubio-Vandellòs-Tarragona Thrust. **B)** Main structures active during latest Oligocene to Miocene extension. **A:** Pla de Barcelona Fault; **B:** Vallès-Penedès Fault; **C:** El Camp Fault; **D:** Baix Ebre Fault. **VPB:** Vallès-Penedès Basin; **ECB:** El Camp Basin; **GMH:** Gaià-Montmell High; **PH:** Prades High; **GMtH:** Garraf-Montnegre High (modified from Roca *et al.*, 2004).

1.4.1.4. Location of the study area within the tectonic context

In this complex structural setting, the study area is located in the central part of the CCR in the Gaià-Montmell High, which is the transfer zone developed between two major Neogene extensional faults: the Vallès-Penedès Fault and El Camp Fault (Figure 1.20). These two major faults have a right-stepped en-echelon arrangement and are bounded towards the southeast by the Baix Penedès and El Camp basins respectively. The Vallès-Penedès Fault, which extends for more than 100 km towards the northeast, experienced a Neogene extensional displacement of up to 4 km, though it previously acted as a Paleogene NW-directed thrust with a transpressive component (Fontboté, 1954; Roca *et al.*, 1999) (Figure 1.19A). The Montmell Fault (Figure 1.20) is considered as the southwestern continuation of the Vallès-Penedès Fault, the assemblage of which comprises the Montmell- Vallès Fault System (Marín *et al.*, 2023, paper included in chapter 2 of this dissertation).

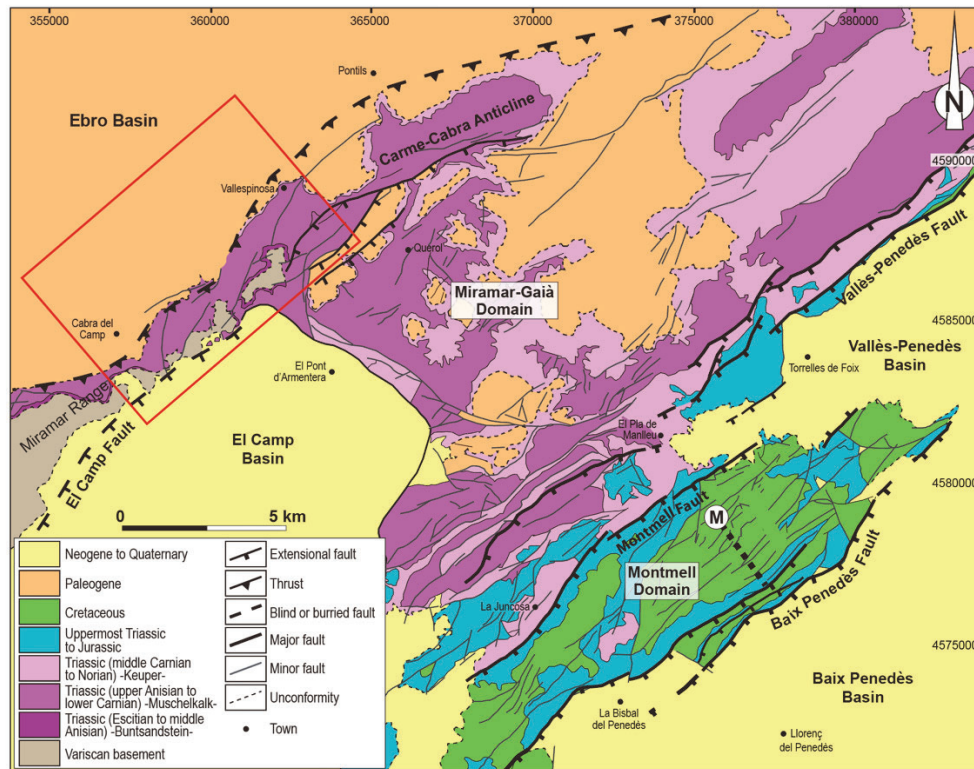


Figure 1.20. Geological map of the Gaià-Montmell High, the transfer zone of the two major Neogene extensional faults: the Vallès-Penedès and El Camp Neogene faults. The two main domains characterizing the Gaià-Montmell High are indicated: the Miramar-Gaià and the Montmell domains. Label "M" and the thick dashed line indicates the approximate location of the Mesozoic type-succesion (Salas, 1987). The red square indicates the area between Vallespinosa and Cabra del Camp in the Ebro Basin margin, the tectonostratigraphy of which was studied in detail in this thesis.

The Montmell Fault separates the Gaià-Montmell High into two domains: the Miramar-Gaià and the Montmell domains, which are basically distinguished by their different Mesozoic stratigraphic record since the Montmell Fault limits to the northwest a thicker Mesozoic succession that includes Jurassic and Cretaceous rocks. This fact led to interpret this fault as the northwest boundary of the Late Jurassic-Early Cretaceous Garraf-Montmell Basin (Salas, 1987).

The northwestmost part of the study area belongs to the central southeastern margin of the Ebro Basin, between Cabra del Camp and Vallespinosa towns (Figure 1.20). Previous studies suggested the presence of a progressive unconformity at this location, indicating that the growth and uplift of the Paleogene frontal contractional structure of the CCR in this area (i.e., Carme-Cabra Anticline) was contemporaneous with the deposition of conglomeratic units during the middle Eocene (Benzaquen *et al.*, 1972a; Anadón *et al.*, 1985 and 1986), fact that is refined and clarified in this dissertation. However, the ages of the contractional structures located towards the hinterland of the CCR and responsible for the contractional deformation of the Miramar-Gaià and Montmell domains remained uncertain due to the lack of preserved syn-kinematic strata in the footwall of the Montmell Fault.

1.4.2 Overview on the stratigraphy

The Catalan Coastal Ranges (CCR) and the southeastern margin of the Ebro Basin present a diverse stratigraphic record developed from the Paleozoic to the Quaternary times. Four main tectonostratigraphic assemblages, which reflect the tectonic evolution of the region, have been differentiated: 1) the basement that resulted from the Variscan/Hercynian orogenic, metamorphic and magmatic processes affecting the region; 2) a late Paleozoic (Permian) - Mesozoic sedimentary record overlying this basement that was deposited during an extensional period resulting in the generation of rift basins across the Iberian Peninsula; 3) a Paleogene sedimentary succession filling the Ebro Foreland Basin as it evolved in response to the Alpine-Pyrenean Orogeny that gave rise to the CIC; and 4) Miocene to Quaternary sedimentary successions infilling series of extensional basins developed during the Neogene structuration of the CCR (e.g., El Camp, Vallès-Penedès and Baix Penedès basins). All the listed stratigraphic assemblages are illustrated in the chronostratigraphic chart of Figure 1.21.

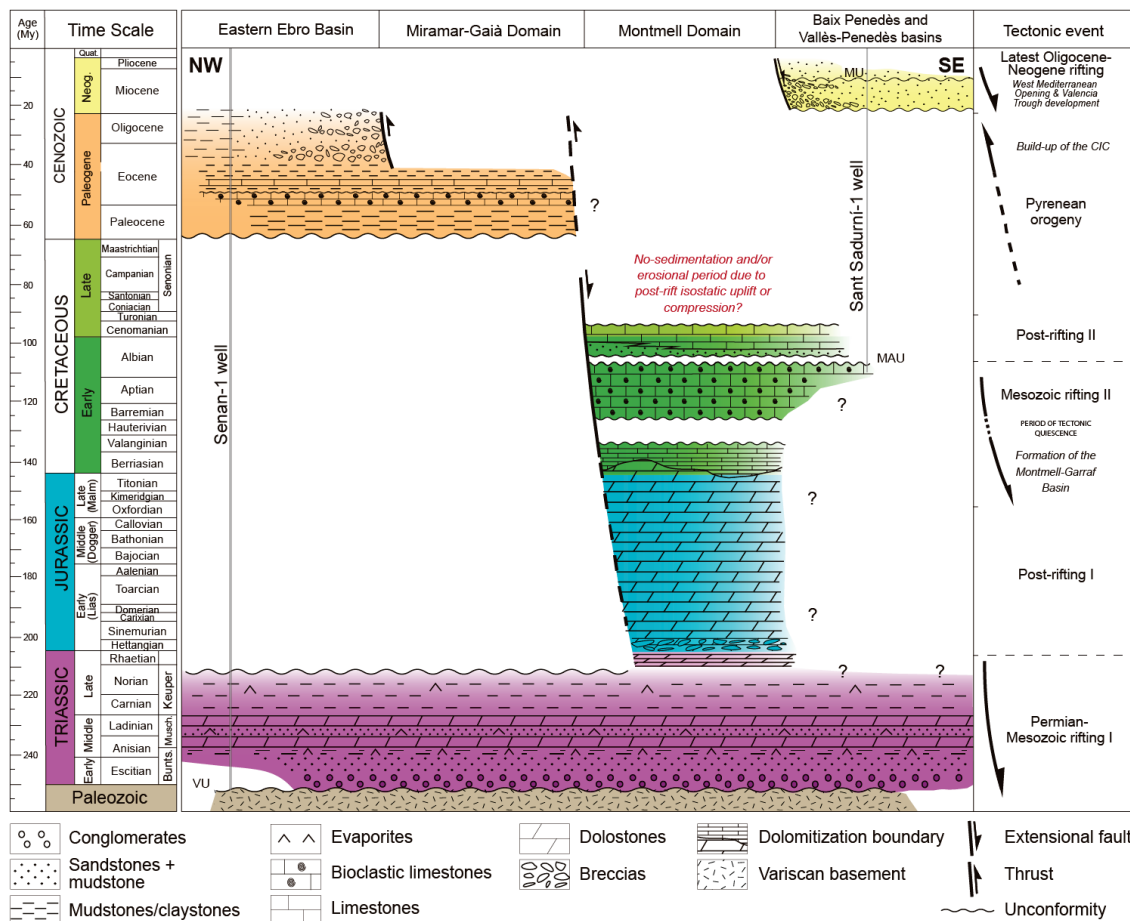


Figure 1.21. Chronostratigraphic chart of the study and the adjoining areas. Main tectonic events are indicated. Major unconformities are labelled as follows: **MU**: Messinian Unconformity; **MAU**: Middle Albian Unconformity; **VU**: Variscan Unconformity. Lithostratigraphy has been compiled from Ortí (1974), Anadón *et al.* (1978), Colombo (1986), Lanaja (1987), Salas (1987), Casas and Permanyer (1991), Calvet and Marzo (1994), Cabrera and Calvet (1996), Salas *et al.* (2001), Mercedes-Martín *et al.* (2014), Ortí *et al.* (2017) and Escudero-Mozo *et al.* (2017).

This differentiation in stratigraphic groups or assemblages reflects the dynamic geological history of the region, characterized by multiple phases of extension and compression. Considering these complexities and the fact that the better-preserved diverse stratigraphic records occur at different areas, the stratigraphic descriptions below are assigned to specific structural units, basins, sectors and/or domains for the clarity of the reader (Figure 1.22).

1.4.2.1. Variscan/Hercynian Basement

Most of the pre-Alpine basement in the CCR encompasses Cambro-Ordovician to early and middle Carboniferous sequences that were intruded by late Carboniferous to Permian plutonic rocks (Julivert, 1955; Sáez and Anadón, 1989; Serra and Enrique, 1989; Julivert and Durán, 1990; Enrique and Solé, 2004). Permian sediments are reported overlaying an erosional surface developed on these basement rocks (i.e., Variscan/Hercynian Unconformity, Figure 1.21; López-Gómez *et al.*, 2002; Galán-Abellán *et al.*, 2013). This unconformity affected both the plutonic intrusions as well as the sedimentary and metamorphic rocks of the basement.

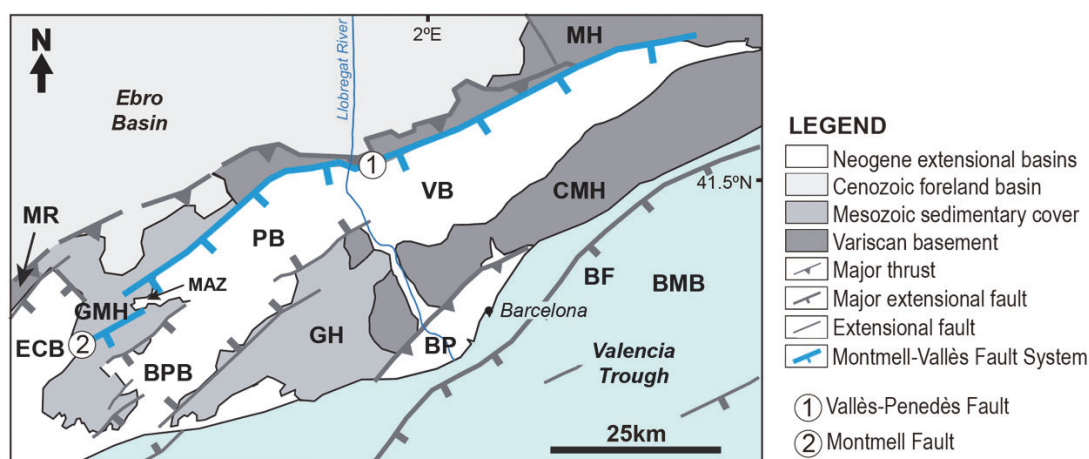


Figure 1.22. Detail of the central Catalan Coastal Ranges highlighting the structural units, basins, sectors, and domains present in the study area. From west to east, **MR**: Miramar Range; **ECB**: El Camp Basin; **GMH**: Gaià-Montmell High; **BPB**: Baix Penedès Basin; **PB**: Penedès Basin; **VP**: Vallès Basin; **GH**: Garraf High; **BP**: Barcelona Plain; **CMH**: Collserola-Montnegre High; **MH**: Montseny High; **BF**: Barcelona Fault; **BMB**: Barcelona-Maresme Basin; **MAZ**: Marmellar Accommodation Zone.

In the study area, Paleozoic rocks of the Variscan Basement have been described at the bottom of the Senant-1 well in the Ebro Basin (Lanaja, 1987), in the adjoining Miramar Range (Julivert, 1955; Melgarejo, 1987) and Prades High as well as in the Montseny and Collserola-Montnegre Highs in the northern sectors of the CCR (Julivert and Durán, 1990; Enrique and Solé, 2004) (Figure 1.22). The Paleozoic succession in the Miramar Range is made up by Cambrian to Carboniferous slates with thin interbeds of Devonian carbonates (Julivert, 1955; Sáez and Anadón, 1989; Julivert and Durán, 1990). Upper Carboniferous to Permian granitoids have been reported in the Prades High (Serra and Enrique,

1989; Enrique and Solé, 2004). In this work it is assumed that Paleozoic rocks like the ones in the adjoining Miramar Range (Figure 1.23) also characterize the basement underneath the Gaià-Montmell High. These Paleozoic rocks are considered as the structural basement unconformably overlaid by the middle-late Permian and Mesozoic successions. Further details about the potential nature and lithology of the Variscan Basement in the Gaià-Montmell High are included in the discussion of the magnetotelluric model interpretation presented in the first research paper included in Chapter 2.

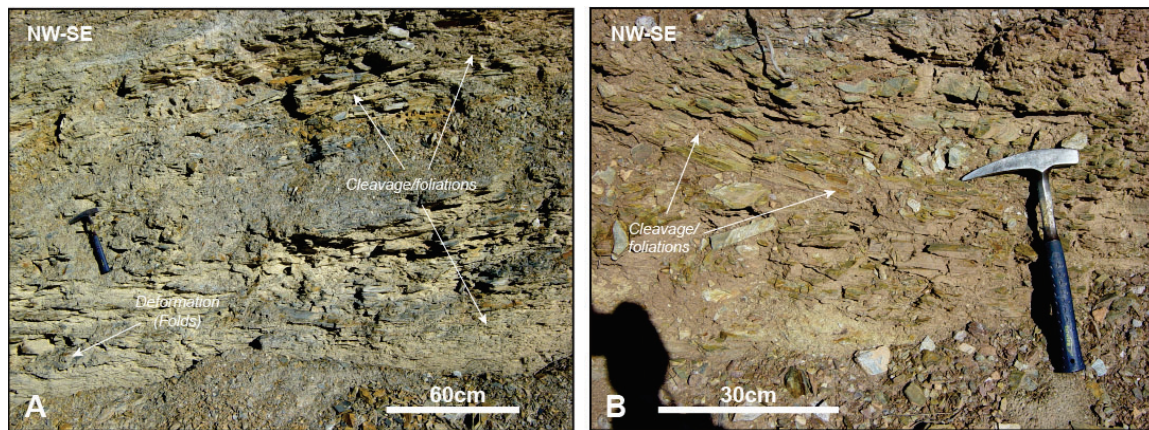


Figure 1.23. Paleozoic outcrops in the Miramar Range (see Figure 1.22 for its location). **A)** Highly deformed Silurian black-grey slates with quartzitic levels showing folds and cleavage/foliations. **B)** Carboniferous slates and red sandstones with cleavage/foliations.

1.4.2.2. Late Permian - Mesozoic stratigraphic record

In the CCR, the Permian - Mesozoic stratigraphic record is characterized by significant thickness variations between the different domains in the area. The Miramar-Gaià Domain and the adjoining Ebro Basin and Miramar Range are characterized by a thin Mesozoic succession that only includes Triassic rocks ranging between 200 to 350 m in thickness (Lanaja, 1987; Virgili *et al.*, 2006; Galán-Abellán *et al.*, 2013; Mercedes-Martín *et al.*, 2014). In contrast, to the southeast, the Mesozoic succession of the Montmell-Garraf Basin exceeds 2 km in thickness (Salas, 1987). This second realm shows a more complete stratigraphic record that includes some localized Permian successions as well as more widespread Triassic, Jurassic, and Cretaceous sequences that show noticeable northwest-southeast lateral thickness variations, which are summarized in the Figure 1.24.

Permian and Triassic successions

The Alpine cycle regionally starts with a Middle-Late Permian-Early Triassic extensional period that controlled the deposition of siliciclastic and carbonate units along NE-SW-trending basins (Galan-Abellán *et al.*, 2013; Mercedes-Martín *et al.*, 2014; López Gómez *et al.*, 2019; Mercedes-Martín and Buatois, 2020). The Triassic stratigraphic record is constituted by limestones, dolomites, siliciclastic and evaporitic rocks, ascribed to the threefold stratigraphical Germanic subdivision that includes the

Buntsandstein, Muschelkalk and Keuper magnafacies (Virgili, 1958; Calvet and Marzo, 1994; Arnal *et al.*, 2002; Galán-Abellán *et al.*, 2013; Escudero-Mozo *et al.*, 2017; Ortí *et al.*, 2017; Mercedes-Martín and Buatois, 2020) (Figure 1.25). This succession is related to the extensional tectonics that gave rise to several large intraplate Mesozoic rifts systems formed in the eastern Iberian Plate during the opening of the western Neotethys (Salas *et al.*, 2001; García-Senz and Salas, 2011). Subsidence in these grabens was not coetaneous and caused thickness differences in the sedimentary record (Marzo 1980; Calvet and Marzo, 1994). Within this regional extensional context, however, in the study area, the Permian succession is only observed in the Garraf High realm. Additionally, Triassic strata does not show major lateral thickness variations between the Senant-1 well northwest in the Ebro High and the successions preserved in the Gaià, Montmell and Garraf domains in the southeast (Figure 1.24A).

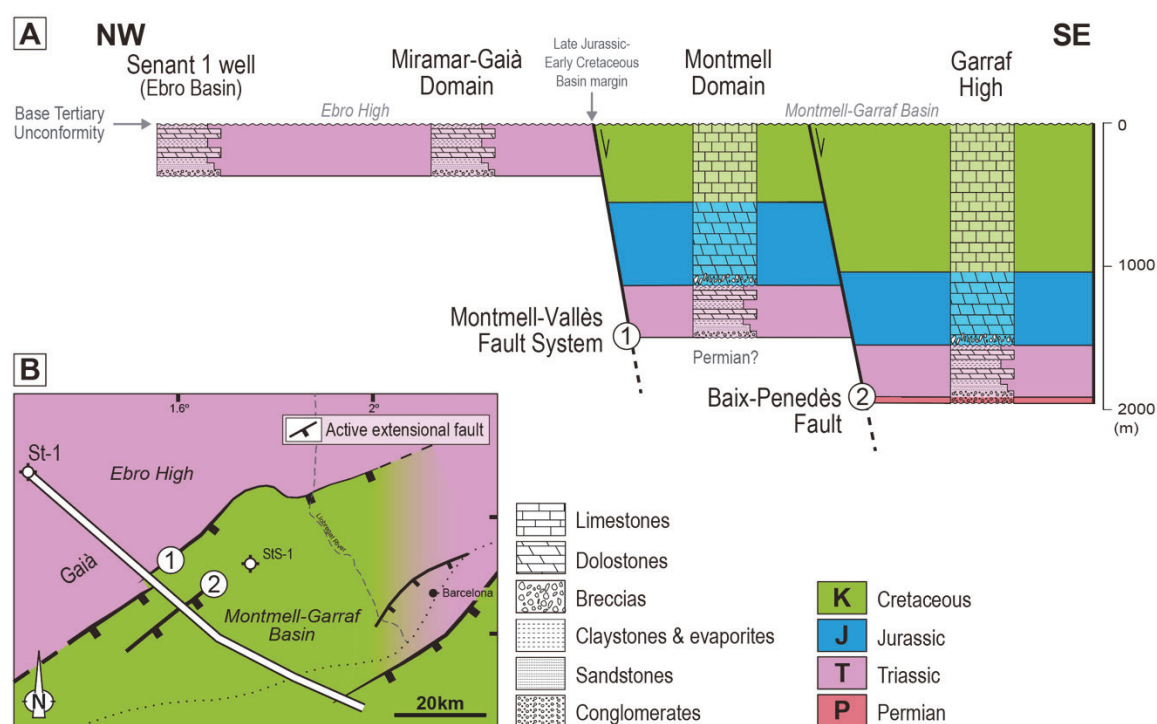


Figure 1.24. A) Permian-Mesozoic thicknesses across the Ebro Basin and the central Catalan Coastal Ranges. Upper reference datum corresponds to the base of the Tertiary. Mesozoic thicknesses are based on Salas (1987), Lanaja (1987) and ICGC (2005); Permian is based on Marzo (1980), Marzo and Calvet (1985), López-Gómez (2002) and López-Gómez *et al.* 2019). Horizontally not-to-scale. **B)** Tectonostratigraphic map of the central Catalan Coastal Ranges at the end of the late Jurassic - early Cretaceous extensional phase. **St-1:** Senant-1 well; **StS-1:** Sant Sadurní-1 well.

The Escitian-lowermost Anisian (Buntsandstein magnafacies) succession is basically constituted by continental clastics grading from base to top from conglomerates to red sandstones and lutites. The Anisian-Ladinian (Muschelkalk magnafacies) succession is subdivided in the region in three main assemblages: a lower succession of marine carbonates (Mu1), a middle succession mainly constituted by red beds and evaporites (Mu2) and a third and upper one also constituted by marine carbonate

deposits (Mu3). This succession is overlaid by the Carnian-Norian (Keuper magnafacies) succession consisting of tidal-flat and sabkha fine detrital and evaporite deposits (Marzo, 1981; Virgili *et al.*, 1983; Mercedes-Martín *et al.*, 2013) (Figure 1.21). In the area of study, these stratigraphic units are well exposed in the Miramar-Gaià Domain (Figures 1.20 and 1.25). The Triassic succession ends with a 70 m thick uppermost unit of Triassic dolomites.



Figure 1.25. Triassic outcrops in the Gaià-Montmell High. S_0 indicates bedding orientation **A)** Quartz clast-rich conglomerates and red lutites Lower Buntsandstein facies; **B)** Quartz clast-rich Lower Buntsandstein conglomerate facies; **C)** Fine laminated Lower Muschelkalk (Mu1) marine carbonate facies; **D)** Deformed (see folds in the upper left corner of the image) Middle Muschelkalk (Mu2) red-beds and evaporitic facies; **E)** Foliated and faulted Upper Muschelkalk (Mu3) marine carbonate facies; **F)** Keuper fine detrital and evaporite facies.

Jurassic-Cretaceous successions

The Jurassic-Cretaceous successions only occur in the Montmell-Garraf Basin area, which includes the Montmell Domain, the southwestern end of the Vallès-Penedès Basin, the Garraf High and some adjacent offshore areas (Figure 1.22). From bottom to top, the sequence consists of a 300 m thick unit of Lower-Middle Jurassic dolomitic breccias followed by a 1200 m thick succession of shallow marine limestones, dolomites, and shales of Late Jurassic (Oxfordian) - Early Cretaceous age (Salas, 1987; Salas and Casas, 1993; Salas *et al.*, 2001; Albrich *et al.*, 2006). In terms of subsidence and sedimentation rates, the first hints of extensional activity did not start until the Late Jurassic. Subsequently, Upper Oxfordian to Lower Valanginian thick carbonate-dominated successions were deposited in the Montmell-Garraf Basin (Figure 1.26).

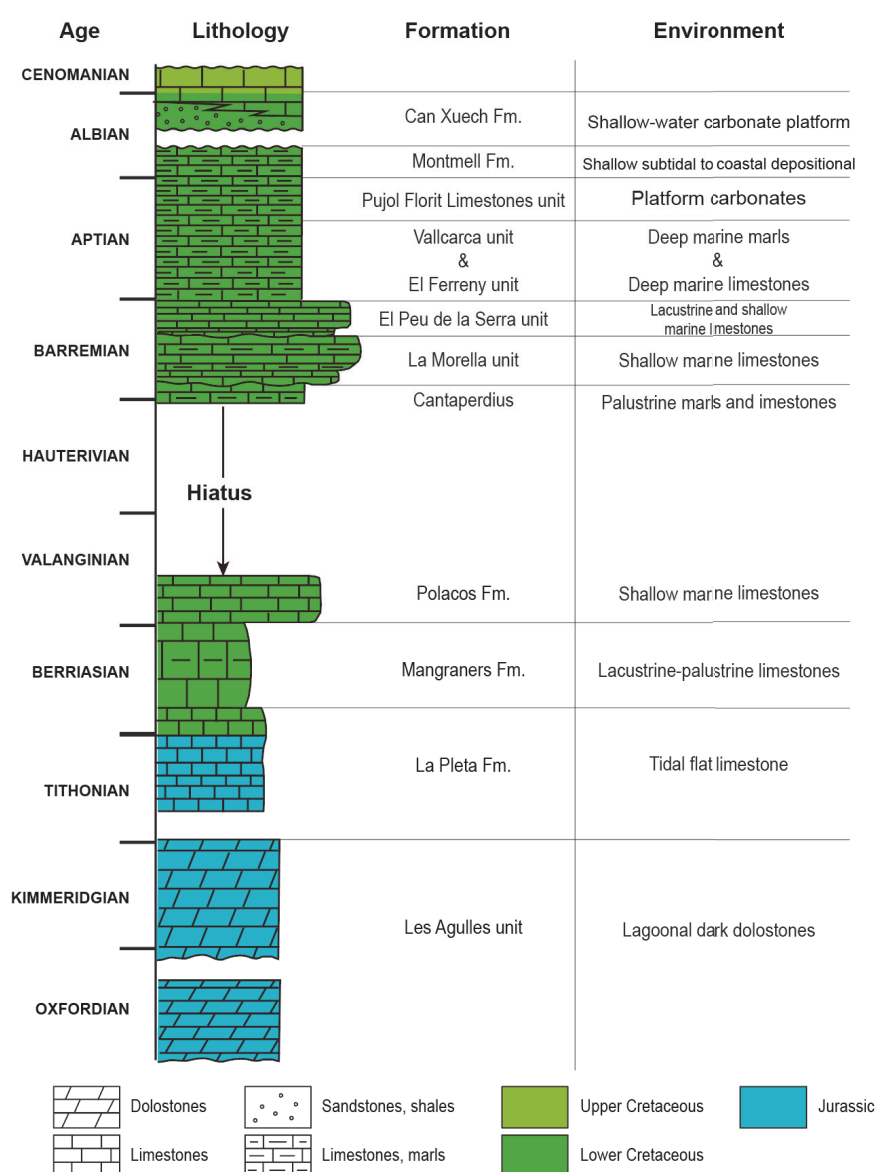


Figure 1.26. Chrono-lithostratigraphic diagram showing the Upper Jurassic-Lower Cretaceous succession recognized in the Montmell-Garraf Basin (compiled from Salas *et al.* 2001, Moreno-Bedmar *et al.*, 2017 and Martín-Closas *et al.*, 2021).

In the study area, the Valanginian shows a constant thickness, which may indicate that this unit was deposited over a planar extensional ramp (McClay, 1995; Withjack and Schlische, 2006; Ferrer *et al.*, 2016). This fault corresponds to the breakaway fault of the extensional system, limit that has been related to the Montmell-Vallès Fault System (Marín *et al.*, 2021). Middle/Late Valanginian to Hauterivian strata are absent in the Montmell-Garraff Basin therefore, Barremian sediments paraconformably overlay the preserved Lower Valanginian record (Figure 1.26). This transgressive Neocomian hiatus is regionally recognized and has been interpreted either as a phase of low subsidence and relative tectonic quiescence (Anadón *et al.*, 1979; Salas *et al.*, 2001), or as related to a post-Late Jurassic-early Valanginian lower thermal subsidence stage. From Barremian on, subsidence rates increased in the Montmell-Garraff Basin up to the Early Albian. During this period, shallow marine carbonates were deposited with significant thickness variations in the Montmell Domain. The absence of Jurassic to Cretaceous sediments in the Miramar-Gaià Domain indicates a hiatus scenario controlled by the presence of a paleo-structural high to the NW of the Montmell Fault (Ebro High, Figure 1.24) (Salas *et al.*, 2020).

Jurassic and Cretaceous rocks are thoroughly connected to the rifting processes that characterized the evolution of the Iberian Rift System during this time span, leading to the development of numerous extensional sub-basins (Anadón *et al.*, 1979; Salas, 1987). Accordingly, the Upper Albian to Cenomanian succession of fluvial and shallow marine carbonates and clastics, which corresponds to the youngest Mesozoic record preserved in the Montmell Domain and the Garraf High (Esteban, 1973; Salas, 1987; Salas *et al.*, 2001), would represent the transition to post-rift conditions setting the stage for later Paleogene compressional tectonics and foreland basin development.

1.4.2.3. Paleogene stratigraphic record

The Paleogene stratigraphy reflects the change of the tectonic situation from the Mesozoic rift basin sedimentation into the development of the basin fill of the Ebro Foreland Basin. In the study area, the preserved Paleogene successions are restricted to the Miramar-Gaià Domain and the southeast margin of the Ebro Basin. In the Miramar-Gaià Domain, the thin Mesozoic cover is unconformably overlain by Paleocene (Thanetian) to Lower Eocene (Ypresian) continental and marine sediments (Ferrer, 1971; Anadón, 1978; Colombo, 1986), whereas a more complete succession including up to Lower Oligocene deposits occurs at the southeast margin of the Ebro Basin. As previously indicated, Paleogene rocks were either not deposited or not preserved in the Montmell Domain (Figures 1.20 and 1.21).

In the study area, Paleogene sediments represent the pre and the syn-tectonic fill of the Ebro Foreland Basin, and they vary from marine to continental facies. In the northwestern part of the Ebro Basin, this succession reaches a thickness of up to 1.5 km, although it tends to thin toward the CCR margin (Barberà *et al.*, 2001). From the Paleocene to the upper Eocene, the Ebro Basin was connected to the Atlantic, allowing for marine sedimentation, particularly in the basin's central and northern regions

(Serra Kiel *et al.*, 2003; Garcés *et al.*, 2020). However, by the late Eocene (late Priabonian), marine connections were severely restricted, and the basin became endorheic leading finally to the exclusive deposition of alluvial-fan and fluvial-fan deposits as well as lacustrine carbonates and evaporites (Reguant, 1967; Pueyo, 1975; Colombo, 1980; Benzaquen *et al.*, 1972a; Cabrera and Colombo, 1986; Anadón *et al.*, 1987; Anadón *et al.*, 1989; Colldeforns *et al.*, 1994b).

Colldeforns *et al.* (1994a and b) split the Paleogene record in the study area into four lithostratigraphic assemblages: 1) a basal assemblage encompassing the Mediona and the Orpí formations; 2) the Pontils-Cornudella Group; 3) the Santa Maria Group; and 4) the Barberà-Anoia Group, the basal part of which is a lateral equivalent of the Santa Maria Group towards the northeast. A schematic summary of these four assemblages is illustrated by the chrono-lithostratigraphic chart of Figure 1.27. Images of the Paleogene lithologies present in the central southeastern margin of the Ebro Basin in the Vallespinosa Cabra del Camp sectors are shown in Figure 1.28.

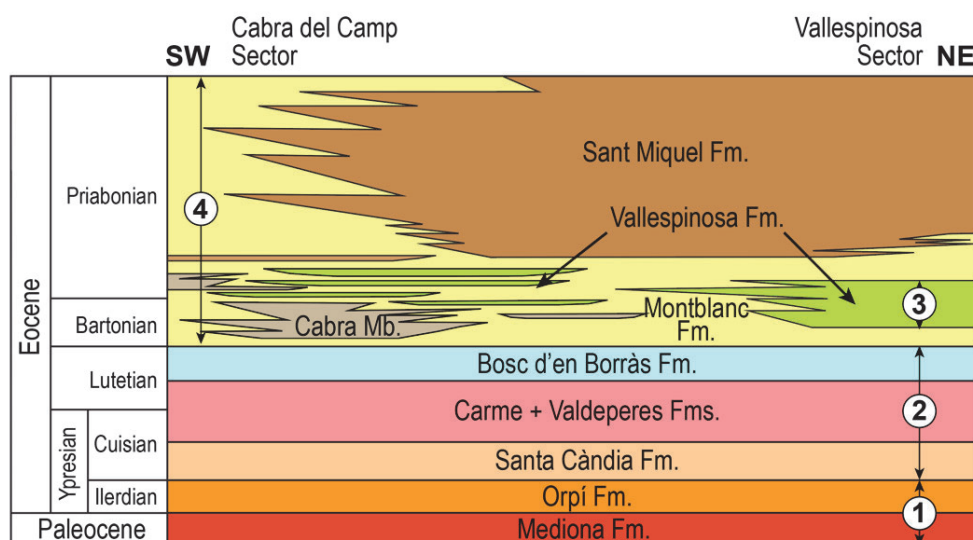


Figure 1.27. Not-to-scale schematic chrono-lithostratigraphic panel for the Paleocene-Eocene units outcropping between Vallespinosa and Cabra del Camp towns (see Figure 1.20 for location). Numbers in the panel indicate the four major lithostratigraphic assemblages defined in the area by Colldeforns *et al.* (1994a and b): **1)** basal continental unit (Mediona Fm.) and a lower marine unit (Orpí Fm.); **2)** Pontils-Cornudella Group; **3)** Santa Maria Group, and **4)** Barberà-Anoia Group.

The lowermost assemblage (label 1 in Figure 1.27) is present in the Miramar-Gaià Domain and the northwestern limb of the Carme-Cabra Anticline (Figure 1.20). It starts with the Thanethian Mediona Fm. (Anadón, 1978 a and b), a discontinuous continental unit constituted by alluvial mudstones affected by intense pedogenic processes. This unit paraconformably overlays the Triassic cover and is in turn overlaid by the marine lower Ypresian (Ilerdian) Orpí Fm. (Figure 1.28A), which is mainly made up by often-dolomitized Alveolina limestones deposited in shallow carbonate platform environments (Ferrer, 1971; Anadón, 1978 a and b; Anadón *et al.*, 1979).

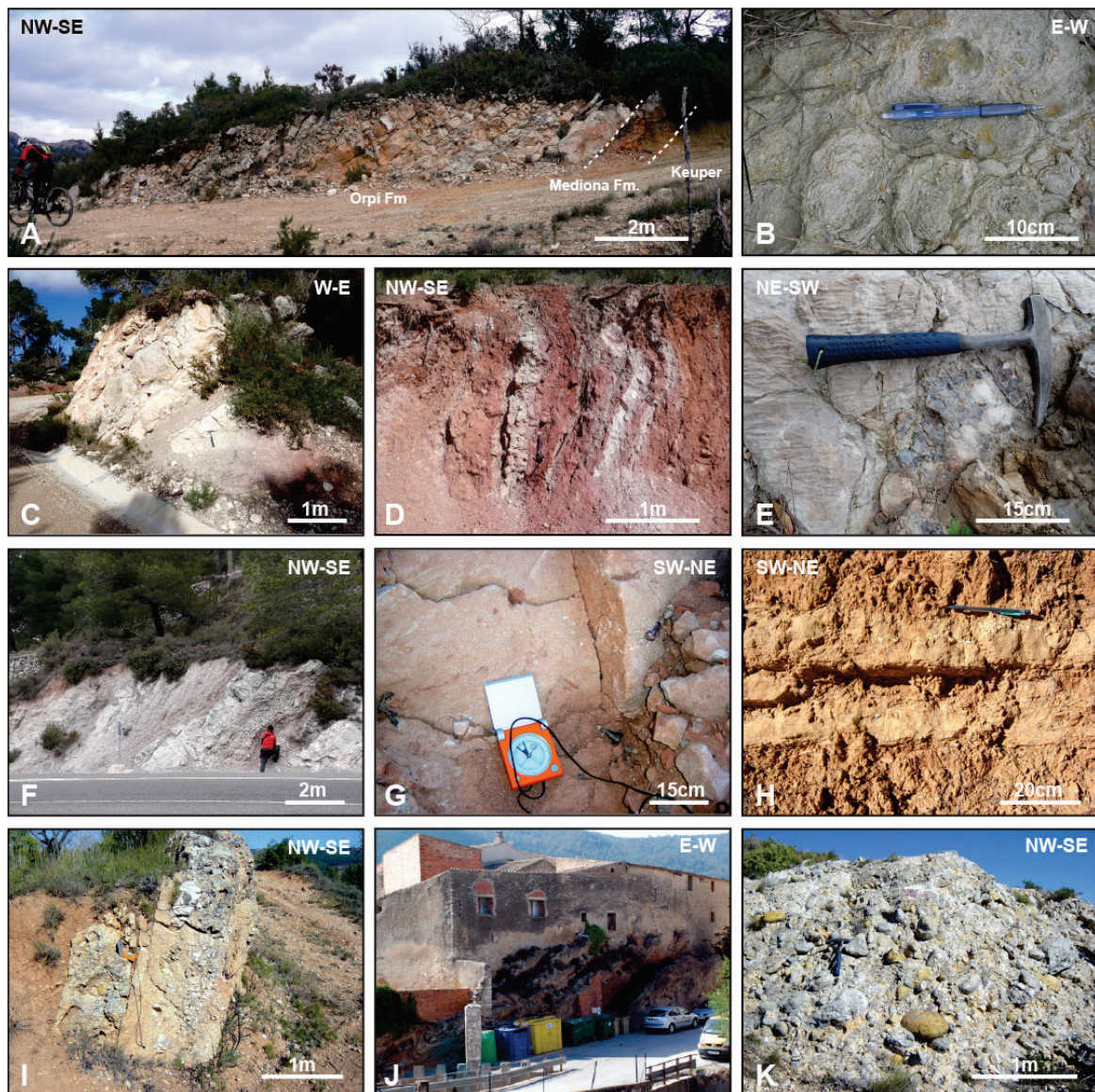


Figure 1.28. Paleogene outcrops of the central southeastern margin of the Ebro Basin in the Cabra-Vallespinosa area. **A)** Mediona and Orpi formations (non-marine and marine carbonatic basal succession) on top of Upper Triassic Keuper; **B)** Mediona Fm., continental unit constituted by alluvial mudstones affected by intense pedogenic processes; **C)** Lacustrine limestones alternating with versicoloured mudstones of the Santa Cándia Fm.; **D)** Red mudstones with minor sandstone and carbonate bed intercalations of the Carme Fm.; **E)** Sulphate evaporites and lacustrine carbonates of the Valdeperes Fm.; **F)** Lacustrine and palustrine limestones with interbedded marls and cherts bearing beds of the Bosc d'en Borràs Fm.; **G)** Shallow marine fine-grained sandstones of the Vallespinosa Fm.; **H)** Red beds of the Montblanc Fm.; **I)** Cabra del Camp Mb. verticalized bed (Montblanc Fm.); **J)** Inverted beds of the Cabra del Camp Mb. (Montblanc Fm.); **K)** Sant Miquel del Montclar massive conglomerates with centimetric to decimetric carbonate clasts.

The Pontils-Cornudella Group (label 2 in Figure 1.27) (Anadón, 1978 a and b; Anadón *et al.*, 1979, 1983, 1992; Colombo, 1980, 1986, Colldeforns *et al.*, 1994b) encompasses upper Ypresian to Lutetian in age non-marine alluvial and lacustrine sediments. The lowermost part of this assemblage is also present in the Miramar-Gaià Domain. From bottom to top, four stratigraphic formations have been

distinguished in this group (Anadón, 1978): Santa Càndia Fm. (lacustrine limestones alternating with versicoloured mudstones) (Figure 1.28C); Carme Fm. (mud flat plain red mudstones with minor sandstone and carbonate bed intercalations) (Figure 1.28D); Valdeperes Fm. (sulphate evaporites and lacustrine carbonates) (Figure 1.28E); and finally the Bosc d'en Borràs Fm. (lacustrine and palustrine limestones with interbedded marls and cherts bearing beds, which grade towards the southwest to distal alluvial mudstones) (Figure 1.28F).

The overlying Bartonian and Priabonian sequences of the Santa Maria and Barberà-Anoia groups (labels 3 and 4 respectively in Figure 1.27) are preserved in the northwest limb of the Carme-Cabra Anticline (Figure 1.20). In the study area, the Santa Maria Group embraces a variety of shallow marine and transitional facies (i.e., deltaic, fan-deltaic conglomerates, sandstones, coral-bearing limestones, and marlstones with bioclastic sandstone intercalations integrated in the Vallespinosa Fm. (Figure 1.28G) (Ferrer, 1971; Anadón and Marzo, 1986; Colldeforns *et al.*, 1994a; Serra Kiel *et al.*, 2003).

On the other hand, the Barberà-Anoia Group (Colombo, 1980, 1986, Colldeforns, 1994a) comprises the Bartonian to Early Oligocene alluvial and lacustrine deposits that crop out in the area. It includes up to six different formations: Montblanc, Sant Miquel, Sarral, Rocafort, Rauric and Santa Coloma (Colombo, 1980, 1986; Colldeforns *et al.*, 1994a and b) (Figure 1.27). The Montblanc Fm. (Figure 1.28H) is made up of distal alluvial red beds that interfinger with the marine sandstones of the Vallespinosa Fm. in its lower part. To the southwest instead, discontinuous alluvial conglomerate intercalations of the Cabra del Camp Mb. (Colldeforns 1994a) (Figure 1.28I and J) occur showing a maximum thickness of around 200 m in the Cabra del Camp area (Figure 1.20). The Sant Miquel Fm. (Colombo, 1980, 1986) corresponds to a thick succession of proximal alluvial fan conglomerates (Figure 1.28K) that unconformably overlay the marine sediments of the Santa Maria Group (Priabonian Riu de Boix Fm.) (Anadón *et al.*, 1986; Colldeforns *et al.*, 1994a). Towards the north and northeast, these conglomerates laterally change to late Priabonian to early Oligocene successions. These ones include the lacustrine gypsums, carbonates, and marls of the Sarral and Rocafort formations, the fluvial and lacustrine shales, marls, and lenticular conglomerates of the Rauric Fm. and the lacustrine marl and gypsum beds of the Santa Coloma Fm. (Benzaquen *et al.*, 1972a; Colombo, 1980, 1986, Colldeforns *et al.*, 1994a and b).

The ages of these marine and non-marine lithostratigraphic successions were initially established and subsequently refined by various authors through the analysis of biostratigraphic assemblages and biozones (Ferrer, 1971; Anadón, 1978 a and b; Anadón and Feist, 1981; Anadón *et al.*, 1983, 1987, 1992; Agustí *et al.*, 1987; Feist *et al.*, 1994; Serra-Kiel *et al.*, 2003; Sanjuan *et al.*, 2014; Tosal *et al.*, 2019; Minwer-Barakat *et al.*, 2023). Moreover, magnetostratigraphic studies conducted in nearby areas have provided additional constraints, significantly enhancing the precision of these biostratigraphic age determinations

(Barberà 1999; Barberà, 1999, Barberà *et al.*, 2001; Beamud *et al.*, 2012; Costa *et al.*, 2010 and 2013; Gomez-Paccard *et al.*, 2011; Garcés *et al.*, 2020; Marín *et al.*, 2025).

1.4.2.4. Neogene succession

The Neogene stratigraphic record in the CCR is closely linked to the extensional tectonics that followed the compressive phase of the Alpine orogeny and affected the region from latest Oligocene to Miocene. During this tectonic phase half-graben basins, tilted blocks and structural culminations developed due to the extensional reactivation of the inherited compressive Paleogene faults. Significant sediment accumulation took place in the onshore half-grabens and in the neighbouring offshore continental margin zones particularly during the Miocene and Pliocene (Bartrina *et al.*, 1992; Roca and Guimerà, 1992; Cabrera and Calvet, 1996).

The lower deposits of the Neogene succession, Miocene in age (Aquitania (?) to late Burdigalian), are dominated by thick alluvial-fan red bed deposits and thin lacustrine successions associated with extensional faulting. These deposits are extensive across the Vallès-Penedès and Baix Penedès basins and reach considerable thicknesses (Cabrera, 1979 and 1981; Agustí *et al.*, 1987; Cabrera and Calvet, 1996). By the late Burdigalian-early Langhian the region experienced several marine transgressive-regressive pulses that lead to the development of a variety of transitional marine to open marine depositional environments, with the deposition of coastal sabkha, carbonate coralgal platform, and siliciclastic fan-delta and bay sequences. This fact reflects the interplay between marine and continental conditions and are well-recorded in the Langhian sequences (Cabrera and Calvet, 1996). From the Serravallian to the Tortonian, the region was still affected by some transgressive-regressive pulses that finally resulted in the retreat of the marine and transitional environments and the larger spreading of the alluvial-fan and fluvial sedimentation during Tortonian times (Cabrera *et al.*, 2004).

In the study area, growth strata geometries in Middle-Upper Miocene sediments were reported in the Marmellar area, located in the hangingwall of the Vallès-Penedès Fault (Baqués *et al.*, 2012), indicating the extensional reactivation of this fault during the Neogene. Lastly, a very significant Messinian erosional surface marks the upper boundary of the Miocene sediments. This erosional surface, formed during the Messinian Salinity Crisis, deeply incised in the Miocene successions as well as in the older rocks of the Paleozoic basement and the Mesozoic and Paleogene cover (Almera, 1894; Gallart, 1981; Corregidor *et al.* 1997).

Pliocene alluvial-fan, fluvial, transitional marine, and open marine sediments were deposited overlying the above-mentioned unconformity in the onshore incised valleys that formed because of the Messinian marine level drop (Almera, 1894; Gallart, 1981; Martinell, 1988; Roca *et al.*, 1999). These deposits would record the final phase of Neogene extension when it was not regionally widespread and it was more localized next to some faults. Alluvial-fan and fluvial Quaternary deposits were deposited mainly as

down-stepped, terraced units whose deposition was largely influenced by the glacioeustatic processes (Gallart, 1981).

1.4.3. Final remarks

The geology of the Catalan Coastal Ranges (CCR) reflects the complex tectonics–sedimentation interactions developed during its Paleozoic to Recent evolution, a fact well recorded in the stratigraphic record.

The tectonic history has been characterized by three major phases since the late Paleozoic:

- Middle-Late Permian to Mesozoic extensional phase.
- Paleogene contractional phase.
- Latest Oligocene to Miocene extensional phase.

This tectonic evolution has significantly influenced the present-day configuration and the deformation of the stratigraphic record in the region.

The Mesozoic rift-related sedimentation, consisting mainly of Triassic to Cretaceous deposits, led to the development of multiple basins and sub-basins, with notable lateral variations in areal extent and thickness of the stratigraphic record. This period was followed by a Paleogene compressional phase, which inverted pre-existing rift structures, contributing to the development of the Catalan Intraplate Chain fold-and-thrust belt. Some structures of this period are still preserved in outcrops of the present extensional structural highs in the central CCR. The final tectonic phase during the Neogene reactivated the Paleogene faults as extensional features, resulting in the formation of the modern-day half-grabens (e.g., Vallès-Penedès and El Camp basins) and the extensional culminations in the area (Garraf, Montmell). This final widespread extensional stage concealed the previous tectonic events and makes difficult their reconstruction.

1.5. Problem approach and methodologies

1.5.1. Problem approach

This methodology section explains the different techniques that have been employed to investigate the stratigraphic and structural characteristics of the study area. As stated in the Motivation Section (Section 1.1), the performed research aims to answer a set of key questions related to the tectonic evolution, deformation history, and stratigraphic record in the central Catalan Coastal Ranges. The methodology applied in this thesis has been planned as a fit-for-purpose approach to achieve this objective. Accordingly, the research tasks have been split in three different phases, each one answering the partial objectives and covered in each of the publications included in this dissertation (Figure 1.29).

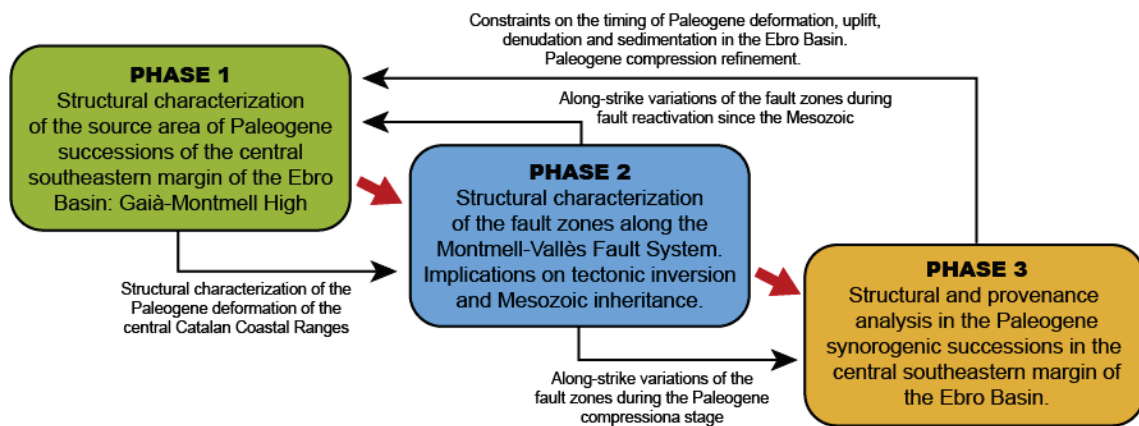


Figure 1.29. Flow diagram showing the three phases that covers the performed research.

The methodology involves a combination of multidisciplinary techniques such as field-based geological mapping, the acquisition, processing, and interpretation of magnetotelluric data, the construction of balanced structural sections and their restoration, magnetostratigraphy along key stratigraphic successions as well as tectono-stratigraphic analysis, and provenance analysis in syn-tectonic strata. The integration of the results of each of these techniques provides insights on the deformation history of the study area, the possibility to constrain the ages of individual tectonic and sedimentary processes and their interactions, and the identification of the source areas controlling the alluvial depositional systems preserved in the studied segment of the southeastern margin of the Ebro Basin. The following section provides a brief description of each of the methodologies and techniques applied in the research.

1.5.2. Methodology and applied techniques

1.5.2.1. Fieldwork

The fieldwork activities conducted in this research encompass several activities such as geological mapping, the collection of structural and stratigraphic data, gathering samples for magnetostratigraphic analysis, and the acquisition of magnetotelluric data. Due to their specific nature, the magnetostratigraphic and magnetotelluric techniques are discussed in detail in separate sections below.

The fieldwork campaigns that have fed the research presented in this dissertation were mainly performed from 2006 to 2010, with some minor complementary activities between 2017 and 2019. These activities principally focussed on the recognition and characterization of the stratigraphic units for the construction of structural cross-sections across the Gaià-Montmell High and the neighbouring areas paying special attention to the central southeastern margin of the Ebro Basin at the Cabra del Camp (Figure 1.30).

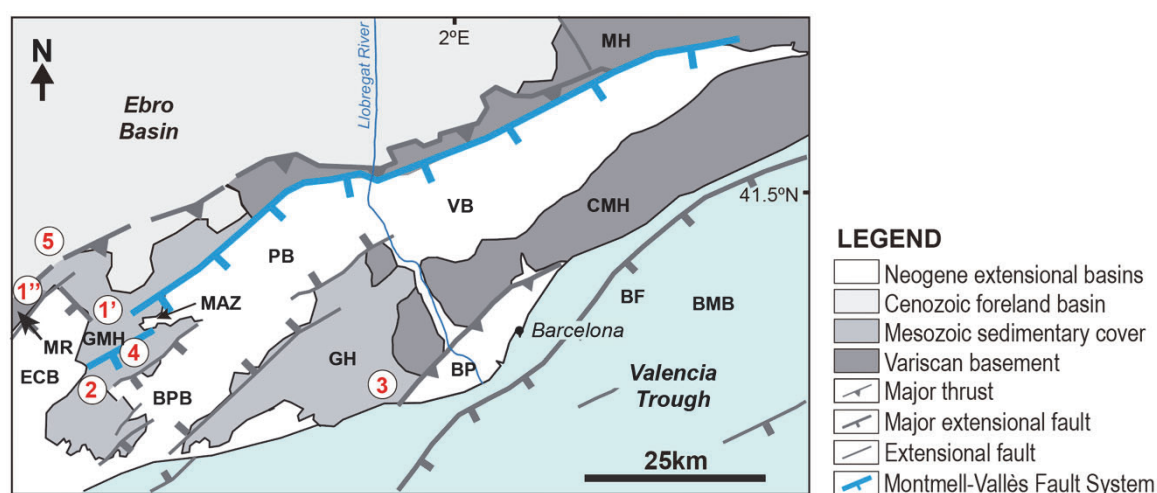


Figure 1.30. Simplified geological map of the central Catalan Coastal Ranges indicating the areas where the stratigraphic recognition and characterization of specific stratigraphic successions and the gathering of structural data have been performed: **1)** Triassic successions in Querol in the centre of the Miramar-Gaià Domain (1') and the Miramar Range (1"); **2)** Lower Cretaceous successions in Coll de Santa Cristina - La Rubiola at the Montmell Domain; **3)** Upper Jurassic-Lower Cretaceous (Early Valanginian) successions; **4)** Upper Jurassic-Lower Cretaceous successions nearby la Juncosa del Montmell town; **5)** Paleogene units preserved both in the southeastern margin of the Ebro Basin between Vallespinosa and Cabra del Camp.

The recognition of the Paleozoic to Cenozoic stratigraphic sequences present in the study area involved the identification of the best outcrops in which the successions are well preserved. The characterization of the Triassic units (i.e., Buntsandstein, Muschelkalk and Keuper magnafacies) was performed in two areas, the surroundings of Querol in the centre of the Miramar-Gaià Domain and in Miramar Range (label 1, Figure 1.30). The stratigraphic succession cropping out in the Coll de Santa Cristina - La

Rubiola at the Montmell Domain (label 2, Figure 1.30) was used to characterize the Lower Cretaceous units, which were previously defined by Salas (1987). However, the poor preservation of these outcrops did not allow a complete identification, fact overcome by the more complete Upper Jurassic-Lower Cretaceous (Early Valanginian) succession located in the La Pleta succession - Penya Ginesta in the Garraf High (label 3, Figure 1.30). These stratigraphic successions were later compared and completed with the one of same age cropping out nearby la Juncosa del Montmell town in the Montmell Domain (label 4, Figure 1.30). Moreover, the Paleogene units were studied in two different areas: the incomplete preserved (i.e., highly eroded) sequences in the Miramar-Gaià Domain, and the roughly complete series outcropping in the southeastern margin of the Ebro Basin between Vallespinosa and Cabra del Camp (label 5, Figure 1.30).

Geological mapping was systemically conducted during the stratigraphic recognition and its characterization thru positioning the cartographic limits of stratigraphic units, faults and, when present, unconformities. Moreover, gathering of approximately 1500 structural measurements (e.g., dip and dip direction of beds, faults, and kinematic indicators) mainly allocated along the Gaià-Montmell High, the Baix Penedès Basin and the southeastern margin of the Ebro Basin (Figure 1.30), paleocurrent directions, landscape observations and correlations, and gathering rock samples for their later recognition using thin sections were also performed. All field observations and their spatial relationships were later processed, analysed, and interpreted at outcrop and regional scale for their integration.

In terms of specific material and gear, fieldwork included the use of geological tools such as hammer, compass, and hand magnifier, a GPS device, mapping boards to support topographic maps and orthophotograph, as well as digital elevation models (DEM). Cartographic base maps included 1:5.000 and 1:10.000 topographic maps and orthophotographs covering both the Gaià-Montmell High and the central southeaster margin of the Ebro Basin. These were provided by the Institut Cartogràfic i Geològic de Catalunya and were used for an accurate location of the mapping features. Moreover, in the last fieldwork period, which involved mapping refinements and enhancements performed between years 2017 and 2019, digital geological applications such as Field Move® and Clino® (Emerson, 2024) were used to complete the databases. Detailed field notes, sketches, and photographs were systematically done to create an accurate archive.

1.5.2.2. Magnetotelluric data

The magnetotelluric method (MT) has been used to determine the electrical properties of the upper crust across the Gaià-Montmell High (Figure 1.31) and to attempt to constrain the deep structure when possible. MT is an electromagnetic geophysical method based on the simultaneous measurement of naturally occurring electric and magnetic field variations on Earth's surface (Chave and Jones, 2012). The relationship between electric and magnetic fields at different periods is therefore used to define

the impedance tensor, whose components provide information about the electrical resistivity distribution at depth (Simpson and Bahr, 2005).

This technique is highly sensitive to conductive bodies that, in turn, may be associated with the presence of specific minerals, partial melts, or fluids at depth. Considering the marked lithological differences between the stratigraphic sequences across the Gaià-Montmell Section, the main goals of the MT survey, modelling and interpretation in this study have been: 1) to identify the geometry of boundaries between the primary stratigraphic and structural units, and 2) to detect basement conductivity anomalies that could indicate the presence of damage zones and fluid circulation, because of the region's complex tectonic evolution.

In the present research, the MT has been used to both constrain and validate the structure of the Gaià-Montmell High. Nineteen MT soundings with recording times ranging from 8 to 12 hours were acquired along the Gaià-Montmell High (Figure 1.31). Data acquisition and time series processing were performed in collaboration with the Electromagnetic and Seismic Exploration Group of the University of Barcelona. Time series processing used the Egbert and Booker (1986) method and applied remote reference when possible. Apparent resistivity and phase resulting curves cover periods from 0.001 to 1 seconds. A dimensionality analysis was later performed using the WALDIM code (Martí *et al.*, 2009a) that is based on the invariant rotation parameters of the impedance tensor. Once the analysis of the MT model was performed, the observed resistivity values of the basement were compared to two additional parametric MT soundings acquired 30 km southwest of the study area in the Prades High on top of Paleozoic rocks. These two MT soundings enhanced the understanding and helped on the analysis of the geoelectric behaviour of the basement in the study area. Their results were later compared to other studies performed in other locations in the northeastern Iberian Peninsula (e.g., Muñoz *et al.*, 2008; Ledo *et al.*, 1998; Campanyà *et al.*, 2018; Martí *et al.*, 2009b).

The results of the analysis and interpretations of the MT data and models carried out by the Electromagnetic and Seismic Exploration Group of the University of Barcelona are presented as part of the results of the first publication included the Chapter 2 of this dissertation.

1.5.2.3. Geological cross-section construction and structural restoration

The present research includes the construction of three structural cross-sections at key locations of the study area in order to cover specific objectives of the research: the Gaià-Montmell Section, the Marmellar Section, and the Cabra Section (Figure 1.31). These sections have been constructed based on the data collected in the field during the geological mapping (e.g., cartographic traces, bedding and fault attitudes), as well as the analysis of available geological maps and observed thicknesses of the sedimentary units. When the stratigraphic units do not crop out in the studied area, thicknesses have

been estimated from the regional reviews from literature as well as the information of the Senant-1, Sant Sadurní-1, and Martorell-1 wells (Lanaja, 1987) (Figure 1.32).

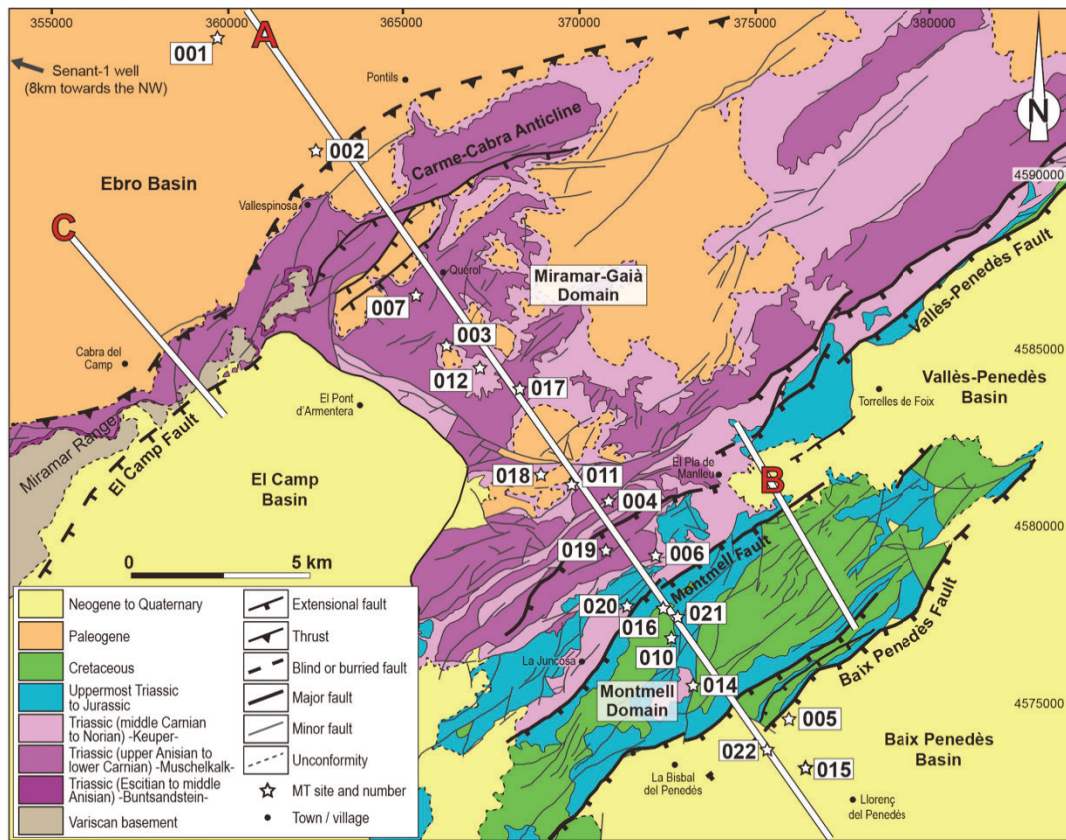


Figure 1.31. Geological map of the Gaià-Montmell High and surrounding areas (modified from ICC, 2017). The map includes the location of the constructed sections: **A)** Gaià-Montmell Section; **B)** Marmellar Section and **C)** Cabra Section. The map also shows the acquired parametric MT soundings along the Gaià-Montmell Section.

The Gaià-Montmell Section is approximately 40 km long and, from NW to SE, runs from the undeformed Ebro Basin to the Baix Penedès Basin across the Gaià-Montmell High (section A in Figure 1.3.2). It has been constructed using well and field data being later constrained by a 2D MT model. The Marmellar sections is approximately 7 km long and covers the relay area between the southern end of the Vallès-Penedès Fault at the NE edge of the Montmell Domain. The Cabra Section instead crosses the SE margin of the Ebro Basin and the NW frontal structure of the Cabra-Carme Anticline (hereinafter CCR) at the locality of Cabra del Camp. The orientation of the three sections is approximately orthogonal to the predominant NE-SW trend of the Alpine structures of the CCR. In the specific case of the Gaià-Montmell Section, the geometry of the Baix Penedès Basin has been also constrained by the gravimetric studies performed by Hernández and Casas (1985) and Casas and Permanyer (1991). The construction of the structural sections assumes in cases projection of dip data. This exercise has been performed defining cylindrical domains and using the kink-band method in the 2DMove software (Emerson, 2024).

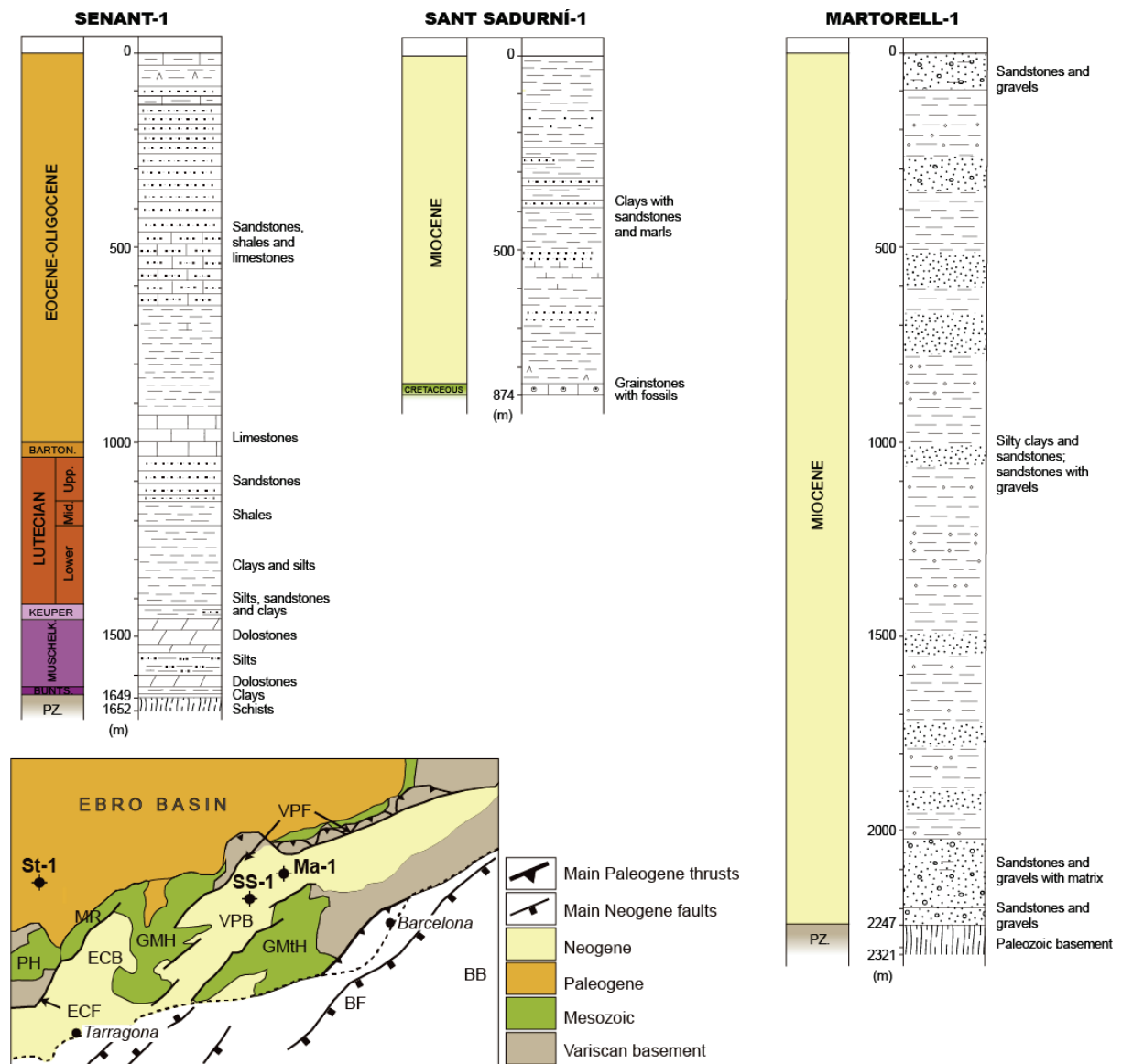


Figure 1.32. Senant-1, Sant Sadurní-1 and Martorell-1 boreholes (St-1, SS-1 and Ma-1 respectively in the map) used during the construction of the structural sections and tectonostratigraphic maps (modified from Lanaja, 1987). From west to east, **PH**: Prades High; **MR**: Miramar Range; **ECB**: El Camp Basin; **ECF**: El Camp Fault; **GMH**: Gaià-Montmell High; **VPB**: Vallès-Penedès Basin; **VPF**: Vallès-Penedès Fault; **GMtH**: Garraf-Montnegre High; **BF**: Barcelona Fault; **BB**: Barcelona Basin. In the stratigraphic columns, **PZ**: Paleozoic

Palinspastic sequential restorations of the Gaià-Montmell Section have been carried out to validate the structural interpretation from both geometric and kinematic perspectives. These restorations consider the contribution of inherited faults and syn-tectonic sedimentation and include the integration of the results from the magnetostratigraphic study as well as regional tectonic constraints. The reconstructions illustrate the tectonic evolution of the area and estimate the amount and direction of the deformation.

The structural restoration was performed using a geomechanical approach performed using Dynel2D® from SLB. During the restorations, the line-length unfold method (Dahlstrom, 1969), which straightens

the beds while maintaining constant the line length, was considered. Because the sections were constructed using the kink method, layer thicknesses remained constant during the unfolding process. This process allows calculating shortening and stretching value for each of the restored paleo-steps as well as fault slip and accumulated stresses.

During the different steps and phases indicated in the research approach, an initial structural restoration of the Gaià-Montmell Section including three tectonic stages from the Mesozoic to the present-day is presented in the results of Chapter 2.1. Additionally, the work presented in Chapter 2.3 allowed the refinement of the structural restoration with two additional time-steps during the compressional stage affecting the area during the Paleogene in the central Catalan Coastal Ranges.

1.5.2.4. Magnetostratigraphy

Magnetostratigraphic studies are divided into two different phases: the rock sampling and analytical laboratory procedure. The analysis aims for an accurate refinement of the age of the Paleogene succession in the central southeastern margin of the Ebro Basin to constrain the timing of the synorogenic sedimentation. The sampling was carried out north and northwest of Vallespinosa where a relatively continuous northwest-dipping Paleogene succession (Pontils, Santa Maria and Barberà-Anoia groups) exists. The sampled section consists of 238 measurement sites along ~1,430m of sedimentary record, which yields an average sampling resolution of 6m/sample. Rock sampling focused on mudstones, limestones, and fine-grained sandstones, considering coarser lithologies are less proficient for recording the geomagnetic field. Electrical and petrol power drills equipped with diamond core bits cooled with water were used to obtain 2 samples per station. Samples were in situ oriented with a magnetic compass coupled with an orienting device with clinometer to have a coordinate system to refer the paleomagnetic vector obtained in the later laboratory labour, which was carried out by the specialists from the Paleomagnetic Laboratory of Barcelona (CCiTUB and GEO3BCN CSIC).

Laboratory treatment consisted in stepwise thermal demagnetization and subsequent measurement of the Natural Remanent Magnetization (NRM). Samples were heated in an MMTD-80 thermal demagnetizer (Magnetic Measurements Ltd.) with a residual field less than 10nT. The NRM was measured in a superconducting rock magnetometer (2G Enterprises). The magnetic noise in the superconducting rock magnetometer is around $1 \cdot 10^{-6}$ A/m, well below the intensity of the samples. Stepwise thermal demagnetization was performed in 14 to 18 temperature steps, from 100°C up to 520°C in limestones and grey mudstones and up to 680-690°C in red mudstones and fine-grained sandstones. Magnetic susceptibility was measured after each demagnetization step with a kappabridge KLY2 (Geofyzika Brno) to monitor the undesired formation of magnetic minerals upon heating, since it can be detected by a sharp increase in magnetic susceptibility. Stable Characteristic Remanent Magnetization (ChRM) directions were calculated by means of Principal Component Analysis

(Kirschvink, 1980) after visual inspection of demagnetization diagrams using the Paldir software (University of Utrecht).

The analysis of the results was carried out together with the magnetostratigraphy specialists from the Paleomagnetic Laboratory of Barcelona (CCiTUB and GEO3BCN CSIC), which were compared with established paleomagnetic reference data to determine the age of the sampled succession and therefore establish their paleomagnetic polarity and put in context with the structural evolution implications of the area. The results were later compared and integrated with key fossil sites reported, which provided a detailed constraint on the age of the sampled rocks.

1.5.2.5. Provenance analysis

Provenance analysis was conducted on key sedimentary units along the margin of the Ebro Basin. This analysis aims to determine the source materials of the sediments (i.e., source area), provides insights into past sediment transport processes and directions, and supports the reconstruction of the areal distribution of lithofacies. Additionally, from a tectonostratigraphic perspective, this analysis links sediment sources to the geodynamic evolution of the region. The structural and genetic characteristics of synorogenic strata are closely associated to tectonic and orogenic processes, which include thrusting, uplift, exhumation, and erosion. Consequently, studying these synorogenic (or syn-tectonic) strata enables paleo-reconstructions and offers insights into the timing of specific phases of tectonic activity, sediment transport pathways, paleoenvironments and erosion rates in the orogenic-related regions.

Two different tasks were carried out for the provenance analysis in this research. First, the sampling of clasts from synorogenic conglomerates and sandstones collected during the different fieldwork campaigns (Figure 1.33). This sampling was followed by the analysis of the clast fossil content in thin sections, which was carried out by specialists from the Sedimentary Geology Research Group of the University of Barcelona. Second, the measurements of paleocurrent indicators (e.g., paleochannels axis, sedimentary base marks) also carried out during the fieldwork.

Up to fourteen samples were gathered through the Paleogene synorogenic succession along the Ebro Basin margin between Cabra del Camp and Vallespinosa towns, then followed by their analysis using thin sections made in the Thin-Section Service of the University of Barcelona.

Thin sections were examined under an optical microscope in the Petrology Laboratory of the Mineralogy, Petrology, and Applied Geology Department, University of Barcelona, to identify paleontological content within individual conglomerate clasts and in some cases their associated matrix and sandstones. High-resolution imaging and the use of both transmitted and polarized light aid in discerning structural details, enabling taxonomic classification and identification of fossil species. Considering that certain fossil types are diagnostic of specific geologic periods, their identification provide key information about the ages and environments of the source areas (i.e., specific lithofacies),

allowing determining which areas were exhumed and eroded in the past. The comparison of the clast analysis results with known sedimentary successions of the same age in the Catalan Coastal Ranges allows tracing clasts back to their source units in the orogenic belt (i.e., parent lithologies). The results from a provenance analysis must also account for potential sediment reworking processes, including the cannibalization of older conglomerates. This reworking may occur when previously deposited sediments are later uplifted and exhumed, subsequently being redeposited as younger strata by secondary erosion-transport processes. Provenance analysis also integrates paleocurrent indicators (i.e., base marks, channels axis) in order to determine the relative location of source areas. Figure 1.33 shows some examples of sampled clasts from the Cabra de Camp Mb. (Montblanc Fm.) in the Cabra del Camp town surroundings as well as outcrops where paleocurrent directions were measured.

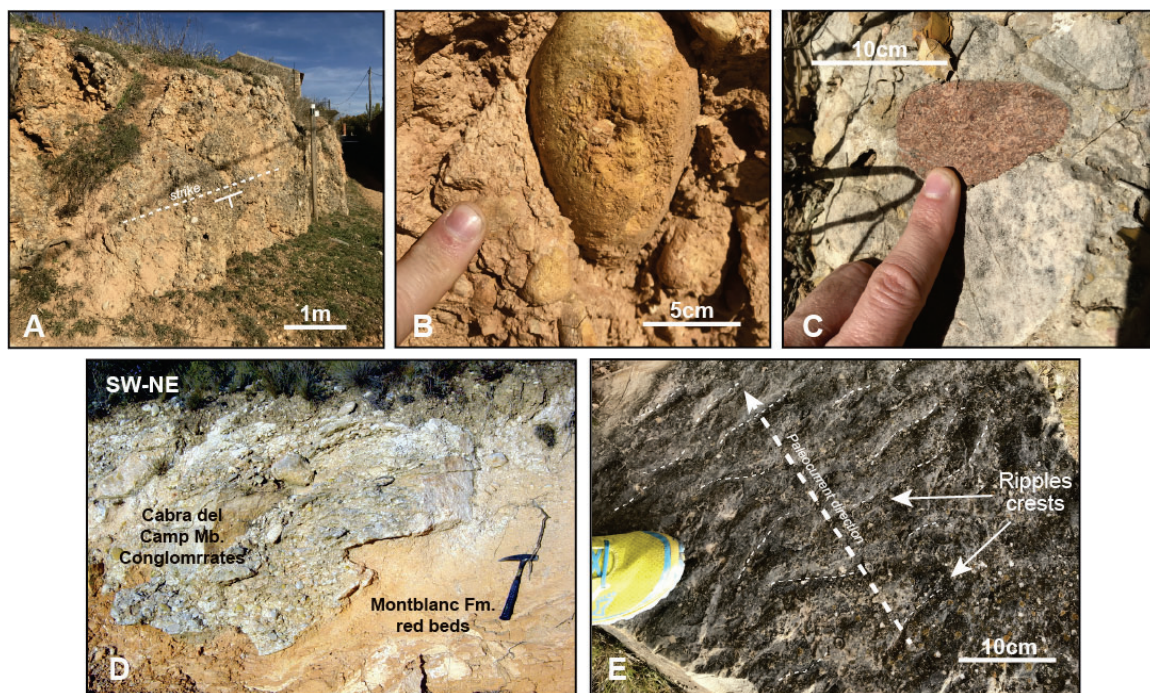


Figure 1.33. **A)** Cabra de Camp Mb. (Montblanc Fm.) verticalized conglomerate bar; **B)** Example of yellowish centimetric Mesozoic bioclastic clast sampled from the Cabra del Camp Mb.; **C)** Example of Mesozoic reddish centimetric bioclastic clast sampled from the Cabra del Camp Mb.; **D)** Paleochannel bottom outcrop in conglomerates of the Cabra del Camp Mb. used for paleocurrent measurements; **E)** Ripples at the bed top of marine-continental transitional facies. Dashed white arrow indicates the paleocurrent direction.

1.5.3. Concluding remarks on the applied techniques

This research has applied a detailed approach and workflow designed to investigate the stratigraphic and tectonic evolution of the central Catalan Coastal Ranges combining the methodologies previously described. The multi-disciplinary approach, including field-based geological mapping, structural section construction and restoration supported by magnetotelluric data clast provenance analysis and magnetostratigraphic dating, allows together for a comprehensive analysis of the deformation history,

focussing on the timing of key sedimentary and tectonic processes. This in turn allows the characterization of the source areas responsible for deposits in the southeastern margin of the Ebro Basin during the compressional phase that affected the area during the Paleogene. Additionally, the integrated methodology also offers a multi-scale perspective that connects surface and subsurface observations, thus illustrating the tectonostratigraphic development of the region.

Provenance analysis is considered a central part of the workflow. It incorporates fossil identification and paleocurrent measurements to determine source-to-sink mechanisms. This approach links clasts in synorogenic conglomerates to specific parent lithologies, highlighting how the compressional tectonic evolution influenced on the sedimentary deposition patterns. By employing this approach, the research addresses the stated objectives and key research questions outlined in the motivation of this thesis.

CHAPTER 2

FIRST PUBLICATION

Structure and Mesozoic structural inheritance in the Gaià-Montmell High

Marín, M., Roca, E., Marcuello, A., Cabrera, L. and Ferrer, O., 2021. Mesozoic structural inheritance in the Cenozoic evolution of the central Catalan Coastal Ranges (western Mediterranean): Structural and magnetotelluric analysis in the Gaià-Montmell High. *Tectonophysics*, 814, p.228970.

DOI: <https://doi.org/10.1016/j.tecto.2021.228970>

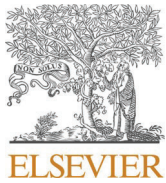
Journal metrics (data from Journal Citation Report for 2021):

- Journal Impact Factor: **3.660**
- Journal Impact Factor excluding self-citations: **3.334**
- Category: **Geochemistry and Geophysics**
- Position: **32/87** (based on category and year of publication)
- Quartil: **Q2**

The main objective of the first paper included in this dissertation (Marín *et al.*, 2021) was to explore the tectonic evolution of the source area(s) of the synorogenic successions preserved in the central southeastern margin of the Ebro Basin. This source area corresponds to the Gaià-Montmell High (GMH) and the neighbouring areas in the central CCR. The study focusses on the role of pre-existing Mesozoic structures during the later Cenozoic evolution of the area. In the present-day configuration of the CCR, the GMH represents a Neogene structural high that preserves Mesozoic and Paleogene successions, the stratigraphic and structural records of which are key for the study. The results of the work illustrate the structural configuration and the evolution of the upper crust across the GMH and highlights the structural inheritance played by the Mesozoic Montmell Fault throughout the Cenozoic, including two tectonic inversion phases.

Data and supplementary material can be found in the following link: [data and supplementary material](#)

[Tectonophysics](#) a journal focussing on original research and reviews in the fields of kinematics, structure, composition, and dynamics of the solid earth at all scales published by Elsevier at Science Direct. The journal encourages submission of papers based on the integration of a multitude of geophysical, geological, geochemical, geodynamic, and geo-tectonic methods.



Mesozoic structural inheritance in the Cenozoic evolution of the central Catalan Coastal Ranges (western Mediterranean): Structural and magnetotelluric analysis in the Gaià-Montmell High

Miquel Marín ^{a,b,*}, Eduard Roca ^b, Alex Marcuello ^b, Lluís Cabrera ^b, Oriol Ferrer ^b

^a Schlumberger, Aachen Technology Center, Ritterstraße 23, 52072 Aachen, Germany

^b Institut de Recerca Geomodels, Departament de Dinàmica de la Terra i de l'Oceà, Universitat de Barcelona, Martí i Franquès s/n, 08028 Barcelona, Spain

ARTICLE INFO

Keywords:

Structural inheritance
Inversion tectonics
Western Mediterranean
Catalan Coastal Ranges
Magnetotellurics
Tectonic evolution

ABSTRACT

The control exerted by the Mesozoic basin configuration on the Cenozoic tectonic evolution of the Catalan Coastal Ranges has been frequently recognized as a key factor to explain its present-day structure. However, details of this structural inheritance and its evolution through geological time is still under discussion. In this work we present two structural cross-sections based on fieldwork, well and magnetotelluric data in order to illustrate the structural styles and tectonic evolution of the Gaià-Montmell High. Here, the Montmell Fault not only constitutes the SW segment of one of the major Neogene faults in the Catalan Coastal Ranges (the Montmell-Vallès Fault System), but also the NW limit of a Late Jurassic-Early Cretaceous extensional basin (the Montmell-Garraf Basin), facts that denote a major role of this fault in the tectonic evolution of the area. The present-day structure of the Gaià-Montmell High resulted, therefore, from two successive episodes of inversion during the Cenozoic. The first one reactivated the Montmell Fault as compressional during the Paleogene. As a result, and among other inversion-related structures, the Gaià-El Camp Thrust developed a major NW-directed basement footwall shortcut. Later on, the previously formed compressional structure during the Paleogene became reactivated as extensional during the Neogene. During this phase, the reactivation of the Montmell Fault looks limited and, hence, the extension is transmitted to the Baix Penedès Fault. The reactivation of the Gaià-El Camp Thrust is also manifest in the development of an array of extensional faults in the backlimb of the Carme-Cabra Anticline that corresponds to the NE-end of El Camp Fault. This episode of negative inversion developed accommodation zones between the four major faults present in the area (Vallès-Penedès, Montmell, El Camp and Baix Penedès faults) that are characterized by the presence of relay ramps with breaching faults.

1. Introduction

Pre-existing faults and stratigraphic variations commonly play a major role in determining regional evolution during later deformation (Jackson, 1980; Cooper et al., 1989; Williams et al., 1989; Coward, 1994; Buchanan and Buchanan, 1995; Butler et al., 2006). It has been widely described how pre-existing faults control not only the location and kinematics of later structures (i.e., folds and faults) but also the shape and location of orogenic belts and rifts. The structural configuration during the opening of the Bay of Biscay and western Tethys during the Mesozoic has been widely recognized as a key factor that controlled the location and kinematics of the orogenic belts developed in the NE Iberian Peninsula during Late Cretaceous-Cenozoic. Examples of this

structural control are found in the Pyrenees (Muñoz, 1992; Bond and McClay, 1995; García-Senz, 2002; Mencos et al., 2015; Muñoz, 2017), the Iberian Chain (Salas and Casas, 1993; Guimerà et al., 1995; Salas et al., 2001; Nebot and Guimerà, 2016; Guimerà, 2018; Aldega et al., 2019), the Columbrets Basin in the Valencia Trough (Etheve et al., 2018; Roma et al., 2018) and the Betic Chain (Calvert et al., 2000; Vergés et al., 2002). Nevertheless, the role played by the Mesozoic structures in the Catalan Intraplate Chain (CIC), an orogenic belt also developed NE of the Iberian Peninsula during the Cenozoic (Guimerà, 1984; Gaspar-Escribano et al., 2004; Juez-Larré and Andriessen, 2006), is not completely understood.

The development of the present-day basin-and-range configuration of the Catalan Coastal Ranges (CCR) (Fig. 1) resulted from the

* Corresponding author at: Schlumberger, Aachen Technology Centre, Ritterstraße 23, 52072 Aachen, Germany.

E-mail address: mperez92@slb.com (M. Marín).

<https://doi.org/10.1016/j.tecto.2021.228970>

Received 19 August 2020; Received in revised form 9 June 2021; Accepted 14 June 2021

Available online 17 June 2021

0040-1951/© 2021 Published by Elsevier B.V.

extensional reactivation of the main Paleogene contractional structures (Fontboté, 1954; Gaspar-Escribano et al., 2004; López-Blanco et al., 2000; Marcén et al., 2018). Thus, the presence of pre-existing faults has been considered as a key factor controlling the tectonic evolution of the CCR during the Neogene (Guimerà et al., 1995; Roca et al., 1999; Marín et al., 2008; Baqués et al., 2012).

The control played by pre-Cenozoic structures is still poorly constrained and mostly supported by changes in stratigraphic thicknesses and regional observations (e.g., Esteban and Robles, 1976; Salas and Casas, 1993; Salas et al., 2001). Other studies state the potential Cenozoic reactivation of Mesozoic extensional faults in the region (Roca and Guimerà, 1992; Gómez and Guimerà, 1999) and the control the stratigraphic changes of the Mesozoic succession had in the development of Paleogene contractional structures (Anadón et al., 1985; Guimerà and Álvaro, 1990). Moreover, some works based on geochemical analysis in crustal-scale fault damage zones and gouges (i.e., neoformation of minerals, fluid circulation) reveal multiple reactivations in response to the tectonic phases affecting the Iberian Peninsula since the Mesozoic (e.g., Baqués et al., 2013; Cantarero et al., 2014) and even before the Mesozoic (Marcén et al., 2018; Aldega et al., 2019).

In this paper, we define the structure of a portion of the NW margin of the Montmell-Garraf Basin (Salas, 1987), one of the stratigraphically differentiated rift basins developed in NE Iberian Peninsula Late Jurassic-Early Cretaceous. This area is characterized by the presence of a

strip of Paleogene folds and thrusts, located at the southern prolongation of the major Neogene Vallès-Penedès extensional Fault (Fig. 1). The study is essentially focused on the recognition of the main structural features and the description of the role played by the Mesozoic basin architecture during the Cenozoic tectonic evolution.

The work is supported by the construction of two structural cross-sections based on field and well data (Gaià-Montmell and the Marmellar sections, Fig. 2) that allow the delineation of the structures of the uppermost crust. The geometry of the basement and major faults is also sustained at depth by a magnetotelluric (MT) survey carried out along the Gaià-Montmell section, which yields information on the electrical response of the crust up to about 4 km depth.

2. Geological setting

2.1. Tectonic setting

Located in northeastern Iberian Peninsula, the CCR is a structural unit with a NE-SW-oriented basin and range physiography that extends parallel to the coastline for more than 250 km (Fig. 1). It is approximately 30 km wide and, in the present-day, constitutes the onshore expression of the extensional continental margin that separates the thinned crust of the Valencia Trough from the relatively thick crust of the Iberian Plate (Dañobeitia et al., 1992; Roca and Guimerà, 1992;

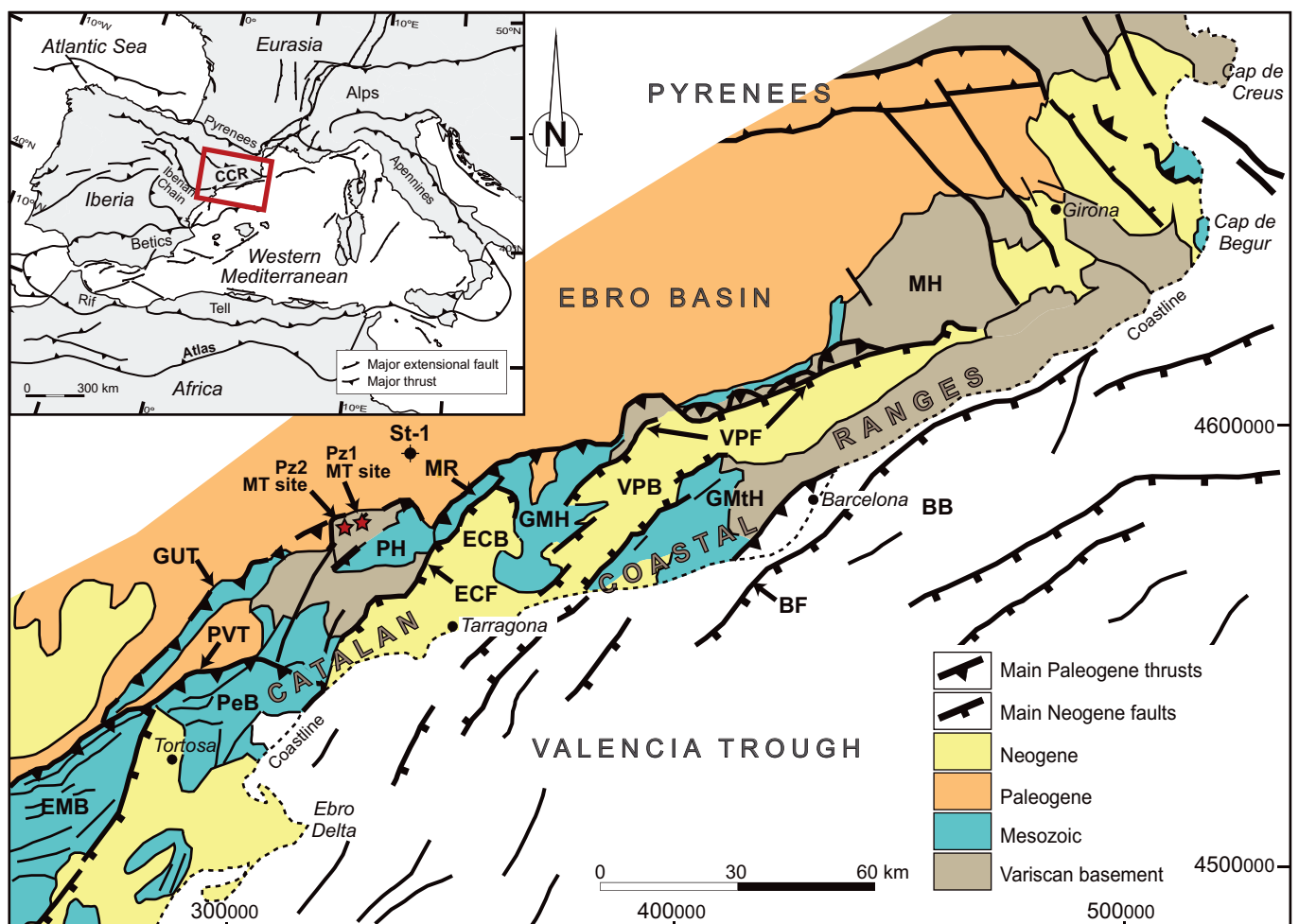


Fig. 1. Schematic structural map of the Catalan Margin (Western Mediterranean). ECB: El Camp Basin; ECF: El Camp Fault; GMtH: Garraf-Montnegre High; GMH: Gaià-Montmell High; MR: Miramar Range; PH: Prades High; VPB: Vallès-Penedès Basin; VPF: Vallès-Penedès Fault; MH: Montseny High; BF: Barcelona Fault; BB: Barcelona Basin; GUT: Gandesa-Ulldemolins Thrust; PVT: Portlirubio-Vandellòs Thrust; PeB: Perelló Mesozoic Basin; EMB: Eastern Maestrat Mesozoic Basin; St-1: Senant-1 well. Red stars in the Prades High indicate the location of the two MT soundings recorded on top of Paleozoic rocks. (For interpretation of the references to color in this figure legend, the reader is referred to the web version of this article.)

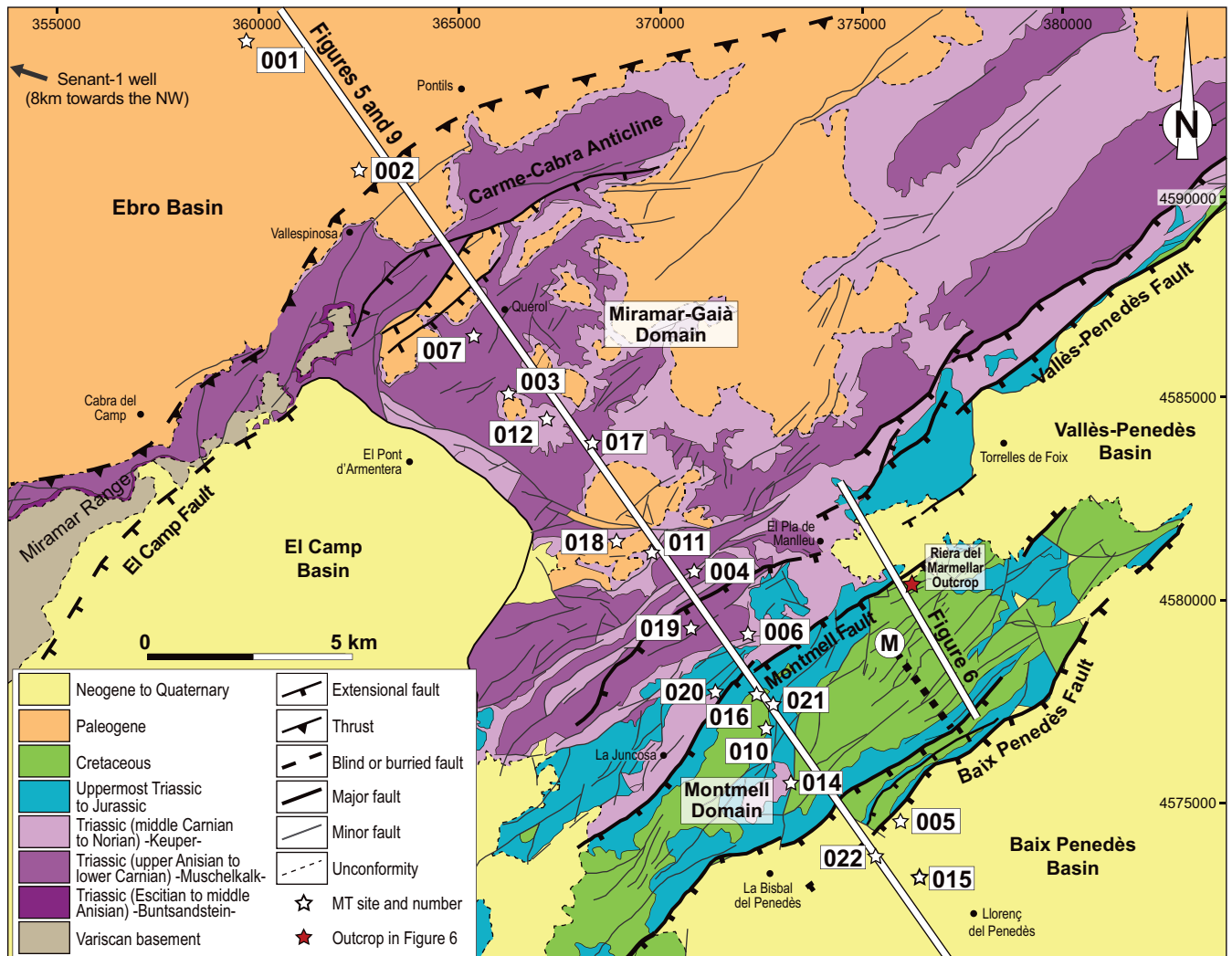


Fig. 2. Geological map of the Gaià-Montmell High and surrounding areas. The map includes the location the Gaià-Montmell and the Marmellar cross-sections (Figs. 5 and 6 respectively) and the acquired parametric MT soundings along the Gaià-Montmell section. M-labelled thick dashed line indicates the approximate location of the Mesozoic succession-type described by Salas (1987) in the Marmellar area. Black dots are village locations used in the text to facilitate the explanations. See Fig. 1 for the exact location of the Senant-1 well.

Vidal et al., 1995). The CCR is formed by several ENE- to NE-striking basement blocks bounded by 50 to 150 km-long faults that display a right-stepping *en-echelon* arrangement (Fig. 1). These major faults mostly dip towards the SE and show reverse, normal and limited left-lateral strike-slip motion (Ashauer and Teichmüller, 1935; Llopis-Lladó, 1947; Anadón et al., 1985; Guimerà, 2004). The general structure of the CCR is essentially the result of a multiphasic and complex Alpine evolution that included: 1) two extensional episodes from Late Paleozoic to Mesozoic, 2) a compressional period during the Paleogene, and 3) an extensional period from latest Oligocene to middle Miocene (Roca and Guimerà, 1992; Salas et al., 2001; Roca et al., 2004; Marín et al., 2008; Baqués et al., 2012).

The first extensional episode, Late Permian to Triassic in age, is related to the opening of the Neotethys. The second, latest Oxfordian to Aptian, is related to the opening of the North Central Atlantic and the Bay of Biscay (Salas and Casas, 1993; Salas et al., 2001) that later, led to the uncoupling of the Iberian Plate from the Eurasian Plate during Albian-early Santonian times (Srivastava et al., 1990; Sibuet et al., 2004).

From late Santonian, a faster opening of South Atlantic Ocean produced the northward drift of Africa and, consequently, the convergence and later collision of the recently uncoupled Iberian and Eurasian plates

(Srivastava et al., 1990; Rosenbaum et al., 2002). This drastic change in the relative motion of Iberia generated the Pyrenean fold-and-thrust belt from the inversion of the Mesozoic rift-system (Muñoz, 1992; Vergés et al., 2002; Muñoz, 2017; García-Senz et al., 2019). In this scenario the contractional deformation progressed southwards leading to the inversion of the Mesozoic rift basins developed in the Iberian Plate and forming the Iberian Range and the Catalan Intraplate Chain (CIC). The preserved structure of the CIC consists of NNW-directed, ENE- to NE-trending thick-skinned and thin-skinned thrusts as well as strike-slip faults (Guimerà and Álvaro, 1990). According to preserved growth strata, the development of the CIC started during Paleocene times and progressed from northeast to southwest up to the middle Oligocene (Guimerà and Santanach, 1978; Guimerà, 1984; Anadón et al., 1985). From that moment and up to the middle Miocene, the rollback of the subduction of the Maghreb Tethys beneath the Iberian Plate produced the extension of the eastern Iberian Plate from the development of widespread back-arc processes (Horváth and Berckhemer, 1982; Carminati et al., 1998; van Hinsbergen et al., 2014). This episode led to the formation of the northwestern Mediterranean Basin, which, in the CIC area, developed as result of the extensional reactivation of Paleogene thrusts (Roca, 2001; Gaspar-Escribano et al., 2004; Marín et al., 2008; Baqués et al., 2012). The extensionally reactivated faults were

responsible of the splitting of the CIC into a set of ENE-WSW blocks bounded by crustal-scale SE- to SSE-dipping extensional faults with kilometric displacements (Bartrina et al., 1992; Roca and Guimerà, 1992) (Fig. 1). The extension induced the development of a series of basins in the extensional fault hangingwalls filled by more than 4 km of sediments ranging in age from Oligocene to Recent (Bartrina et al., 1992) and an isostatic rebound in the footwalls up to 1.2 km (Gaspar-Escribano et al., 2004).

In this complex structural setting, the study area is located in the central part of the CCR in the transfer zone of the two major Neogene extensional faults: the Vallès-Penedès Fault and El Camp Fault (Fig. 2). This transfer zone is known as the Gaià-Montmell High, has a right-stepped *en-echelon* arrangement and is bounded southeastwards by the Baix Penedès Fault.

2.2. Stratigraphy and thickness variations

Four stratigraphic assemblages can be distinguished in the study area: the Variscan basement, the Mesozoic cover, the Paleogene fill of the Ebro Basin and Neogene basin infill of the Baix Penedès Basin

(Fig. 3). From a Mesozoic stratigraphy point of view two main domains can be differentiated: the Miramar-Gaià Domain in the NW and the Montmell Domain in the SE (Figs. 2 and 3).

Paleozoic rocks of the Variscan basement have been reported and described at the bottom of the Senant-1 well in the Ebro Basin (Lanaja, 1987; Fig. 1) as well as in the adjoining Miramar Range (Julivert, 1955; Melgarejo, 1987) and Prades High (Figs. 1 and 2). The Paleozoic succession would be made up by Cambrian to Carboniferous slates with thin interbeds of Devonian carbonates (Julivert, 1955; Sáez and Anadón, 1989; Julivert and Durán, 1990) and Upper Carboniferous to Permian granitoids (Serra and Enrique, 1989; Enrique and Solé, 2004). The present work assumes similar Paleozoic rocks under the Gaià-Montmell High, which are considered as the structural basement.

Unconformably overlying the Variscan basement, the Mesozoic succession shows significant variations across the study area (Figs. 2 and 3). In the Miramar-Gaià Domain, the Mesozoic succession is thin and only includes 200 to 350 m of Triassic rocks (Fig. 3) (Virgili et al., 2006; Galán-Abellán et al., 2013; Mercedes-Martín et al., 2014). Towards the SE, however, the Mesozoic of the Montmell Domain exceeds 2 km of thickness (Salas, 1987) and is stratigraphically more complete including

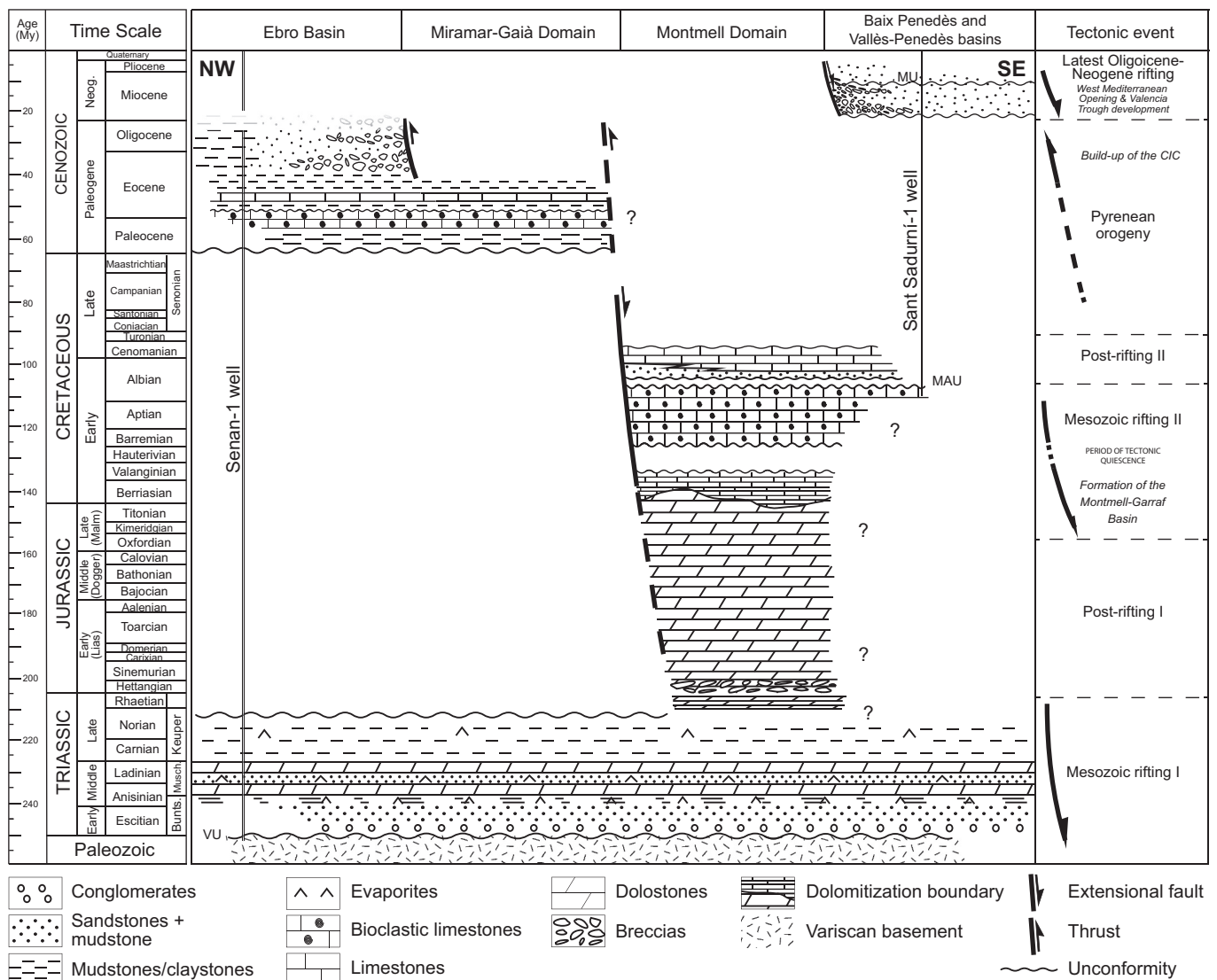


Fig. 3. Chronostratigraphic chart of the study and the adjoining areas. Main tectonic events are indicated. Major unconformities are labelled as follows. MU: Messinian Unconformity; MAU: Middle Albian Unconformity; VU: Variscan Unconformity. Lithostratigraphy has been compiled from Ortí (1974), Anadón et al. (1978), Colombo (1986), Lanaja (1987), Salas (1987), Casas and Permanyer (1991), Calvet and Marzo (1994), Cabrera and Calvet (1996), Salas et al. (2001), Mercedes-Martín et al. (2014), Ortí et al. (2017) and Escudero-Mozo et al. (2017).

Triassic, Jurassic and Cretaceous rocks. On top of the Germanic Triassic, there is a 70 m-thick unit of uppermost Triassic dolomites, followed by a 300 m unit of Lower-Middle Jurassic dolomitic breccias and a 1200 m-thick succession of shallow marine limestones, dolomites and shales of Late Jurassic-Early Cretaceous age (Salas, 1987; Salas et al., 2001; Albrich et al., 2006). The Upper Jurassic-Lower Albian succession is part of a major extensional basin (the Montmell-Garraf Basin) that includes the southern end of the Vallès-Penedès Basin, the Garraf High and some adjacent offshore areas (Anadón et al., 1979; Salas, 1987; Salas and Casas, 1993) (Fig. 1). An Upper Albian to Cenomanian sequence of fluvial and shallow marine carbonates complete the Mesozoic record in the Montmell Domain (Salas, 1987; Salas et al., 2001).

Whereas Paleogene strata are absent in the Montmell Domain, the thin Mesozoic of the Miramar-Gaià Domain appears unconformably overlaid by the Paleogene sediments of the Ebro Basin infill. These are 350 to 500 m-thick marine and continental sediments, and range in age between Paleocene and early Eocene (Ferrer, 1971; Anadón, 1978; Colombo, 1986). Towards the northwest, in the undeformed Ebro Basin, the Paleogene succession thickens up to 1.5 km and includes sediments up to late Oligocene in age (Barberà et al., 2001).

Towards the E and SE of the Gaià-Montmell High, the Mesozoic succession is unconformably overlaid by the basin infill of the Vallès-Penedès and Baix Penedès basins. These sediments are made up by alluvial fan, lagoonal evaporites, carbonate coralgal and fan-delta siliciclastic deposits mainly early to late Miocene in age (Cabrera and Calvet, 1996) unconformably overlaid by Pliocene alluvial sediments (Gallart, 1981) (Figs. 2 and 3).

3. Methods

The present work is based on the construction of structural sections across the area of study using well, field data and later constrained by one 2D magnetotelluric model. Two NW-SE-oriented cross-sections have been constructed in the study area: the Gaià-Montmell section (Fig. 4) and the Marmellar section (Fig. 5). The Gaià-Montmell section is approximately 40 km long and, from NW to SE, runs from the undeformed Ebro Basin to the Baix Penedès Basin (Fig. 2). The Marmellar section is 7 km long and runs approximately 10 km east of the Gaià-Montmell section. This second section crosses the southern end of the Vallès-Penedès Fault at the NE edge of the Montmell Domain (Figs. 2 and 4). The orientations of the sections are respectively N146° and N161°, both orthogonal to the NE-SW predominant trend of the Alpine structures. The cross-sections are based on field data (mostly bedding and fault attitudes), geological map analyses and observed thicknesses of the sedimentary units. When the stratigraphic units do not crop out in the area (e.g., Lower and Middle Triassic), thicknesses have been estimated from the regional reviews of Marzo (1980) and Calvet and Marzo (1994), as well as from information from the Senant-1 and Sant Sadurní-1 wells (Lanaja, 1987, Figs. 1 and 3). The Senant-1 well has also been used to define the depth of the basement in the undeformed areas of the Ebro Basin (Fig. 3). The geometry and location of the bottom of the Baix Penedès Basin (Fig. 2) has been constrained by the gravimetric studies performed by Hernández and Casas (1985) and Casas and Permanyer (1991).

During the construction of the cross-sections, projection and extrapolation of dip data were performed defining cylindrical domains and using the kink-band method. The sections have been constructed and balanced using 2Dmove software. To show the tectonic evolution of the area, the Gaià-Montmell section has been partially restored at the end of (a) the Mesozoic rifting phase, and (b) the contractional Paleogene deformation. During such restorations, the *line-length unfold* method (Dahlstrom, 1969), which straightens the beds while maintaining constant the line length, was used. Because the sections were constructed using the kink method, layer thicknesses remained constant during the unfolding process. This process allows calculating shortening and stretching value for each of the restored paleo-steps.

The magnetotelluric method (MT) has been used to determine the electrical properties of the upper crust across the Gaià-Montmell section and constrain the structure when possible. The MT is an electromagnetic geophysical method based on the simultaneous measurements on Earth's surface of naturally occurring electric and magnetic fields variations. The relations between electric and magnetic fields at different periods are used to define the impedance tensor whose components provide information about the electrical resistivity distribution at depth (Simpson and Bahr, 2005). This technique is very sensitive to conductive bodies that, in depth, can be associated with the presence of conductive rocks, minerals and partial melts, and also to the presence of fluids. Taking into consideration the marked lithological differences between the stratigraphic sequences present along the Gaià-Montmell section the main goals of the MT study were: 1) to recognize the geometry of the boundaries between the main stratigraphic and structural units in depth, and 2) to identify basement conductivity anomalies that could denote the presence of damage zones and fluid circulation.

4. Structure of the Gaià-Montmell High

4.1. Gaià-Montmell section

The structure of the Gaià-Montmell High is illustrated in the Gaià-Montmell section (Fig. 4). The Gaià-Montmell High relates to the positive relief located between the Baix Penedès Basin and the SE margin of the Ebro Basin, which is represented by the Carme-Cabra Anticline (Fig. 2). This anticline is an ENE-WSW-trending structure that involves the Variscan basement as well as Triassic and Paleogene sediments. It has a 13 km long and nearly horizontal backlimb and a shorter 1 km long vertical to overturned forelimb (Fig. 4 and Fig. A of the Supplementary material). This uplifted area has been interpreted as the result of the emplacement of a NW-vergent basement thrust (Gaià-El Camp Thrust), the ramp of which constantly dips less than 30° underneath the ensemble of the Gaià-Montmell High and branches at the lower part of the Montmell Fault. Such geometry is constrained by the width of the uniformly uplifted area (~13 km) and supported by the ESCI-Catalanides deep seismic profile that shows that basement-involved thrusts in the CCR do not affect the top of the lower reflective crust located at 12 to 15 km depth (Fernández et al., 1990; Sàbat et al., 1997; Roca et al., 2004). In this scenario, the geometry of the frontal limb of the Carme-Cabra Anticline is interpreted as controlled by a triangular zone of distributed shear at the tip of this propagating thrust (Allmendinger, 1998; Mitra and Mount, 1998; Allmendinger et al., 2004).

From a structural point of view, the Gaià-Montmell High can also be divided in two domains. In the Miramar-Gaià Domain, the hangingwall of the Gaià-El Camp Thrust is practically horizontal and shows little deformation, except for the presence of sets of minor post-Paleogene SE-directed normal faults located in the Carme-Cabra Anticline backlimb, affecting the basement and generating extensional rollovers on their hangingwalls. On the other hand, the Montmell Domain shows gentle NW-vergent fault-bend folds compatible to the presence of basement reverse faults. These and their related folds involving the basement appear affected by high-angle SE-dipping extensional faults. The syncline present east of La Juncosa, for instance, appears controlled by the emplacement of one these basement-involved faults west of Masies de Sansuies (Fig. 4). This reverse fault develops a frontal structure with a discrete, relatively steep front limb and a flat crest behind it that is similar to the overall geometry observed in the Miramar-Gaià Domain but at minor scale.

Both structural domains are separated by a highly deformed and narrow strip located SE of L'Arboçar (labeled "L'Arboçar deformation strip" in Fig. 4). In this area, Middle Triassic and Lower Ypresian (Ilerdian) rocks belonging to the Miramar-Gaià Domain are strongly deformed by NW-verging recumbent folds, thrust faults and backthrusts mostly interpreted as detached at the top of the Lower Triassic (Buntsandstein). A pre-Paleogene nearly vertical extensional basement fault

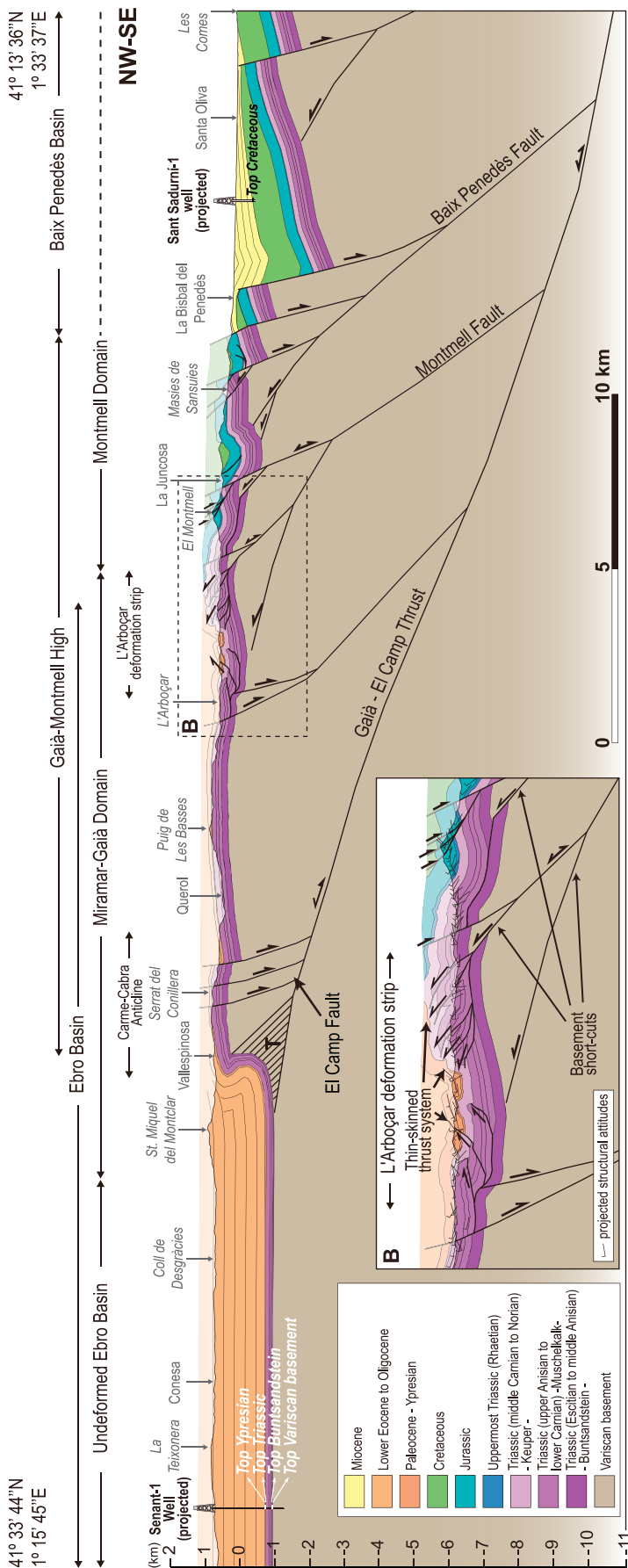


Fig. 4. Gaia-Montmell section showing the Alpine structure at the linkage zone between the Neogene Vallès-Penedès and El Camp faults in the central Catalan Coastal Ranges. See location of the section in Fig. 3. The hatched area labelled with “T” indicates the zone of distributed shear at the upper tip of the Gaia-El Camp Thrust. B) Detail of the structure of the L'Arboç deformation strip.

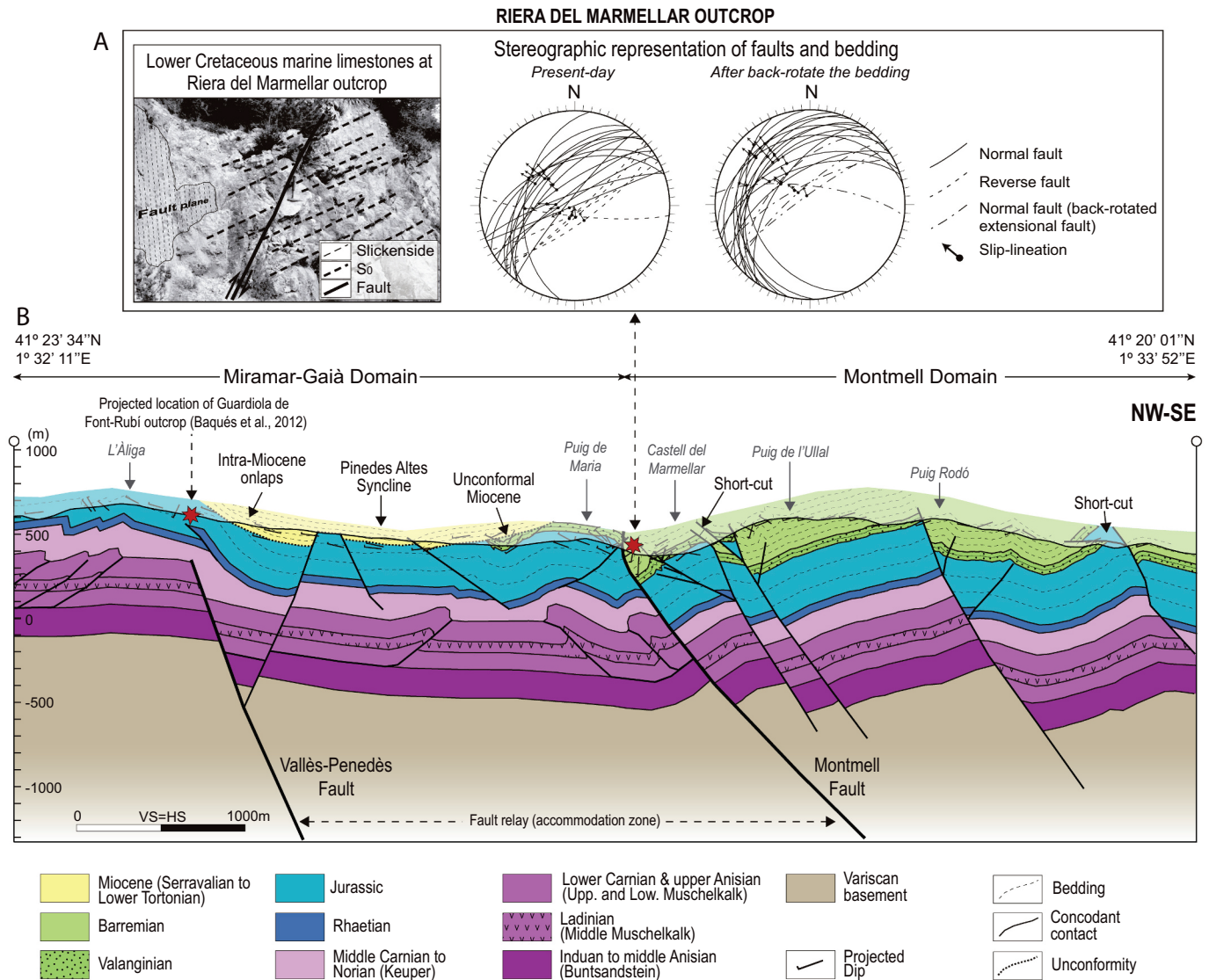


Fig. 5. A) Riera del Marmellar outcrop exemplifying collected structural data and stereographic plots (lower hemisphere) with measured fault planes and slip directions in the present-day and their orientations after unfolding the bedding. B) Marmellar Section showing the structure at the NE sector of the Montmell Domain and adjoining Miramar-Gaià Domain areas. Location of the Riera del Marmellar and Guardiola de Font-Rubí outcrops are indicated with a red star. See Fig. 3 for the location of the section and the outcrop in map view. (For interpretation of the references to color in this figure legend, the reader is referred to the web version of this article.)

seems to control the location and development of the backthrusts in the NW limit of the deformation strip. Northwest and southeast of this strip, the Triassic is located at the same structural high. However, the base of the Cenozoic occupies a significantly lower position in the Miramar-Gaià Domain than in the Montmell Domain, where the top of the outcropping thick Mesozoic succession indicates that this would be located at least 500 m higher. This structural and stratigraphic configuration, in conjunction with the NW vergence of the structures developed along the L'Arboçar deformation strip, suggest interpreting the NW limit of the Montmell Domain as a nearly complete inverted SE-dipping Mesozoic extensional fault. In this scenario, the L'Arboçar deformation strip would correspond to the transmission of the compressional deformation to the Montmell Fault footwall, which induced the formation of detachment folds and thin-skinned thrusting facilitated by the presence of evaporitic decollement levels within the Triassic (Fig. 4).

The age of this suggested inversion of the Montmell Fault is poorly constrained due to the lack of preserved growth and post-growth strata around this fault. Only the presence of Paleocene to lower Ypresian strata contractionally deformed in the L'Arboçar deformation strip

indicates that it had to take place after early Ypresian (post-Ilerdian). On the other hand, the development of the Gaià-El Camp thrust sheet is well constrained by the presence of syntectonic sediments preserved in the Sant Miquel del Montclar area (Figs. 2 and 4). At this location, the Carme-Cabra Anticline forelimb presents series of NW-dipping upper Eocene conglomerates unconformably overlying overturned lower Eocene conglomerates, sandstones and mudstones (Anadón et al., 1985). These growth geometries allow establishing the age of the emplacement of the Gaià-El Camp thrust sheet as middle Eocene.

The Gaià-Montmell section also shows several extensional faults affecting the previously outlined compressional structure. A set of SE-dipping, basement-involved extensional faults bound the Baix Penedès Basin towards the NW and show an accumulative displacement of about 2.5 km. The existence of the Mesozoic succession underneath the Baix Penedès Basin remains uncertain due to the absence of subsurface data in this area. However, we assume its presence taking into consideration data from the Sant Sadurní-1 well, which cuts fossil-rich limestones rocks of Early Cretaceous age (Neocomian) (Lanaja, 1987; see Fig. 1 for its location).

In addition, a set of minor SE-dipping faults that affect Mesozoic and Paleogene strata of the Carme-Cabra Anticline backlimb is present between the villages of Vallespinosa and Querol as well as NW of L'Arboçar. Cartographically, these faults are NE-SW-oriented, laterally disappearing towards the NE (Fig. 2), they display relatively high angles ($>75^\circ$) and show metric to decametric fault throws. Taking into consideration roll-over geometries and the fact that they are only present in the Gaià-El Camp thrust sheet hangingwall, these are interpreted as rooted in the Gaià-El Camp Thrust. If this fault linkage exists, this would imply the Gaià-El Camp Thrust plane also underwent extensional reactivation during the Neogene.

4.2. Marmellar section

The Marmellar section is located at the southeast of the Gaià-Montmell High and includes the southeasternmost part of the Miramar-Gaià Domain, the SW end of the Vallès-Penedès Fault and the Montmell Domain (Figs. 2 and 5). At this location, the Miramar-Gaià and the Montmell domains are separated by a NE-SW-oriented fault that laterally corresponds to what has been described in the Gaià-Montmell section as the Montmell Fault. Additionally, the section is adjacent to the Mesozoic succession-type described by Salas (1987) and labeled "M" in Fig. 2, which allows a detailed recognition of the Mesozoic rocks outcropping in the area.

The structure of the Montmell Domain belongs to an array of NE-SW-oriented, SE-dipping basement extensional faults that split the area into a system of NW-tilted fault blocks filled by up to 1100 m thick Jurassic to Barremian rocks (Fig. 5). These faults have throws of hectometric displacement up to 300–400 m and kilometric lengths up to 5 km, which allows considering these extensional faults as vertically restricted (Nicol et al., 1996). At depth, these basement-involved extensional faults show domino style dipping $55\text{--}60^\circ$ towards the SE and display reverse and normal drag folding in their hangingwalls. Moreover, minor compressional features deforming the Mesozoic sedimentary cover are present in the Montmell Domain. Basically, these are represented by SE-directed reverse faults and low angle NE-vergent thrusts respectively located at the hangingwalls and footwalls of some of the major extensional faults.

Structural data was collected at the Riera del Marmellar outcrop in Lower Cretaceous marine limestones belonging to the Montmell Fault hangingwall. At this location, beds are 1 to 4 m-thick, trend NE-SW, dip around 31° to the NW and contains metric-scale faults, tension veins and numerous stylolite surfaces. Gathered structural data mainly consists of normal faults with orientations ranging $N30\text{--}70$, dipping 65 to 80° towards the NW with 80° WNW of slip, as well as reverse faults with orientations $N50\text{--}65$, dipping 70 to 80° towards the SE with 70° E of slip. Data was displayed on stereoplots and later restored to their original geometry by rotating bedding to horizontal (Fig. 5). Once restored, all collected faults originally look as normal faults with orientations mainly ranging $N15\text{--}75$, dipping 30 to 85° towards the NW and with slip direction towards the NW. Fluid geochemistry analysis performed by Baqués et al. (2012) in the same area relates these mesostructures to the Mesozoic *syn*-rift stage that led to the development of the Montmell-Garraf Basin.

The Montmell Fault, a basement-involved SE-dipping extensional fault, represents the NW boundary of the Montmell Domain. This fault is nearly vertical ($>85^\circ$) at surface that progressively decreases its dip at depth up to 45° . This major structure also coincides with the NW boundary relatively thick Lower Cretaceous successions outcropping in the Montmell Domain, the map view configuration of which corresponds to series of NE-SW-oriented normal faults separated by narrow transfer zones that can be correlated with the presence of a basement fault that becomes segmented at surface (Fig. 2). Its interpreted location matches the NE prolongation of the Montmell Fault as interpreted in the Gaià-Montmell section (Fig. 4). Contractional structures such as low-angle NW-directed thrusts and their related fault-bend and fault-propagation folds are present in the Montmell Fault footwall. These structures

involve Jurassic and Middle to Upper Triassic rocks and, because of they show short wavelengths in the geological map, they have been interpreted as rooted at the evaporitic levels of the uppermost Lower Triassic (Buntsandstein) that is considered a good regional detachment.

At surface, the Miramar-Gaià Domain is characterized by a Jurassic to Miocene cover deformed in a 2 km-wide gentle syncline (Pinedes Altes Syncline, Fig. 5) bounded towards the NW by a SE-dipping monocline. Miocene is only present in this syncline and unconformably overlies Lower Cretaceous and Jurassic rocks that show a more high syncline geometry. The syncline appears affected by some minor extensional faults mainly developed at its lower part and includes internal onlaps in its NW limb. At smaller scale, the outcropping Jurassic-Lower Cretaceous cover appears affected by minor NW and SE-verging folds. These, locally cut by small thrusts, are interpreted as drape/fault-bend folds developed over Muschelkalk thrust horses limited by the Keuper and the uppermost Buntsandstein evaporite decollements.

The NE-SW orientation of the monocline limiting the Pinedes Altes Syncline to the NW and its lateral continuity with the cartographic trace of the Vallès-Penedès Fault towards the NE allow interpreting this structure in the Marmellar section. In map view, the Vallès-Penedès Fault shows splays and relay faults developed at the termination of a fault segment. Approximately 1 km NE of the Marmellar section, Jurassic rocks outcrop in both the hangingwall and the footwall of the Vallès-Penedès Fault denoting the loss of displacement of this towards the SW (Fig. 2). Therefore, in the Marmellar section, the Vallès-Penedès Fault has been interpreted as a SE-dipping ($\sim 65^\circ$) basement-involved normal fault that dies out in the Upper Triassic interval and drape folds the overlying Jurassic and Miocene rocks.

Based on these geometrical relationships, it is possible to establish the relative kinematic ages of some of the structures illustrated in the Marmellar section. The relatively thick Mesozoic succession and the structural data collected in the Riera del Marmellar outcrop (Fig. 5), indicate this fault experienced extensional motion during, at least, the Lower Cretaceous coevally to the formation of the Montmell-Garraf Basin (Salas, 1987). Compressional features along the Montmell Fault cartographic trace are essentially located in its hangingwall and affect Mesozoic rocks. This may suggest a post-Lower Cretaceous compressional phase that, at this location, did not reactivate the Montmell Fault but developed buttressing against the previously formed extensional fault (Gillcrist et al., 1987; Cooper et al., 1989). Minor reverse faults also developed in the Miramar-Gaià Domain, basically consisting of NW- and SE-directed thrusts at the NW and SE limbs of the Pinedes Altes Syncline and affecting Jurassic rocks (Fig. 5). Although the age of the compression is poorly constrained by preserved strata (mostly Mesozoic rocks coeval or previous to the extensional phase), it is possible to sustain that compression occurred after their deposition (post- Lower Cretaceous), and previously to the deposition of the Miocene sediments that unconformably overlie the observed contractional structures. This fact makes possible relating the compressional features observed in the Marmellar area to the regional compressional phase that affected the central part of the CCR during Paleocene to Eocene. On the other hand, onlap geometries in Miocene sediments preserved above the monocline that characterizes the NW limb of the Pinedes Altes Syncline indicate these sedimented deposited during the extensional motion of the Vallès-Penedès Fault during Miocene times.

5. Magnetotelluric data and 2D inversion model

Nineteen magnetotelluric (MT) soundings with recording times ranging from 8 to 12 h were acquired along the Gaià-Montmell section (Fig. 2). Time series were processed using the Egbert and Booker (1986) method and applying remote reference when possible. Apparent resistivity and phase resulting curves cover periods from 0.001 s to 1 s.

To determine if the geoelectrical structure is 1D, 2D, 3D/2D (2D structures with galvanic distortion) or 3D, a dimensionality analysis was performed using the WALDIM code (Martí et al., 2009b) that is based on

the invariant rotation parameters of the impedance tensor. The dimensionality results (Fig. B of the supplementary material) show that for periods shorter than 1 s, this behavior can be considered highly variable with a rather frequent 2D component, whereas at periods longer than 1 s, the geoelectrical behavior is strongly 3D. In all 2D and 2D/3D cases, the strike is rather parallel with a trend that ranges between N015° and N065°; orientation that is consistent with the N40–60° trend of the geological structures (Figs. 1 and 3). So, the dimensionality analysis results reveal that a 2D MT model could be rather reliable to determine the geoelectrical structure in periods shorter than 1 s, but not at longer ones where the dominant 3D data structure can induce wrong interpretations (Ledo, 2005). Considering this dimensional breakdown, a directionality analysis was performed using the STRIKE code developed by McNeice and Jones (2001). It states a geoelectrical direction of N55° although it also indicates a 3D effect of the regional structure. The elements of the impedance tensor were rotated applying this direction to obtain the two main directions for the 2D modeling: the transverse electric (TE) mode when the electric field is parallel to the strike and the transverse magnetic (TM) mode if the parallel one is the magnetic field. The obtained apparent resistivity and phase curves for each sounding are shown in the Fig. C of the Supplementary material. Data and model responses are presented as pseudo-sections built by plotting the data in an x-T map, where x-axis corresponds to the data position on the profile and T-axis to the period, which is considered as a proxy of the depth: TE and TM apparent resistivity and phase responses (Fig. D of the Supplementary material).

The 2D modeling is based on the simultaneous fit of the TE and TM data and has been done using the 2D RLM2DI inversion code (Rodi and Mackie, 2001) considering a 5% error floor that reaches an RMS of 2.7. The final 2D model is presented in Fig. 6A, which shows the calculated apparent resistivities.

5.1. Correspondence between the 2D magnetotelluric model and the Gaià-Montmell section

The MT model illustrates the geoelectrical structure along the Gaià-

Montmell section with the presence of different conductivity/resistivity bodies (Fig. 6A). In general terms, the MT model shows a geoelectrical structure shaped by two stacked up layers. The lower layer has a very resistive ($\geq 1000 \Omega\cdot\text{m}$) and homogeneous character below 0.5–2.5 km, although some less-resistant bands ($\sim 100\text{--}600 \Omega\cdot\text{m}$) are also present (e. g. below the Montmell Domain and the NW limit of the Miramar- Gaià Domain). The geoelectrical behavior of the upper layer is, on the other hand, highly heterogeneous where the presence of conductive bodies with low lateral continuity (mostly isolated conductive bodies) prevails.

The comparison between the resistivity model and the Gaià-Montmell section (Fig. 6B) allows the correlation of the geoelectrical structure to different types of rheologies. The highly resistive and laterally continuous response of the lower geoelectrical layer (R1 and R3, Fig. 6A) can be correlated to the Variscan basement, which is made up by epimetamorphic and plutonic rocks. The high resistivity of the basement is corroborated by two additional parametric MT soundings acquired 30 km southwest of the study area in the Prades High on top of Paleozoic rocks (soundings Pz1 and Pz2, see Fig. 1 for location). MT soundings at this location reveal that Carboniferous slates and Permian granitoids show resistivities $\geq 1000 \Omega\cdot\text{m}$ (Fig. E in the supplementary material), fact which is also documented in other locations of the Iberian Peninsula such as the Iberian Massif (Muñoz et al., 2008), the Pyrenees (Ledo et al., 1998; Campanyà et al., 2018) and the Betic Cordillera (Martí et al., 2009a; Rubín et al., 2010).

The upper geoelectrical layer is, instead, very variable in depth and in resistivity character. From NW to SE, it includes conductive/resistive bodies C1, C2, C3, C4, R2, C5 and C6. Comparing the geoelectrical character to geological data and interpretations along the Gaià-Montmell section (Fig. 6B), these bodies can be divided in two different groups, those that correlate with the Mesozoic and/or Cenozoic sedimentary cover (C1, C2, R2, C5 and C6) and those that suit with positions of the Variscan basement (C3 and C4). Located in the northernmost part of the section, C1 agrees with the Mesozoic and Cenozoic sedimentary infill of the Ebro Basin, the thickness of which accounts to 1649 m of sedimentary cover above the Variscan basement as described in the Senan-1 well (Lanaja, 1987; see Figs. 1 and 3 for well location).

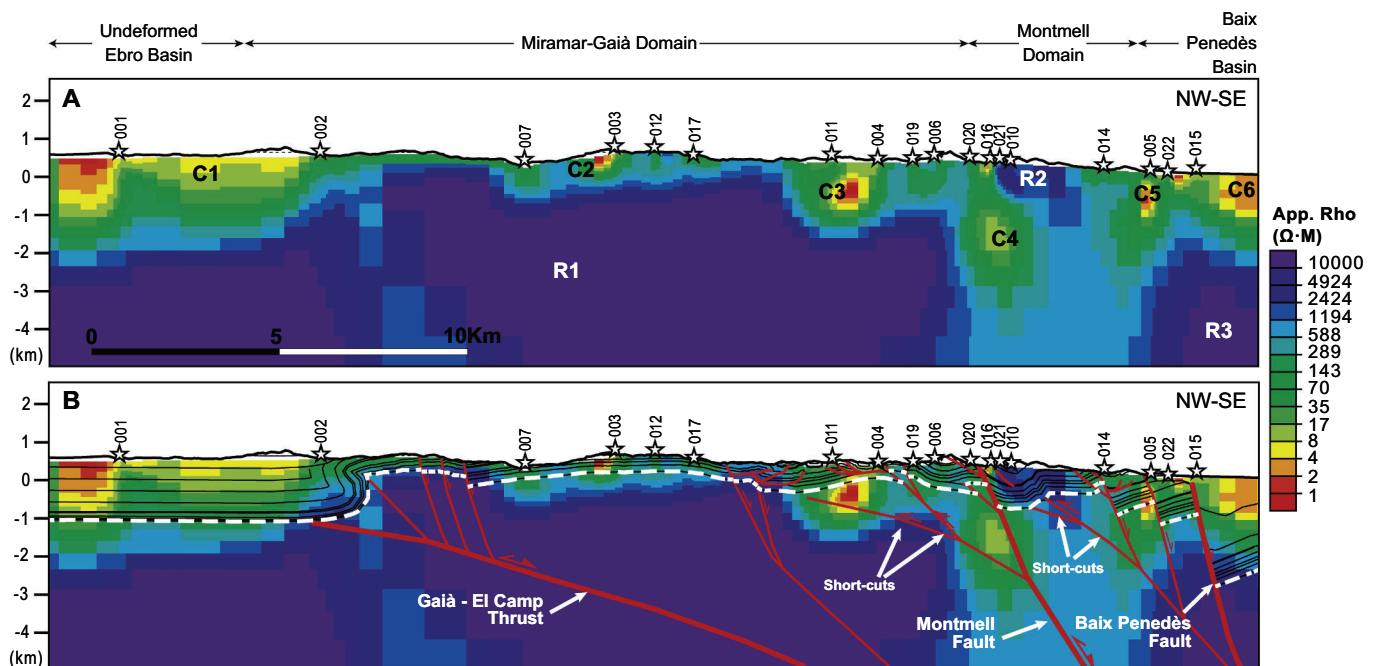


Fig. 6. A) Final magnetotelluric 2D model of the Gaià-Montmell section showing the differentiated conductive (C labels) and resistive (R labels) bodies. B) The model with the interpreted stratigraphic boundaries (black lines), faults (red lines) and the top of the Variscan basement (dashed white line). White stars indicate the location of the MT soundings (see Fig. 3 for their location). (For interpretation of the references to color in this figure legend, the reader is referred to the web version of this article.)

Likewise, conductive body C2 coincides in thickness and location with the Triassic succession, which, in the Miramar-Gaià Domain, mainly consists of clastic sediments with evaporitic episodes and carbonates (Fig. 3). On the other hand, resistive body R2 agrees with the position of Jurassic and Lower Cretaceous rocks, which mainly consist of massive limestones and dolostones present in the Montmell Domain. Geoelectrical body C5 also coincides with the clastic sediments with evaporitic and carbonate episodes of the Triassic of the southeastern Montmell Domain. At the southeastern end of the section, the conductive body C6 agrees with the Neogene infill of the Baix Penedès Basin, the thickness of which is pointed out by Casas and Permanyer (1991) as approximately 2000 m of mainly terrigenous sediments (Cabrera and Calvet, 1996).

Taking into consideration the intrinsic resistive character of the Variscan basement, the explanation about the nature of the conductive body C3 is conjectural. Low resistive values at this location ($\leq 10 \Omega\cdot\text{m}$) can be related to highly fractured rocks (e.g., Pous et al., 2001; Martí et al., 2020) and/or metallic mineralizations (Martí et al., 2009a) similar to those recognized in the central CCR southwest of the study area in the Prades High (Fig. 1). Examples of documented metal mineralizations in this area consist of Pb-Zn-Ba-Ag-Ni-Cu sediment-hosted veins, late Hercynian to Triassic in age, formed along intra-Paleozoic and Lower Triassic fractures (Cardellach et al., 1990; Canet et al., 2005; Alfonso et al., 2012). Hence, metal mineralizations, which include highly conductive elements, would enhance the conductive character of the Variscan basement rocks at C3 (Fig. 6).

The geoelectrical body C4 belongs to a 1–2 km wide, SE-dipping band of relatively low resistivity ($\geq 15 \Omega\cdot\text{m}$) 2 km depth underneath the NW limit of the Montmell Domain (Fig. 6). This band is clearly differentiated from the surrounding high resistive and homogeneous signature that characterizes Variscan basement and appears in agreement with the location of the NW limit of the Montmell Domain. The origin of this low resistivity is uncertain, although it seems to be related to a different type or degree of deformation between the Miramar-Gaià and the Montmell domains. While the Miramar-Gaià Domain formed during the Paleogene compression concentrating its deformation at the tip of the Gaia-El Camp Thrust and the frontal limb of the Cabra-Carme Anticline, the structural analysis in the Montmell Domain indicates a higher degree of deformation that includes thick-skinned extensional and contractional structures. The Variscan basement is highly deformed in the central CCR and only planar-type Paleozoic structures such as low-angle thrusts have been described (Julivert and Durán, 1990). However, this type of geometries does not suit with the description of C4. Considering C4 is related to the presence of a SE-dipping basement fault, its 1 to 2 km width would correspond to the damage zone located at the Montmell Fault footwall where conductivity has been enhanced by the presence of fluids within a fractured and permeable zone (e.g., Pous et al., 2001) and, perhaps, metal conductive mineralizations.

Considering these interpretations, the MT model has allowed constraining three key structural aspects along the Gaià-Montmell section (Fig. 6): 1) the depth of the base of the Mesozoic to Cenozoic sedimentary infill of the Ebro Basin over the Variscan basement in the northernmost sector (conductive body C1 between MT soundings 001 and 002); 2) the geometry of the Montmell Fault underneath the northern limit of the Montmell Domain and the location at depth of its related shortcut (conductive body C4 between MT soundings 020 and 010); and 3) the base of the Mesozoic to Miocene sedimentary infill of the Baix Penedès Basin in the southernmost sector (conductive body C6 south of the MT sounding 015).

6. Discussion: tectonic evolution and structural inheritance of the central CCR

Structural and stratigraphic observations along the Gaià-Montmell and Marmellar sections, together with regional geophysical data and geological maps allow the characterization of the deformation history of

the linking zone between the Vallès-Penedès and El Camp basins (Figs. 1 and 2). The tectonic evolution of this area includes three major Alpine events: A Late Jurassic-Early Cretaceous extension, a latest Cretaceous-early Oligocene compression and uplift, and a late Oligocene-Neogene extension.

6.1. Late Jurassic (Oxfordian) – early cretaceous extension: Montmell-Garraf Basin formation

The Alpine cycle regionally starts with a Late Permian-Early Triassic extensional period that controlled the deposition of siliciclastic and carbonate units along NE-SW-trending basins (Galán-Abellán et al., 2013; Mercedes-Martín et al., 2014; Mercedes-Martín and Buatois, 2020). However, in the study area Triassic strata show no lateral thickness variations indicating a relative tectonic quiescence during this period. The first hints of Mesozoic tectonic activity do not appear until the Late Jurassic. Upper Oxfordian to Valanginian carbonate-dominated sediments deposited in an incipient depocenter (the Montmell-Garraf Basin), bounded towards the NW by a high-angle SE-dipping extensional fault. The constant thickness of the Valanginian sediments indicates they were deposited over a planar extensional ramp (McClay, 1995; Withjack and Schlische, 2006; Ferrer et al., 2016). This fault would correspond to the breakaway fault of the extensional system, the present-day location of which corresponds to the SE limit of L'Arboç deformation strip (Fig. 4). Laterally towards the NE, this fault corresponds to the SW prolongation of the Vallès-Penedès Fault (Figs. 2 and 5).

Late Valanginian to Hauterivian strata are absent in the Montmell-Garraf Basin and Barremian sediments paraconformably overlie preserved Valanginian (Fig. 5). This hiatus throughout the Neocomian is widespread recognized in the region and, with a diachronic character, has been interpreted in two ways: as a period of decelerated subsidence, emersion and relative tectonic quiescence in the external zones of the rift basin system (Anadón et al., 1979; Salas et al., 2001), or related to a thermal post-Late Jurassic-early Valanginian rifting phase (Salas et al., 2020). From Barremian on, an acceleration of the subsidence takes place in the Montmell-Garraf Basin following two different phases: 1) Barremian to early Albian, 2) late Albian to Cenomanian. During this period, the breakaway fault shifts towards the SE to the present-day location of the Montmell Fault (Figs. 4 and 5). Considering this scenario, the Montmell Fault, can therefore be considered as the SW segment of a major structure that we call the Montmell-Vallès Fault System.

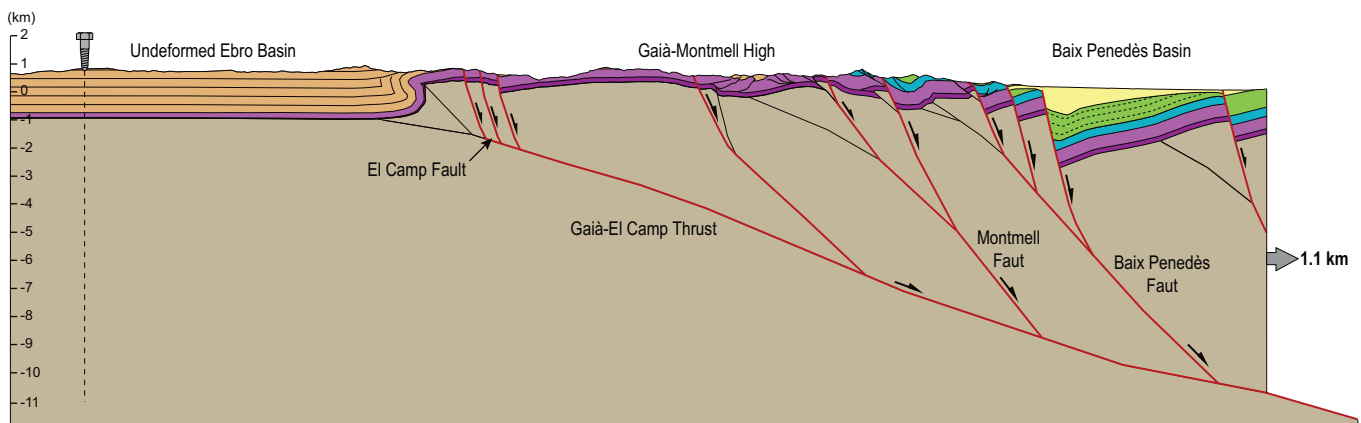
Barremian to Lower Albian sediments were deposited in the Montmell-Marmellar area with significant thickness variations. Up to 550 m of Barremian to Lower Aptian shallow marine carbonates deposited on the Montmell Fault hangingwall in the Marmellar area. In comparison, towards the NW in the Miramar-Gaià Domain, Paleocene sediments conformably lie over Triassic strata (Fig. 4) and Jurassic to Cretaceous sediments are absent. This fact can be explained by erosion or non-deposition. The nonexistence of clastic deposits during this period, which would represent the erosion of Jurassic and Cretaceous strata before the Paleocene, most likely indicates a hiatus scenario due to the presence of a paleo-structural high NW of the Montmell Fault (Ebro High, Fig. 7C) during, at least, the extensional motion of the Montmell Fault from Barremian to early Albian.

The end of the extensional motion of the Montmell Fault cannot be established with precision with the analyzed data. However, regional criteria associate the end of the extension to the development of the Middle Albian Unconformity (Fig. 3) (Salas, 1987; Salas et al., 2001; Salas et al., 2020). From this time and up to the Cenomanian, a relatively constant thickness unit characterized by the entrance of clastic sediments is deposited (Salas and Casas, 1993). This period has been traditionally interpreted as post-rift thermal relaxation with associated homogeneous subsidence (Robles, 1982; Alonso et al., 1993; Salas et al., 2001). However, new interpretations relate this period to late crustal extension over a low angle fault that passively transports the area

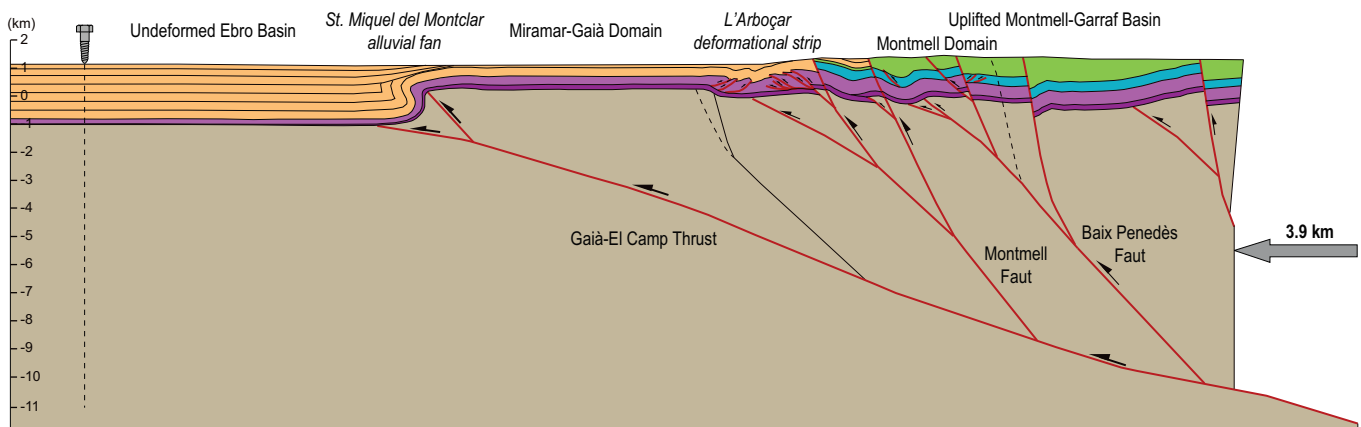
A: Present-day (after the Neogene extension) .

CIC compartmentalized by Neogene extensional faults linked to the opening of the Western Mediterranean.

NW-SE

**B: Early Oligocene (end of the Paleogene compression).**

Catalan Intraplate Chain build-up and full inversion of the Garraf-Montmell Basin.

**C: Middle Albian (end of the Late Jurassic-Early Cretaceous extension).**

End of the Montmell-Garraf Basin formation

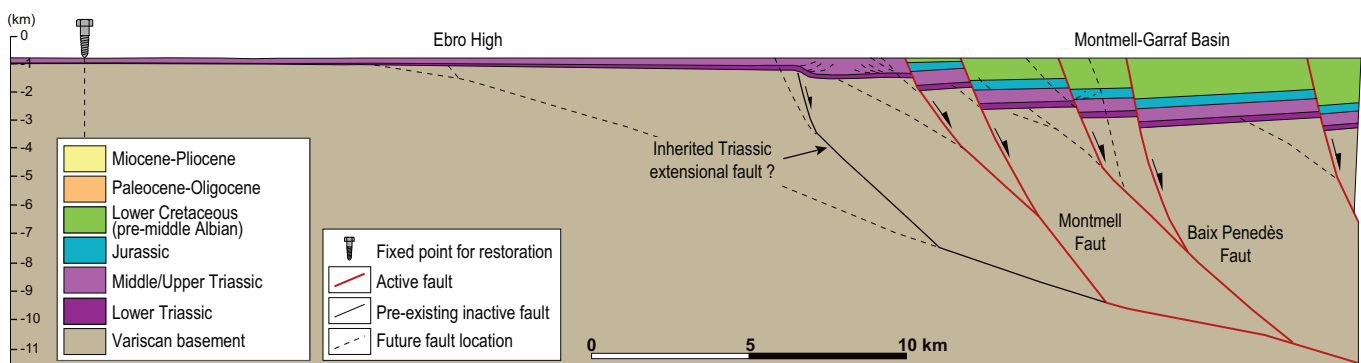


Fig. 7. Sequential structural restoration of the Gaià-Montmell section applying flexural slip and bed length preservation. A) Present-day after the latest Oligocene-Neogene extension. B) Early Oligocene (end of the Paleogene compression). C) Late Cenomanian (end of the Late Jurassic-Early Cretaceous extension). No vertical exaggeration.

previously formed by high-angle extensional faults (Tugend et al., 2015) and, hence, with the resulting extensional displacement of the Montmell Fault.

6.2. Late cretaceous - early Oligocene compression: positive inversion of the Montmell Fault and emplacement of the Gaià-El Camp thrust sheet

From late Santonian (Late Cretaceous), the convergent motion between the Iberian and Eurasian plates is activated (Roest and Srivastava,

1991; Rosenbaum et al., 2002), yet the transmission of compressional stresses into the study area arises in the lattermost Cretaceous (Maastriichtian?). During this period of the convergence, up to three phases can be distinguished. The first phase takes place at the end of the Cretaceous and is recorded in the Miramar-Gaià Domain by the presence of a paraconformity that brings the basal Paleocene and the Keuper into contact (Figs. 3 and 4). The presence of this unconformity indicates a regional pre-Paleocene uplift that can be linked to an uppermost Cretaceous contractional deformation over the entire area or, conversely, to an

isostatic adjustment of the Montmell Fault footwall after the Late Jurassic to Lower Cretaceous rifting phase. From a tectonic point of view, this period can be both contractional and quiescent. The second phase occurs from Paleocene to early Eocene times, and is characterized by the sedimentation of concordant fine-grained terrigenous beds and carbonates with little lateral thickness variations deposited in the distal areas of the Pyrenean foreland (Anadón et al., 1979; Anadón et al., 1985). These deposits indicate the absence of significant deformation or creation of relief in the adjacent areas of the central CCR and, therefore, a period of tectonic quiescence. The third and most relevant compressional phase in the study area takes place from Middle Eocene to early Oligocene. During this period compressional structures emerged in both Miramar-Gaià and Montmell domains. The footwall of the Montmell Fault was strongly deformed by a set of basement shortcuts that laterally become thin-skinned-controlled fold-and-thrust systems detached at top Buntsandstein and Keuper evaporitic levels. On the other hand, minor deformation appeared in the Montmell Domain where SE-vergent backthrusts and pop-up structures developed (Figs. 4 and 5), possibly as a result of slight buttressing effect. This structural style around the Montmell Fault is also observed in several parallel minor extensional faults in the Montmell Domain (Figs. 4 and 5), which denote the contractional reactivation of pre-existent Mesozoic extensional faults in the area. The tectonic inversion is basically characterized by minor hangingwall buttressing later passively transported by shortcuts developed in the upper part of the reactivated faults, and thin-skinned thrust systems detached in the Triassic evaporite levels of the Miramar-Gaià Domain.

The whole ensemble of the Miramar-Gaià Domain became uniformly uplifted by the Gaià-El Camp Thrust. Considering the dip of this thrust and the fact that it merges at depth to the Montmell Fault, the Gaià-El Camp Thrust can be interpreted as a major footwall shortcut developed to provide a smoother fault trajectory during the inversion of the Montmell Fault (Fig. 7B).

Paleogene growth geometries at the SE margin of the Ebro Basin consisting of Upper Eocene to lower Oligocene sediments unconformably deposited over Lower to Middle Eocene strata (St. Miquel del Montclar area, Figs. 4 and 7B) allow establishing the precise age of the Gaià-El Camp Thrust emplacement as late Bartonian to Lower Oligocene. Conversely, the age of the inversion of the Montmell-Garraf Basin cannot be fully constrained due to the lack of preservation of growth sequences. Nevertheless, taking into consideration that up to Lower Ypresian (Ilerdian) sediments are involved in the Montmell Fault footwall deformation with no growth geometries, it can be stated that the contractional motion in this area is, at least, late Ypresian (Cuisian). Additionally, the fact that the Gaià-El Camp Thrust has been interpreted as a major shortcut supports the idea that the primary reactivation of the Montmell Fault was to some extent older (late Ypresian to Lutetian).

6.3. Latest Oligocene(?)/early Miocene - late Miocene extension: Baix Penedès Basin formation and partial reactivation of the Gaià-El Camp Thrust

The Paleogene structure described in the previous section is affected by extensional deformation that cuts or, at times, reactivates previously formed faults. Most of the interpreted extensional faults have a predominant ENE-WSW orientation, dip towards the SE and generally display decametric to hectometric displacements (Figs. 2 and 7A). Four major faults (Vallès-Penedès, Montmell, El Camp and Baix Penedès faults) show kilometric fault traces and display an overlapped arrangement linked by large NW-SE-oriented accommodation zones (Fig. 8).

The Vallès-Penedès Fault progressively loses its displacement towards the SW overstepping with the Montmell and the Baix Penedès faults in the respectively Marmellar and Sant Martí Sarroca transfer zones (Fig. 8). In this area, the Vallès-Penedès Fault throw becomes less than 300–400 m, displaying a drape-fold detached in the Upper Triassic evaporites on its hangingwall (Fig. 5). Extensional displacement is,

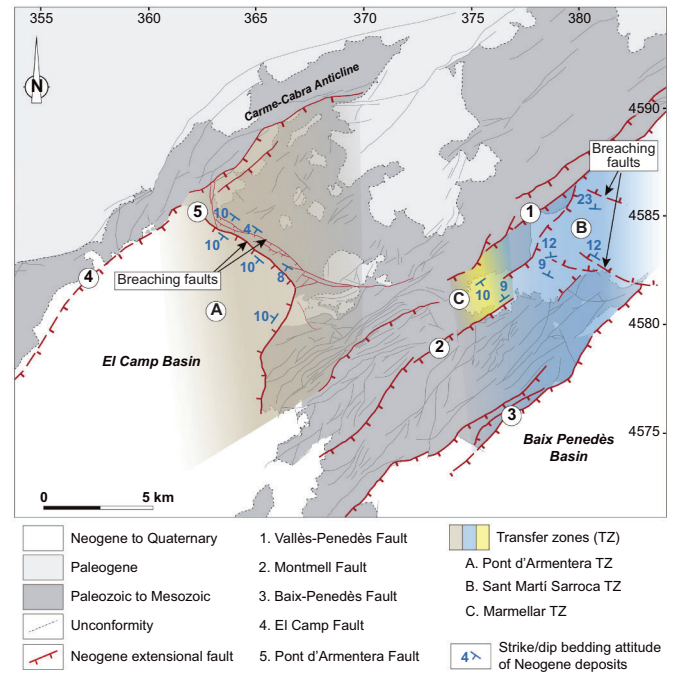


Fig. 8. Schematic geological map of the Gaià-Montmell High showing the major Neogene extensional faults and their related relay ramps.

hence, relayed to the Montmell and the Baix Penedès faults, which extends towards the SW with a similar orientation. The Montmell Fault shows decametric fault throws and a low accumulated extensional displacement. The Baix Penedès Fault, in turn, shows a segmented fault pattern with several SE-dipping splays at surface and a considerably higher accumulated throw reaching several hundreds of meters. NW-SE-trending breaching faults are present in the Sant Martí Sarroca Transfer Zone (Fig. 8). The Baix Penedès Fault is interpreted as rooted at the deep NW-vergent basement ramp underneath the area (Fig. 7).

On the other hand, the displacement of the El Camp Fault drastically decreases towards the NE and becomes a narrow array of SE-dipping faults with hectometric accumulated displacements at the Carne-Cabra Anticline backlimb (Figs. 2 and 8). Considering the geometry of the Miramar-Gaià Domain as the result of the displacement and uplift over a low angle basement ramp shallowing towards the NW (Fig. 7B), this array of extensional faults at the NE end of El Camp Fault has been interpreted as rooted in the Gaià-El Camp Thrust (Figs. 4 and 7A).

In this context of overlapped major extensional faults, the NW-SE-trending faults present in the Sant Martí Sarroca Transfer Zone as well as the Pont d'Armentera Fault (Fig. 8) are considered as relay ramp-breaching faults of a soft linked extensional system (Fossen and Rotevatn, 2016). These zones would transfer displacement between the Vallès-Penedès and the Baix Penedès faults and between El Camp Fault and the Montmell-Vallès Fault System respectively.

The extensional reactivation (or negative inversion) of preexisting faults is suggested by several evidences such as: 1) the development of an array of extensional faults rooted at the discrete fault plane of the Paleogene Gaià-El Camp Thrust at the NE end of El Camp Fault; 2) the extensional geometry of the Montmell Fault (although this fault has a reverse movement during Paleogene times); or 3) the Baix Penedès Fault and its splays which are also rooted at a Paleogene reverse fault footwall ramp. However, the reactivation of the Montmell Fault is relatively limited, and the extension seems basically relayed to the Baix Penedès Fault, which induced the development of a 1.5 km deep basin on its hangingwall (Fig. 7A).

All these structural observations indicate a post-early Oligocene extensional period that resulted in the extensional reactivation of the previously formed Paleogene and Late Jurassic-Early Cretaceous faults,

the age of which can be constrained based on the tectonostratigraphic relationships. Undeformed Pleistocene alluvial deposits fossilize most of the major faults in the central CCR, hence, indicating their extensional motion is pre-Pleistocene. Additionally, major faults, which often show drape-folds on their hangingwalls, cut or fold Serravallian sediments. Therefore, their extensional motion must be considered as post-Serravallian. Yet, extensional growth strata geometries are indeed observed in upper Serravallian-lower Tortonian sediments deposited over the hangingwall of the Vallès-Penedès Fault in the Marmellar area (Fig. 5), which would indicate, at least for this fault, extensional motion during this period. This fact agrees to previous regional studies that indicate extension in the CCR occurred between Burdigalian and Messinian times (Gallart, 1981; Cabrera et al., 1991; Cabrera and Calvet, 1996; Porta and Civís, 1996; Cabrera et al., 2004). The lack of upper Oligocene and Neogene sediments preserved over in the Miramar-Gaià and Montmell domains prevent establishing a relative chronology of the observed extensional faults.

7. Conclusions

A new field-based dataset integrated with MT data acquired across the Gaià-Montmell High has allowed the recognition of the main features characterizing the upper crustal Alpine structure. MT data along the Gaià-Montmell section has allowed a better definition of the structure at depth and the identification of zones with potential fractures and conductive fluids.

The structure of the Gaià-Montmell High consists of two domains with a differentiated tectono-stratigraphic evolution: the Miramar-Gaià and the Montmell domains. The Miramar-Gaià Domain belongs to an area with a very thin Mesozoic succession (only Triassic) uplifted over the Ebro Basin by a NW-vergent low-angle basement thrust (the Gaià-El Camp Thrust). The Montmell Domain belongs to an area with a well-developed Mesozoic succession that includes Triassic, Jurassic and Cretaceous rocks. This domain is limited towards the NW by the Montmell Fault and its structure consists of NW-vergent compressional faults affected by high-angle SE-dipping extensional basement faults. A highly deformed area with prominent NW-vergent thrust imbrications characterizes the limit between the two domains.

The Montmell Fault corresponds to the SW prolongation of the Vallès-Penedès Fault. Both faults are partially overlapped and linked by the Marmellar Accommodation Zone. We call this major structure the Montmell-Vallès Fault System. This constituted the NW limit of the Montmell-Garraf extensional basin, which developed during the Late Jurassic-Early Cretaceous (Oxfordian to middle Aptian).

A period of tectonic inversion and contractional reactivation related to the Paleogene compressional phase is attested by the presence of highly deformed areas (thin-skinned thrusting and footwall shortcut development) along the Montmell-Vallès Fault System footwall. These contractional structures belong to the positive inversion of the Mesozoic Montmell-Garraf Basin and the emplacement of a NW-directed basement thrust (Gaià-El Camp Thrust) that uplifted the Montmell-Garraf Basin and the adjoining marginal areas of the Ebro High. Reactivation of the Montmell Fault appears to be by some means restricted and, hence, deformation propagated to the fault footwall resulting in shortcut formation. The areas where footwall shortcut structures formed are characterized by conductive bodies at depth.

The age of the positive inversion can be relatively well established by syn-kinematic sediments preserved in the SE margin of the Ebro Basin. These indicate that the Gaià-El Camp Thrust emplacement is late Bartonian to lower Oligocene. The absolute age of the Montmell-Vallès Fault reactivation is uncertain. However, taking into consideration preserved pre-kinematic strata in its footwall, it can be established as, at least, late Ypresian (Cuisian).

Negative tectonic inversion of the previously formed Paleogene and Late-Jurassic faults is also within reach in the Gaià-Montmell High. During Latest Oligocene(?) / early Miocene - late Miocene extensional

displacement at the SW-end of the Vallès-Penedès Fault is relayed to the Baix Penedès Fault and, at minor scale, to the Montmell Fault. Accordingly, accommodation zones characterized by the presence of relay ramp-breaching faults developed. The negative inversion of the Gaià-El Camp Thrust is also identified at the NE-end of El Camp Fault, where an array of extensional faults developed in the Miramar-Gaià Domain. Tectonostratigraphic relationships indicate that extension occurred between Burdigalian and Messinian times.

The following are the supplementary data related to this article.

Declaration of Competing Interest

The authors declare that they have no known competing financial interests or personal relationships that could have appeared to influence the work reported in this paper.

Acknowledgements

This work was funded by the projects CGL2014-54118-C2-1-R/BTE MINECO/FEDER, UE; CGL2017-85532-P AEI/FEDER, UE and CGL2014-55900-P from the Spanish Ministerio de Economía y Competitividad, the project PID2019-106440GB-C21 from the Spanish Ministerio Ciencia Innovación y Universidades, the GEOMODELS Research Institute and the Grup de Geodinàmica i Anàlisi de Conques (grant no. 2017SGR-596). The authors acknowledge Schlumberger and Petroleum Experts for providing academic licenses for Dynel2D© and Move© software respectively, used in the geological mapping and structural interpretation. Constructive reviews from Christopher Connors and an anonymous reviewer significantly improved the original manuscript, for which the authors are very thankful. Ramon Carbonell is also thanked for his role as editor of the present journal.

Appendix A. Supplementary data

Supplementary data to this article can be found online at <https://doi.org/10.1016/j.tecto.2021.228970>.

References

- Albrich, S., Bernaus, J.M., Boix, C., Caus, E., Martín-Closas, C., Salas, R., Vicedo, V., Villalonga, R., 2006. Caracterización bioestratigráfica y paleoambiental del Cretácico Inferior (Berriasiense-Barremiense) del Macizo de Garraf (Cadena Costera Catalana). *Rev. Esp. Micropaleontol.* 38 (2-3), 429–451.
- Aldega, L., Viola, G., Casas-Sainz, A., Marcen, M., Roman-Berdiel, T., van der Lelij, R., 2019. Unraveling multiple thermotectonic events accommodated by crustal-scale faults in Northern Iberia, Spain: insights from K-Ar dating of clay gouges. *Tectonics* 38, 3629–3651.
- Alfonso, P., Canet, C., Melgarejo, J.C., Mata-Perello, J.M., Fallick, A.E., 2012. Stable isotope geochemistry of the Ulldemolins Pb-Zn-Cu deposit (SW Catalan Coastal Ranges, Spain). *Geol. Acta* 10 (2), 145–157.
- Allmendinger, R., Zapata, T., Mancada, R., Dzelalija, F., 2004. Trishear kinematic modeling of structures, with examples from the Neuquen Basin, Argentina. In: McClay, K.R. (Ed.), *Thrust Tectonics and Hydrocarbon Systems*, AAPG Memoir, vol. 82, pp. 356–371.
- Allmendinger, T., 1998. Inverse and forward numerical modeling of tri-shear fault propagation folds. *Tectonics* 17, 640–756.
- Alonso, A., Floquet, M., Mas, R., Meléndez, A., 1993. Late cretaceous carbonate platforms: origin and evolution. Iberian Range, Spain. In: Simó, T., Scout, R.W., Masse, J.P. (Eds.), *Cretaceous Carbonate Platforms*, AAPG Memoir, vol. 56, pp. 297–316.
- Anadón, P., 1978. El Paleógeno continental anterior a la transgresión Biarritzense (Eoceno medio) entre los ríos Gaià y Ripoll (prov. de Tarragona y Barcelona). *Estud. Geol.* 34, 341–440.
- Anadón, P., Colombo, F., Esteban, M., Marzo, M., Robles, S., Santanach, P., Solé-Sugrañes, L., 1979. Evolución tectonoestratigráfica de los Catalánides. *Acta Geol. Hispánica* 14, 242–270.
- Anadón, P., Cabrera, L., Guimerà, J., Santanach, P., 1985. Paleogene strike-slip deformation and sedimentation along the southeastern margin of the Ebro Basin. In: Biddle, K.T., Christie-Blick, N. (Eds.), *Strike-Slip Deformation, Basin Formation and Sedimentation*, Society of Economic Paleontologists and Mineralogists Special Publication, vol. 37, pp. 301–318.
- Ashauer, H., Teichmüller, R., 1935. Die variszische und alpidische Gebirgsbildung Kataloniens. *Abhandlungen Gesellschaft Wissenschaften Göttingen. Math. Phys. Kl.* (3F), 16.

- Baqués, V., Travé, A., Roca, E., Marín, M., Cantarero, I., 2012. Geofluid behaviour in successive extensional and compressional events: a case study from the southwestern end of the Vallès-Penedès Fault (Catalan Coastal Ranges, NE Spain). *Pet. Geosci.* 18 (2012), 17–31.
- Baqués, V., Travé, A., Cantarero, I., 2013. Development of successive karstic systems within the Baix Penedès Fault zone (onshore of the Valencia Trough, NW Mediterranean). *Geofluids* 14, 75–94.
- Barberà, X., Cabrera, L., Marzo, M., Parés, J.M., Agustí, J., 2001. A complete terrestrial Oligocene magnetobiostratigraphy from the Ebro Basin, Spain. *Earth Planet. Sci. Lett.* 187, 1–16.
- Bartrina, M.T., Cabrera, L., Jurado, M.J., Guimerà, J., Roca, E., 1992. Evolution of the central margin of the Valencia trough (western Mediterranean). *Tectonophysics* 203, 219–247.
- Bond, R.M.G., McClay, K.R., 1995. Inversion of lower cretaceous extensional basin, south central Pyrenees, Spain. In: Buchanan, J.G., Buchanan, P.G. (Eds.), *Basin Inversion*, Geological Society Special Publication, vol. 88, pp. 415–431.
- Buchanan, J.G., Buchanan, P.G., 1995. Basin Inversion. *Geol. Soc. Spec. Publ.* 88 (596pp.).
- Butler, R., Tavarnelli, E., Grasso, M., 2006. Tectonic inversion and structural inheritance in mountain belts. *J. Struct. Geol.* 28, 1891–1892.
- Cabrera, L., Calvet, F., 1996. Onshore Neogene record in NE Spain: Vallès-Penedès and El Camp half-grabens (NW Mediterranean). In: Friend, P.T., Dabrio, D. (Eds.), *Tertiary Basins of Spain*, pp. 97–105.
- Cabrera, L., Calvet, F., Guimerà, J., Permanyer, A., 1991. El registro sedimentario miocénico en los semigrabens del Vallès-Penedès y de El Camp: organización secuencial y relaciones tectónica sedimentación. In: I Congreso del Grupo Español del Terciario: Libro-guía Excursión, 84 (132pp.).
- Cabrera, L., Roca, E., Garcés, M., de Porta, J., 2004. Estratigrafía y evolución tectonosedimentaria oligocena superior-neógena del sector central del margen catalán (Cadena Costero-Catalana). In: Vera, J.A. (Ed.), *Geología de España*. SGE-IGME, Madrid, pp. 569–573.
- Calvert, A., Sandvol, E., Seber, D., Barazangi, M., Roecker, S., Mourabit, T., Vidal, F., Alguacil, G., Jabour, N., 2000. Geodynamic evolution of the lithosphere and upper mantle beneath the Alboran region of the western Mediterranean: constraints from travel time tomography. *J. Geophys. Res. Solid Earth* 105, 10871–10898.
- Calvet, F., Marzo, M., 1994. El Triásico de las Cordilleras Costero-Catalanas: estratigrafía, sedimentología y análisis secuencial. In: Field guide III Coloquio de Estratigrafía y Sedimentología del Triásico y Pérmico de España, pp. 1–53.
- Campanyà, J., Ledo, J., Queralt, P., Marcuello, A., Muñoz, J.A., Liesa, M., Jones, A.G., 2018. New geoelectrical characterization of a continental collision zone in the Central – E astern Pyrenees: constraints from 3-D joint inversion of electromagnetic data. *Tectonophysics* 742–743, 168–179.
- Canet, C., Alfonso, P., Melgarejo, J.C., Fallick, A.E., 2005. Stable isotope geochemistry of the carboniferous Zn-Pb-Cu sediment-hosted sulfide deposits, Northeastern Spain. *Int. Geol. Rev.* 47, 1298–1315.
- Cantarero, I., Travé, A., Aliás, G., Baqués, V., 2014. Polyphasic hydrothermal and meteoric fluid regimes during the growth of a segmented fault involving crystalline and carbonate rocks (Barcelona Plain, NE Spain). *Geofluids* 14, 20–44.
- Cardellach, E., Canals, A., Tritlla, J., 1990. Late and post-Hercynian low temperature veins in the Catalanian Coastal ranges. *Acta Geol. Hispan.* 25 (1–2), 75–81.
- Carminati, E., Wortel, M.J.R., Meijer, P.T., Sabadini, R., 1998. The two-stage opening of the western-Central Mediterranean basins: a forward modeling test to a new evolutionary model. *Earth Planet. Sci. Lett.* 160, 667–679.
- Casas, A., Permanyer, A., 1991. Disposición y estructura del zócalo de la depresión terciaria del Penedés. *Rev. Inst. Investig. Geol.* 35 (1891/82), 23–30.
- Colombo, F., 1986. Continental Paleogene stratigraphy and sedimentology of the western southern border of the Catalanides, Tarragona Province, Spain. *Cuadern. Geol. Ibérica* 10, 55–115.
- Cooper, M.A., Williams, G.D., de Graciansky, P.C., Murphy, R.W., Needham, T., de Paor, D., Stonley, R., Todd, S.P., Turner, J.P., Ziegler, P.A., 1989. Inversion Tectonics – A Discussion. In: Cooper, M.A., Williams, G.D. (Eds.), *Inversion Tectonics*, Special Publication of the Geological Society of London, vol. 44. Blackwell Scientific Publications, pp. 335–347.
- Coward, M.P., 1994. Inversion tectonics. In: Hancock, P.L. (Ed.), *Continental Deformation*. Pergamon, Oxford, pp. 289–304.
- Dahlstrom, C.D.A., 1969. Balanced cross sections. *Can. J. Earth Sci.* 6, 743–757.
- Dañoibeitia, J.J., Arguedas, M., Gallart, F., Banda, E., Makris, J., 1992. Deep crustal configuration of the Valencia Trough and its Iberian and Balearic borders from extensive refraction and wide-angle reflection profiling. *Tectonophysics* 203, 37–55.
- Egbert, G.D., Booker, J.R., 1986. Robust estimation of geomagnetic transfer functions. *Geophys. J. Int.* 87, 173–194.
- Enrique, P., Solé, J., 2004. El basamento ígneo. Las rocas intrusivas de la Cordillera Costero-Catalana. In: Vera, J.A. (Ed.), *Geología de España*. SGE-IGME, Madrid, pp. 481–484.
- Escudero-Mozo, M.J., Márquez-Aliaga, A., Goy, A., Martín-Chivelet, J., López-Gómez, J., Márquez, L., Arche, A., Plasencia, P., Pla, C., Marzo, M., Sánchez-Fernández, D., 2017. Middle Triassic carbonate platforms in eastern Iberia: Evolution of their fauna and palaeogeographic significance in the western Tethys. *Palaeogeogr. Palaeoclimatol. Palaeoecol.* 417, 236–260.
- Esteban, M., Robles, S., 1976. Sobre la paleogeografía del Cretácico Inferior de los Catalánides entre Barcelona y Tortosa. *Acta Geol. Hispan.* XI, 73–78.
- Etheve, N., Mohn, G., Frizon de Lamotte, D., Roca, E., Tugend, J., Gómez-Romeu, J., 2018. Extreme Mesozoic crustal thinning in the Eastern Iberia margin: the example of the Columbrets Basin (Valencia Trough). *Tectonics* 37–2, 636–662.
- Fernández, M., Torné, M., Zeyen, H., 1990. Lithospheric thermal structure of NE Spain and the North-Balearic Basin. *J. Geodyn.* 12, 253–267.
- Ferrer, J., 1971. El Paleoceno y Eoceno del borde suroriental de la Depresión del Ebro (Cataluña). In: *Memories Suisses de Paléontologie*, 90 (70pp.).
- Ferrer, O., McClay, K.R., Sellier, N.C., 2016. Influence of fault geometries and mechanical anisotropies on the growth and inversion of hanging-wall synclinal basins: insights from sandbox models and natural examples. *Geol. Soc. Lond., Spec. Publ.* 439, 487–509.
- Fontboté, J.M., 1954. Las relaciones tectónicas de la depresión del Vallès-Penedés con la Cordillera Prelitoral Catalana y con la Depresión del Ebro. In: *Tomo Homenaje a Prof. E. Hernández-Pacheco*. Real Sociedad Española de Historia Natural, Madrid, pp. 281–310.
- Fossen, H., Rotevatn, A., 2016. Fault linkage and relay structures in extensional settings – a review. *Earth-Sci. Rev.* 154, 14–28.
- Galán-Abellán, B., López-Gómez, J., Berrechea, J.F., Marzo, M., De la Horra, R., Arche, A., 2013. The beginning of the Buntsandstein cycle (Early–Middle Triassic) in the Catalan Ranges, NE Spain: Sedimentary and palaeogeographic implications. *Sediment. Geol.* 296, 86–102.
- Gallart, F., 1981. Neógeno superior y Cuaternario del Penedés (Catalunya, España). *Acta Geol. Hispan.* 16, 151–157.
- García-Senz, J., 2002. Cuencas extensivas del Cretácico Inferior en los Pirineos centrales. In: *Formación y subsecuente inversión*. Universitat de Barcelona. Ph.D. Thesis. (310pp.).
- García-Senz, J., Pedrera, A., Ayala, C., Ruiz-Constán, A., Robador, A., Rodríguez-Fernández, L.R., 2019. Inversion of the north Iberian hyperextended margin: the role of exhumed mantle indentation during continental collision. *Geol. Soc. Spec. Publ.* 490, 177–198.
- Gaspar-Escribano, J., García-Castellanos, D., Roca, E., Cloetingh, S., 2004. Cenozoic vertical motions of the Catalan Coastal Ranges (NE Spain): the role of tectonics, isostasy, and surface transport. *Tectonics* 23, 1–18.
- Gillcrist, R., Coward, M.P., Mugnier, J.L., 1987. Structural inversion and its controls: examples from the Alpine foreland and the French Alps. *Geodin. Acta* 1, 5–34.
- Gómez, M., Guimerà, J., 1999. Estructura Alpina de la Serra de Miramar y del NE de las Muntanyes de Prades (Cadena Costera Catalana). *Rev. Soc. Geol. Esp.* 12 (3–4), 405–418.
- Guimerà, J., 2018. Structure of an intraplate fold-and-thrust belt: the Iberian Chain. A synthesis. *Geol. Acta* 16–4, 427–438.
- Guimerà, J., 1984. Paleogene evolution of deformation in the northeastern Iberian Peninsula. *Geol. Mag.* 121, 413–420.
- Guimerà, J., 2004. La Cadena Costera Catalana. In: Vera, J.A. (Ed.), *Geología de España*. SGE-IGME, Madrid, pp. 603–605.
- Guimerà, J., Alvaro, M., 1990. Structure et évolution de la compression alpine dans la Chaîne ibérique et la Chaîne côtière catalane (Espagne). *Bull. Soc. Géol. France* 6 (2), 339–348.
- Guimerà, J., Santanach, P., 1978. Sobre la compresión alpina en el sector central de las Cadenas Costeras Catalanas. *Acta Geol. Hispan.* 2 (13), 33–42.
- Guimerà, J., Alonso, A., Mas, J.R., 1995. Inversion of an extensional-ramp basin by a newly formed thrust: The Cameros basin (N. Spain). In: Buchanan, J.G., Buchanan, P. G. (Eds.), *Basin Inversion*, Geological Society Special Publication, vol. 88, pp. 433–453.
- Hernández, E., Casas, A., 1985. Estudio gravimétrico de la depresión del Penedés. *Acta Geol. Hispan.* 20 (3–4), 191–198.
- Horváth, F., Berckhemer, H., 1982. Mediterranean backarc basins. In: Berckhemer, H., Hsü, K. (Eds.), *Alpine Mediterranean Geodynamics*, American Geophysical Union, Geodynamic Series A, vol. 7, pp. 141–173.
- Jackson, J.A., 1980. Reactivation of basement faults and crustal shortening in orogenic belts. *Nature* 283, 343–346.
- Juez-Larré, J., Andriessen, P.A.M., 2006. Tectonothermal evolution of the northeastern margin of Iberia since the break-up of Pangea to present, revealed by low-temperature fission-track and (U-Th)/He thermochronology. A case history of the Catalan Coastal Ranges. *Earth Planet. Sci. Lett.* 243, 159–180.
- Julivert, M., 1955. Geología de la Sierra de Miramar. *Memor. Comunicac. Inst. Geol.* 13, 79–118.
- Julivert, M., Durán, H., 1990. The Hercynian structure of the Catalanian Coastal Ranges (NE Spain). *Acta Geol. Hispan.* 25 (1–2), 13–21.
- Lanaja, J.M., 1987. Contribución de la explotación petrolífera al conocimiento de la geología de España. IGME, Madrid.
- Ledo, J., 2005. 2-D versus 3-D magnetotelluric data interpretation. *Surv. Geophys.* 26–5, 511–543.
- Ledo, J., Queralt, P., Pous, J., 1998. Effects of galvanic distortion on magnetotelluric data over three-dimensional regional structure. *Geophys. J. Int.* 132, 295–301.
- Llopis-Lladó, N., 1947. Contribución al conocimiento de la morfoestructura de los Catalánides. Inst. “Lucas Madalla”, Barcelona CSIC (373pp.).
- López-Blanco, M., Marzo, M., Burbank, D.W., Vergés, J., Roca, E., Anadón, P., Piña, J., 2000. Tectonic and climatic controls on the development of foreland fan deltas: Montserrat and Sant Llorenç del Munt systems (Middle Eocene, Ebro Basin, NE Spain). *Sediment. Geol.* 138, 17–39.
- Marcén, M., Casas-Sainz, A.M., Román-Berdiel, T., Grier, A., Santanach, P., Pocoví, A., Gil-Imaz, A., Aldega, L., Izquierdo-Llavall, E., 2018. Multiple movements recorded in a crustal weakness zone in NE Iberia: the Vallès-Penedès Fault revisited. *J. Geodyn.* 121, 96–114.
- Marín, M.A., Roca, E., Rosell, O., Marcuello, A., Cabrera, L., 2008. La Falla del Montmell: un ejemplo del control ejercido por las fallas extensivas mesozoicas en la arquitectura cenozoica de las Cadenas Costaneras Catalanas. *Geotemas* 10, 461–464.
- Martí, A., Queralt, P., Roca, E., Ledo, J., Galindo-Zaldívar, J., 2009a. Geodynamic implications for the formation of the Betic-Rif orogen from magnetotelluric studies. *J. Geophys. Res.* 114-B1, 1–14.

- Martí, A., Queralt, P., Ledo, J., 2009b. WALDIM: a code for the dimensionality analysis of magnetotelluric data using the rotational invariants of the magnetotelluric tensor. *Comput. Geosci.* 35 (12), 2295–2303.
- Martí, A., Queralt, P., Marcuello, A., Ledo, J., Rodríguez-Escudero, E., Martínez-Díaz, J., Campaña-Llovet, J., Meqbel, N., 2020. Magnetotelluric characterization of the Alhama de Murcia Fault (Eastern Betics, Spain) and study of magnetotelluric interstation impedance inversion. *Earth Planets Space* 72, 16.
- Marzo, M., 1980. El Buntsandstein de los Catalánides: estratigrafía y procesos de sedimentación. PhD Thesis. Universitat de Barcelona (317pp.).
- McClay, K., 1995. 2D and 3D analogue modelling of extensional fault structures; templates for seismic interpretation. *Pet. Geosci.* 1, 163–178.
- McNeice, G.W., Jones, A.G., 2001. Multisite, multifrequency tensor decomposition of magnetotelluric data. *Geophysics* 66 (1), 158–173.
- Melgarejo, J.C., 1987. Estudi geològic i metal·logenètic del Paleozoic del Sud de les Serralades Costaneres Catalanes. PhD Thesis Universitat de Barcelona, pp. 1–615.
- Mencos, J., Carrera, N., Muñoz, J.A., 2015. Influence of rift basin geometry on the subsequent postrift sedimentation and basin inversion: the Organyà Basin and the Boixols thrust sheet (south central Pyrenees). *Tectonics* 34, 1452–1474.
- Mercedes-Martín, R., Buatois, L.A., 2020. Microbialites and trace fossils from a Middle Triassic restricted carbonate ramp in the Catalan Basin, Spain: evaluating environmental and evolutionary controls in an epicontinental setting. *Lethaia* 54 (1), 4–25. <https://doi.org/10.1111/let.12378>.
- Mercedes-Martín, R., Arenas, C., Salas, R., 2014. Diversity and factors controlling widespread occurrence of syn-rift Ladinian microbialites in the western Tethys (Triassic Catalan Basin, NE Spain). *Sediment. Geol.* 313, 68–90.
- Mitra, S., Mount, V.S., 1998. Foreland-involved basement structures. *Am. Assoc. Pet. Geol. Bull.* 82, 70–109.
- Muñoz, G., Mateus, A., Pous, J., Heise, W., Santos, F.M., Almeida, E., 2008. Unravelling middle-crust conductive layers in Palaeozoic Orogens through 3D modeling of magnetotelluric data: the Ossa-Morena Zone case study (SW Iberian Variscides). *J. Geophys. Res.* 113 (B06106), 1–23.
- Muñoz, J.A., 1992. Evolution of a continental collision belt: ECORS-Pyrenees crustal balanced cross-section. In: McClay, K. (Ed.), *Thrust Tectonics*. Chapman & Hall, London, pp. 235–246.
- Muñoz, J.A., 2017. Fault-related folds in the southern Pyrenees. *AAPG Bull.* 101-4, 579–587.
- Nebot, G., Guimerà, J., 2016. Structure of an inverted basin from subsurface and field data: the Late Jurassic-Early Cretaceous Maestrat Basin (Iberian Chain). *Geol. Acta* 14 (2), 155–177.
- Nicol, A., Watterson, J., Walsh, J.J., Childs, C., 1996. The shapes, major axis orientations and displacement patterns of fault surfaces. *J. Struct. Geol.* 18 (2–3), 235–248.
- Ortí, F., 1974. El Keuper del Levante español. *Estud. Geol.* 30, 7–46.
- Ortí, F., Pérez-López, A., Salvany, J.M., 2017. Triassic evaporites of Iberia: Sedimentological and palaeogeographical implications for the western Neotethys evolution during the Middle Triassic–Earliest Jurassic. *Palaeogeogr. Palaeoclimatol. Palaeoecol.* 471, 157–180.
- Porta, J., Civís, J., 1996. La sucesión bioestratigráfica del mioceno marino en el Penedés y el horst de Tarragona-Bonastre (Neógeno del Sistema Mediterráneo). *Geogaceta* 19, 97–102.
- Pous, J., Marcuello, A., Queralt, P., 2001. Magnetotelluric signature of the western Cantabrian Mountains. *Geophys. Res. Lett.* 28, 1795–1798.
- Robles, S., 1982. El Cretácico de los Catalánides. In: *El Cretácico de España*. Universidad Complutense de Madrid, Madrid, pp. 199–272.
- Roca, E., 2001. The Northwest-Mediterranean basin (Valencia Trough, Gulf of Lions and Lliguro-Provençal basins): structure and geodynamic evolution. In: Ziegler, P.A., Cavazza, W., Robertson, A.H.F., Crasquin-Soleau, S. (Eds.), *Peri-Tethys Memoir 6: Peri-Tethyan Rift/Wrench Basins and Passive Margins*, French National Museum of Natural History, vol. 186, pp. 671–706.
- Roca, E., Guimerà, J., 1992. The Neogene structure of the eastern Iberian margin: structural constraints on crustal evolution of the Valencia Trough (western Mediterranean). *Tectonophysics* 203, 203–218.
- Roca, E., Sans, M., Cabrera, I., Marzo, M., 1999. Oligocene to Middle Miocene evolution of the central Catalan margin (northwestern Mediterranean). *Tectonophysics* 315, 209–233.
- Roca, E., Frizon de Lamotte D., Mauffret, A., Bracène, R., Vergés, J., Benaouali, N., Fernández, M., Muñoz, J. A. and Zeyen, H. 2004. Transect II: Aquitaine Basin - Pyrenees - Ebro Basin - Catalan Range - Valencia Trough - Balearic Block - Algerian Basin - Kabylies - Atlas - Saharan Platform. In: Cavazza, W., Roure, F. M., Spakman, W., Stampfli, G. M. and Ziegler, P. A. (Eds.), 2004. *The Transmed Atlas – The Mediterranean Region from Crust to Mantle*, Springer, Berlin, Heidelberg.
- Rodi, W.L., Mackie, R.L., 2001. Nonlinear conjugate gradients algorithm for 2-D magnetotelluric inversion. *Geophysics* 66, 174–187.
- Roest, W.R., Srivastava, S.P., 1991. Kinematics of the plate boundaries between Eurasia, Iberia and Africa in the North Atlantic from the Late Cretaceous to the present. *Geology* 19, 613–616.
- Roma, M., Ferrer, O., Roca, E., Pla, O., Escosa, F.O., Butillé, M., 2018. Formation and inversion of salt-detached ramp-syncline basins. Results from T analog modeling and application to the Columbrets Basin (Western Mediterranean). *Tectonophysics* 745, 214–228.
- Rosenbaum, G., Lister, G.S., Duboz, C., 2002. Relative motions of Africa, Iberia and Europe during Alpine orogeny. *Tectonophysics* 359, 117–129.
- Rubinat, M., Ledo, J., Roca, E., Rosell, O., Queralt, P., 2010. Magnetotelluric characterization of a salt diapir: a case study on Bicorn-Biqua Diapir (Prebetic Zone, SE Spain). *J. Geol. Soc.* 167, 145–153.
- Sàbat, F., Roca, E., Muñoz, J.A., Vergés, J., Santanach, P., Sans, M., Masana, E., Estévez, A., Santisteban, C., 1997. Role of extension and compression in the evolution of eastern margin of Iberia: the ESCI-Valencia Trough seismic profile. *Rev. Soc. Geol. Esp.* 8 (4), 431–448.
- Sáez, A., Anadón, P., 1989. El Complejo turbidítico del Carbonífero del Priorat (Tarragona). *Acta Geol. Hispán.* 24 (1), 33–47.
- Salas, R., 1987. El Malm i el Cretaci inferior entre el Massís de Garraf i la Serra d'Espadà. PhD Thesis. Universitat de Barcelona (345pp.).
- Salas, R., Casas, A., 1993. Mesozoic extensional tectonics, stratigraphy and crustal evolution during the Alpine cycle of the eastern Iberian basin. *Tectonophysics* 228 (1–2), 33–55.
- Salas, R., Guimerà, J., Mas, R., Martín-Closas, C., Meléndez, A., Alonso, A., 2001. Evolution of the Mesozoic Central Iberian Rift System and its Cainozoic inversion (Iberian Chain). In: Ziegler, P.A., Cavazza, W., Robertson, A.H.F., Crasquin-Soleau, S. (Eds.), *Peri-Tethys Memoir 6: Peri-Tethyan Rift/Wrench Basins and Passive Margins*, French National Museum of Natural History, vol. 186, pp. 145–185.
- Salas, R., Guimerà, J., Bover-Arnal, T., Nebot, M., 2020. The Iberian-Catalan Linkage: the Maestrat and Garraf Basin. In: Quesada, Oliveira (Eds.), *The Geology of Iberia: A geodynamic approach*, Regional Geology Reviews, vol. 3, pp. 228–230. Ch. 5.
- Serra, P.R., Enrique, P., 1989. The Late-Hercynian intrusives from southern Catalanian Coastal Ranges (NE Spain), and their epilitonic to subvolcanic level of magma emplacement. *Rend. Soc. Ital. Mineral. Petrol.* 43, 817–829.
- Sibuet, J.C., Srivastava, S., Spakman, W., 2004. Pyrenean orogeny and plate kinematics. *J. Geophys. Res.* 109, B08104.
- Simpson, F., Bahr, K., 2005. *Practical Magnetotellurics*. Cambridge University Press (270pp.).
- Srivastava, S.P., Roest, W.R., Kovacs, L.C., Oakey, G., Lévesque, S., Verhoef, J., Macnab, R., 1990. Motion of Iberia since the Late Jurassic: results from detailed aeromagnetic measurements in the Newfoundland Basin. *Tectonophysics* 184, 229–260.
- Tugend, J., Manatschal, G., Kuszniir, N.J., 2015. Spatial and temporal evolution of hyperextended rift systems: implication for the nature, kinematics, and timing of the Iberian-European plate boundary. *Geology* 43 (1), 15–18.
- Van Hinsbergen, D.J.J., Vissers, R.L.M., Spakman, W., 2014. Origin and consequences of western Mediterranean subduction, rollback, and slab segmentation. *Tectonics* 33, 393–419.
- Vergés, J., Fernández, M., Martínez, A., 2002. The Pyrenean origin: pre-, syn-, and post-collisional evolution. In: Rosenbaum, G., Lister, G.S. (Eds.), *Reconstruction of the Evolution of the Alpine-Himalayan Orogen*, Journal of the Virtual Explorer, vol. 8, pp. 57–76.
- Vidal, R., Gallart, J., Dañobeitia, J., Díaz, J., 1995. Mapping the Moho in the Iberian Mediterranean margin by multicoverage processing and merging of wide-angle and near-vertical reflection data. In: Banda, E., Torné, M., Talwani, M. (Eds.), *Rifted Ocean Continent Boundaries*, NATO ASI Series C, Mathematical and Physical Sciences, vol. 463, pp. 291–308.
- Virgili, C., Cassinis, G., Broutin, J., 2006. Permian to Triassic sequences from selected continental areas of Southwestern Europe. *Geol. Soc. Lond. Spec. Publ.* 265, 231–265.
- Williams, G.D., Powell, C.M., Cooper, M.A., 1989. Geometry and kinematics of inversion tectonics. In: Cooper, M.A., Williams, G.D. (Eds.), *Inversion Tectonics*, Geological Society of London, Special Publication, vol. 44, pp. 3–15.
- Withjack, M.O., Schlische, R.W., 2006. Geometric and experimental models of extensional fault-bend folds. In: Buitier, S.J.H., Schreurs, G. (Eds.), *Analogue and Numerical Modelling of Crustal-Scale Processes*, Geological Society of London, Special Publication, vol. 253, pp. 285–305.

SECOND PUBLICATION

Paleogene compression reconstruction in the central Catalan Coastal Ranges

Marín, M., Carola, E., Beamud, E., Bover-Arnal, T., López-Blanco, M., Garcés, M., Roca, E., Costa, E., Ferrer, O., Cabrera, L., 2025. Paleogene kinematics of the central Catalan Coastal Ranges: temporal constraints from magneto-chronology and provenance analysis in synorogenic deposits in the SE margin of the Ebro Basin (NE Spain). *Geologica Acta* 23.2, 1-25.

DOI: <https://doi.org/10.1344/GeologicaActa2025.23.2>

Journal metrics (data from Journal Citation Report for 2023; 2024/2025 not available):

- Journal Impact Factor: **1.3**
- Journal Impact Factor excluding self-citations: **1.3**
- Category: **Geology**
- Position: **22/61** (based on category and year of publication)
- Quartil: **Q2**

This paper (Marín *et al.*, 2025) aims to refine the chronology of the contractional Paleogene structure in the central Catalan Coastal Ranges, utilizing magnetostratigraphy and provenance analysis performed in synorogenic deposits from the central southeastern margin of the Ebro Basin. The results of the paper constrain the timing of the emplacement of the compressional structures that conformed the northwesternmost part of the Catalan Intraplate Belt during the Paleogene, including the onset of the inversion of the Montmell-Vallès Fault System, the development of the Gaià-El Camp Thrust as recorded by the coeval deposition of the synorogenic successions. The results are then integrated within the evolution of the whole southeastern margin of the Ebro Basin during the Paleogene.

The paper is included in a special volume in homage to Ramon Salas.

Data and supplementary material can be found in the following link: [data and supplementary material](#)

[Geologica Acta](#) a journal providing innovative and high-quality means of scientific dissemination, with researchers and specialists in the Earth Science field as the main audience. It is a non-profit DIAMOND OPEN ACCESS (neither submission nor reading fees are charged) which has the aim to stimulate rapid diffusion of results and efficient exchange of ideas between the widespread communities of researchers in Earth Science.

Barcelona, 7th of January 2025

Dear authors,

I am pleased to inform you that your revised paper “Paleogene kinematics of the central Catalan Coastal Ranges: temporal constraints from magneto-chronology and provenance analysis in synorogenic deposits in the SE margin of the Ebro Basin (NE Spain)” by Miquel Marín, Eloi Carola, Elisabet Beamud, Telm Bover-Arnal, Miguel López-Blanco, Miguel Garcés, Eduard Roca, Elisenda Costa, Oriol Ferrer and Lluís Cabrera is accepted for publication in *Geologica Acta*.

Thank you for your fine submittal to *Geologica Acta*.

With best regards,

The editorial committee
Geologica Acta

Paleogene kinematics of the central Catalan Coastal Ranges: temporal constraints from magneto-chronology and provenance analysis in synorogenic deposits in the SE margin of the Ebro Basin (NE Spain)

Miquel Marín^{1,2} Eloi Carola^{2,3} Elisabet Beamud^{2,4} Telm Bover-Arnal^{2,5} Miguel López-Blanco^{2,3} Miguel Garcés^{2,3}
Eduard Roca^{2,3} Elisenda Costa^{3,6} Oriol Ferrer^{2,3} Lluís Cabrera^{2,3}

¹SLB

Abingdon Technology Centre, OX14 4RU Abingdon, United Kingdom

²UB-Geomodels Research Institute

Facultat de Ciències de la Terra, University of Barcelona (UB), Martí i Franquès s/n, 08028 Barcelona, Spain

³Departament de Dinàmica de la Terra i de l'Oceà

Facultat de Ciències de la Terra, University of Barcelona (UB), Martí i Franquès s/n, 08028 Barcelona, Spain

⁴ Paleomagnetic Laboratory CCiTUB - GEO3BCN CSIC

Carrer Lluís Solé i Sabarís s/n, 08028 Barcelona, Spain

⁵Departament de Mineralogia, Petrologia i Geologia Aplicada

Facultat de Ciències de la Terra, University of Barcelona (UB), Martí i Franquès s/n, 08028 Barcelona, Spain

⁶INS Torrent de les Bruixes (Departament d'Educació Generalitat Catalunya)

c/ Sta. Eulàlia s/n, 08921 Santa Coloma de Gramenet, Spain

ABSTRACT

The precise determination of the tectonic deformation timing such as thrust emplacement has always been a challenge for understanding the evolution of fold-and-thrust belts. In the Catalan Coastal Ranges, this issue has traditionally been addressed through the mapping and the analysis of the syn-tectonic successions preserved in the SE margin of the Ebro Basin. However, the age of the Paleogene contractional structures located towards the hinterland and responsible of the inversion and uplift of the inherited Mesozoic structure remained uncertain due to the lack of preserved syn-kinematic strata in these areas. With the aim of better understand the contractional evolution of the area during the Paleogene, this work presents a tectono-stratigraphic analysis approach that combines structural reconstructions, provenance analysis and magnetostratigraphic dating in well-exposed synorogenic sediments in the central SE margin of the Ebro Basin. The results of the study allow to establish the precise age of the main contractional structures present in the central Catalan Coastal Ranges. The combined analysis has revealed that: 1) the inversion of the Montmell-Vallès Faults System started in the Bartonian and continued up to the late Priabonian, and 2) the emplacement of the Gaià-El Camp Thrust and the formation of the Cabra-Carme Anticline took place from early to late Priabonian and was the responsible of the sudden increased of the sedimentation rates. A later decrease of the sedimentation rates during late Priabonian (chron C15n) has been interpreted as the prelude of the end of the Paleogene compressional phase in the area.

KEYWORDS | Catalan Coastal Ranges. Ebro Foreland Basin. Synorogenic. Magnetostratigraphy. Provenance Analysis. Paleogene.

INTRODUCTION

Thrust systems in orogenic belts have traditionally been interpreted as usually propagating toward the foreland in a forward-breaking thrusting sequence (Boyer and Elliott, 1982; Butler, 1982, 1987). In this sequence, foreland basin sediments are progressively incorporated in the deformation wedge (Fig. 1). Thrusting can also develop towards the hinterland, a process known as break-back sequence (Boyer and Elliott, 1982; Butler, 1982, 1987). Moreover, out-of-sequence thrusts might develop in the hinterland of the fold-and-thrust belt, thus conditioning the advance of deformation as well as the configuration of the orogen (McClay, 1992). On the other hand, the configuration of fold-and-thrust belts can also be influenced by the presence of pre-existing extensional faults. The reactivation of these faults can lead to the development of inversion-related structures such as footwall shortcuts, hanging-wall folding and backthrusting as the effect of the buttressing (e.g. Butler, 1989; Hayward and Graham, 1989; Coward *et al.*, 1991; Coward, 1994; Scisciani *et al.*, 2001; Amilibia

et al., 2008; Ferrer *et al.*, 2023) or by changes in the mechanical stratigraphy (Couzens *et al.*, 1996; Gross *et al.*, 1997; Ferril *et al.*, 2008). Understanding the sequence of emplacement of thrusts is important in order to better interpret the changes in the sedimentation pattern over time due to the fact that tectonics and sedimentation are closely interconnected in orogenic belts. Thus, changes in depositional systems are often interpreted as responses to regional or local tectonic activity, such as the uplift and growth of nearby thrusts or folds. Moreover, the geometrical and genetic analysis of syn-tectonic strata can be used to understand the kinematics of individual structures (e.g. Vergés and Muñoz, 1990; Suppe *et al.*, 1992; Burbank *et al.*, 1992; Hardy *et al.*, 1996; Ford *et al.*, 1997; Vergés *et al.*, 2002; Salvini and Storti, 2002; Fernández *et al.*, 2004).

A thorough understanding of key geological elements and their critical moments is essential for accurately assessing natural resources like hydrocarbons, CO₂ storage, minerals, and geothermal energy. Determining the absolute and relative ages of structures is vital to assess

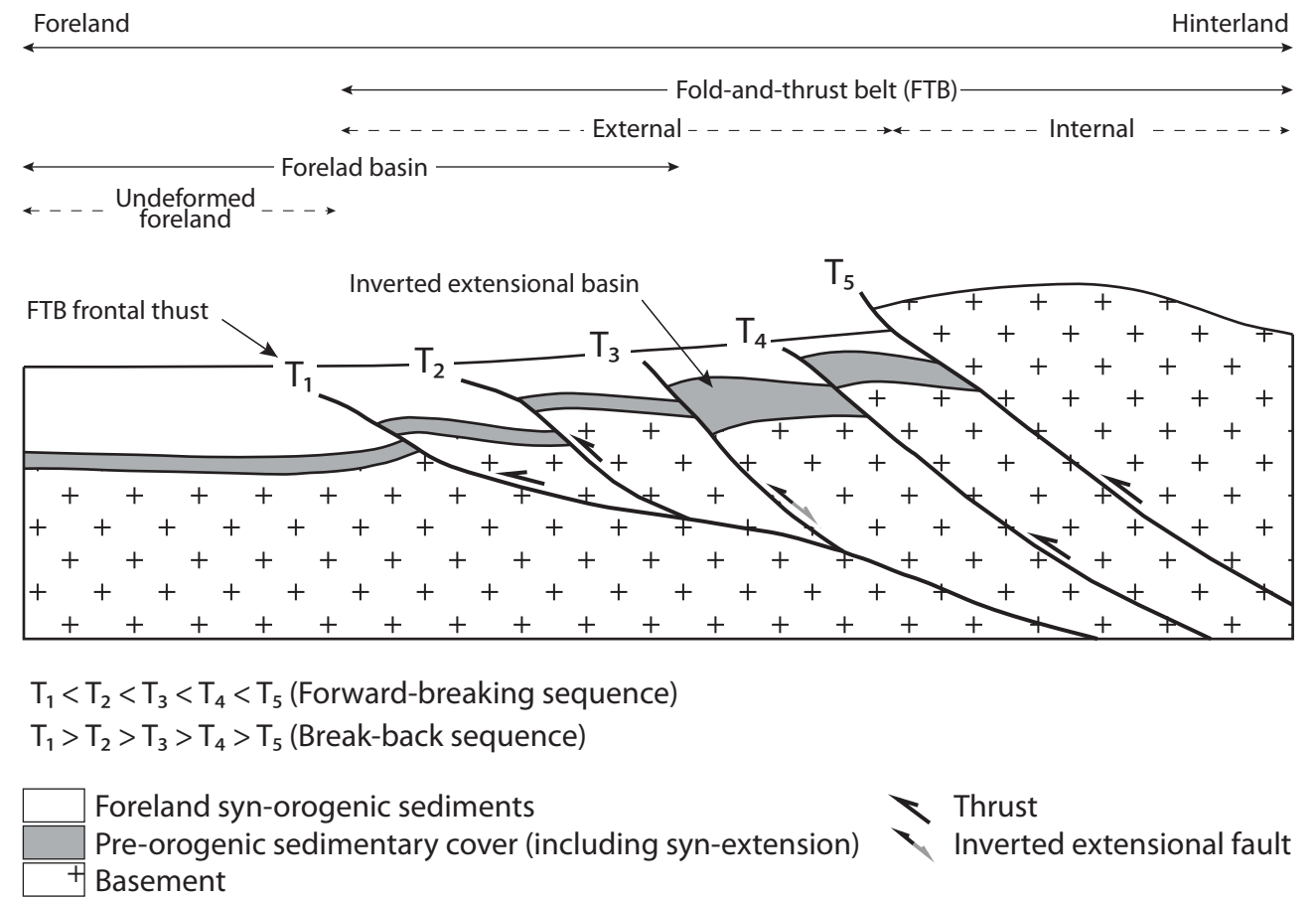


FIGURE 1. Schematic diagram of a thick-skinned fold-and-thrust belt, which includes an inverted extensional basin and its related foreland basin. T_i to T_v stand for relative timing of deformation. End-member thrusting sequences (forward-breaking and break-back) are also specified. Other combinations of relative timing imply out-of-sequence thrusting.

uncertainties and exploration risks, like the timing between hydrocarbon generation and trap formation (Magoon, 1987; Al-Hajeri *et al.*, 2009; Makeen *et al.*, 2016) or cross-cutting relationships in non-accessible areas. Analyzing syn-kinematic sedimentation and growth geometries is crucial to determine the age and movement of structures in orogenic belts.

The Ebro Basin is the southern foreland of the Pyrenean orogen (northeastern Iberia) that developed from Late Cretaceous to middle Miocene times (Muñoz, 1992; Vergés and García-Senz, 2001; Mouthereau *et al.*, 2014). To the southwest and southeast, the Ebro Basin is limited by two intraplate chains that resulted from the inversion of pre-existent Mesozoic basins: the Iberian Range, and the Catalan Coastal Ranges (CCR) respectively (Fig. 2). The

Ebro Basin infill is made up by both marine and continental sediments that thickens northwards and northwestwards up to over 5,000m (Rioja-3 borehole; Lanaja, 1987). At the basin margins, these sediments record the growth of the three mountain ranges. World-class examples of growth strata have been documented along the three margins (*e.g.* Riba, 1973, 1976; Anadón, 1978; Anadón *et al.*, 1985, 1986; Vergés and Muñoz, 1990; Suppe *et al.*, 1992, 1997; Colombo, 1994; Ford *et al.*, 1997; Lawton *et al.*, 1999; López-Blanco, 2002; Gómez-Paccard *et al.*, 2011). Such growth strata geometries in the southeastern margin, together with clast composition and paleocurrents analysis performed in the alluvial and fan-delta sediments deposited at the toe of the CCR have been used to decipher the age and kinematics of some frontal fold-and-thrust structures both, regionally (Anadón, 1978a, b; Anadón *et al.*, 1985;

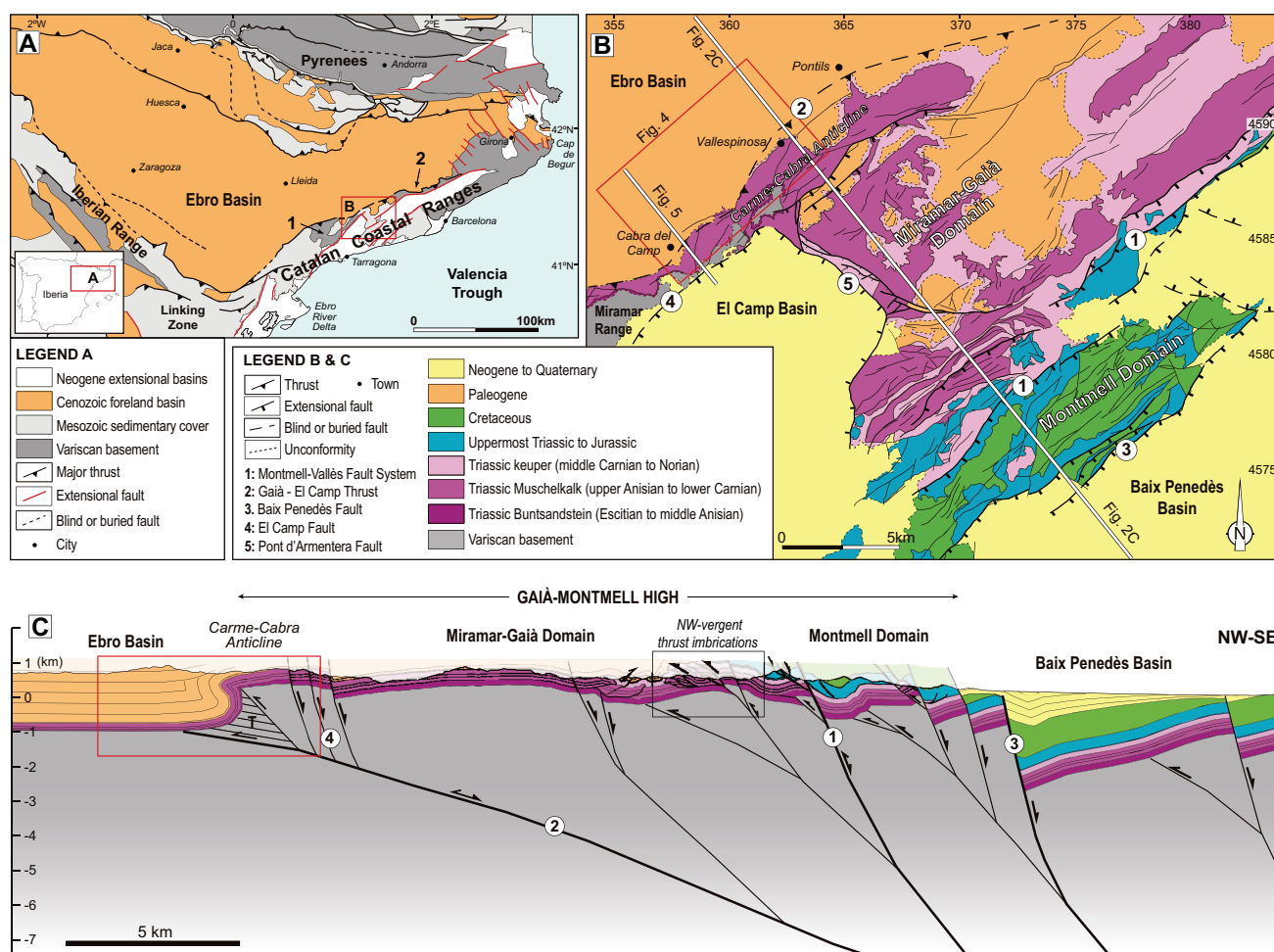


FIGURE 2. A) Geologic map of NE Iberia showing the major Cenozoic structural units including its three bounding orogenic belts: the Pyrenees and the intraplate Iberian and Catalan ranges. Cenozoic foreland basin-fill is highlighted in orange. Coordinates in geographical system. Labels 1 and 2 respectively correspond to the Prades Block and the Montserrat-Sant Llorenç del Munt areas referred in the text. B) Geological map of the Gaià-Montmell High in the central Catalan Coastal Ranges and adjoining areas. The area corresponds to the linkage zone between the Neogene Montmell-Vallès Fault System and El Camp Fault. Coordinates in UTM kms. C) Cross-section across the Gaià-Montmell High and its neighbouring areas. The hatched area labelled with "T" indicates the zone of distributed shear at the tip of the Gaià-El Camp Thrust (modified from Marín *et al.*, 2021). Legend for B and C is the same.

1989; Colombo, 1994; López-Blanco *et al.*, 2000a, b; López-Blanco, 2002; Gómez-Paccard *et al.*, 2011) and of the study area (Anadón, 1978 a and b; Anadón *et al.*, 1986).

The study area is located along the central southeastern margin of the Ebro Basin, between Cabra del Camp and Vallespinosa towns (Fig. 2B). Previous studies have suggested the presence of a progressive unconformity at this location, indicating that the growth and uplift of the frontal structure of the central CCR (Carme-Cabra Anticline) were contemporaneous with the deposition of conglomeratic units during the middle Eocene (Benzaquen *et al.*, 1973; Anadón *et al.*, 1985 and 1986) (Fig. 2). Nevertheless, the age of the contractional structures located towards the hinterland and responsible for the inversion and contractional uplift of the pre-existent Mesozoic basins (Montmell Domain in Fig. 2B, C) remain uncertain due to the lack of preserved syn-kinematic strata in the footwall of the Montmell Fault.

To address this problem, the current study presents a detailed tectonostratigraphic analysis of the whole Paleogene succession preserved in the central southeastern margin of the Ebro Basin along the northwestern limb of the Carme-Cabra Anticline which in the study area resembles more of a monocline (Fig. 2). It integrates results from a detailed geological map, clast composition and paleotransport direction analysis, and a magnetostratigraphic section performed across the 1,450m of the well-exposed Ebro Basin infill succession in the area. This approach enables the precise determination of the age and kinematics not only of the Carme-Cabra Anticline but also of the structures responsible for uplift and denudation of the inner parts of the central CCR during the Paleogene compressional phase.

GEOLOGICAL SETTING

Tectonostratigraphic framework

The Catalan Coastal Ranges is a NE-SW-oriented structural unit that extends for up to 250km parallel to the NE coastline of Iberia (Fig. 2A). It is around 30 km wide, and its basin-and-range configuration constitutes the onshore expression of the mainly extensional, divergent continental margin that separates the thicker crust of the Iberian Plate from the thinned crust of the Valencia Trough (Dañobeitia *et al.*, 1992; Roca and Guimerà, 1992; Vidal *et al.*, 1995). The current structure of the CCR is the result of three main tectonic phases: i) a multiphasic extensional phase from late Paleozoic to Mesozoic, ii) a compressional phase during the Paleogene and iii) an extensional phase from latest Oligocene to middle Miocene (Llopis, 1947; Anadón *et al.*, 1979; Roca and Guimerà, 1992; Bartrina *et al.*, 1992; López-Blanco *et al.*, 2000a, b; Baqués *et al.*,

2012; Cantarero *et al.*, 2014 a, b; Marín *et al.*, 2021).

The Late Jurassic to Early Cretaceous extensional episode, well recorded in the neighbour Iberian Range (Salas and Casas, 1993; Guimerà 2018), is represented by two right-stepped extensional basins, the Montmell-Garraf and Barcelona-Maresme basins bounded towards the northwest by two main extensional faults: the Montmell-Vallès Fault System and the Barcelona Fault (Fig. 3). These faults limit towards the NW the upper crust extensively deformed during the opening of the Tethys, in such a way that in their footwall blocks there are no Upper Jurassic or Lower Cretaceous sediments (Roca and Guimerà, 1992; Salas, 2001; Gaspar-Escribano *et al.*, 2004; Marín *et al.*, 2021).

Convergence and later collision between the Iberian and Eurasian plates took place from Late Cretaceous (Santonian) to middle-late Oligocene (Srivastava *et al.*, 1990; Rosenbaum *et al.*, 2002; Andeweg, 2002; Angrand *et al.*, 2020; Angrand and Mouthereau, 2021). In the NE of Iberia, this period led to the formation of the Pyrenees (Muñoz, 1992; Vergés *et al.*, 2002; Muñoz, 2017; García-Senz *et al.*, 2019), the Iberian Chain (Guimerà, 1984; Guimerà *et al.*, 1995; Nebot and Guimerà, 2016; Guimerà, 2018), and the Catalan Intraplate Chain (CIC) in the current location of the CCR (Anadón *et al.*, 1985; Guimerà and Álvaro, 1990; Salas *et al.*, 2001; López-Blanco, 2002) (Fig. 2A). In the study area, this entailed to the formation of the CIC from early Eocene to early Oligocene (Guimerà and Santanach, 1978; Guimerà, 1984; Anadón *et al.*, 1985; López-Blanco, 2002) by the tectonic inversion of the inherited Mesozoic extensional basins, and, towards the northwest, of the Ebro Foreland Basin (Anadón *et al.*, 1985; Roca and Guimerà, 1992; Juez-Larré and Andriessen, 2006; Salas *et al.*, 2001; Baqués *et al.*, 2012; Marín *et al.*, 2021). The CIC fold-and-thrust belt growth was controlled by the emplacement of major NW-directed NE-trending basement involving thrust sheets that incorporated the marginal parts of the developing Ebro Basin (Anadón *et al.*, 1986; Colombo, 1994; López-Blanco *et al.*, 2000a, b; López-Blanco, 2002; Gómez-Paccard *et al.*, 2011; Marín *et al.*, 2021).

The Paleogene contractive structure in the study area includes two domains with a differentiated stratigraphy in the Gaià-Montmell High (Marín *et al.*, 2021) (Fig. 2B, C). The Miramar-Gaià Domain in the NW comprises a very thin Mesozoic succession made up of only a Triassic succession uplifted over the Ebro Basin by a NW-directed low-angle basement thrust (the Gaià-El Camp Thrust). On the other hand, the Montmell Domain includes a well-developed Jurassic-Cretaceous succession (Fig. 3). The boundary between both domains corresponds to the Montmell-Vallès Fault System, a high-angle SE-dipping Mesozoic fault that was inverted during the Paleogene compressional phase

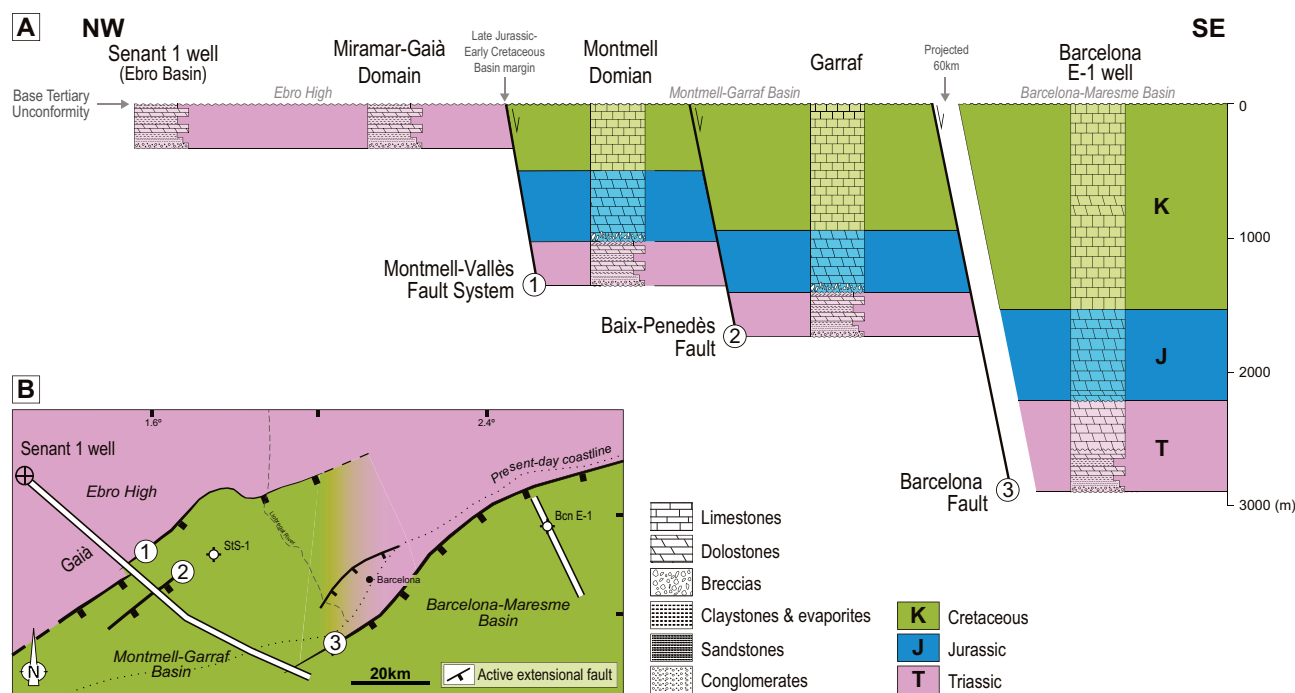


FIGURE 3. A) Mesozoic thicknesses across the central Catalan Coastal Ranges and the present-day offshore Barcelona-Maresme Basin. Upper reference datum corresponds to the base of the Tertiary. Mesozoic thicknesses based on [Salas \(1987\)](#), [Lanaja \(1987\)](#) and [ICGC \(2005\)](#). B) Tectonostratigraphic map of the central Catalan Coastal Ranges and offshore areas at the end of the Late Jurassic - Early Cretaceous extensional phase. Bcn E-1: Barcelona Marina E-1 well; StS-1: Sant Sadurní-1 well.

as it is attested by the presence of NW-directed thrust imbrications developed along its footwall ([Fig. 2C](#)) ([Baqués et al., 2012](#); [Marín et al., 2021](#)).

Throughout the Neogene, an extensional period associated to the rollback of the Tethyan Ocean plate during its subduction beneath the Iberian Plate took place ([Roca, 1994](#); [Sabat et al., 1995](#); [Carminati et al., 1998](#); [Roca et al., 2004](#); [van Hinsbergen et al., 2014, 2020](#); [Romagny et al., 2020](#)). This period resulted in the present-day horst-and-graben configuration of the CCR and the display of series of NNW-tilted blocks limited by major SE-dipping extensional faults ([Fig. 2C](#)). These faults resulted from the negative tectonic inversion (*i.e.*, extensional reactivation) of the Paleogene faults ([Bartrina et al., 1992](#); [Roca, 2001](#); [Gaspar-Escribano et al., 2004](#); [Baqués et al., 2012](#); [Marín et al., 2021](#)). In this scenario, the study area comprises the footwall block of the northeastern end of one of these major Neogene extensional faults (El Camp Fault) and the northeastern edge of the extensional relay zone developed between this fault and the Montmell-Vallès Fault System ([Fig. 2B](#)).

Alpine stratigraphic record of the central CCR and the SE Ebro Basin margin

The Alpine stratigraphy of the study area includes an upper Permian-Cretaceous cover unconformably overlain

by the Paleogene sedimentary infill of the Ebro Basin. In the footwall of the Montmell-Vallès Fault System, this sedimentary cover is formed by an up to 200 to 350 m succession of upper Permian-Triassic rocks ([Virgili et al., 2006](#); [Galán-Abellán et al., 2013](#); [Mercedes-Martín et al., 2014](#)) (Miramar-Gaià Domain, [Figs. 2; 3](#)) encompassing siliciclastic, limestone, dolostone, and evaporitic rocks ascribed to Buntsandstein, Muschelkalk and Keuper facies ([Virgili, 1958](#); [Calvet and Marzo, 1994](#); [Arnal et al., 2002](#); [Galán-Abellán et al., 2013](#); [Escudero-Mozo et al., 2017](#); [Ortí et al., 2017](#); [Mercedes-Martín and Buatois, 2020](#)). In contrast, Jurassic and Cretaceous rocks are present in the hangingwall of the Montmell-Vallès Fault System (Montmell Domain, [Figs. 2; 3](#)). This succession exceeds 2 km in thickness ([Salas, 1987](#)) and includes Lower-Middle Jurassic dolomitic breccias, a relatively thick succession of Late Jurassic-Early Cretaceous (Barremian-Aptian) shallow marine limestones, dolomites, and shales ([Salas, 1987](#); [Salas et al., 2001](#); [Albrich et al., 2006](#)), and an upper Albian to Cenomanian sequence of fluvial and shallow marine carbonates that represents the youngest Mesozoic rocks preserved in the Montmell Domain ([Salas, 1987](#); [Salas et al., 2001](#); [ICGC, 2005, 2018](#)). The Upper Jurassic to lower Albian succession is part of the extensional Montmell-Garraf Basin ([Fig. 3](#)) that developed during this period ([Anadón et al., 1979](#); [Salas, 1987](#); [Salas and Casas, 1993](#)).

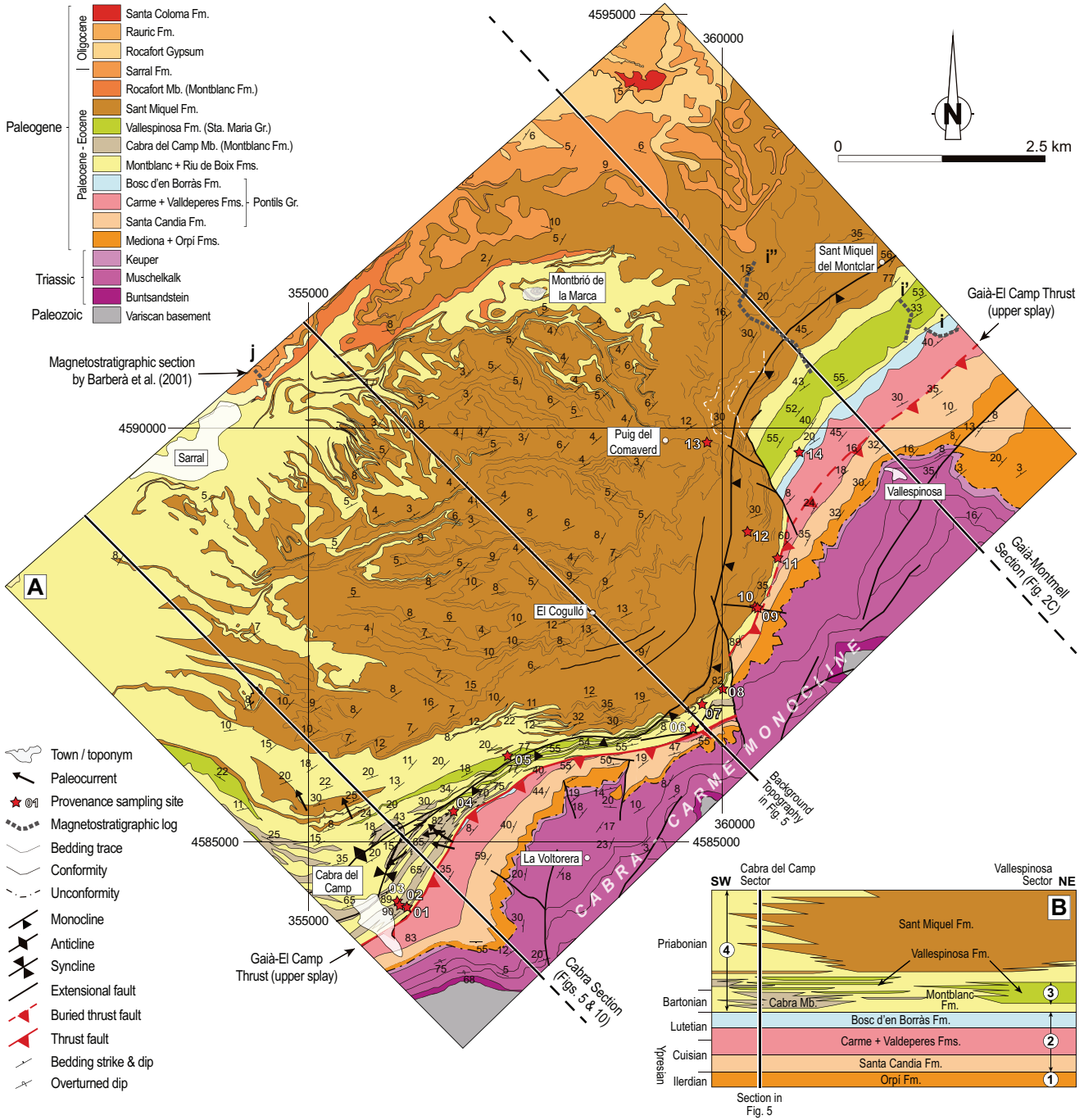


FIGURE 4. A) Geological map of the SE margin of the Ebro Basin between Cabra del Camp and Vallespinosa locations based on [Carrera et al. \(2020\)](#) and extended towards the northeast using the map from [Colldeforns \(unpublished\)](#). Labels i, i', i'' stand for the Pontils magnetostratigraphic logs from [Beamud et al., \(2012\)](#). The basal portion of the magnetostratigraphic log corresponding to the Carme Fm. present in [Figure 8](#), is located in the map shown in [Figure 1 of the supplementary material](#). Label j indicates the location of the Rocafort de Queralt magnetostratigraphic log from [Barberà et al. \(1999, 2001\)](#). The location of the cross-section in [Figure 5](#) is shown. The map uses UTM projection for zone 31N (ETR96 datum) and the coordinates are in meters. B) Not-to-scale schematic lithostratigraphic panel for the Eocene units. Numbers in the panel indicate the four major lithostratigraphic units defined in the area by [Colldeforns et al. \(1994a, b\)](#): 1) basal continental unit (Mediona Fm.) and a lower marine unit (Orpi Fm.); 2) Pontils-Cornudella Group; 3) Santa Maria Group, and 4) Barberà-Anoia Group.

The Cenozoic stratigraphic record in the Ebro Basin infill consists of marine and continental sediments ranging from the Paleocene to the upper Eocene (Figs. 4; 5). As

reported by the well Senant-1 (Lanaja, 1987) and from the geological maps (Figs. 2; 4) the Cenozoic succession, in some areas, rests directly on top of the Triassic succession.

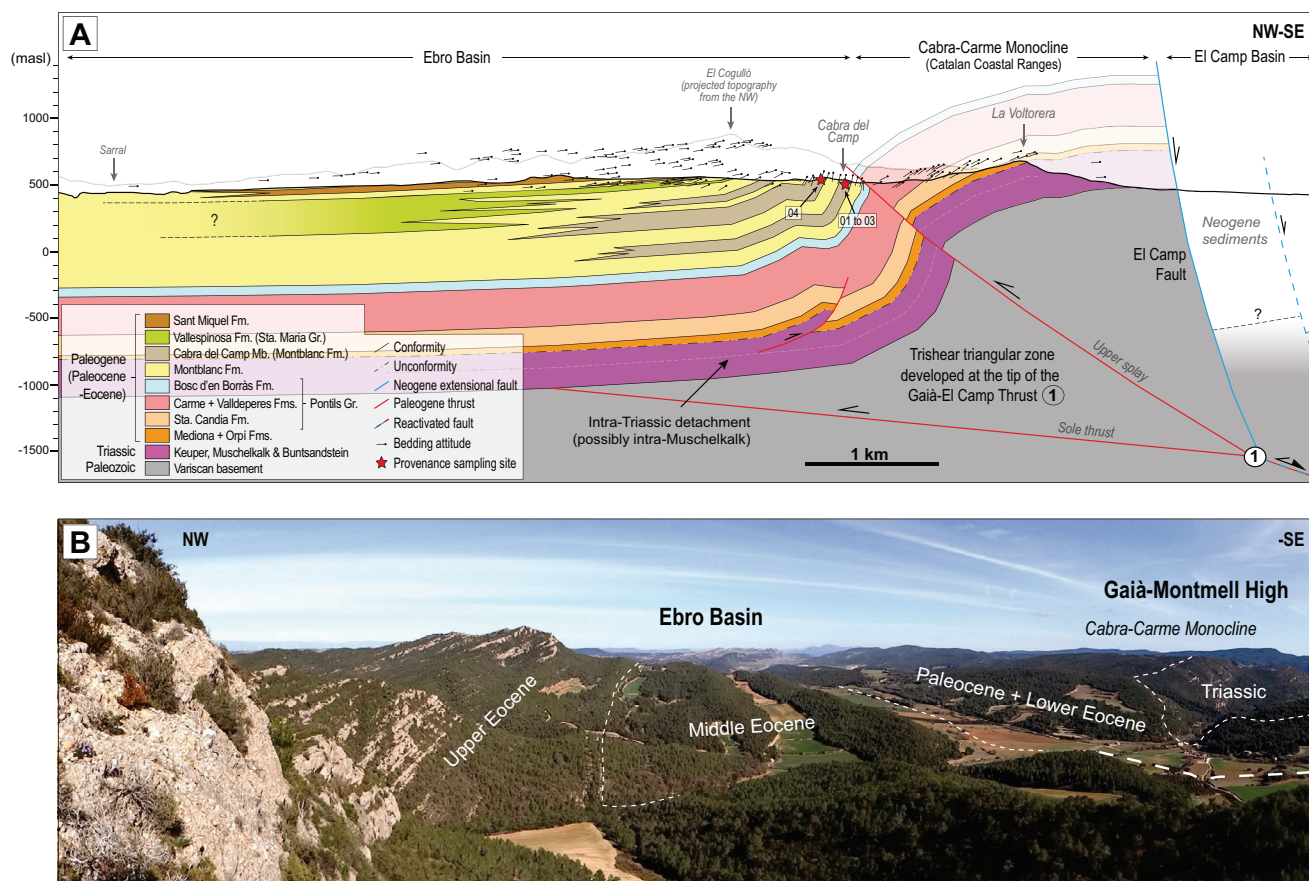


FIGURE 5. A) Geological cross-section of the SE margin of the Ebro Basin across the locality of Cabra del Camp. The section includes the NW frontal structure of the Catalan Coastal Ranges (Cabra-Carme Monocline). B) Field image of the limit between the Triassic and the succession of the foreland. See map in Figure 2 for location at regional scale and map in Figure 4 for a detail section location in the study area.

From the Paleocene to middle Eocene (middle Bartonian), the basin was connected to open Atlantic waters to the northwest (Serra Kiel *et al.*, 2003; Garcés *et al.*, 2020 and references therein). Yet, by the late Bartonian, the marine connections became restricted, leading to a change in sedimentation patterns over time (Costa *et al.*, 2010; Garcés *et al.*, 2020). This was recorded by the shift from marine marls to alternations of shales and anhydrite, halite, carnallite and sylvinites, recorded in the central parts of the basin and corresponding to the final stages of marine Priabonian sedimentation (Reguant, 1967; Pueyo, 1975; Busquets *et al.*, 1985; Travé *et al.*, 1996; Costa *et al.*, 2010). From the late Eocene (Priabonian) (Arche *et al.*, 2010; Arasa and Cabrera, 2018) the Ebro Foreland Basin became an endorheic sedimentary trough filled exclusively with continental deposits including siliciclastic sediments in the margins grading to lacustrine evaporites and carbonates towards the inner basin parts (Anadón *et al.*, 1989; Valero-Montesa *et al.*, 2014).

The Paleocene to Oligocene deposits present in the study area belong to the first marine basin-fill hemicycle

and a part of the second endorheic hemicycle (Serra Kiel *et al.*, 2003). Colldeforns *et al.* (1994a, b) subdivided these Paleogene series into four lithostratigraphic assemblages: i) a basal assemblage formed by the Mediona and the Orpí formations; ii) the Pontils-Cornudella Group; iii) the Santa Maria Group from which only the Riu de Boix and the Vallespinosa formations are present in the studied area and iv) the Barberà-Anoia Group, the basal part of which is a lateral equivalent of the Santa Maria Group towards the northeast.

The basal assemblage is present in the Miramar-Gaià Domain and the northwestern limb of the Carme-Cabra Monocline. It begins with the Thanethian Mediona Fm. (Anadón, 1978a, b), a discontinuous continental unit formed by alluvial shales affected by intense pedogenic processes that unconformably overlies the Triassic cover. This basal unit is overlaid by the well dated marine Ypresian (Ilerdian) Orpí Fm. (Ferrer, 1971; Anadón, 1978 a and b; Anadón *et al.*, 1979), a frequently dolomitized Alveolina limestone unit deposited in a shallow carbonate platform environment.

The Pontils-Cornudella Group (Anadón, 1978 a, b; Anadón *et al.*, 1979, 1983, 1992; Colombo, 1980, 1986, Colldeforns *et al.*, 1994b) mainly encompasses non-marine detrital and lacustrine units Ypresian to Lutecian in age. The lower part of this unit is also present in the Miramar-Gaià Domain (Fig. 2). From bottom to top, in the study area, five formations have been distinguished in this group (Anadón, 1978): a 80 to 110m thick succession of lacustrine limestones alternating with varicoloured mudstones of the Santa Càndia Fm.; a 170m thick mud flat plain facies (red mudstones with minor sandstone and calcareous intercalations) of the Carme Fm.; a variable thickness (up to a maximum of 100m) of evaporites and lacustrine carbonates of the Valldeperes Fm.; the lacustrine and palustrine limestones with interbedded marl and chert of the Bosc d'en Borràs Fm., which reaches its maximum thickness (about 100 m) at the NE end of the study area and grades towards the southwest to distal alluvial mudstones.

Above, the Bartonian and Priabonian deposits of the Santa Maria and Barberà-Anoia groups are preserved in the northwest limb of the Carme-Cabra Monocline (Fig. 4). In the study area, the Santa Maria Group embraces up of nearly 300m-thick succession of shallow marine and transitional facies (*i.e.* deltaic, fan-deltaic conglomerates, sandstones, coral-bearing limestones, and marlstones with bioclastic sandstones intercalations) (Ferrer, 1971; Anadón and Marzo, 1986; Serra Kiel *et al.*, 2003) integrated in the Vallespinosa Fm. (Colldeforns *et al.*, 1994a).

On the other hand, the Barberà-Anoia Group (Colombo, 1980, 1986; Colldeforns, 1994a) comprises the Bartonian to Oligocene continental and lacustrine deposits. It includes up to six different formations: Montblanc, Sant Miquel, Sarral, Rocafort, Rauric and Santa Coloma (Colombo, 1980, 1986; Colldeforns *et al.*, 1994a, b). The Montblanc Fm. is made up of distal alluvial red beds that are interbedded with the marine sandstone of the Vallespinosa Fm. in its lower part, which becomes thicker and predominant towards the northeast. To the southwest, discontinuous alluvial conglomerate intercalations of the Cabra del Camp Mb. (Colldeforns, 1994a) are present showing a maximum thickness of around 200 m in the Cabra del Camp area instead (Fig. 4). The Sant Miquel Fm. (Colombo, 1980, 1986) corresponds to a 600m-thick succession of proximal alluvial fan conglomerates that unconformably overlay the marine sediments of the Santa Maria Group (Priabonian Riu de Boix Fm.) (Anadón *et al.*, 1986; Colldeforns *et al.*, 1994a). Towards the north and northeast, these conglomerates laterally change to late Priabonian to early Oligocene successions. These ones include the lacustrine carbonates and marls of the Sarral and Rocafort formations, the fluvial and lacustrine shales, marls, and lenticular conglomerates of the Rauric Fm. and the lacustrine marls and gypsums of the Santa Coloma Fm. (Benzaquen *et al.*,

1973; Colombo, 1980, 1986; Colldeforns *et al.*, 1994a, b).

The dating of these marine and non-marine lithostratigraphic units was formerly established and lately refined through the definition of biostratigraphic assemblages and biozones (Ferrer, 1971; Anadón, 1978a, b; Anadón and Feist, 1981; Anadón *et al.*, 1983, 1987, 1992; Agustí *et al.*, 1987; Feist *et al.*, 1994; Serra-Kiel *et al.*, 2003; Sanjuan *et al.*, 2014; Tosal *et al.*, 2019; Minwer-Barakat *et al.*, 2023). Further on, magnetostratigraphic studies done in neighbouring areas allowed the refinement of the biostratigraphic ages (Barberà 1999; Barberà *et al.*, 1999, 2001; Beamud *et al.*, 2012; Costa *et al.*, 2010, 2013; Gomez-Paccard *et al.*, 2011; Garcés *et al.*, 2020).

METHODOLOGY

The present study uses an integrated approach that combines geological mapping, the construction of a geological section, provenance analysis and magnetostratigraphic dating. A NW-SE-oriented structural section was constructed combining up to 140 bedding dips in Triassic to Eocene rocks. This section uses a new geological map of the SE margin of the Ebro Basin between Cabra del Camp and Vallespinosa towns (Carrera *et al.*, 2020), which partially covers the area of study and was extended towards the northeast using a geological map done by Colldeforns (unpublished). All the data provided with the map (Fig. 4) are obtained from the field and the location was acquired with a device equipped with a GPS. The use of both maps allows constraining the contacts between stratigraphic units, stratigraphic thicknesses as well as structural relationships and attitudes (Fig. 5). Additionally, the use of 3D digital outcrop models was used to better refine the contact of some of the stratigraphic units (Annex I of the supplementary material).

The provenance analysis includes two main parts: the analysis of the palaeontological content in clasts from foreland conglomerates in order to define the tectonically uplifted areas exposed to erosion in the hinterland of the orogenic system, and the integration of paleocurrent indicators (*i.e.* base marks, channels) to determine the relative location of the alluvial deposits source. Up to 14 samples gathered through the Paleogene succession along the Ebro Basin margin between Cabra del Camp and Vallespinosa towns were analysed using thin sections (see map in Fig. 4 for their location).

The magnetostratigraphic analysis aims for an accurate reconstruction of the Paleogene compressional deformation in the central CCR by refining the age of the Paleogene succession to constrain the timing of the synorogenic sedimentation. The Pontils magnetostratigraphic section

was carried out north and northwest of Vallespinosa where a relatively continuous northwest-dipping Paleogene succession occurs (Fig. 4). The sampled section consists of 238 measurement sites along ~1,430m of sedimentary record, which yields an average sampling resolution of 6 m/sample (Fig. I supplementary material). The succession shows a relatively steep dip of 64° at the base of the section which progressively decreases to a gentle dip of 15° at the top. The first 410 m of the Pontils section include the Carme, Valldeperes, Bosc d'en Borràs and Montblanc formations of the Pontils-Cornudella Group, followed by 300 m of the Vallespinosa Fm. of the Santa Maria Group, extending up to the meter 716. The Montblanc-Riu de Boix formations along the Pontils section were not suitable for magnetostratigraphic purposes and no samples were obtained until the meter 800, where the first Sant Miquel conglomerates of the Barberà-Anoia Group crop out (Fig. 4). Details about the sampling and laboratory procedures of the magnetostratigraphic analysis are provided in the Annex II of the supplementary material.

RESULTS

Structure of the central SE margin of the Ebro Basin

The structure of the SE margin of the Ebro Basin across Cabra del Camp is illustrated in the section of the Figure 5A. Overall, the margin in the study area depicts an anticline-syncline geometry developed at the tip of a low-angle thrust that uplifts the basement and the sedimentary cover over a gently northwest-dipping regional level of the Ebro Basin (Fig. 5B). The most prominent structure in the section is the Cabra-Carme Monocline, which is cored by a trishear triangular zone (understood as the model proposed by Erslev, 1991) developed at the tip of the Gaià-El Camp Thrust. This monocline represents the northwest deformation front of the CCR and involves the Variscan Basement and the unconformably overlying sedimentary cover made up by a Germanic Triassic succession (Buntsandstein, Muschelkalk and Keuper) and the Paleogene strata of the Ebro Basin fill. A splay of the Gaià-El Camp Thrust propagates up to the surface showing a relatively low displacement. The trace of this thrust can be followed at surface for around 6 km towards the northeast up to a zone characterized by the presence of NW-SE-oriented faults and the relatively thick conglomerates of the Sant Miquel Fm. (Fig. 4). From this point on, towards the northeast, the thrust appears progressively buried by the lower to middle Eocene Santa Cándia and Carme formations.

As shown by dip data and the cartographic traces, the geometry of the thrust footwall displays a pair of anticline-syncline structures that extend westward, parallel to the deformation front (Figs. 4; 5). Towards the northeast, the

folds plunge and merge into a monocline structure (Fig. 4). The southern limb of the footwall syncline is characterized by the presence of nearly vertical beds of the Cabra del Camp Mb., which rapidly reduce their dip towards the northwest. This trend continues further northwest where dips between 5° and 8° are present around the location of Sarral town (Fig. 4). At depth, the aforementioned anticline-syncline pair has been interpreted as the result of the propagation of a southeast-directed out-of-syncline thrust, probably detached within the ductile levels of the middle Muschelkalk in the Triassic succession (Fig. 5). This structure transfers slip along the anticline forelimb to accommodate the tectonic shortening (Mitra, 2002).

In terms of lithostratigraphy, the conglomerates of the Cabra del Camp Mb. laterally and vertically grade towards the northwest into the finer-grained sediments of the Montblanc Fm. and, towards the northwest, into the marine succession of the Vallespinosa Fm. (Figs. 4B; 5). These three formations are overlaid by the massive conglomerates of the Sant Miquel Fm.

Additionally, the Cabra-Carme Monocline is affected near its hinge by the El Camp Fault, a high-angle, SE-dipping Neogene extensional fault that is interpreted as rooted in the Gaià-El Camp Thrust. This Neogene structure bounds towards the northwest the El Camp Basin and controls the development of a semi-graben depocenter on its hangingwall (Figs. 2; 5).

Paleocurrents and Provenance analysis

Paleocurrent indicators such as base marks, imbrications, channel base axis (Fig. 6A, B) were collected in the field in conglomeratic beds around Cabra del Camp (Figs. 4; 6C). Dips at these locations range from the nearly verticalized beds in the Cabra del Camp town area in the southern limb of the syncline at this location to the 25° of the Sant Miquel Fm. north of Cabra del Camp (Figs. 4; 5). Once restored to the horizontal, paleocurrent lineaments reveal a main flow direction towards the west and northwest (Fig. 6D), therefore implying a source area located east to southeast of the study area.

On the other hand, the analysis of the fossil content of carbonate clasts, which were sampled from coarse grained beds at 14 different sites distributed through the Paleogene succession along the margin (see locations in Fig. 4), has been performed aiming to provide information about their provenance and, therefore, the determination of the tectonically active areas. Samples 01 to 08 and 12 to 14 were collected at different levels of the Montblanc and Vallespinosa formations and Cabra del Camp Mb. Samples 09 to 11 were collected in undetermined alluvial deposits. To help in the tectonostratigraphic analysis, which is the

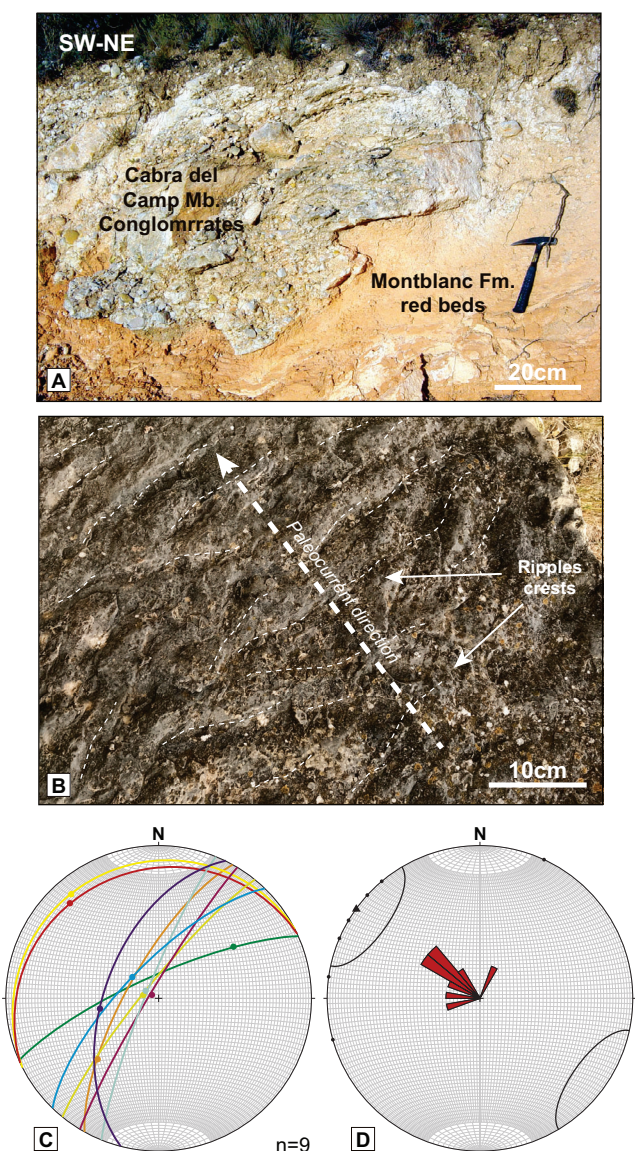


FIGURE 6. A) Paleochannel bottom outcrop in conglomerates of the Cabra del Camp Mb. used for paleocurrent measurements. B) Ripples at the bed top of marine-continental transitional facies. Dashed white arrow indicates the paleocurrent direction. C) Stereographic plot of paleocurrent measurements in the Cabra Fm. around the Cabra del Camp (n= number of measurements). See map in Figure 4 for location. D) Restored paleocurrent directions showing the predominant direction of the sediment supply.

objective of this study, only the sites close to the Cabra section (sites 01 to 04 sampled in the Cabra del Camp Mb.) are detailed while descriptions for each investigated sample can be found in the [Table I of the supplementary material](#).

Site 1 clasts are mainly grainstones dominated by *Alveolina*, *Opertorbitolites*, miliolids, other foraminifera and recrystallized green algae (Fig. 7A), as well as packstones containing peloids, orbitolinids, and fragments of rudist bivalves, other molluscs, and echinoids. Clasts

exhibiting wackestone to packstone textures with ostracods occur (Fig. 7B) and sometimes the ostracod-bearing clasts include gastropods and can show bioturbation traces. Mudstones, dolostones, and wackestone to packstone textures with small miliolids and other foraminifera (Fig. 7C), bivalves and serpulids, are also common. Other clast facies identified include sandy limestone, a mudstone-wackestone with characean remains, a grainstone with recrystallized ooids and calcareous algae, a grainstone with ooids exhibiting radial and concentric coatings (Fig. 7D), and grainstone textures with ooids, peloids, intraclasts, orbitolinids, and fragments of oysters and other molluscs. *Alveolina* and fragments of orbitolinids were also recognized within the conglomerate matrix.

Site 2 clasts are made up of dolomitic limestone with a grainstone texture containing peloids (Fig. 7E), miliolids, other foraminifera, fragments of molluscs, echinoids, and calcareous algae, as well as a highly recrystallized limestone clast with abundant calcareous green algae (Fig. 7F). Fragments of oysters, gastropods, echinoids, and bryozoans occur. Non-skeletal components found in this latter highly recrystallized grainstone include peloids, silt-sized quartz grains and intraclasts. Non-skeletal components found in the highly recrystallized grainstone also include peloids, silt-sized quartz grains and intraclasts. Intraclasts are made up of packstone to grainstone textures with scarce ooids, other coated grains, peloids and silt-sized quartz. Furthermore, conglomerate clasts with packstone to grainstone textures including miliolids, *Alveolina*, *Opertorbitolites*, small rotaliids, other foraminifera, and fragments of echinoids and molluscs, were also recognized.

Site 3 sample contains clasts with orbitolinids (Fig. 7G), encrusting and agglutinating foraminifera, other foraminifera, fragments of oysters, other molluscs, calcareous algae and serpulids, as well as non-skeletal components such as peloids, intraclasts and silt-sized quartz. An additional investigated clast was made up of a recrystallized packstone texture with peloids, silt-sized quartz, miliolids, other foraminifera, and fragments of oysters, other molluscs, bryozoans, echinoids, and calcareous algae. Further analysed conglomerate clasts exhibit wackestone textures with small foraminifera, mudstone to wackestone textures, occasionally bioturbated, with ostracods and gastropods, packstone to grainstone textures with orbitolinids, peloids, and fragments of oysters, other molluscs, echinoids, corals, and calcareous algae, and grainstone textures with miliolids, *Alveolina* and other foraminifera. Finally, a clast made up of a “bacinellid” fabric was also identified (Fig. 7H).

Site 4 clasts exhibit grainstone textures with abundant orbitolinids. Miliolids, other foraminifera, and fragments of *Marinella lugeoni*, *Permocalculus*, other calcareous

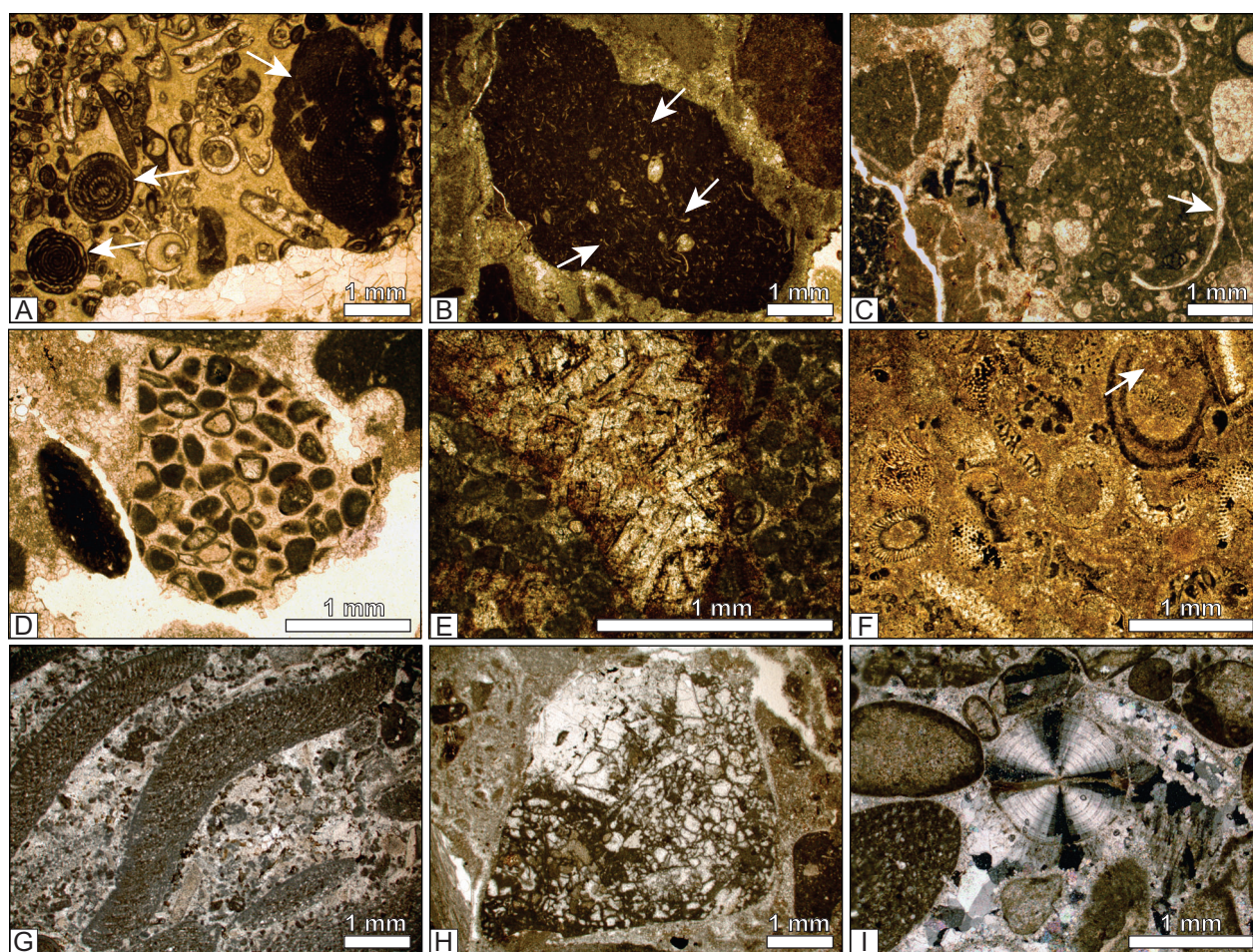


FIGURE 7. Clast microfacies. A) Photomicrograph of a grainstone texture from the Ypresian Orpí Fm. showing two *Alveolina* tests (left) and one of *Opertorbitolites* (upper right). Sampling site 1. B) Detail of a pebble-sized clast with ostracods giving rise to a wackestone texture. Santa Cándia Fm. (late Ypresian-Bartonian?). Sampling site 1. C) Close-up view of a packstone clast (centre to right) with small foraminifera and a section of a bivalve. Basal part of the Orpí Fm. (Ypresian). Sampling site 1. D) Sand-sized clast exhibiting a grainstone texture with ooids perhaps eroded from the Cenomanian Can Xuech Fm. Note the presence of an orbitolinid within the conglomerate matrix (right). Sampling site 1. E) Close-up view of a dolomitized miliolid and peloidal grainstone of Barremian-Aptian age. Sampling site 2. F) Photomicrograph of a recrystallized limestone exhibiting abundant sections of calcareous green algae. Cretaceous? Sampling site 2. G) Detail of an orbitolinid grainstone of Barremian-Aptian age. Sampling site 3. H) Pebble-sized clast of Aptian age showing a “bacinellid” fabric. Sampling site 3. I) Barremian-Aptian grainstone texture exhibiting a section of a belemnite rostrum (centre) under cross polarized light. Note the presence of an orbitolinid in the lower left part of the image. Sampling site 4.

algae, bryozoans, echinoids, oysters, other bivalves, corals, and sections of belemnite rostra also occur (Fig. 7I). Non-skeletal components include well-rounded intraclasts, peloids and silt-sized quartz grains. A calcilithite sample with silt to sand-sized quartz grains, peloids, ooids, miliolids, other undetermined benthic foraminifera and fragments of orbitolinids was also collected. The calcilithite also includes small dolostone, mudstone and grainstone clasts. The latter is mainly made up of peloids and fragments of molluscs.

The Pontils magnetostratigraphic section

Thermal demagnetization of the studied samples reveals, in general, two stable paleomagnetic components after removal of a low temperature component that

parallels either the present-day magnetic field or the drilling direction. This low temperature component is usually removed below 200-230°C and will not be further considered. Above this, characteristic components pointing north with positive inclinations or south with negative inclinations are found along section. The temperature intervals selected to calculate each characteristic component are compiled in the Table II of the supplementary material. In general, characteristic components of grey mudstones and limestones are defined between 300-500°C pointing to (titano)magnetite as the main remanence carrier. Characteristic components in red mudstones and fine-grained sandstones are defined at higher temperatures, up to 650-690°C, pointing to hematites as the main remanence carrier. Despite this, some components

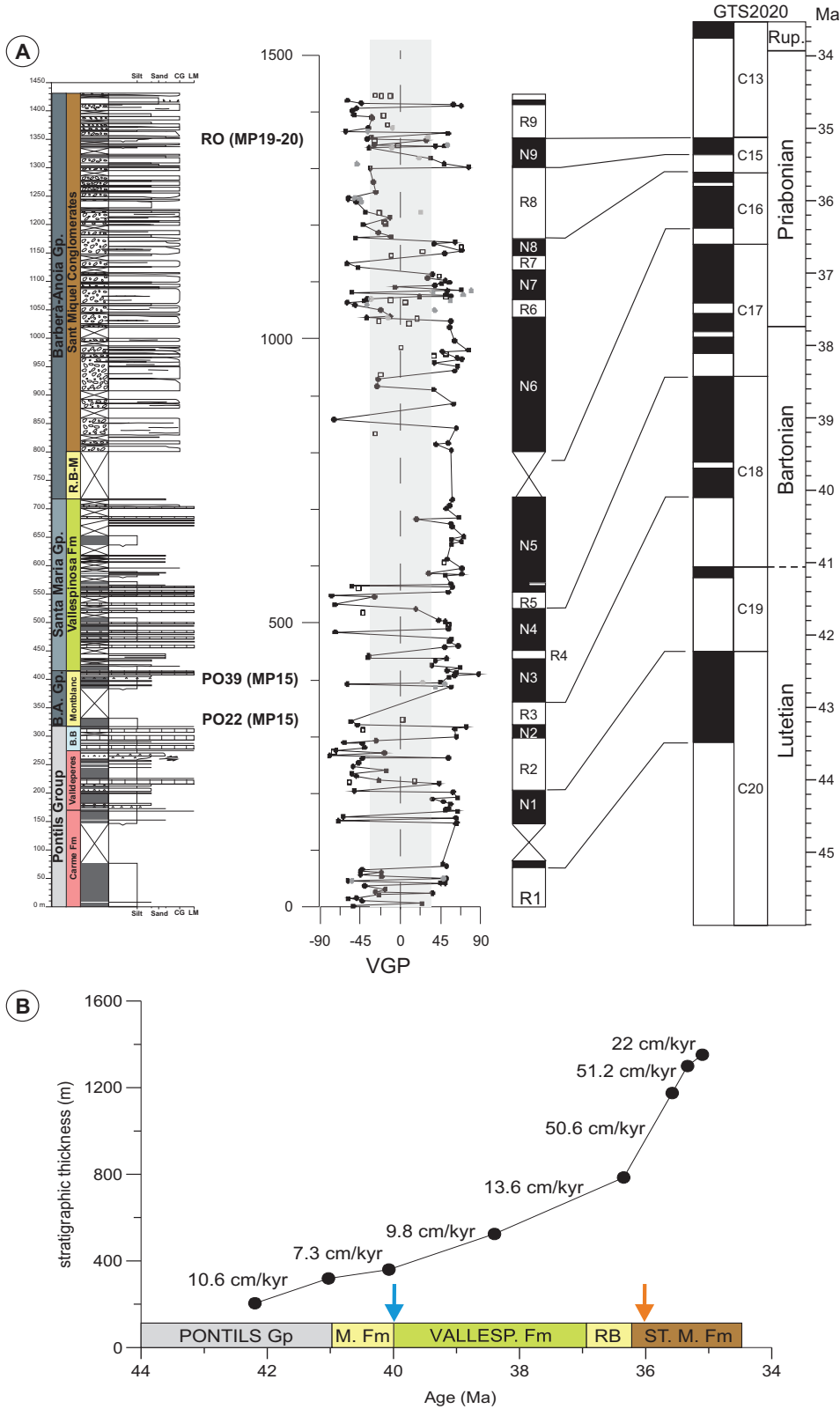


FIGURE 8. Magnetostratigraphy of the Pontils section. A) Magnetostratigraphic section and correlation to the GPTS (Gradstein et al., 2020). PO and RO correspond to Pontils and Rocafort de Queralt fossil sites, respectively, with their attribution to Mammal Paleogene Reference Levels in brackets. White squares in the VGP graph represent type 3 directions, discarded to build the local magnetostratigraphy. B.A. Gp., B.B. and R.B.-M stand for Barberà-Anoia Group, Bosc d'en Borràs and Riu de Boix-Montblanc formations in the stratigraphic column. B) Sedimentation rates values and evolution for the Pontils section. Blue arrow: Bartonian transgressive event at the base of Santa Maria Group. Orange arrow: time of disconnection from the ocean of the Ebro Basin.

are defined at temperatures around 400°C thus suggesting a mixture of (titano)magnetite and hematite in the red beds. No substantial changes in magnetic susceptibility are observed upon progressive thermal demagnetization (Table III of the supplementary material), indicating that not significant mineral neoformation occurred inside the thermal demagnetizer. The calculated characteristic components have been assigned to three qualities. Type 1 quality is assigned when the paleomagnetic direction can be calculated with more than 3 demagnetization steps and demagnetization diagrams yield linear trends to the origin of coordinates with maximum angular deviations (MAD) around 5°. Directions are defined as type 2, when MAD >5°, yet they can still be calculated by at least three demagnetization steps. Samples with erratic trends in which directions can be hardly calculated, often with only two demagnetization steps, yield type 3 directions, which are not considered for building the sequence of polarity zones in the magnetostratigraphic section. Nevertheless, this is not a significant issue since 205 directions out of 238 sites have been assigned to either type 1 or 2, which represents that 86% of the demagnetized samples yield reliable paleomagnetic directions. Magnetic polarities are deduced after computing the virtual geomagnetic pole latitude (VGP) from the characteristic component of each site. Positive values of VGP are interpreted as normal polarities and are represented in black when building the local magnetostratigraphic column (Fig. 8). Accordingly, negative VGP values are interpreted as reversed polarities and represented in white in the local magnetostratigraphic column. To define the magnetozones that constitute the local magnetostratigraphy at least two consecutive sites of the same polarity are needed. By doing so, 9 reversed and 9 normal magnetozones have been identified in the Pontils magnetostratigraphic section which can be correlated to the Geomagnetic Polarity Timescale (GPTS).

The magnetostratigraphic section is located a few km southwest of the Pontils village (Fig. 2B), where the fossil locality of Pontils was reported (Anadón, 1978; Anadón and Feist, 1981; Minwer-Barakat et al., 2023). The Pontils fossil site was assigned to the MP15 Mammal Paleogene Reference Level by Schmidt-Kittler (1987). Lithostratigraphic correlation of the fossil site to the Pontils magnetostratigraphic section places the first levels containing significant fossil mammal remains (sample PO22 from Minwer-Barakat et al., 2023) around the meter 330 and the last levels containing significant mammal fossil remains (PO39 from Minwer-Barakat et al., 2023) around the meter 400. Therefore, both levels are contained respectively between the base and the top of the Montblanc Fm. (Fig. 8). Additionally, the fossil site Rocafort de Queralt (RO), assigned to MP19-20 (Anadón et al., 1987), can be lithostratigraphically correlated from the neighbouring Rocafort magnetostratigraphic section (Barberà et al.,

2001) to the meter 1,350 of the Pontils section, within the Sant Miquel conglomerates of the Barberà-Anoia Group (Fig. 8).

DISCUSSION

This discussion is divided into three parts: first, the attribution of age of the clasts sampled in the Cabra del Camp conglomerates; second, the age of the sampled Eocene units from the paleomagnetic study; and third, the tectono-stratigraphic interpretations and their implications in the tectonic evolution of the central CCR.

Source area age attribution of the upper Eocene clasts in the central SE margin of the Ebro Basin

The northwest-directed paleocurrents measured within the sampled upper Eocene strata (Figs. 4; 6) suggest the presence of higher reliefs toward the southeast of the study area, indicating a possible source of sediment input from elevated terrains. This pattern implies that the southeast region may have acted as a topographic high or a tectonically active area during the deposition of these strata, influencing sediment transport and depositional processes across the basin.

The detailed fossil content description carried out on clasts from the upper Eocene alluvial units (Cabra Mb., Montblanc Fm. and Sant Miquel Fm.) and the shallow marine units (Vallespinosa Fm.) provides key information about the formations that were exhumed and eroded in the source area at the time of sedimentation. A detailed summary with the attributed ages for each studied sample can be found in Table I of the supplementary material.

A series of clast-types have been used to determine the original stratigraphic units where these clasts are derived from. These types are described below from younger to older and are summarized in Figure 9.

Sampled unit	Source area age attribution				
	Cretaceous			Paleogene	
	Lower Cretaceous		Upper Cretaceous	Eocene	
	Barremian-Aptian		Cenomanian	Ypresian	
Sant Miquel Fm.		E			B
Vallespinosa Fm.		E			B
Cabra del Camp Mb.	G	D E F H	D	C H	A D H

FIGURE 9. Source area age attribution of the upper Eocene clasts in the central SE margin of the Ebro Basin. Clast type classification: A: Ypresian wackestones-packstones. B: Alveolina limestone. C: Cenomanian ooidal grainstones. D: Lacustrine limestones (Barremian-Aptian, Upper Cretaceous, Ypresian). E: Barremian-Aptian: orbitolinid limestone. F: Barremian Aptian grainstones. G: Undifferentiated Cretaceous limestone. H: Undifferentiated Cretaceous or Early Eocene dolostones.

Type A clasts: Ypresian

The wackestone and packstone textures with undetermined small foraminifera (Fig. 7C) recognized in sites 01 and 03 are characteristic of the basal part of the Orpí Fm. (see figure 28 in Anadón, 1978a, b) and, therefore, are Ypresian (Ilerdian) in age.

Type B clasts: Ypresian

Grainstone clasts rich in *Alveolina*, *Opertorbitolites* (Fig. 7A), miliolids, gypsinids, and algae are prevalent throughout the studied clastic deposits and consistently present across nearly all sampling sites. These clasts, as well as the *Alveolina*, *Opertorbitolites* and gypsinid tests found in the conglomerate matrix in sites 07, 08, 09, 11 and 12, were also eroded from the Ypresian (Ilerdian) Orpí Fm. (see Anadón, 1978).

Type C clasts: Cenomanian

The grainstone with well-formed ooids (Fig. 7D) exhibiting radial and concentric coatings sampled in site 01 is probably Cenomanian in age. Esteban (1973) reported similar facies from the Cenomanian Can Xuech Fm. in the Montmell area (Fig. 2).

Type D clasts: Barremian-Aptian, Upper Cretaceous, Ypresian

The age of the freshwater limestone facies with ostracods (Fig. 7B) and characeans recognized in clasts from sites 01 and 03 could have been sourced from the Barremian-Aptian and/or Upper Cretaceous as have been reported in the CCR (e.g. Esteban, 1973; Salas, 1987; Martín-Closas *et al.*, 2018, this volume), but also from the Ypresian (Cuisian) Santa Cándia Fm., which belongs to the Pontils-Cornudella Group and overlies the Ypresian (Ilerdian) Orpí Fm. (Anadón, 1978).

Type E clasts: Barremian-Aptian

Clasts and matrix samples containing orbitolinids also occur in almost all sampled sites (Figs. 7D, G, I). The presence of orbitolinids, and occasionally of *Nummuloculina*, *Marinella lugeoni*, *Permocalculus*, as well as fragments of rudist bivalves and belemnites (Fig. 7I), indicate a Barremian-Aptian age (Esteban, 1973; Robles, 1982; Salas, 1987).

Type F clasts: Barremian-Aptian

The grainstones dominated by the presence of peloids, scarce ooids, miliolids (Fig. 7E) and fragments of molluscs and echinoids found in sites 01 to 04 also show facies like

those observed in Barremian-Aptian platform carbonates from the CCR (Esteban, 1973; Robles, 1982; Salas, 1987) and are therefore ascribed to this age interval. The “bacinellid” fabric-bearing clast (Fig. 7H) recognized in sampling site 03 is also representative of the Aptian Stage (see Schlagintweit and Bover-Arnal, 2013).

Type G clasts: undifferentiated Cretaceous

In sampling site 02, a clast made up of highly recrystallized limestone with abundant calcareous green algae was collected (Fig. 7F). The age of this sample is unknown. Similar deposits dominated by calcareous green algae, which are common in Cretaceous platform carbonates (e.g. Esteban, 1973; Salas, 1987), have not been reported in the Paleogene record of the CCR (Anadón, 1978). Therefore, the age of this sample has been ascribed to the Cretaceous.

Type H clasts: undifferentiated Cretaceous or early Eocene

In the CCR, dolostone stratigraphic intervals that could have sourced the dolostone clasts found in the investigated conglomerate deposits of the Cabra del Camp Mb. (Sites 01 to 04) include the Barremian-Aptian succession (Robles, 1982; Salas, 1987), the Cenomanian Can Xuech Fm. (Esteban, 1973) and the Orpí Fm. of Ypresian age (Anadón, 1978). The Jurassic and Triassic record also includes dolostone intervals (e.g. Salas, 1987). However, non-dolomitized clasts older than Lower Cretaceous have not been recognized in the sampling sites. Therefore, the dolostone clasts identified are more likely to be of Cretaceous or early Eocene in age.

Age of the Pontils magnetostratigraphic section

The proposed correlation of the Pontils local magnetostratigraphic section to the GPTS (Gradstein *et al.*, 2020) suggests that the deposition of the Pontils section occurred between C20r to C13r chrons (Lutetian to Priabonian) (Fig. 8A). This correlation is based on both the reversal pattern, the location of fossil sites PO and RO along the section and cartographic relationship with neighbouring sections (López-Blanco *et al.*, 2024). Fossil site RO (MP19-20) is located around the meter 1350 in the Pontils section coinciding with the upper part of the normal magnetozone N9 (Fig. 8A). Correlation of RO to C15n by Barberà *et al.* (2001) also favours the correlation of N9 to C15n in the Pontils section, which pins the upper part of the section. The base of the Sant Miquel conglomerates is also characterized by a long normal magnetozone N6, which we propose to correlate to C16n based on the geological mapping-deduced vertical and lateral relationships with the Tossa Fm. (López-Blanco *et al.*, 2024) that is correlated

to C16n by Costa *et al.* (2013). Therefore, deposition of the Sant Miquel conglomerates occurred from C16n up to C13r (36.2 Ma up to 34.5 Ma according to GPTS version of Gradstein *et al.* (2020)). The Riu de Boix-Montblanc Fm. does not provide a characteristic reversal pattern since no data are available due to bad outcrop conditions. However, it has been assigned to C16r.2r-C17n.1n (Fig. 8A). Below, the Vallespinosa Fm. within the Santa Maria Gp. yields N5, N4 and part of N3 normal magnetozones and R4 and R5 reversed magnetozones. N5 is correlated to C17n.2n and 3n (Priabonian-Bartonian), whereas R5, N4, R4 and top of N3 are correlated to Bartonian chrons C17r.3r, C18n.1n, C18r.1r and top of 18n.2n, respectively. The Montblanc Fm., in a stratigraphic position equivalent to the Pontils fossil site (MP15, Fig. 8), also records the magnetozones N3 and the reversed magnetozones R3, which are correlated to C18n.2n and the base of C18r.2r respectively. Therefore, the Pontils fossil site correlation to the GPTS confirms the Bartonian age assigned by Minwer-Barakat *et al.* (2023) and not the uppermost Lutetian age as previously suggested by Beamud *et al.* (2003) and Beamud (2013) due to an imprecise location of the fossil site on top of the Bosc d'en Borràs Fm. Limestones and the heterochronous character of its top due to the transition to SW to detrital Montblanc Fm. strata. From this correlation the fossil site spans from approximately 41 Ma (PO22, reversed polarity) to 39.8 Ma (PO39, normal polarity). Following down-section, the Bosc d'en Borràs, Valldeperes and Carme formations reversal pattern formed by magnetozones N2, R2, N1 and R1 are proposed to correlate to C19n, C19r, C20n and C20r respectively (Fig. 8A).

Although bio- and chronostratigraphic implications of the European Paleogene reference levels are beyond the scope of this study, it is worth pointing out that the Bartonian age of the Pontils fossil site derived from this work only refers to the Pontils fossil site and not to the calibration of the MP15 reference level. As an example, the Sant Jaume de Frontanyà, (SJF) fossil site (Busquets *et al.*, 1992; Moyà-Solà and Kohler, 1993), which is also assigned to MP15 reference level, has been traditionally dated as early Bartonian (Bonilla-Salomón *et al.*, 2016). However, a new 6.5 km thick composite magnetostratigraphic section within the Ripoll syncline, in the south Pyrenean foreland, correlates the SJF fossil site to C20n (late Lutetian) (Juvany *et al.*, 2024). This implies a time span of more than 3Myr between SJF and Pontils fossil sites, both belonging to the MP15 reference level. Therefore, further studies are needed in order to understand the chronostratigraphic significance of the Paleogene mammal reference levels.

Using the absolute ages obtained from the correlation of the magnetostratigraphic log with the GPTS 2020 and the stratigraphic thickness corresponding to the different magnetozones, values of sedimentation rates have also been

calculated (Fig. 8B). The Pontils-Cornudella Group (C20n to C19n) correlates to low sedimentation rates with an average value of 10.6cm/kyr. The Montblanc, Vallespinosa and Riu de Boix formations (C18n to C16r) also represent low sedimentation rates, although slightly increasing the values between 7.3 at the base and 13.6 cm/kyr towards the top (Fig. 8B). Conversely, the base of the Sant Miquel Fm. at C16n shows an abrupt change in the sedimentation rates to much higher values sustained for 1Myr (from 50.6cm/kyr at C16n to 51.2 cm/kyr at C15r), finally decreasing to 22cm/kyr at C15n.

Tectonostratigraphic evolution of the central Catalan Coastal Ranges during the Paleogene compression: relative and absolute timing of thrust emplacement

The compressional phase related to the convergent motion between the Iberian and Eurasian plates started in the late Santonian (Late Cretaceous) (Roest and Srivastava, 1991; Rosenbaum *et al.*, 2002). However, the first evidence of the transmission of the compressional stresses into the Catalan Coastal Ranges area occurs at the end of the Cretaceous (possibly Maastrichtian), as recorded in the Miramar-Gaià Domain by the presence of a paraconformity that brings in contact basal Paleogene and Triassic (Keuper) strata (Figs. 4; 5). This unconformity denotes a period of regional uplift linked to either, a Late Cretaceous contractional deformation, or an isostatic adjustment after the Late Jurassic to Early Cretaceous rifting phase (Marín *et al.*, 2021). A subsequent period of tectonic quiescence from Paleocene to middle Eocene (late Lutetian) is illustrated by the sedimentation of conformable fine-grained terrigenous and carbonate beds deposited in the distal areas of the South-Pyrenean foreland (Anadón, 1978 a, b; Anadón *et al.*, 1985). The presence of *Alveolina* and *Opertorbitolites*, as well as freshwater limestone facies in clasts from the first conglomeratic beds present in the basin margin suggests that, at least, Paleocene-Ypresian (Ilerdian to lower Cuisian) strata from the Mediona, Orpí and Santa Càndia formations and, probably, upper Cuisian to Lutetian from the Carme, Valldeperes and Bosc d'en Borràs formations, were unconformably overlying Cretaceous rocks of the Montmell-Garraf Basin area (Fig. 10A). This stratigraphic succession indicates the absence of significant deformation or creation of relief in the adjacent areas and its extension towards the southeast remains uncertain.

The first significant compressional period in the study area corresponds to the beginning of the tectonic inversion of the Montmell Fault, which drives the uplift of Montmell-Garraf Basin and the overlying strata over the undeformed Ebro Basin (Fig. 10B). This inversion is characterized by the development of footwall shortcuts in the upper part of the reactivated faults as well as the presence of minor buttressing (*e.g.* SE-directed backthrusts and pop-up

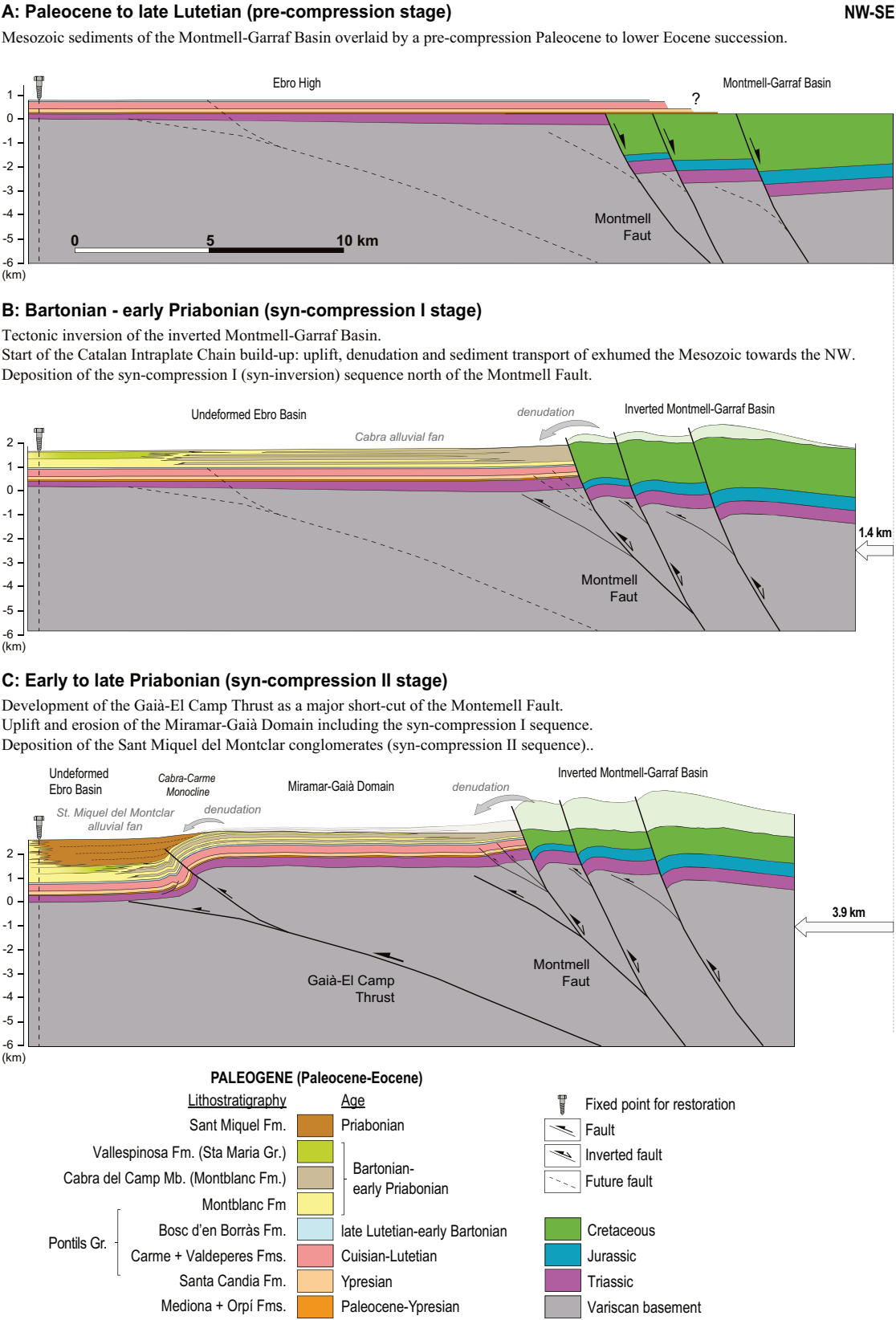


FIGURE 10. Schematic sequential structural restoration of the Gaià-Montmell section applying flexural slip and bed length preservation. A) late Lutetian pre-compressional stage. B) late Lutetian – middle Bartonian syn-compressional stage. C) middle Bartonian to late Priabonian latest stages of the compressional stage. No vertical exaggeration.

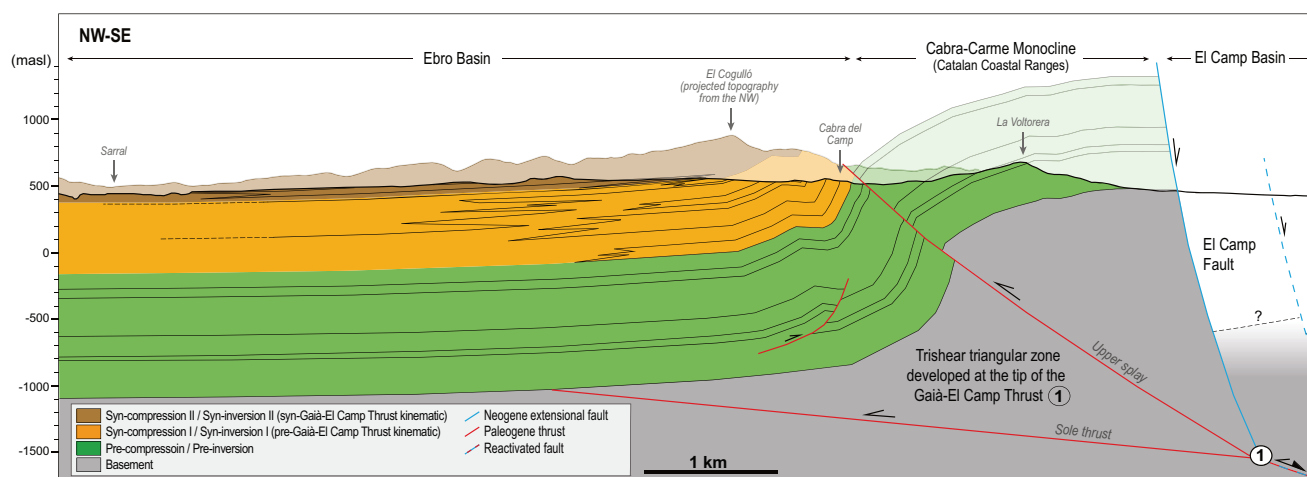


FIGURE 11. Geological cross-section of the SE margin of the Ebro Basin across the locality of Cabra del Camp showing the tectono-sequences differentiated by the tectono-stratigraphic analysis. See Figure 4 for section location.

structures) in the Montmell Fault hangingwall (Marín *et al.*, 2021). The uplift of the Montmell-Garraf Basin controlled the denudation of the positive reliefs and the deposition of the first syn-compression succession recorded in the studied sector of the Ebro Basin margin (Fig. 11). The base of this succession corresponds to the first conglomerates of the Cabra del Camp Mb. (Montblanc Fm.). The observed parallelism with the strata underneath denotes that their deposition was before the emplacement of the Gaià-El Camp Thrust (pre-Gaià-El Camp Thrust kinematic, Fig. 11) therefore contradicting previous interpretations that included these conglomerates as part of a growth sequence (*i.e.* Anadón *et al.*, 1986).

The analysis of the fossil content in clasts from the Cabra del Camp Mb. conglomerates and coeval units (Montblanc and Vallespinosa formations) reveals that the source area contained rocks from the Lower Cretaceous (Barremian-Aptian), Upper Cretaceous (Cenomanian, Turonian and, possibly, Senonian) and lower to middle Eocene (Ypresian-Lutetian). Despite the current levels of erosion south of the Montmell Fault in the Miramar-Gaià Domain does not allow the recognition of rocks younger than Paleocene (Figs. 2B, C), an alluvial system at the footwall of the Montmell Fault and extending up to the present-day location of Cabra del Camp is proposed for this period (Cabra alluvial fan, Fig. 10B). This reconstruction contemplates the presence of (unpreserved) proximal alluvial facies at the foothills of the inverted Montmell-Garraf Basin laterally changing to distal facies towards the northwest above the still inactive Gaià-El Camp Thrust. This reconstruction is supported by the measured NW-directed paleocurrents and the fact that one of the main sources of the sediments consisted of Cretaceous rocks comparable to the formations described in the Mesozoic basins located southeast of the study

area (*e.g.* Montmell-Garraf) (Esteban, 1973; Esteban and Robles, 1976; Salas *et al.*, 2001; Moreno-Bedmar *et al.*, 2017; Martín-Closas *et al.*, this volume). Consequently, the conglomerate beds currently outcropping in the surroundings of Cabra del Camp in the Ebro Basin margin (Cabra del Camp Mb., Fig. 4) can be described as the distal remains of an alluvial system that expanded over the Miramar-Gaià Domain (Fig. 10B). To the northwest, the Cabra alluvial system would laterally transition into the finer-grained facies of the Montblanc Fm. and the marine sediments of the Vallespinosa Fm. (Fig. 4B)

The beginning of the inversion and the uplift of the Montmell-Garraf Basin can be established from the paleomagnetic analysis performed in sediments of the Santa Maria and Barberà-Anoia groups (Fig. 8), which constrains the age of the base of the Montblanc Fm. and its lateral equivalent the Cabra del Camp Mb. (Figs. 4; 5) as early Bartonian (41Ma). This age of initial contractional movements and inversion agrees with the fact that the compressional deformation in the Catalan Coastal Ranges progressed from northeast to southwest up to the middle Oligocene (Guimerà and Santanach, 1978; Guimerà, 1984; Anadón *et al.*, 1985). The earliest syn-tectonic sediments recorded along the SE Ebro Basin margin are the early Eocene Cairat Fm. (Ypresian-early Cuisian in age), which were deposited northeast of the study area in the Montserrat-Sant Llorenç del Munt area (López-Blanco, 2002) (Fig. 2A).

The compressional deformation continued and the whole ensemble of the Miramar-Gaià Domain became uniformly uplifted by the Gaià-El Camp Thrust (Fig. 10C), a low-angle thrust previously interpreted as a major footwall shortcut that provided a smoother fault trajectory

during the inversion of the Montmell Fault (Marín *et al.*, 2021). The emplacement of the Gaià-El Camp Thrust is the responsible of the Cabra-Carme Monocline formation, which represents the deformation front of the Catalan Coastal Ranges. The deformation was first accommodated within a trishear triangular zone developed at the tip of the Gaià-El Camp Thrust. As deformation progressed, an out-of-syncline back-thrust developed to accommodate the shortening, folding the previously deposited syn-compression I succession (Figs. 5; 10C; 11) and resulting in the characteristic anticline-syncline pair observed north of Cabra del Camp (Fig. 4). Similar out-of-syncline structures have been previously recognized in the Miramar Range southwest of the study area by Gómez and Guimerà (1999) (see map in Fig. 2B for location).

The Sant Miquel conglomerates were deposited during this period as the result of the uplift, denudation, and transport of coarse-grained sediments from the adjoining reliefs towards the southeast (Fig. 10C). The projection of topographically higher dip data from the Sant Miquel Fm. located to the northeast (Fig. 5), shows that this formation probably onlaps and/or truncates the strata underneath. The internal structure of these conglomerates seen northeast of the Vallespinosa town (Fig. 4), which includes at least two intraformational angular unconformities (López-Blanco *et al.*, 2025), is coherent with its deposition during the coeval development of the Cabra-Carme Monocline. The observed geometries would suggest that this monocline developed following a limb rotation model that generated a fan of beds with intraformational unconformities (Fig. 10C). This fact agrees with the interpretation of the frontal structure as a fault-propagation fold developed by a triangular shear zone at the tip of the Gaià-El Camp Thrust (Marín *et al.*, 2021).

If we consider the results of the magnetostratigraphic analysis (Fig. 8) and the above-mentioned geometrical relationships of the Sant Miquel conglomerates, it is possible to refine the age of the deformation as Priabonian and not late Bartonian as previously suggested by Marín *et al.* (2021). The end of the compressional deformation is difficult to establish in the study area considering that the stratigraphic record is limited. However, it probably ended in the uppermost Priabonian, as suggested by the end of the conglomeratic sedimentation and the presence of lacustrine facies that would denote tectonic quiescence (Anadón *et al.*, 1985, 1989).

Combining thickness and precise age control provided by magnetostratigraphic analysis sedimentation rates have been calculated for the Pontils magnetostratigraphic section. The evolution of these sedimentation rates shows a tight correlation with the deduced tectonic evolution of the Ebro Basin margin (Fig. 8B). The calculated values for the Pontils Group and Montblanc Formation (10.6cm/

kyr and 7.3cm/kyr, respectively) show, in average, the lowest sedimentation rates of the section. These low values correspond to areas of low subsidence attributed to a relative quiescence episode during the Late Lutetian pre-compression stage (Fig. 10A). The Bartonian-early Priabonian units (Vallespinosa and Riu de Boix Formations) show higher sedimentation rates (9.8cm/kyr and 13.6cm/kyr, respectively). These values still represent relatively low subsidence rates. However, they correspond to syn-compression I stage (Fig. 10B) and thus, associated to the first significant compressional period in the study area. In this case, it can be interpreted that the inversion of high-angle faults bounding the Montmell-Garraf Basin did not induce a major change in subsidence rates. However, the increasing trend in sedimentation rates would record a progressive rise in subsidence rates due to a change in the tectonic activity. The calculated values for Sant Miquel Formation imply an abrupt increase in the sedimentation rates of up to 51.2cm/kyr. This shift corresponds to the beginning of the early Priabonian late Priabonian syn-compression II stage (Fig. 10C) and can be interpreted as related to the continuation of the Montmell-Garraf Basin inversion and mostly to the onset of the Gaia-El Camp emplacement. This resulted in a major load of basement units causing an increase in subsidence rates in the basin. However, this period (C16n and C15r) also shows relatively high sedimentation rates in other sections and sub-basins from the South-Pyrenean foreland (Garcés *et al.*, 2020). In these other areas, the increase in values has been interpreted as being related to the disconnection of the South-Pyrenean foreland from the Atlantic Ocean (Garcés *et al.*, 2020). Thus, the abrupt increase in sedimentation rates observed in the Pontils section could be interpreted as a combination of the basin margin tectonics and the evolution of the Ebro Basin from exoreic to endorheic conditions during C16n (Costa *et al.*, 2010). The final decrease in the sedimentation rates from 51.2cm/kyr to 22cm/kyr (in C15r and C15n respectively) at the top of Sant Miquel Fm. can be interpreted as related either to the end of the whole syn-compression stage or to a gradual return to trends of the previous externally drained stage (Garcés *et al.*, 2020). This decreasing trend is also recorded by the very low sedimentation rates (6 cm/kyr) in C13r at the neighbouring Sarra section (Barberà *et al.*, 2001) corresponding to the strata just overlying the Sant Miquel conglomerates.

Additionally, the results of the provenance analysis in clasts from the Sant Miquel conglomerates indicate that Barremian-Aptian orbitolinids and Ypresian (Ilerdian) *Alveolina* are prevalent throughout the studied samples. This denotes the continuation of tectonic inversion of the Montmell Fault, the uplift and denudation of the Montmell-Garraf Basin and, the potential cannibalization of the proximal zones of the previously deposited Cabra alluvial system (Fig. 10C).

In terms of Paleogene compression, uplift and its related denudation, significant erosion estimates of up to 2-3km are reported from fission-track thermal modelling southwest of the study area in an equivalent structural position in the Prades Block (Fig. 2A) (Juez-Larré and Andersen, 2002).

CONCLUSIONS

The integration of a new geological map, structural analysis as well as magnetostratigraphic and provenance analyses has allowed the refinement of the tectono-stratigraphic evolution of the central Catalan Coastal Ranges and the SE margin of the Ebro Basin during the Paleogene compression.

The correlation of the new Pontils magnetostratigraphic section with the Geomagnetic Polarity Time Scale allows constraining the absolute ages of the Paleogene stratigraphic units along more than 1,400m of succession from Lutetian to Priabonian. The sedimentation of the uppermost Carme Fm. occurred during the late Cuisian, while the Valldeperes and the Bosc d'en Borràs formations occurred during the Lutetian. The age of the deposition of the Vallespinosa and Montblanc formations (including the Cabra del Camp Mb.) has been established as Bartonian to early Priabonian. The paleomagnetic study also dates the Pontils fossil site (MP15 reference level) as Bartonian, ranging from 41 to 39.8Ma.

The conglomerates of the Cabra del Camp Mb. correspond to distal facies of an alluvial system (Cabra alluvial system). This system expanded to the northwest of the Montmell Fault over the Miramar-Gaià Domain due to the onset of compression and the tectonic inversion of the fault during the Bartonian to early Priabonian. This proposed age refines previous estimates for the timing of the Montmell Fault inversion that placed the reactivation in the late Ypresian (Cuisian). Additionally, it aligns with the diachronous record of the compression observed along the SE margin of the Ebro Basin, where the timing varies from Ypresian in the northern sector to Bartonian in the central area, and middle to late Eocene in the south.

The provenance analysis of the Cabra del Camp conglomerates indicates that the source area of this alluvial system was located southeast of the studied area and corresponded to the Montmell-Garraf Basin. The proximal facies of Cabra alluvial system would have been located in the footwall of the Montmell Fault although these have not been preserved due to later uplift and denudation. The composition of clasts suggests that the Mesozoic Basin included Upper Cretaceous (Cenomanian, Turonian and minor Senonian), and Lower Cretaceous (Barremian-

Aptian) strata. The Mesozoic Basin was overlaid by Paleocene to Lutetian sediments (Mediona and Orpí formations and Pontils-Cornudella Group), which confirms this as a period of tectonic quiescence. However, the extent of these Paleogene successions towards the southeast remains uncertain.

A second pulse of compression is recorded by intraformational angular unconformities in the conglomerates of the Sant Miquel Formation (syn-compression II stage) during the Priabonian. The deformation of these conglomerates is associated with the growth of a fault-propagation fold known as the Cabra-Carme Monocline, which resulted from the emplacement of the Gaià-El Camp Thrust. This thrust uplifted the Miramar-Gaià Domain over the Ebro Basin. The Cabra-Carme Monocline constitutes the deformation front of the Catalan Coastal Ranges at this location. Additionally, out-of-syncline backthrusting deformed the previously deposited syn-compression I sequence, which includes the conglomerates of the Cabra del Camp Mb. The beginning of this stage is marked by the abrupt increase in the sedimentation rates, which is related to the increase in the tectonic subsidence caused by the onset of the Gaià-El Camp low angle thrust.

ACKNOWLEDGMENTS

The authors thank the Paleomagnetic Laboratory CCiTUB - Geo3BCN (CSIC) for the support on paleomagnetic analyses. We would like to thank the kind and useful review performed by Drs. Antonio Casas and Mar Moragas as well as the Editor, Dr. Joan Guimerà, and finally, all the staff members of *Geologica Acta* for handling the paper. This research has been carried out within the framework of the following projects: the IBERINSULA (PID2020-113912GB-I00), funded by MCIN/AEI/10.13039/501100011033; the MCIN Project IMPACISIS (PID2019-106440GB-C21) European Regional Development Fund (ERDF); the SABREM-PID2020-117598GB-I00 funded by MCIN/AEI/10.13039/501100011033; the DGICYT PID2021-122467NB-C22 Ministerio de Ciencia, Innovación y Universidades/Agencia Estatal de Investigación/Fondo Europeo de Desarrollo Regional; GEODIGIT (TED2021-130602B-I00) research projects funded by MCIN/AEI/10.13039/501100011033 for the European Union "NextGenerationEU"/PRTR. The Grups Consolidats de Recerca "Geologia Sedimentària" (2021-SGR-Cat 00349) and "Geodinàmica i Anàlisi de Conques" (2021-SGR 00076) of the Generalitat de Catalunya, and the UB Geomodels Research Institute are also acknowledged. The research has also been benefited by the project "Caracterització litoestratigràfica i estructural i cartografia geològica del Paleogen dels fulls de Sarra (67-31) i Montblanc (67-32) del Mapa Geològic de Catalunya 1:25000" funded by the Institut Cartogràfic i Geològic de Catalunya.

REFERENCES

- Agustí, J., Anadón, P., Arbiol, S., Cabrera, L., Colombo, F., Sáez, A., 1987. Biostratigraphical characteristics of the Oligocene sequences of north-eastern Spain (Ebro and Campins basins). *Münchner Geowissenschaften Abhandlungen (A)* 10, 35-42.
- Albrich, S., Bernaus, J.M., Boix, C., Caus, E., Martín-Closas, C., Salas, R., Vicedo, V., Villalonga, R., 2006. Caracterización bioestratigráfica y paleoambiental del Cretácico Inferior (Berriasiense-Barremiense) del Macizo de Garraf (Cadena Costera Catalana). *Revista Española de Micropaleontología* 38 (2-3), 429-451.
- Al-Hajeri, M.M., Al-Saeed, M., Derks, J., Fuchs, T., Hantschel, T., Kauerauf, A., Neumaier, M., Schenk, O., Swientek, O., Tessen, N., Welte, D., Wygrala, B., Kornpohl, D., Peters, K., 2009. Basin and petroleum system modeling. *Oilfield Review* 21(2), 14-29.
- Amilibia, A., Sàbat, F., McClay, K.R., Muñoz, J.A., Roca, E., Chong, G., 2008. The role of inherited tectono-sedimentary architecture in the development of the central Andean Mountain belt: Insights from the Cordillera de Domeyko. *Journal of Structural Geology* 30(12), 1520-1539.
- Anadón, P., 1978a. El Paleógeno continental anterior a la transgresión biarrtziense (Eoceno medio) entre los ríos Gaia y Ripoll. PhD Thesis, University of Barcelona, Barcelona, 267pp.
- Anadón, P., 1978b. El Paleógeno continental anterior a la transgresión biarrtziense (Eoceno medio) entre los ríos Gaiá y Ripoll. *Estudios Geológicos*.
- Anadón, P., Colombo Piñol, F., Esteban Cerdà, M., Marzo Carpio, M., Robles Orozco, S., Santanach, P., Solé Sugrañes, L., 1979. Evolución tectonoestratigráfica de los Catalánides. *Acta Geologica Hispánica* 14. Hommage to Lluís Solé i Sabarís. 242-270.
- Anadón, P., Feist, M., 1981. Charophytes et biostratigraphie du Paléogène inférieur du bassin de l'Ebre oriental. *Palaeontographica Abteilung B* 178, 143-168.
- Anadón, P., Feist, M., Hartenberger, J.L., Muller, C., Villalta-Comella, J., 1983. Un exemple de corrélation biostratigraphique entre échelles marines et continentales dans l'Éocène: la coupe de Pontils (Bassin de l' Ebre, Espagne), *Bulletin de la Société Géologique de la France* XXV (5), 747-755.
- Anadón, P., Cabrera, L., Guimerà, J., Santanach, P., 1985. Paleogene strike-slip deformation and sedimentation along the southeastern margin of the Ebro Basin, In: Biddle, K.T. and Christie-Blick, N. (eds.), *Strike-Slip Deformation, Basin Formation, and Sedimentation. The Society of Economic Paleontologists and Mineralogists*, 303-318. <https://doi.org/10.2110/pec.85.37.0303>
- Anadón, P., Cabrera, L., Colombo, F., Marzo, M., Riba, O., 1986. Syntectonic intraformational unconformities in alluvial fan deposits, eastern Ebro Basin margins (NE Spain). In: Allen, P.A. and Homewood, P. (eds.), *Foreland basins, Special Publication Number 8 of the International Association of Sedimentologists*, 259-271.
- Anadón, P., Vianey-Liaud, M., Cabrera, L., Hartenberger, J.L., 1987. Gisements à vertébrés du paléogène de la zone orientale du bassin de l'Ebre et leur apport à la stratigraphie. *Paleontologia i Evolució*, 21, 117-131.
- Anadón, P., Marzo, M., 1986. Sistemas deposicionales eocenos del margen oriental de la cuenca del Ebro: Sector Igualada-Montserrat. In: Reguant, S. (ed.), *XI Congreso Español de Sedimentología: guía de las excursiones*. Barcelona, 1-4.
- Anadón, P., Cabrera, L., Colldeforns, B., Sáez, A., 1989. Los sistemas lacustres del Eoceno superior y Oligoceno del sector oriental de la Cuenca del Ebro. *Acta Geologica Hispánica*, 24 (3-4): 205-230.
- Anadón, P., Cabrera, L., Choi, S. J., Colombo, F., Feist, M., Sáez, A., 1992. Biozonación del Paleógeno continental de la zona oriental de la Cuenca del Ebro mediante carófitas: implicaciones en la biozonación general de carófitas de Europa occidental. *Acta Geologica Hispánica*, 27 (1-2), 69-94.
- Andeweg, B., 2002. Cenozoic tectonic evolution of the Iberian Peninsula: effects and causes of changing stress fields. PhD Thesis Vrije Universiteit, Amsterdam, 178pp.
- Angrand, P., Mouthereau, F., Masini, E., Asti, R., 2020. A reconstruction of Iberia accounting for Western Tethys–North Atlantic kinematics since the late-Permian–Triassic. *Solid Earth*, 11(4): 1313-1332. <https://doi.org/10.5194/se-11-1313-2020>
- Angrand, P., Mouthereau, F., 2021. Evolution of the Alpine orogenic belts in the Western Mediterranean region as resolved by the kinematics of the Europe-Africa diffuse plate boundary. *BSGF-Earth Sciences Bulletin*, 192, (1). 44 pp. <https://doi.org/10.1051/bsgf/2021016>
- Arasa-Tuliesa, A., Cabrera, L., 2018. Neogene-Quaternary onshore record in the lower Ebro River incised palaeovalley (Ebro margin, Catalan Coastal Range, NE Iberia). *Geologica Acta*, 16 (3), 265-292.
- Arche, A., Evans, G., Clavell, E., 2010. Some considerations on the initiation of the present SE Ebro River drainage system: Post- or pre-Messinian? *Journal of Iberian Geology* 36 (1), 73-85.
- Arnal, I., Calvet, F., Márquez, L., Márquez-Aliaga, A., Solé de Porta, N., 2002. La plataforma carbonatada epeírica (Formaciones Imón e Isábena) del Triásico superior del Noreste de la Península Ibérica. *Acta Geológica Hispánica* 37 (4), 299-328.
- Baqués, V., Travé, A., Roca, E., Marín, M., Cantarero, I., 2012. Geofluid behavior in successive extensional and compressional events: a case study from the southwestern end of the Vallès-Penedès Fault (Catalan Coastal Ranges, NE Spain). *Petroleum Geosciences*, 18, 17-31.
- Barberà, X., 1999. Magnetostratigrafia de l'Oligocè del sector sudoriental de la Conca de l'Ebre: implicacions magnetobiocronològiques i seqüencials. PhD Thesis. University of Barcelona, Barcelona, 247pp.
- Barberà, X., Cabrera, L., Marzo, M., Parés, J.M., Agustí, J., 2001. A complete terrestrial Oligocene magnetobiostratigraphy from the Ebro Basin, Spain. *Earth and Planetary Science Letters*, 187, 1-16.
- Bartrina, M.T., Cabrera, L., Jurado, M. J., Guimerà, J., Roca, E., 1992. Evolution of the central Catalan margin of the Valencia

- trough (western Mediterranean). *Tectonophysics*, 203(1-4), 219-247.
- Beamud, E., 2013. Paleomagnetism and thermochronology in Tertiary syntectonic sediments of the South-Central Pyrenees: Chronostratigraphy, kinematic and exhumation constraints. PhD Thesis, University of Barcelona, Barcelona, 251pp.
- Beamud, E., Garcés, M., Cabrera, L., Muñoz, J.A., Almar, Y., 2003. A new late Eocene continental chronostratigraphy from NE Spain. *Earth and Planetary Science Letters*, 216, 501-514.
- Beamud, E., Costa, E., Garcés, M., Cabrera, L., Roca, E., Gómez-Paccard, M., 2012. An integrated Eocene chronostratigraphy for the central sector of the SE margin of the Ebro Basin. *Geotemas*, 13, 1116-1119.
- Benzaquen, M., Nuñez, A., Martínez, W., 1973. Hoja nº 418 (Montblanc), Mapa Geológico de España E. 1: 50.000. Segunda Serie (MAGNA). Instituto Geológico y Minero de España, Madrid.
- Bonilla-Salomón, I., Minwer-Barakat, R., Vianey-Liaud, M., Moyà-Solà, S., 2016. Middle Eocene rodents from Sant Jaume de Frontanyà (eastern Pyrenees, northern Spain) and biochronological implications. *Journal of Vertebrate Paleontology*, 36(4), e1121149. <https://doi.org/10.1080/02724634.2016.1121149>
- Boyer, S.E., Elliott, D., 1982. Thrust systems. *AAPG Bulletin*, 66(9), 1196-1230.
- Burbank, D.W., Verges, J., Munoz, J.A., Benthams, P., 1992. Coeval hindward-and forward-imbricating thrusting in the south-central Pyrenees, Spain: Timing and rates of shortening and deposition. *Geological Society of America Bulletin*, 104(1), 3-17.
- Busquets, P., Ortí, E., Pueyo, J.J., Riba, O., Sáez, A., Salas, R., Taberner, C., 1985. Evaporite deposition and diagenesis in the saline (potash) Catalan basin, Upper Eocene. Excursion Guidebook 6th European Meeting, Lleida, Spain, 13-59.
- Busquets, P., Ramos Guerrero, E., Moya, S., Agustí, J., Colombo, E., Checa, L., Kohler, M., 1992. La Formación de Bellmunt (Unidad del Cadi, Pirineo Oriental); aportaciones bioestratigráficas de los sistemas lacustres y palustres asociados. *Acta Geologica Hispánica*, 27, 109-116.
- Butler, R.W.H., 1989. The influence of preexisting basin structure on thrust system evolution in the Western Alps. In: Cooper, M.A., Williams, G.D. (eds.), *Inversion Tectonics*. Geological Society of London Special Publication, 44, 105-122.
- Butler, R.W.H., 1982. The terminology of structures in thrust belts. *Journal of structural Geology*, 4(3), 239-245.
- Butler, R.W.H., 1987. Thrust sequences. *Journal of the Geological Society*, 144(4), 619-634.
- Calvet, E., Marzo, M., 1994. El Triásico de las Cordilleras Costero Catalanas: estratigrafía, sedimentología y análisis secuencial. In: *Field guide III Coloquio de Estratigrafía y Sedimentología del Triásico y Pérmico de España*, pp. 1-53.
- Cantarero, I., Travé, A., Alías, G., Baqués, V., 2014a. Polyphasic hydrothermal and meteoric fluid regimes during the growth of a segmented fault involving crystalline and carbonate rocks (Barcelona Plain, NE Spain). *Geofluids*, 14, 20-44.
- Cantarero, I., Lanari, P., Vidal, O., Alías, G., Travé, A., Baqués, V., 2014b. Long-term fluid circulation in extensional faults in the central Catalan Coastal Ranges: P-T constraints from neoformed chlorite and K-white mica. *International Journal of Earth Sciences*, 103, 165-188.
- Carminati, E., Wortel, M.J.R., Meijer, P.T., Sabadini, R., 1998. The two-stage opening of the western-central Mediterranean basins: a forward modeling test to a new evolutionary model. *Earth and Planetary Science Letters*, 160(3-4), 667-679.
- Carrera, N., López-Blanco, M., Arbués, P., Beamud, E., Garcés, M., Marín, M., Cabrera, L., 2020. Caracterització litostratigràfica i estructural i cartografia geològica del Paleogen dels fulls de Sarrià (67-31) i Montblanc (67-32) del Mapa Geològic de Catalunya 1:25000. Institut Cartogràfic i Geològic de Catalunya Technical Report CG-0006/20 (unpublished), 70 pp.
- Coldeforns, B. (unpublished). Mapa Geològic de Catalunya. 1:25.000, Sheet nº 418-2-1 (68-31) (Querol). Geological map advised by P. Anadón. Servei Geològic, de Catalunya, Barcelona, Spain.
- Coldeforns, B., Anadón, P., Cabrera, L., 1994a. Litoestratigrafia del Eoceno superior-Oligoceno inferior de la zona oriental de la Cuenca del Ebro. Sector Igualada-Santa Coloma de Queralt. *Geogaceta* 15, 55-58.
- Coldeforns, B., Anadón, P., Cabrera, L., 1994b. Nuevos datos sobre la litoestratigrafía del Eoceno-Oligoceno inferior de la zona suroriental de la Cuenca del Ebro (Sector Pontils-Montblanc, provincias de Tarragona y Barcelona). *Geogaceta* 16, 98-101.
- Colombo, E., 1980. Estratigrafía y sedimentología del Terciario inferior continental de los Catalánides. PhD Thesis, University of Barcelona, Barcelona, 608pp.
- Colombo, E., 1986. Continental Paleogene stratigraphy and sedimentology of the western southern border of the Catalanides, Tarragona Province, Spain. *Cuadernos de Geología Ibérica*, 10, 55-115.
- Colombo, E., 1994. Normal and reverse unroofing sequences in syntectonic conglomerates as evidence of progressive basinward deformation. *Geology*, 22(3), 235-238.
- Costa, E., Garcés, M., López-Blanco, M., Beamud, E., Gómez-Paccard, M., Larrasoana, J.C., 2010. Closing and continentalization of the South Pyrenean foreland basin (NE Spain): magnetochronological constraints. *Basin Research*, 22(6), 904-917.
- Costa, E., Garcés, M., López-Blanco, M., Serra-Kiel, J., Bernaola, G., Cabrera, L., Beamud, E., 2013. The Bartonian-Priabonian marine record of the eastern South Pyrenean foreland basin (NE Spain): a new calibration of the larger foraminifers and calcareous nannofossil biozonation. *Geologica Acta*, 11(2), 177-193.
- Couzens, B.A., Wiltshko, D.V., 1996. The control of mechanical stratigraphy on the formation of triangle zones. *Bulletin of Canadian Petroleum Geologists*, 44, 165-179.
- Coward, M.P., 1994. Inversion tectonics. In: Hancock, P.L. (ed.) *Continental Deformation*. Pergamon Press, 280-304.

- Coward, M.P., Gillcrist, R., Trudgill, B., 1991. Extensional structures and their tectonic inversion in the Western Alps. In: Roberts, A.M., Yielding, G., Freeman, B. (eds.), *The Geometry of Normal Faults*, Geological Society Special Publication, 56, 93–113.
- Dañoibeitia, J.J., Arguedas, M., Gallart, J., Banda, E., Makris, J., 1992. Deep crustal configuration of the Valencia trough and its Iberian and Balearic borders from extensive refraction and wide-angle reflection seismic profiling. *Tectonophysics*, 203(1–4), 37–55.
- Escudero-Mozo, M.J., Márquez-Aliaga, A., Goy, A., Martín-Chivelet, J., López-Gómez, J., Márquez, L., Arche, A., Plasencia, P., Pla, C., Marzo, M., Sánchez-Fernández, D., 2017. Middle Triassic carbonate platforms in eastern Iberia: evolution of their fauna and palaeogeographic significance in the western Tethys. *Palaeogeogr. Palaeoclimatol. Palaeoecol.* 417, 236–260.
- Erslev, E. A. 1991. Trishear fault-propagation folding. *Geology*, 19(6), 617–620.
- Esteban, M., 1973. *Petrología de las calizas Cretácicas del Sector Central de los Catalánides (Prov. de Tarragona y Barcelona)*. PhD Thesis, University of Barcelona, Barcelona, 425pp.
- Esteban, M., Robles, S., 1976. Sobre la paleogeografía del Cretácico Inferior de los Catalánides entre Barcelona y Tortosa. *Acta Geológica Hispánica* 11(3), 73–78.
- Feist, M., Anadón, P., Cabrera, L., Choi, S. J., Colombo, F., Sáez, A., 1994. Upper Eocene-Lowermost Miocene charophyte succession in the Ebro basin (Spain). Contribution to the charophyte biozonation in Western Europe. *Newsletters on Stratigraphy*, 30 (1): 1–32.
- Fernández, O., Muñoz, J.A., Arbués, P., Falivene, O., Marzo, M., 2004. Three-dimensional reconstruction of geological surfaces: An example of growth strata and turbidite systems from the Ainsa basin (Pyrenees, Spain). *AAPG Bulletin*, 88(8), 1049–1068.
- Ferrer, J., 1971. El Paleoceno y Eoceno del borde suroccidental de la Depresión del Ebro (Cataluña). *Mémoires suisses de Paléontologie*, 90, 1–70.
- Ferrer, O., Carola, E., McClay, K., 2023. Structural control of inherited salt structures during inversion of a domino basement-fault system from an analogue modelling approach. *Solid Earth*, 14(5), 571–589.
- Ferrill, D.A., Morris, A.P., 2008. Fault zone deformation controlled by carbonate mechanical stratigraphy, Balcones fault system, Texas. *AAPG Bulletin*, 92(3), 359–380.
- Fontboté, J.M., Guimerà, J., Roca, E., Sàbat, E., Santanach, P., Fernández-Ortigosa, E., 1990. The Cenozoic geodynamic evolution of the Valencia trough (western Mediterranean). *Revista Sociedad Geológica de España*, 3(3–4), 249–259.
- Ford, M., Williams, E.A., Artoni, A., Vergés, J., Hardy, S., 1997. Progressive evolution of a fault-related fold pair from growth strata geometries, Sant Llorenç de Morunys, SE Pyrenees. *Journal of structural Geology*, 19(3–4), 413–441.
- Galán-Abellán, B., López-Gómez, J., Berenechea, J.F., Marzo, M., De la Horra, R., Arche, A., 2013. The beginning of the Buntsandstein cycle (Early–Middle Triassic) in the Catalan Ranges, NE Spain: Sedimentary and palaeogeographic implications. *Sediment. Geol.* 296, 86–102.
- Garcés, M., López-Blanco, M., Valero, L., Beamud, E., Muñoz, J.A., Oliva-Urcia, B., Vinyoles, A., Arbués, P., Cabello, P., Cabrera, L., 2020. Paleogeographic and sedimentary evolution of the South Pyrenean foreland basin. *Marine and Petroleum Geology*, 113, 104105.
- García-Senz, J., Pedrera, A., Ayala, C., Ruiz-Constán, A., Robador, A., Rodríguez-Fernández, L.R., 2019. Inversion of the north Iberian hyperextended margin: the role of exhumed mantle indentation during continental collision. *Geol. Soc. Spec. Publ.* 490, 177–198.
- Gaspar-Escribano, J.M., García-Castellanos, D., Roca, E., Cloetingh, S.A.P.L., 2004. Cenozoic vertical motions of the Catalan Coastal Ranges (NE Spain): The role of tectonics, isostasy, and surface transport. *Tectonics*, 23(1), TC1004.
- Gómez, M., Guimerà, J., 1999. Estructura Alpina de la Serra de Miramar y del NE de las Muntanyes de Prades (Cadena Costera Catalana). *Rev. Soc. Geol. Esp.*, 12(3–4), 405–418.
- Gómez-Paccard, M., López-Blanco, M., Costa, E., Garcés, M., Beamud, E., Larrasoña, J.C., 2011. Tectonic and climatic controls on the sequential arrangement of an alluvial fan/fan-delta complex (Montserrat, Eocene, Ebro basin, NE Spain). *Basin Research*, 23, 1–19.
- Gradstein, F.M., Ogg, J.G., Schmitz, M. D., Ogg, G. M. (Eds.), *Geologic time scale 2020*. Elsevier, 159–192.
- Gross, M.R., Gutierrez-Alonso, G., Bai, T., Wacker, M.A., Collingsworth, K.B., Behl, R.J., 1997. Influence of mechanical stratigraphy and kinematics on fault scaling relations. *Journal of Structural Geology*, 19, 171–183.
- Guimerà, J., 1984. Paleogene evolution of deformation in the northeastern Iberian Peninsula. *Geol. Mag.*, 121, 413–420.
- Guimerà, J., 2018. Structure of an intraplate fold-and-thrust belt: the Iberian Chain. A synthesis. *Geologica Acta*, 16 (4): 427–438.
- Guimerà, J., Santanach, P., 1978. Sobre la compresión alpina en el sector central de las Cadenas Costeras Catalanas. *Acta Geológica Hispánica* 2(13), 33–42.
- Guimerà, J., Álvaro, M., 1990. Structure et évolution de la compression alpine dans la Chaîne ibérique et la Chaîne côtière catalane (Espagne). *Bull. Soc. Géol. France* 6 (2), 339–348.
- Guimerà, J., Alonso, A., Mas, J.R., 1995. Inversion of an extensional-ramp basin by a newly formed thrust: The Cameros basin (N. Spain). In: Buchanan, J.G., Buchanan, P. G. (eds.), *Basin Inversion*, Geological Society Special Publication, vol. 88, 433–453.
- Hardy, S., Poblet, J., McClay, K.R., Waltham, D., 1996. Mathematical modelling of growth strata associated with fault-related fold structures. *Geological Society, London, Special Publications*, 99(1), 265–282.
- Hayward, A.B., Graham, R.H., 1989. Some geometrical characteristics of inversion. In: Cooper, M.A., Williams, G.D.

- (eds.), *Inversion Tectonics*. Geological Society of London Special Publication, 44, 17-39.
- ICGC, 2005. Mapa geològic comarcal de Catalunya 12, Baix Penedès, 1:50.000. Institut Cartogràfic i Geològic de Catalunya. Barcelona.
- ICGC, 2018. Mapa geològic de Catalunya, Sant Martí Sarroca 419-1-2 (69-32), 1:25.000. Institut Cartogràfic i Geològic de Catalunya. Barcelona.
- Juez-Larré, J., Andriessen, P.A.M., 2002. Post Late Paleozoic tectonism in the southern Catalan Coastal Ranges (NE Spain), assessed by apatite fission track analysis. *Tectonophysics*, 349, 113-129.
- Juez-Larré, J., Andriessen, P.A.M., 2006. Tectonothermal evolution of the northeastern margin of Iberia since the break-up of Pangea to present, revealed by low-temperature fission-track and (U-Th)/He thermochronology. A case history of the Catalan Coastal Ranges. *Earth and Planetary Science Letters* 243, 159-180.
- Juvany, P., Garcés, M., López-Blanco, M., Martín-Closas, C., Beamud, E., Tosquella, J., Bekkevold, S.E., 2024. Chronostratigraphy and tectono-sedimentary history of the Eastern South Pyrenean foreland basin (Ripoll Syncline, North-East Spain). *The Depositional Record*, 10, 338-363. <https://doi.org/10.1002/dep2.287>.
- Kirschvink, J.L., 1980. The least-squares line and plane and the analysis of paleomagnetic data. *Geophysical Journal of the Royal Astronomical Society*, 62, 699-718.
- Lanaja, J.M., 1987. Contribución de la exploración petrolífera al conocimiento de la Geología de España. IGME Ministerio de Industria y Energía, Madrid, 465pp.
- Lawton, T.F., Roca, E., Guimerà, J., 1999. Kinematic-stratigraphic evolution of a growth syncline and its implications for tectonic development of the proximal foreland basin, southeastern Ebro basin, Catalunya, Spain. *GSA Bulletin* 111-3, 412-431.
- Llopis, N., 1947. Contribución al conocimiento de la morfoestructura de los Catalánides. PhD Thesis, Instituto Lucas Mallada, CSIC Barcelona, 373pp.
- López-Blanco, M., 2002. Sedimentary response to thrusting and fold growing on the SE margin of the Ebro basin (Paleogene, NE Spain). *Sedimentary Geology*, 146, 133-154.
- López-Blanco, M., Marzo, M., Burbank, D.W., Vergés, J., Roca, E., Anadón, P., Piña, J., 2000a. Tectonic and climatic controls on the development of foreland fan deltas: Montserrat and Sant Llorenç del Munt systems (Middle Eocene, Ebro Basin, NE Spain). *Sedimentary Geology*, 138(1-4), 17-39.
- López-Blanco, M., Marzo, M., Piña, J., 2000b. Transgressive-regressive sequence hierarchy of foreland, fan-delta clastic wedges (Montserrat and Sant Llorenç del Munt, Middle Eocene, Ebro Basin, NE Spain). *Sedimentary Geology*, 138(1-4), 41-69.
- López-Blanco, M., Carrera, N., Arbués, P., Beamud, E., Garcés, M., Marín, M., Cabrera, L., Roca, E., Ferrer, O., Gratacos, O., 2024. Relación entre los Conglomerados de Sant Miquel de Montclar (Eoceno, margen SE de la cuenca del Ebro) y las unidades estratigráficas adyacentes. *Geo-Temas*, 20, 138.
- López-Blanco, M., Ma, M., Beamud, E., Marín, M., Costa, E., 2025. New evidence of synsedimentary folding of the Sant Miquel de Montclar conglomerates (Eocene, Ebro basin, NE Spain). *Geogaceta*, 77.
- Magoon, L., 1987. The Petroleum System-A Classification Scheme for Research, Exploration, and Resource Assessment. In: Magoon (ed.), *Petroleum Systems of the United States*, U.S. Geological Survey Bulletin 1870, 67pp.
- Makeen, Y.M., Abdullah, W.H., Pearson, M.J., Hakimi, M.H., Ayinla, H.A., Elhassan, O.M., Abas, A.M., 2016. History of hydrocarbon generation, migration and accumulation in the Fula sub-basin, Muglad Basin, Sudan: Implications of a 2D basin modeling study. *Marine and Petroleum Geology*, 77, 931-941.
- Marín, M., Roca, E., Marcuello, A., Cabrera, L., Ferrer, O., 2021. Mesozoic structural inheritance in the Cenozoic evolution of the central Catalan Coastal Ranges (western Mediterranean): Structural and magnetotelluric analysis in the Gaià-Montmell High. *Tectonophysics*, 814, 228970.
- Marín, M., Roca, E., Baqués, V., Cantarero, I., Cabrera, L., Ferrer, O., Travé, A., 2023. Fluid-rock interaction control on fault reactivation: A review of the Montmell-Vallès Fault System, central Catalan Coastal Ranges (NE Iberia). *Global and Planetary Change*, 220, 104011.
- Martín-Closas, C., Vicente, A., Pérez-Cano, J., Sanjuan, J., Bover Arnal, T., 2018. On the earliest occurrence of *Tolypella* section *Tolypella* in the fossil record and the age of major clades in extant Characeae. *Botany Letters*, 165, 23-33.
- Martín-Closas, C., Albalat, D., Colombo, E., Vilà, M., Vicente, A., Ossó, A., this volume. A new Iberian refugium for charophytes during the maximum post-Palaeozoic sea-level high stand in Europe: the Cenomanian-Turonian of Tarragona (Catalonia, Spain). *Geologica Acta*.
- McClay, K.R., 1992. Glossary of thrust tectonics terms. In: McClay (ed.) *Thrust tectonics*, Springer Science & Business Media, 419-433.
- Mercedes-Martín, R., Arenas, C., Salas, R., 2014. Diversity and factors controlling widespread occurrence of syn-rift Ladinian microbialites in the western Tethys (Triassic Catalan Basin, NE Spain). *Sediment. Geol.* 313, 68-90.
- Mercedes-Martín, R., Buatois, L.A., 2020. Microbialites and trace fossils from a Middle Triassic restricted carbonate ramp in the Catalan Basin, Spain: evaluating environmental and evolutionary controls in an epicontinental setting. *Lethaia* 54 (1), 4-25.
- Minwer-Barakat, R., Bolet, A., Anadón, P., Alegret, L., Badiola, A., Blanco, A., Cotton, L., Femenias-Gual, J., Furió, M., Godinot, M., Moyà-Solà, S., Peláez-Campomanes, P., Sanjuan, J., Marigó, J., 2023. The fossil assemblage from Pontils, a middle Eocene primate-bearing locality from Northeastern Spain. *Journal of Vertebrate Paleontology*, 43, e2259970. <https://doi.org/10.1080/02724634.2023.2259970>
- Mitra, S., 2002. Fold-accommodation faults. *AAPG Bulletin*, 86(4), 671-693.
- Moreno-Bedmar, J.A., Robert, E., Matamales-Andreu, R., Bover Arnal, T., 2017. Review of the early Albian ammonites of the

- Montmell Formation near Marmellar (Salou-Garraf Basin, Tarragona, Catalonia, Spain). *Carnets Geol.*, 17(1), 1-10. DOI 10.4267/2042/62038
- Mouthereau, F., Filleaudeau, P.-Y., Vacherat, A., Pik, R., Lacombe, O., Fellin, M. G., Castellort, S., Christophoul, F. Masini, E., 2014. Placing limits to shortening evolution in the Pyrenees: Role of margin architecture and implications for the Iberia/Europe convergence. *Tectonics*, 33, 2283-2314.
- Moyà-Solà, S., Kohler, M., 1993. Middle Bartonian locality with *Anchomomys* (Adapidae, Primates) in the Spanish Pyrenees: preliminary report. *Folia Primatologica*, 60, 158-163. <https://doi.org/10.1159/000156684>.
- Muñoz, J.A., 1992. Evolution of a continental collision belt: ECORS-Pyrenees crustal balanced cross-section. In: McClay, K. (Ed.), *Thrust Tectonics*. Chapman & Hall, London, 235-246.
- Muñoz, J.A., 2017. Fault-related folds in the southern Pyrenees. *AAPG Bull.* 101-4, 579-587.
- Nebot, M., Guimera, J., 2016. Structure of an inverted basin from subsurface and field data: the Late Jurassic-Early Cretaceous Maestrat Basin (Iberian Chain). *Geol. Acta* 14 (2), 155-177.
- Ortí, F., Pérez-López, A., Salvany, J.M., 2017. Triassic evaporites of Iberia: sedimentological and palaeogeographical implications for the western Neotethys evolution during the Middle Triassic-Earliest Jurassic. *Palaeogeogr. Palaeoclimatol. Palaeoecol.* 471, 157-180.
- Pueyo, J.J., 1975. Estudio petrológico y geoquímico de los yacimientos potásicos de Cardona, Súria, Sallent (Barcelona, España). PhD Thesis, University of Barcelona, Barcelona, 351pp.
- Reguant, S., 1967. El Eoceno marino de Vic (Barcelona). *Memorias Instituto Geológico y Minero de España*, 68, 1-350.
- Riba, O., 1973. Las discordancias sintectónicas del Alto Cardener (Prepirineo catalán), ensayo de interpretación evolutiva». *Acta Geológica Hispánica* VIII (3), 90-99.
- Riba, O., 1976. Syntectonic unconformities of the Alto Cardener, Spanish Pyrenees: A genetic interpretation. *Sedimentary Geology*, 15 (3), 213-233
- Robles, S., 1982. Catalánides. In: García, A. (ed.), *El Cretácico de España*. Universidad Complutense de Madrid, 199-272.
- Roca, E., 1994. La evolución geodinámica de la Cuenca Catalano-Balear y áreas adyacentes desde el Mesozoico hasta la actualidad. *Acta Geológica Hispánica*, 29, 3-26.
- Roca, E., 2001. The Northwest-Mediterranean basin (Valencia Trough, Gulf of Lions and Liguro-Provençal basins): structure and geodynamic evolution. In: Ziegler, P.A., Cavazza, W., Robertson, A.H.F., Crasquin-Soleau, S. (eds.), *Peri-Tethys Memoir 6: Peri-Tethyan Rift/Wrench Basins and Passive Margins*, French National Museum of Natural History, vol. 186, 671-706.
- Roca, E., Guimerà, J., 1992. The Neogene structure of the eastern Iberian margin: structural constraints on the crustal evolution of the Valencia trough (western Mediterranean). *Tectonophysics*, 203(1-4), 203-218.
- Roca, E., Frizon de Lamotte D., Mauffret, A., Bracène, R., Vergés, J., Benaouali, N., Fernández, M., Muñoz, J.A., Zeyen, H., 2004. Transect II: Aquitaine Basin - Pyrenees - Ebro Basin - Catalan Range - Valencia Trough - Balearic Block - Algerian Basin - Kabylies - Atlas - Saharan Platform. In: Cavazza, W., Roure, F. M., Spakman, W., Stampfli, G. M. and Ziegler, P. A. (eds.), 2004. *The Transmed Atlas – The Mediterranean Region from Crust to Mantle*, Springer, Berlin, Heidelberg.
- Roest, W.R., Srivastava, S.P., 1991. Kinematics of the plate boundaries between Eurasia, Iberia and Africa in the North Atlantic from the Late Cretaceous to the present. *Geology* 19, 613-616.
- Rosenbaum, G., Lister, G.S., Duboz, C., 2002. Relative motions of Africa, Iberia and Europe during Alpine orogeny. *Tectonophysics*, 359, 117-129.
- Romagny, A., Jolivet, L., Menant, A., Bessière, E., Maillard, A., Canva, A., Gorini, Ch, Augier, R., 2020. Detailed tectonic reconstructions of the Western Mediterranean region for the last 35 Ma, insights on driving mechanisms. *Bulletin de la Société géologique de France*, 191, 37, 45pp.
- Sàbat, F., Roca, E., Muñoz, J.A., Vergés, J., Sans, M., Masana, E., Estévez, A., Santisteban Bove, C.D., 1995. Role of extension and compression in the evolution of the eastern margin of Iberia: The ESCI-Valencia Trough seismic profile. *Rev. Soc. Geol. Esp.* 8 (4): 431-448.
- Salas, R., 1987. El Malm i el Cretaci inferior entre el Massís de Garraf i la Serra d'Espadà. *Anàlisi de Conca*. PhD Thesis. University of Barcelona, Barcelona, 541pp.
- Salas, R., Casas, A., 1993. Mesozoic extensional tectonics, stratigraphy and crustal evolution during the Alpine cycle of the eastern Iberian basin. *Tectonophysics*, 228 (1-2): 33-55.
- Salas, R., Guimerà, J., Mas, R., Martín-Closas, C., Melendez, A., Alonso, A., 2001. Evolution of the Mesozoic central Iberian Rift System and its Cainozoic inversion (Iberian chain). *Mémoires du Muséum National d'Histoire Naturelle*, 186, 145-186.
- Salvini, F., Storti, F., 2002. Three-dimensional architecture of growth strata associated to fault-bend, fault-propagation, and décollement anticlines in non-erosional environments. *Sedimentary Geology*, 146(1-2), 57-73.
- Sanjuan, J., Martín-Closas, C., Costa, E., Barberà, X., Garcés, M., 2014. Calibration of Eocene-Oligocene charophyte biozones in the Eastern Ebro Basin (Catalonia, Spain). *Stratigraphy* 11(1), 61-81.
- Schlagintweit, F., Bover-Arnal, T., 2013. Remarks on *Bacinnella* Radoičić, 1959 (type species *B. irregularis*) and its representatives. *Facies*, 59, 59-73.
- Schmidt-Kittler, N., 1987. International Symposium on Mammalian biostratigraphy and paleoecology of the European Paleogene - Mainz, february 18th-21st, in: *Müncher Geowissenschaftliche Abhandlungen*, 10, 312pp.
- Scisciani, V., Tavarnelli, E., Calamita, F., 2001. Styles of tectonic inversion within synorogenic basins: examples from the Central Apennines, Italy. *Terra Nova*, 13, 321-326.
- Serra-Kiel, J., Travé, A., Mató, E., Saula, E., Ferràndez, C., Tosquella, J., Vergés, J., 2003. Marine and transitional Middle/

- Upper Eocene units of the Southeastern Pyrenean Foreland Basin (NE Spain). *Geologica Acta*, 1 (2), 177-200.
- Srivastava, S.P., Roest, W.R., Kovacs, L.C., Oakey, G., Lévesque, S., Verhoef, J., Macnab, R., 1990. Motion of Iberia since the Late Jurassic: results from detailed aeromagnetic measurements in the Newfoundland Basin. *Tectonophysics*, 184, 229–260.
- Suppe, J., Chou, G.T., Hook, S.C., 1992. Rates of folding and faulting determined from growth strata. In: McClay (ed.) *Thrust tectonics*. Springer Science & Business Media, 105-121.
- Suppe, J., Sàbat, F., Muñoz, J.A., Poblet, J., Roca, E., Vergés, J., 1997. Bed-by-bed fold growth by kink-band migration: Sant Llorenç de Morunys, eastern Pyrenees. *Journal of Structural Geology*, 19(3-4), 443-461. [https://doi.org/10.1016/S0191-8141\(96\)00103-4](https://doi.org/10.1016/S0191-8141(96)00103-4)
- Travé, A., Serra-Kiel, J., Zamarreno, I., 1996. Paleogeological interpretation of transitional environments in Eocene carbonates (NE Spain). *Palaios*, 11, 141-160.
- Tosal, A., Valero, L., Sanjuan, J., Martín-Closas, C., 2019. Influence of short-and long-term climatic cycles on floristic change across the Eocene–Oligocene boundary in the Ebro Basin (Catalonia, Spain). *Comptes Rendus Palevol*, 18 (8), 925-947.
- Valero-Montesa, L., Garcés, M., Cabrera, L., Costa Gisbert, E., Sáez, A., 2014. 20 Myr of eccentricity paced lacustrine cycles in the Cenozoic Ebro Basin. *Earth and Planetary Science Letters*, 408, 183-193.
- van Hinsbergen, D.J., Vissers, R.L.M., Spakman, W., 2014. Origin and consequences of western Mediterranean subduction, rollback, and slab segmentation. *Tectonics*, 33(4), 393-419.
- Van Hinsbergen, D. J., Torsvik, T.H., Schmid, S. M., Mañenco, L. C., Maffione, M., Vissers, R.L.M., Gürer, D., Spakman, W., 2020. Orogenic architecture of the Mediterranean region and kinematic reconstruction of its tectonic evolution since the Triassic. *Gondwana Research*, 81, 79-229.
- Vergés, J., Muñoz, J.A., 1990. Thrust sequence in the southern central Pyrenees. *Bulletin de la Société géologique de France*, 6(2), 265-271.
- Vergés, J., & García-Senz, J. (2001). Mesozoic evolution and Cenozoic inversion of the Pyrenean Rift. In: Ziegler, P. A., Cavazza, W. & Robertson A. H. F (eds.), *Peri-Tethys memoir 6: Peri-Tethyan Rift-wrench Basins and Passive Margins*. Mémoires du Muséum national d'histoire naturelle 186, 187–212
- Vergés, J., Marzo, M., Muñoz, J.A., 2002. Growth strata in foreland settings. *Sedimentary Geology*, 146(1-2), 1-9.
- Vidal, N., Gallart, J., Dañobeitia, J.J., Díaz, J., 1995. Mapping the Moho in the Iberian Mediterranean margin by multicoverage processing and merging of wide-angle and near-vertical reflection data. In: Banda, E., Torné, M. and Talwani, M. (eds.) *Rifted Ocean-Continent Boundaries*. Proceedings of the NATO Advanced Research Workshop on Rifted Ocean-Continental Boundaries, 291-308.
- Virgili, C., 1958. El Triásico de los Catalánides. *Bol. Inst. Geol. Min. Esp.* 69, 856.
- Virgili, C., Cassinis, G., Broutin, J., 2006. Permian to Triassic sequences from selected continental areas of Southwestern Europe. *Geol. Soc. Lond. Spec. Publ.* 265, 231–26.

Manuscript received Octubre 2024;
revision accepted December 2024;
published Online January 2025.

CHAPTER 4

THIRD PUBLICATION

Fault zone characterization and structural inheritance along of the Montmell-Vallès Fault System

Marín, M., Roca, E., Baqués, V., Cantarero, I., Cabrera, L., Ferrer, O. and Travé, A., 2023. Fluid-rock interaction control on fault reactivation: A review of the Montmell-Vallès Fault System, central Catalan Coastal Ranges (NE Iberia). *Global and Planetary Change*, 220, p.104011.

DOI: <https://doi.org/10.1016/j.gloplacha.2022.104011>

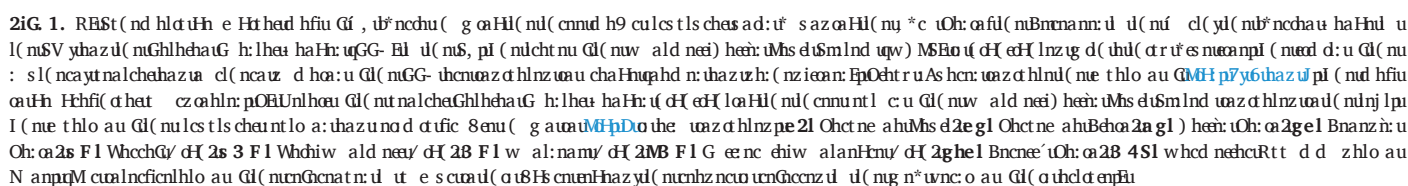
Journal metrics (data from Journal Citation Report for 2023):

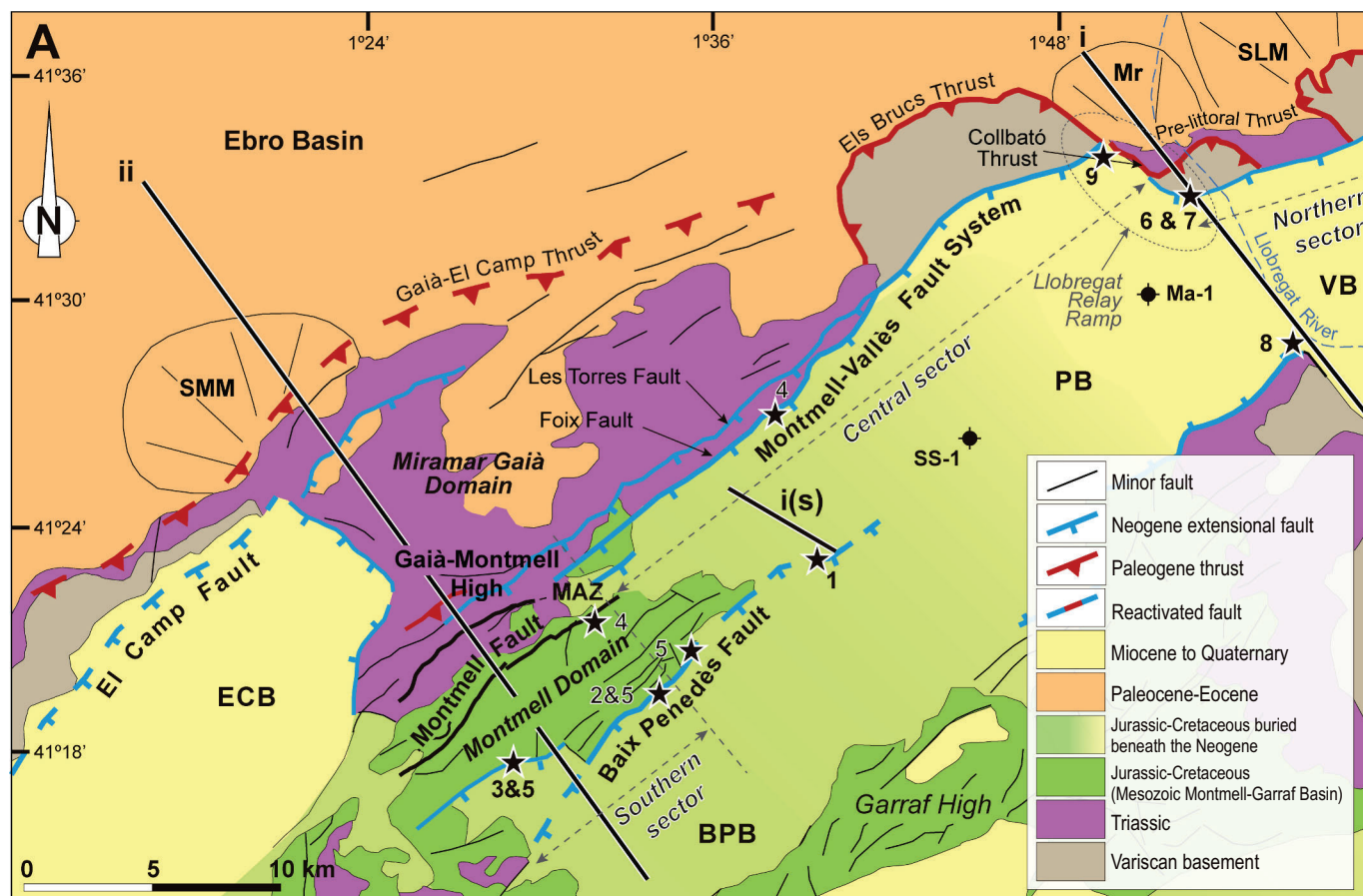
- Journal Impact Factor: **4.0**
- Journal Impact Factor excluding self-citations: **3.7**
- Category: **Geosciences, Multidisciplinary**
- Position: **41/254** (based on category and year of publication)
- Quartil: **Q1**

The goal of this contribution (Marín *et al.*, 2023) was to investigate the variations along strike of the Montmell-Vallès Fault System, which has previously been defined as inherited from the Mesozoic. The study focuses on the characterization of each of three segments that define the entire fault system through the lens of fluid-rock interactions and emphasizing how mineral precipitation and cementation can modify the mechanical properties of fault zones (i.e., damage zone, fault core), therefore influencing their different reactivation during the subsequent tectonic phases that characterize the Cenozoic evolution of the central Catalan Coastal Ranges.

[Global and Planetary Change](#) is a journal addressing all aspects of Earth System Science published by Elsevier at Science Direct. The journal aims to promote a multi-disciplinary understanding of planetary change by exploring global-scale processes across geological, historical, and present-to-future scenarios. It emphasizes studies leveraging observational records, experimental research, or modelling, and welcomes regional or process-specific research that enhances understanding of the Earth System.

hluwa g au(hlu(nulnfinhazut(hchtlnco1d:u Ghs duc tr:ut alc u
 Ghs duc o ficht nd nalific filhHlo auchlo :u[Miccra haz u w cco y7PP52Miccra
 nltheq7P; ; 2M::nay7P7P]PFor ng o nyl(nut fhht dmu GhuGhs d u t nuenht i
 lovhlnz u u d h emt alc eenz t m t(haHh: uau(nud nt(ha c hafeic finclor: u G
 l(nua(ncdnz uGhs d u k anyg (t(u::nalcheemt alc el(nh* admu G l(nuGhs d u
 l t nuenht lovhlnz u s nu l g nhr na o Hu culcnaH l(na o Hu Ghs duc tr:u[V ha Hu
 nltheqy 45P2Iv al:t(unltheqy 4462Iv/hs :nHhcnltheqy7P; P2Rezncunltheqy
 7P; JEpI(nuficet fidhlo au Gnd nal: thaz u d anche y g d(aGhs d u k an: u h: u
 GnaS napem*mauzn: tcof nzuh: uhud nt(ha o d u Gwactnh: o HuGhs duc tr u
 :lcnaH l(u d o Hu l(nuGhs cnuavne finul u d h ncwhe s n:uV al:t(unltheqy

[illegible]

[illegible][illegible]

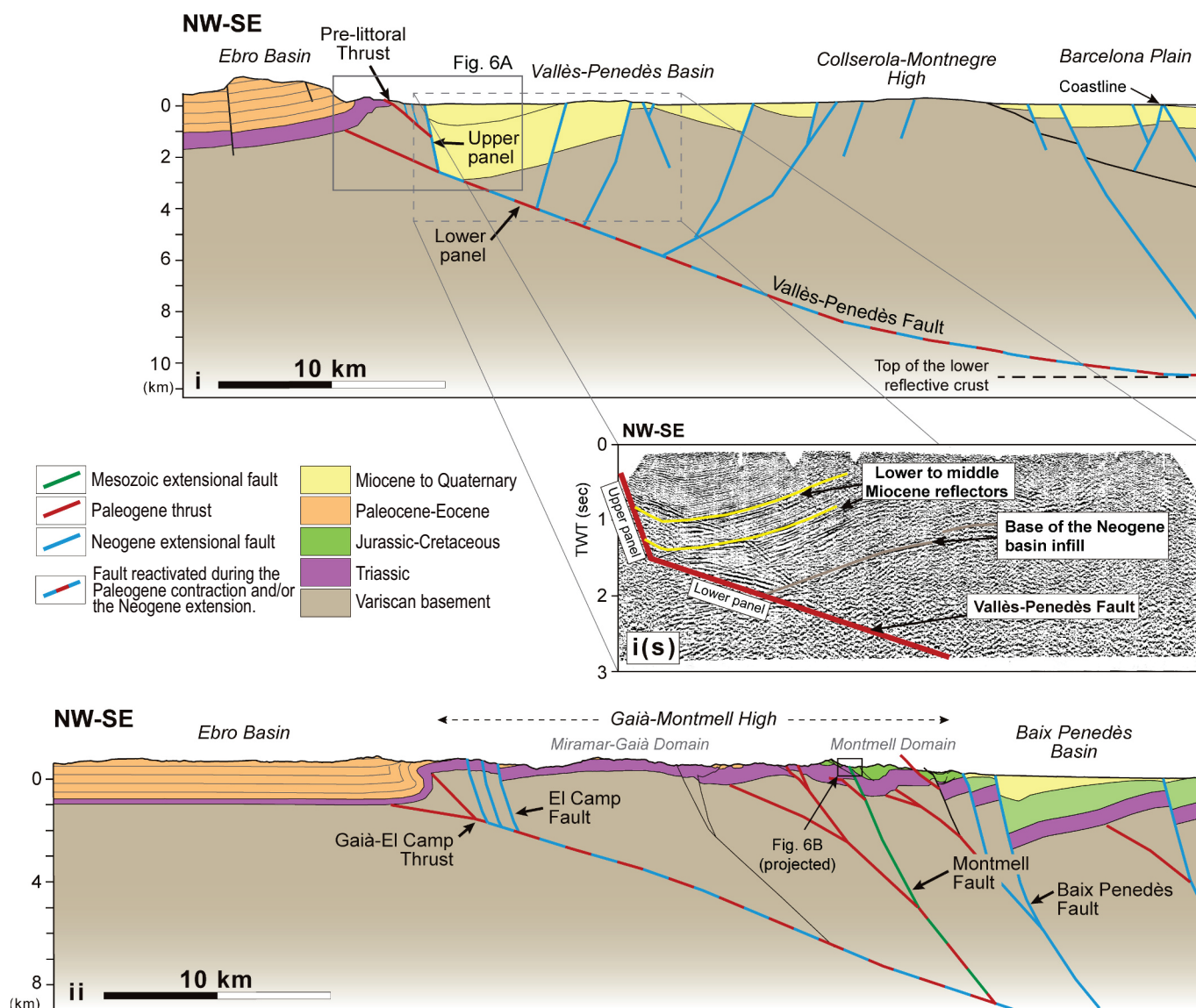
Zig f. Sod fier8nztH e Ht had hfui Ql(nutnalchaGhlheatuG h:lha: haHr:u(dH eH lœHl(nud h9 cŭna k r tũšd:e:thazũl(nuntl c:u Ql(nuw ald nea) heer:tũšdũmĩnd u œz d hlnz wad(nunj lpSihcund * e waz d hlnđ(nue thlo au Gĩs oũl g tha hem o wœũš dufidhan:tfincC đd nz t' mŭg Bĩ chvũnũltheqy 445yũB Ohoxũnltheqy7PP5yũD Ohs Ń:ũ nltheq7P; Pyũ B Ohs Ń:ũ nltheq7P; 7yũB Ohs Ń:ũ nltheq7P; ' yũB Ghalhcnc untheq7P; ' hyũB whct Ńũnltheq7P; 5yũB Bĩ chvũnhaz d Ghevũl q7P; Byũ d B haz d Ghalhcnc untheq7P; ' t Bĩ(nue thlo au Ql(nuštĩls cheant lo a:thazũl nu nũd d tũc 8enu(g a wœfũp dũ the wœz d hlnz pae l) heer: tũ: Oh: œ 2ge l Bnaznĩ: tũ: œ 2ge l Ohj Bnaznĩ: tũ: œ 2ĩ - Mē l, aGhd fiOħ: œ 28 4Sĩ whed nœca Rtt d d zho atũ anũq hœa untheq7P; E2B nhĩ lwchd cnœi; tũ cn(œ 255Hĩ Shaũšz saxi; tũ cn(enpBan Hnanhues vdehazu Chaz ndũh mĩnd: fũd8 1 Šalũfe caQz news al dhes vdeChazaz uaz ued h28 rl w: ncclũthũw hũd253 3 1 Šalũw oš næz new al tũches vdeChapũ

$\therefore \text{Ci6cu66ion}$

I (n: lɛs tɪs cnu Qil (nUGG- uoates z:n; uhu: nlu Ql fɪfɪncu0s ch: dɪf g nc u
Gcnlt n s : unj lna: o aheɪ*: h: ə: uq w ald neɪ Whcc h Gihazu Bncnee *u*: h: ə: yu
MH pɪ uhaz u Bil (nuəd d: u Gg (d (uəls nat nzu au(nuɛ thlo au Qd h9 cu
t d fɪc: o aheɪ lɛs tɪs cr: uz coə Hl (nbhen Hnan c Hnat fi(h: nuɪ : **In* hau**
hazu *e: yu 43J **2Rahz** 'a unl theqy 434^a: t th hazu Ws d nchyu 447**2Sh**: u
haz i Gh: h: yu 44D 2Sh: unl theqy **PP**; Epɪ (n: nu j lna: o aheɪ*: h: ə: un: nal chemu
znvne finz uəl (nutnal chehazu sl (ncaufhlcl Qil (nUGG- uph **Haw** uald neɪu
Whcc h Gihazu Bncnee *u*: h: ə: yu **MH pɪ** Big (emul (nia cl (ncaufhlcl Qil (nUGG- u
cnd hoanz uh: uhu: lɛs tɪs cheu(dh u q d (ua u: d h 08 thaluz nfi : do ausz coə Hu

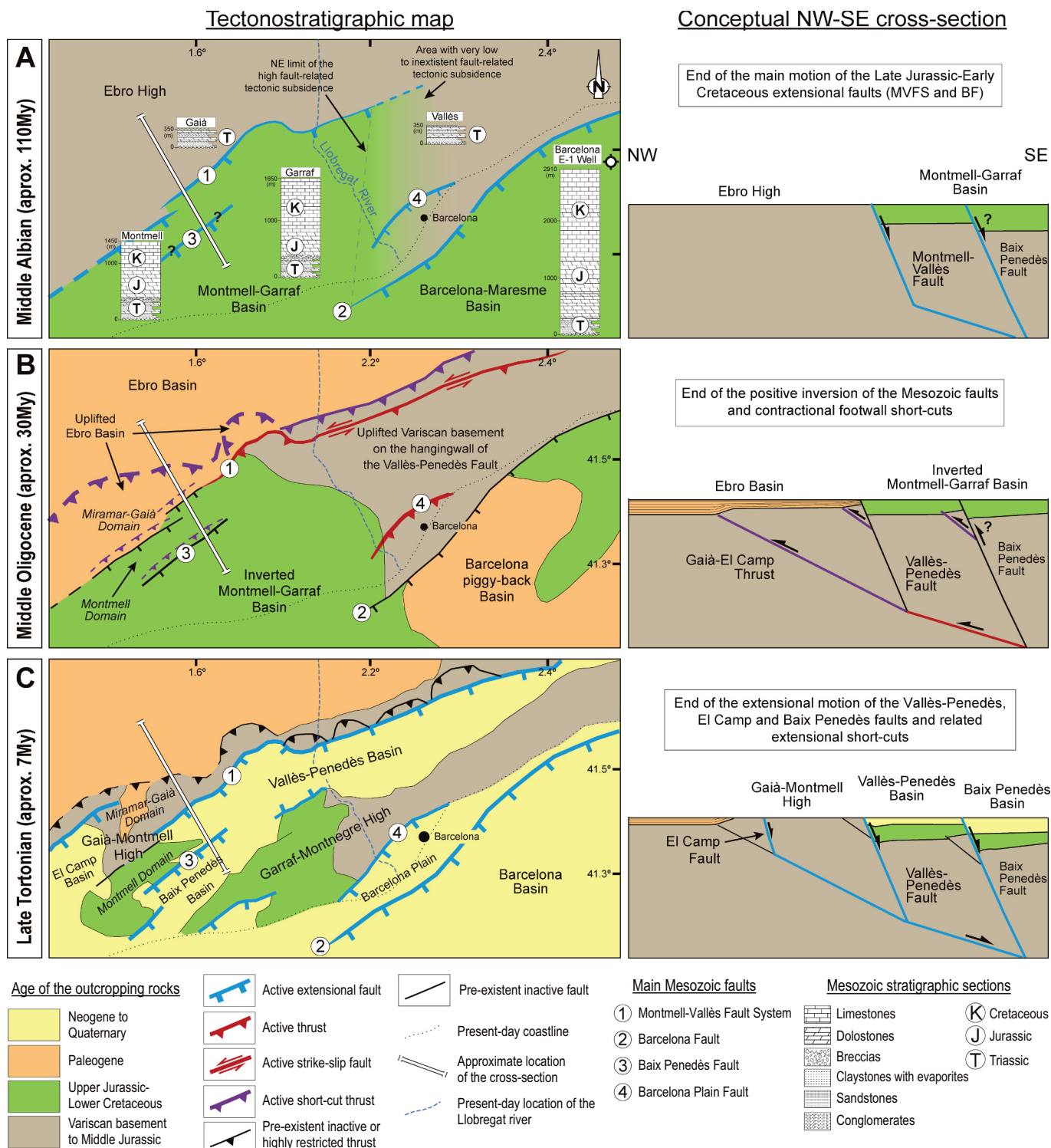
I (nɪGna k dɪtsɪtsɪnu ɒ(nɪnəlcheGG- wɪd hɔɛmɪ ɔlc ɛɛzɪʔmɪ(nu d h9 cɪ j, ɪlcnaɔHɔɪct ne ahy) hɛɛ: iBranzɪn: θazuw ɔld nɛaʔh: nd nalu ɔs d: uɔMɪp; Epɪ (n: nɪɔs d: ɪz dɪʔl ɪl(nɪs, θazunɪ fɪncɔatɪz ɪBhɛn Hɛanɪ t ɔlctɪlo aθaɛzɪ n Hɛanɪlna: o aθɛd lo a: uɔθɪl ɔa hɪnɪ theyɪ 4472ɪ - t θuhazwɛ d nɛhy 4472ɪf ʔfɪnkɪOɔat ɪnɪ theyɪ PPP2ɪwɪ: fɪhɪɪ, ʔ: tɔʔa ɪ nɪ theyɪ PP' 2ɪwɪct nɪ aɪnɪ theyɪ 7: 5Epɪ

baul(nutnalchutlhelu Gil(nuGG- yul(nua d(g:n:lncu* sazhcmu Gil(nu
fien:ncvnu. fifincu0s ch: d(iF g ncuGnrlhtn s :u:sttn:o a:u8aHuI(nu
w ald neeWhchGOh: a:ut a:tozn: ug d(ul(nulcht nu Gil(nu) hee: iBnanz:n: u
hazw ald neeChs d: uMi p7EpI (n: nulg uhs d: uates znunvncat chat(nzu
:nH nal: thazw o fiedmhuch(l: l: InficiaHuAul 6a, TAhchchaHnd nalug d(thu-
7ur d icht nu nfiichlo auMi p: thazw EpRtt cz aHmyd(nmhendcnhlz th: u
:nH nal: u Gil(nu hd nuChs du mInd u(ncuahd nzuw ald nee) hee: uhs du
Smlnd uiw) MiEyl(nurcnhm) Gg(a(ut ccr: fi az: ul (nuwhcd nehcRti
t d d zhlo auN anuzn: tcozn u* muwhca unl uhepu7P7; BuqMi p7EpI (nu
wn: k a:ul vnd nalu Gil(a uhs du mInd w s fidi clnz i: ml (nol d(ranc: u
vhechlo a: u G: fifincu0s ch: d(iF g ncuGnrlhtn s :u:sttn:o a:u *:ncvnu



I g hcz:ul(nú , yaa ul(nuFe *cnHhlu ovcnchaz u) heen: thcnhyul(meod d: u G1

l(nuw ald neeWchcGOh: auy **M-pi** RBhcnuehlovms atndhau:znu d(nu
sfeGuhazunc :o au Gtl(ou:ntl cu Gtl(nuGG- uzs coHil(nuBhen Hhanu
t alchtlo aha:znC cd hlo apil nvncd(nen :yul(nmut ha'u' nuhz zcn: nz uG d u
fic vnahat nuhahenou au d(nuBhen Hhanu nccfha s: u nz cd nal: u Gtl(nuS, u
d hchau Gtl(nu *c tOh: auy (: nuhtl(d nalubhen: yu ncuu(nu nfiic: nalizhm
gG- uF **finkiOhat unluqznuwPPPHil** s: yul(nut d hie :do au Gtl(nut d hie :
u g d au d(nuShaltu: na Qz new s althes vohet auSfw uau d(nu fificnch: lu



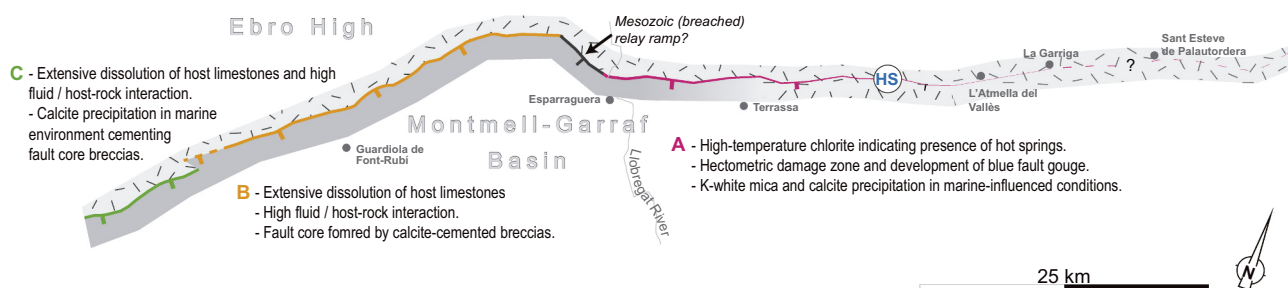
2iGk R. I n t l a : l c h l d t h f i (d u f h i : h a z u t a t n f i l s h e t c : : i n t l o a : u (g æ H l (n u f l i n l o s c h : d u q R l u h l n u w o t n a n u G B n v e s l o a u G l (n u t a l c h e G h l h e a u G h : l h e a h a H r : p i w h f i R u a t e s z n : u r n l t (n z u l c h l d t h f i (d u e s d a : u G l (n u w n : k d p l f a u n t (u d h f i h a z u t c : : i n t l o a u h t l o v n l s d : t h c n u (g a u g d (u l d r u t e c n z u l c h t n : t h a z u a n : y h a z u f i c n v o s : u a h t l o v n l s d : u g d (u l (æ a n c f e h t r u a n : p i

t cancu **GmFp7** Ezna ln: d(hlyau(n) hee: untl cyd(nu slte fific **Hc** tr: u
au(nunc znz ubnhyg ncm d hz nū mī ch: : d thazū Bhen k d t r: ig d(slu cu
g d(uhue thei hazud a cuhd salu Gūs ch: dū u Genlhtn s: u c tr: pu
G a: z nca **Hil** (nu htru GmHb aheunvz natnu Gfici Bhen tnanus fied thazu
nc : o au Gūs ch: : d thazū Genlhtn s: u c tr: yd(a g sēz **HH**: lū(hlū , u Gū
l(nū fē * cnhlū ovncūs ch: : d thaz Y c Genlhtn s: u z nfi : d: ig ncmvnmī(au
ca lufic: nalpū

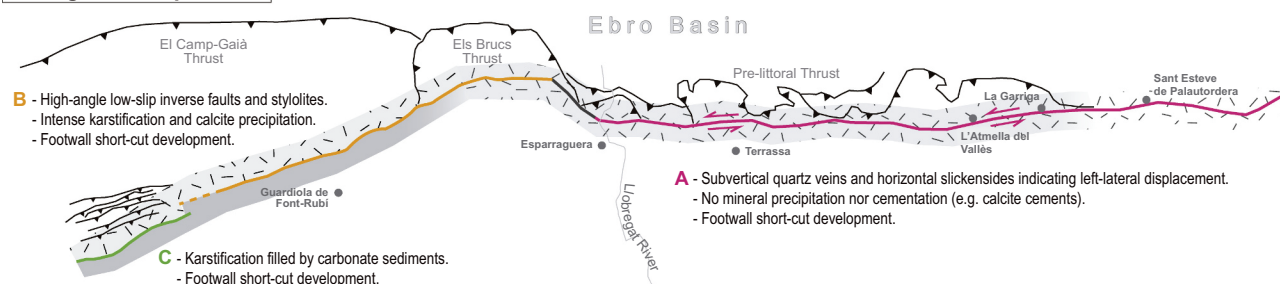
baut alch:lyu:nalntl adubhen hhanuznldt heu:nzɔnal:uəʊl(nu
w al:ncchlutaun dnduhazil(nushaluw oS nez nawn alt dchhes vhechaupwu
hazšwwauMH7Pteates zničnas nalul fienč d əhalut h:l:uzncvəHČ d u
l(nuzod halečHu GŌs ch:d t uhazud hoemF g ncuGnlhtn s:susttn:o:a u
f' finkiOchat unltheq7PPP2aw hca unlthept7P7; ħpi(oiğ səzuəd tlhlnd(hlu
SV uć: d ul(nufie *cnhlit- ɔncvcl(nuthlt(d naluhues: ue thlnzəs, u Gil(nu

w) Məhazul(nənC enul(nunələnficən: nalizhmGG- ug nənud hznur* mGənlihi
tn s:uc tr:prEd(sH yul(nuts cənəlu, uəd du Gil(nuds ch:əuhazuGənlihi
tn s:uc tr:uficən:ncvz us azncənhi(ul(nuf n Hənu) heē:ibNənz:u*:əu
ə8əəu tē hlzn xhifci j əd hlənəm Pürd tSV u Gil(nuFe *cnHlu əvncu:us:i
lhənz tē ml(nuh*:natnu Gz tr:u Gil(əuhHəul nuw hcl cneē; tē cn(əmbazu
d:ufic:natnuəd mshəshəz cə; tē cn(əmudFhaib9yuy 4532Dhcləu hmləpəu
; 447BqMf-p7hazu lchləHhfi(ənt nlo a:uəuMfpi Rəz cəHil(nu fificu
Os ch:ə:tiF g ncuGənlihtn s:yul(nuf , uəd du Gil(nuw əld nēiWhēcGH:əu
g sē:t nē hlzn tē :nū ufic:nalizhmFe *cnHlu əvncpl(nēht ru Gū fificu
Os ch:ə:tiF g ncuGənlihtn s:us ttn:ə a:uf , u Gil(nuFe *cnHlu- əvncuz nī
a ln:ul(hluz cəHil(nuw n: k ə ul(nu) heē:ur nH nal u Gil(nuw) Məg h:u
əht ləv nu cə(hzuhud ə cūz ə fiēht nəluə cl(u Gil(nuFe *cnHlu- əvncu
Mfpi Rəz u6Bq

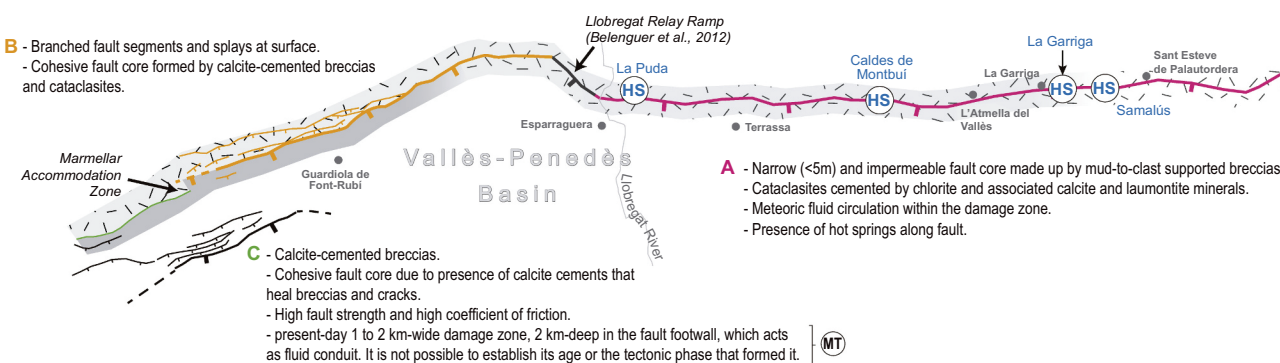
Late Jurassic-Early Cretaceous Extension



Paleogene Compression



Late Oligocene-Neogene Extension



A: Northern sector (Vallès area)

B: Central sector (Penedès area)


C: Southern sector (Montmell area)

HS Hot spring

MT Information from MT

Extensional fault

 Thrust Strike-slip fault

 Main fault trace

Fault splays
 Rooted fault

Related footwall/hangingwall structures

Other data

Host-rock / protolith lithology in the upper part (<1 km) of the fault

 Paleozoic granites and metasedimentary rocks

□ Triassic evaporites, siliciclastics and carbonates

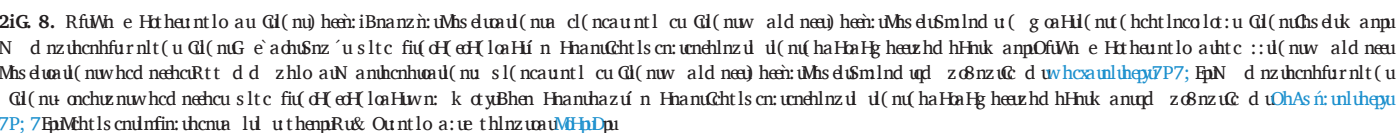
 Mesozoic carbonates

ZiG 7. St (nd hlct u d hfui Ql (nuw ald nee) heh: msh d sm lnd u (g o Hlct d uz h d h hnk anu (hcht lnc o lct: u Ql (nnunt l c: u r y Ouhaz u GBz s coa Hl (nu d GChal u Fhl mts ch: cti u , hcm Gml htn s: yBhen Hanhaz u hlnl d H t nani n Haudnt l ad tzn C d hlo aha l h h: pms o thaz u fnc e Ht haz: t cfilo a: t d fionz th Cnd chv n h az: Ghev n l u 7PP; Bu OhAs r: un l thep 7PP 5y OhAs r: un l thep 7P; 6y OhAs r: un l thep 7P; 7y OhAs r: un l thep 7P; ' Bhaz u GChal hnc un l thep 7P; ' hy 7P; ' t Ep Fe c n l h l u nehma hd fii Q d u Ona Hs nc un l thep d 7P; 7Epw h hnl lncs ct uz h l h u w l RQ d u w hca un l thep 7P7; Ep

I (nuw:n k d t u l c s t l s c n u G l (n u t n a l c h e G G - t h i f i n h : t h e t a l c e e z t f n u l (n u f i h c h e m e u S , i z d i f i c i a H u O h c t n e a h u M i s d p u l (o u d h 9 c u G n a k d t u C s d y u e t h l n z u C c n t e : n u l d (n u f i c n : n a l i z h m t h l e a n u M H p i E t (h : t h e t f n n a u f i : l s d h l n z u h : u a d (n e d n z u t e d d (n u w : n k d t h a z u g s e z t c e n : f i a z d u l (n u h a t o n a l V u e d d u G h a l (n e f h l m o s c h : d t i , h e e n G e n l h t n s : s u n j l n u : o a h e u * h : a u g d u u e d d u l (d r a u G e a u t h u a z u a d n c h y ; 4472 t h u n l u h e p u ; 4442 W h : f i h c i , t : c o h a u n l u h e p u 7 P P ' E p i l (n u w : n k d t u h t o w n u O h c t n e a h u M i s d u h a z u w a l d n e i) h e e n : u M s d t u S m l n d u o f i e h m h u e d H l i : l n f i n f i z u A l a 61 q T a t a 8 H s c h l o a u M H p i R B h a z u h a n c h l n z u h V S V i z d i f i c i a H e n d e m e h d f i e a u l (n e u v n e h f i c i a H i c h n p i l (o u e h d f i y e t h l n z u l d (n u f i c n : n a l i z h m f i : d o a u G u l (n u F e * c n H h l u o n c y z n 8 a n z d (n u , u e d d u G l (n u w a l d n e i W h e c h G O h : a y u h a z u h : u t (h c h t l n e c k n z f m h u l (d r a n : u a t e n h : n u g h c z : u d (n u V S u G l (n u f i f i c u o s c h : d t i F g n c G e n l h t n s : s u s t n : o a : t e d p u d u u a n c h u r d p i

I (nuznvne fid nalu GūBhen Hantut^h:nd naluav evaHu, f. ilcnazæHu
 C ez:thazud(cs:l:u aemæd(nuC lg heu Gī(nuw ald nee) hee: tMš dšmi
 lnd uq^{MH p7}thazud^UEræz d hln: ul(nufihcl dæfi : dovnuævnc: o au Gī(nuficni
 nj o lnalwn: k d u w) Mšuzs cæHu l(nuBhen Hantut d ficn: o aheafi(h: nu
 q^{Mh: fihci, : t cō'ha unluhegu^{7PP}} 2^{awhca unluhegu^{7PP}}; EpBent o nenyd unv d
 znatr: d(nl(cs:lucnht lōvho au Gī(nu eH lenz ofia^He g ncfihaneu Gī(nu
 Cš d: t's lua lu Gī(nulnnfiu fifincufihane uq^{Mh p d}Ep/ nenyd(nuC cd hlo au Gī
 C lg heu: (dtsl: uæz d hln: uhuficht lō hœmia lunj o lnal u cuanfH^æ
 cnht lovhlo au Gī(nuficni o l a H^uCš dufihane: u: unvnc: nuCš d: pš nu ul nœu
 *æa nu conal hlo aul ul(nucnH aheu: (clnæHuizæntlo au q^{mpu}i sU
 : (clnæHuiv: pī , ilcnazæHuCš d: 2^{Wš d nchyr 45' y^{7PP}} Eul(n: nu lnnfiu
 s fifincuCš dufihane u(g uæ: lnhz ucnht lōvho a uh: uenGī dlnchar lœr ni: æfiu
 Cš d: uq^{Rahz 'aunluhegu, 456}Epī nvnd(ner: yst(ulcha: ficn: o aheacnt i
 lōvho au uæ luHanchepil u(h: u' nna u *: nevnz uæ ul(nu) hee: ucnhu Gī(nu
 w) Mšup^sæhuaz i tShal haht(y^{45' y⁴⁴⁵}Er's lua lūæ ul(nu sl(g n lncau
 fihcl uG(o tš dæm lnd p/ nenyhlus cēt nyd(nuwn: k d u w ald neeMš d u
 z n: æ lu g uhamrænd uGBen Hantut alchtlo aheacnt lōvho a u s l d(nu
 znvne fid nalu Gī's llcn: æH lœstis cn: uq d æ uC ez: yul(cs:l:thazut^htri
 l(cs:l: Bæ d(nott haHæHæ heu^{MH p l} Othazu u^OEpū

baucndlo ul ul (nuhcnhaizalco'slo au Gū (nuālnfcnlzuc lg heu
 : (dtsl:yl (nfcn: natnu Gū (o ræzuc Gals tls cr: uul (n) heh: unHl nalu Gū
 l (nw) Mus Hhrl: d (hlū (nwn: k æt uō duf s azæHl (nu ffinco ch: ætu



F g ncuGnlhtn s :uw ald neiWhccGOh: aunj lnaznzU d (ncu u , u(hau
l(nuzn8anzu'h: aue8eued d: yhl'enh: lus fiul(nuficr: nalizhme thlo au Gl(nu
FhuWhccGhul g auMf-h6Epu

Fhlncuzs cœHil(nu dhluT eH t naniwo t nanunj lna: o aheũ: lhHyul(nu
 œ(ncdnz w) Mšig h: the uenht lovhlnz pī(ne g iz dfiœ Hie g nœŭs dufihane u
 d vnz uhHœœœ uhaunj lna: o ahar na: nuqWb: fihci , t cœ ha unluhepu'P7' Bu
 g(ncnh: ũl(nu lnñfius fifinciu an: u(g thũc' hz ũfhcl dœœnht lovhlo ayœũd(œ u
 th: nuh: unj lna: o aheœŭs d: pī(nucnht lovhlo au Gīl(nu lnñfius fifincufihane u o
 cr: lod lnz ũl(nua cl(nca thaz ut nalchœ nt l c: u Gīl(nuw) Mšug hee: thaz u
 Bnanzĩ: ũhngh: Hg(ncm̃l(nu slt c fiœ H) hee: iBnazĩ: ũMš dUc ēē g: ũl(nu
 lcht nu Gīl(nuwn: k œ ŭts dlt ũl(nm̃H b ahaũ thep' g nvncyd(nú n Hnanu
 ŭs dUz n: ũa lueg hmœnht lovlnd(nfucnñj o lnalwñ: k œ ŭts dUz cm̃s lU
 zvnve finz te : nuœũl(noœ(ha Ha Hg heœ qMfp6 Bħ: unj lna: o aheũ(dts l: u Gī
 l(nfucnñj o lnalũd(cs: l: uqM al' lnyy 46' 2Rahz 'auluhepy 4562: thuhazu
 Wš œl nchy; 447 Pũbaũt alch: lyul(nu lnñfius fifincufihane u Gīl(nu sl(nœœ
 :nt l cu Gīl(nuw) Mšuw ald nœœhcnh Bju at nuhHœœœ yœnd hœanz œœht lovw
 zs cœ Hl(nú n Hhanunj lna: o ap' ncnyd(nunj lna: o aheœnht lovhlo au Gīl(nu
 e g iha Hœœ g nœŭs dufihanœœ: s dnz œũd(nuC œd hlo au Ğhaunj lna: o aheũ:
 (dts l ucfcñ: nalnz u' m̃l(nu Ohj uBnazĩ: ũMš dUqWbœœœœ unluhepu'P7'; Bu
 qMfpDœœhazu t Gẽpu

Ss d d hecōaHūl(nuw) M̥ur(g : ucnht lovhlo auzs cōaHil(nuGna k d yu
8c:lusaznct alcht lo auzs cōaHil(nuBhen HhanuQs nkiFhccñhaz uRaz cō: i
:nay7PPJ2w hca unlthep7P7; BqM̥Hpi Obzhaz uhlncs azncunj lna: o auzs cōaHū
l(nuhtlntēH tnanif n HhanuM al* lñy 46' 2Rahz 'a unlthepu 4562i t hu
haz iWš cd nchy 4472F' finkiOha t unlthep7PPP BqM̥Hpi G̥Hpi nvnd(ner: yu
:st(ucnht lovhlo auqua lut d fiendlñ(nuš fificu: lnnfiufihane u G̥il(nu
ca(ncdnz fHln0s ch: d i, hcmGcnlht n s: ūš d: u aemcnht lovhlnz fihel diemu
caul na cl(nh: lncanunt l cu G̥il(nuw) M̥s̥f̥s̥la lwa: u sl(g: lncanau: nu

LkLk mlfanaAl a7bAur6aufgG;nuTAAu CafTr0 grbTAulfur6aU7raaDuGDDanufgG;nu
DgAa,7g,TAEur6aMTAr0 a,1(g,,à7l gGnS: 7ra0 u

. fiid ul(cnnuntl c:ug d(uoCcnalunw: k dthaziGna k dthsdtk anu
znC dld hlo auhcnuzo l o l f o (nz uhe a Hil (nu: lnnfius fifinculCs dufihane u Gi
w) Mfy Bhu d(ncauntl cl(hlt ccr: fi az: ul d(nu) hee: thcnhuMfp7B
hazunj lnaz: C d ul(nFe *cnHlu nehnu hd fiul ul(nu i , thsdumInd wzHu
e thlnz u, u Gi(nuw al: nam/ dH qnue thlo aumMfp; E27Bhut nalche
:ntl kunj lnaz o l hie a Hil(nuBnanzn: thcnhtSV d d ul(nuFe *cnHlu: nehnu
-hd fiul ul(nuwhd nehcrRtt d d z hlo aNu anuMfp; p7y7thaz u6E2haz uBhu
: sl(ncantl cl(hlt ccr: fi az: ul d(nuw al nehcnhuhaz uates zn: d(nu
w ald nehthaziOhq uBnanzn: thsd: uMfp7p7thaz u6Bp

LkLk k x Tr6anAuZalrTnuv(g,,à7gnagBu

I (o:ntl cu Gíl(nuw) Mszuvne finzu vncuhu : lic tru cufic l ed(u d :lemC ed nzuf nuHhad ø:thazud nlh:nzad nalhcmuæt d:th:ldu tr:u Gíl(nu) hca thauh:nd nal thaz yhlus fnc8t cheuvne yf mil(aul cde: d:u hci * ahl nuhazuæt d:th:ldu tr:thazu(d rncGna k d:u Airæand hltuæt d:th:ldunzad nal:u:ntl cRua uH p6Bpí (nuH d nlcotyznC ed hlo ahezazu finle e Ht hcut(hchtlnca ldu Gíl(nua cl(ncau:ntl cu Gíl(nuw) Mszuhcu :sd d hcknz ual(nu h*enu m

I (o u n t l c u a t e s z n : d (c m n u z c c c n a l u t s d u k a n : u o a r n z u l (n u l (c m n u : l h f h : u G l (n u w) M s u n v e s l o a f u h B h t c s : l u s * v n d t h a t s d u k a n u n : l e d l n z u l u l (n u C l g h e u G l (n u B h e n H a n u B c n i e d l c h a i (c s : l 2 r * B u h u n t a z u t s d u k a n u e H l e m z d f i c i a H l u l (n S , u l (h l C e e g : u l (o t B h e n H a n d (c s : l 2 h a z u t B u h d (c z u t s d u k a n u e a r n z u l u l (n e h l m l t e H t n a n i n n H a n u j l n a : o a u G l (n u) h e e i B r a n z i n : u t s d p l (n 8 : l u a n u o t c d n z u t m h u v n d t h a l u n c m u l n n f i S S , i z f i c i a H u t s d u k a n u g d (t h u g u t l (u c h a H a H i C d u r d n e l s a z c n u : u G i d n l n c : u l t h u e d n l n c u R a h z ' a u l t h e p y 4 5 6 2 0 s e h u h a z u S h a l h a h t (y y 4 5 ' y u

pmAvh 1

G(h)chtIncol:d:u Gl(n)ua d(n)cauntl cuq heen:thchBh Gl(n)uw ald nee) heen:thMs d:uSmInd pG d fionzuG: d uRahz 'aunlthepu 456Bhu d:uShahz uShal haht (uq 45' yu 445Bhu
Ghd fi:thazuw cncuq?P: 'BhazuGhalhcnc unltheng?P: 'hBhu

	Northern sector (Vallès area)			
	Fault geometry	Reactivation of pre-existing fault	FAULT ZONE CHARACTERISTICS OF THE ACTIVE FAULTS	
			Fault core	Fault damage zone
Late Jurassic- Early Cretaceous extension	SE-dipping extensional fault with two planar panels: an upper dipping about 60° and a lower dipping less than 30°	Not observed.	Upper fault panels: <ul style="list-style-type: none"> Decametric to hectometric thick formed by blue clay gouges with a sub-horizontal to shallow-dipping foliation and cataclases embedding metric to decametric blocks of Paleozoic Lower and Triassic rocks. No evidence of induced syn-kinematic cement precipitation. 	Upper fault panels: <ul style="list-style-type: none"> Paleozoic rocks cut by metric to decametric faults developed in the finest grained lithologies. No evidence of induced syn-kinematic cement precipitation
Paleogene compression	Upper fault reactivated panels: Steep SE-dipping left-lateral strike-slip fault. New formed short-cut thrusts (Pre-littoral Thrust): ~30° SE-dipping NW-directed short-cut thrust fault.	Reactivation of the upper steep panels of the Mesozoic fault Reactivation of the low angle (~30°) panels of the Mesozoic fault.	Upper fault reactivated panels: Decametric to hectometric thick blue clay gouge with a nearly vertical E-trending foliation and rod-shaped ellipsoidal quartz blocks with a vertical long axis and are encircled by near-horizontal striae New formed short-cut thrusts (Pre-littoral Thrust): <ul style="list-style-type: none"> 1 to 3-m-thick constituted by cemented (calcite) breccias and cataclases and vertical non-cemented stylolites when developed in Triassic carbonate rocks Foliated clay gouges with abundant shear bands and without cement precipitation when formed in metamorphic Paleozoic rocks. 	Upper fault reactivated panels: <ul style="list-style-type: none"> Not observed New formed short-cut thrusts (Pre-littoral Thrust): <ul style="list-style-type: none"> Metric (occasionally decimetric) to decametric thick zone. Amalgamated thrusts and deformation bands that define different scale duplexes
Late Oligocene- Neogene extension	Vallès-Penedès Fault: kinked SE-dipping planar fault with an upper panel dipping around 60° and a lower panel dipping less than 30°.	Partial reactivation of the upper steep panels of the Mesozoic faults Reactivation of the lower fault panel (~30°) of the Mesozoic fault and the Paleogene related short-cut thrusts.	Upper fault panels (Vallès-Penedès Fault): <ul style="list-style-type: none"> Narrow (<5 meters). Mud-to-clast-supported non-cemented breccias with SSE foliation. Cataclases cemented by chlorite and associated calcite and laumontite minerals. 	Upper fault panels (Vallès-Penedès Fault): <ul style="list-style-type: none"> Hectometric to kilometer thick zones. Footwall: <100 meters wide with ENE-trending extensional faults whose intensity increases towards the fault core. Hangingwall: hectometric to kilometer wide extensional fault propagation fold cut by conjugated extensional planar faults.

Maheymul (nuhs duk anuearzul ul (nuhlnul eH tnanif n Hhanunj Inai : o au ufieht nze the aHl (nu) heer: iBnanz: n: uMhs dpliu ut (hcht Inocknz uhls ci Ghtnyf mahecc g uhs dut cr: uq<6ul ul (drys: sheem: 7ul Eihazwznt hd nlctul u nvnaurce d nlctuscc saz aHHzhd hHuk an: pl (nuhs dut cr: theml hznis fiu Qd szil ite: li: sifi dlnz a aitnd nalnzuf cntt d: ug d (uhf e hzu (hee g u SS, uC ehlo ayhazyl g hez: ul (nu i , yhe ufut hlht e: dn: ut nd nalnzuf mu t(e cdnuhazh: t chlznz u het dnuhaz uhs d aldnuul canche u **Ghalhenc unluhegu 7P**; **h**ebad nuC lg heeyC cd nzuf mBhen k d t e tr: yl (nuzhd hHuk anuo u <; PPud ig aueq **Ghalhenc unluhegu 7P**; **h**ihazut a: ol: u G, i, ilcnaz aHu nj Ina: o ahehs d: ug d (uht is cr: ul (hlu d f h8 thalenuat cnh: n: ul (noctfic: i natnuh: uhficc ht (aHl ul (nuhs dut cnplu ul (nu ha Ha Hg heeyhl u ccht nyu

I (nu h d n l c t y z n C c d h l o a h e y h a z u f i n l c e H t h e t (h c h t l n c o l c t : u G i l (n u : s l (n c a u n t l c u G i l (n u w) M s u h n u s d d h e c k n z u a u l (n u i h * e n u D n / n e n y l (n u

G(hchtIncolct:u G(l(nutnalcheuntl cuBranzn:uhenhEi G(l(nuw ald nei) heen:uMsduSmInd pG d fionzUc d uRd dH'ug 45' EhazUChAs n:unlthepu7P; 7Epu

	Central sector (Penedès area)			
	Fault geometry	Reactivation of pre-existing fault	FAULT ZONE CHARACTERISTICS OF THE ACTIVE FAULTS	
			Fault core	Fault damage zone
Late Jurassic- Early Cretaceous extension	SE-dipping fault with two planar panels: one dipping around 60° and a lower dipping less than 30°.	Not observed.	Upper fault panels: <ul style="list-style-type: none"> Metric to, occasionally, decametric thick. Calcite cemented breccias with abundant tension veins. 	Upper fault panels: <ul style="list-style-type: none"> Minor NNW-trending extensional faults filled by calcite
Paleogene compression	New formed short-cut thrusts (Els Brucs and Gaia-El Camp thrusts): ~30° SE-dipping NW-directed short-cut thrusts.	Reactivation of the lower low angle (~30°) fault panel.	New formed short-cut thrusts (Els Brucs Thrust): <ul style="list-style-type: none"> 1 to 3-m-thick constituted by cemented (calcite) breccias and cataclasites and vertical non-cemented stylolites when developed in Triassic carbonate rocks Foliated clay gouges with abundant shear bands and without cement precipitation when formed in metamorphic Paleozoic rocks. 	Upper fault panels: <ul style="list-style-type: none"> Not studied/observed New formed short-cut thrusts: <ul style="list-style-type: none"> Metric (occasionally decimetric) to decametric thick zone. Amalgamated thrusts and deformation bands that define different scale duplexes.
Late Oligocene- Neogene extension	Vallès-Penedès, fault Les Torres and Foix faults: SE-dipping extensional fault with two planar panels: an upper steep with a dip of about 60° and a lower one that dips less than 30°.	Reactivation of the lower panel of the Mesozoic fault as well as of some segments of the Paleogene short-cut thrusts.	Upper fault panels (Vallès-Penedès Fault): <ul style="list-style-type: none"> Metric to exceptionally decametric wide fault core mainly formed by calcite-cemented fault breccias that are affected by calcite-filled tension fractures. 	Upper fault panels (Vallès-Penedès Fault): <ul style="list-style-type: none"> Nearly vertical calcite-cemented tension fractures and high-angle extensional faults whose density increases to the fault core.

G: hchtIncol&:u:G(nu sl(ncauntl cuw ald neehcnhu G(nuw ald nee) hee: tMs el&SmInd pG d fionz uG d tOnchz unl theqz/PP5E5yOhAs r: unl theqz/PyGP; 7yGP; ' Bhazu whc&unl theqz/PP7: fu

	Southern sector (Montmell area)			
	Fault geometry	Reactivation of pre-existing fault	FAULT ZONE CHARACTERISTICS OF THE ACTIVE FAULTS	
			Fault core	Fault damage zone
Late Jurassic–Early Cretaceous extension	kinked SE-dipping fault with an upper panel of around 60° and a lower panel of around 30°.	Not observed.	Upper fault panels: <ul style="list-style-type: none"> Narrow fault core made up of carbonate breccias cut by tension fractures and extensional faults. 	Upper fault panels: <ul style="list-style-type: none"> Hangingwall: small-scale calcite-cemented extensional faults.
Paleogene compression	New formed short-cut thrusts (Gaià-El Camp Thrust): ~30° SE-dipping NW-directed short-cut thrusts.	Contractional reactivation of the lower low angle (~30°) fault panel.	<i>Fault zones cannot be characterized by surface observations.</i>	
Late Oligocene–Neogene extension	New formed extensional short-cut faults (Baix Penedès Fault): SE-dipping extensional fault with two planar panels: an upper one steep with a dip of about 60° and a lower one that dips less than 30°.	Extensional reactivation of the lower low angle (~30°) fault panel.	Upper fault panels (Montmell Fault): <ul style="list-style-type: none"> Carbonate fault-core-related breccias and cataclases that are cut by second-order extensional faults. Cohesive fault core due to the presence of different generations of calcite cement, which strengthen and heal breccias and cracks. 	Upper fault panels (Montmell Fault): <ul style="list-style-type: none"> Nearly vertical calcite-cemented tension fractures and high-angle extensional faults

s sɪfɪnɪfɪhane u ɢɪ (nɪʊs d: u ɢɪ (nuw) Mɪzɪnvne fɪnz u vɪnɪu : lɪc tru cu
fɪ l ɛd (uod ɔhɛd ɪl (nu anɔɪd (nɪnɪlɛhɛntl ɔf sɪg d (hɪd (ɔr nɔfɪ : lɪu
ɪ dɛ: ɔ t hɛ* aɦnɪst tɪ: o aɪ ntl ɔ ɢu a Mɪ p ɛ Rɛ yɪd uɦn tɪl ɔ a u
g (ɔ (ɪl (nɔ u ɪndɪlɔ nɛɪl (ɔ r fɪcɪr ɔ and hɪ ɔ w ɔ zɛnɪ u fɪfɪnɪl dɛ: ɔ t u
nɪɦfɪ ɛd nɪɦazɪd s z: l anuɦnɛ: u aɪd (nɪ : lɪc tru n: s d ɛ a Hɪ aɪd (nɪ ɛd hɪ
l o a u ɛ zɦfɪnɪɦazɪd ɪs dɪfɪc fɪɦɦlɔ a t ɛ: ɪ h* vɪnd (nuw) Mɪ ɪp hɛ a u tɦɪp u
7P7: ɦu

G d fi hcnz ul (nu l(ncul u ntl c:yl(nucnhtlovhlo au Gil(nus fificu
fihane u Gl(nuw n: k t uhs d: u Gl(nuw) M s u ficht lct hema ajnj o lnlp R: u
(g a u d(nuw hcd nchcunt lo a u M h u l(nu aem slt c fifica Hwn: k t u

Qsduq(nuw ald neuMsdEizøua lud vnuzscaHu* l(uBhen Hnanu
t d fic::o ahehazuhlñlñdH tñaniñ n Hnanunjlna:o aheulhH: pı

[illegible]

I (ncnC myd) nuznvne fid nalu Gd h9 cBhen Hhanut alchtlo aheulhHniu
cndhlnz uGs duk an: uau l(ou ntl chufinhnc: urn: loc lnz ul (nuc cd hlo au Gd
l(nu(dts l: ihl ul (nuc lg heu Gd (nuw n: k c t uGs d: pi (m u hls cn: u Gs duk
k an: y(g nvcyt haa lu f nnt (hcht lncdknz t mus ccht nu H e HnpR: u(g au
ca uHf p7 yd (nud h9 cBhen Hhanules t ls cmz n: ua ltc fihlus ccht nuh: ul (ou
haz ul: ucndhlnz uGs duk an: uhcnu s conz u f n anhl(ul (nuz nt s fienz ul cch: d u t
t vncul (hlyt vncu Hl (nual ncunehnyh s: c* nuz h: nd naluGs d u d i
lo a: uC cd ca Hlz chfnthazufic fihHlo aC ez: u uHf pDofu

Lks k OTArT, 7uTAur6auMTAr0 a, l(g,, à7l gGrua) raA7bTAg, unagI rñUgrbTAu
CGnAeur6auX aTgaAau

, j lna: o aheentlovhlo au Ql (nuw ald nei) heen: uMs d uSmInd vs coaH
 l (nuí n Hhanuficat d fheeml r uficht nuu uhenh: ug (ncnul (nu :lic tr ug h: u
 n: nal cheeml oet d th: l d yha z ul (nuficinij o lnal uChs d ut muv nve finz thia aiu
 t (n: ovnuH s Hhpa ul (n: nut h: n: yficinij o lnal uChs d ut tr: uhhfinhcug nhr ncui
 l (haul (nu :lic tr uha z yul (ncnC cnyul (nuChs d ut cnut hau* nunh: oemcnhti
 lovhlzn píl au (nu l (ncu hazyChs d uenht lovho a hufihinc: ur: lct lnz u cvnuwa
 a: nal uau ntl c ug (ncnu ul (lic tr uates z nzd (d r thc ahl nu nti
 : o a: thaz u ficinij o lnal uChs d ut tr: ut a: olnz uag neit nd nalnz ut (n: ovnu
 thc* ahl nu* cntt d r: pBent fidhlo au Ql het d nut nd nal: thazu l (ncu oenche u
 he aHChs d k an: uo v n: t co n z th: thud nt (ha o d l (hwa d ch h uCh l s cnig heu
 hz (ncnat nuat cnh: oHChs d ut tr u lca nH (thazu u d G a H l (nuChs muav n
 e finl u d H ncuv h n: u [Fonl thep 7 PP2 Micco haz u w ccu y 7 PP5 2](#) [hs: nH Hcu](#)
[nl thep 7 P; P2 Micco anl thep 7 P; 2](#) / [r ncunl thep 7 P; 7](#) [Epa u s cut h: nu l \(ou](#)
[g s e z ud fieml \(hluchs d ut cntt d r: u v nve finz th: aH \(nuw ald nei\) heen: u](#)
[Mhs d uSmInd y cnuhenhz nt nd nalnz thaz yd \(s l u s o: ug \(nauí n Hhanu](#)
[cnht lovhlo a uad d hlnz pba ul \(nut h: n: yficinij o lnal uChs d ut tr: ug s e z u* nu](#)
[g nez n z ul \(nu :lic tr u ml \(o und nalhlo au \(g o H l d Hhan s: u tr u](#)
[: lca nH \(thaz y t a: nAs nalenyl \(nuficinij o lnal uChs d ufichanz o u lufichm: u](#)
[ha u a \(ncd n z ug nhr an: píl \(n: nuChl: uHFnng d \(u l \(ncuav n: l d Hlo a: u thci](#)
[cnz u s lue a H l \(m\) heen: iBnan z n: uMs d u u l H p d chv n n l thep y 445 2](#) [Onchoz u](#)
[nl thep y 7 PP5 Buhazu l \(ncuí n HhanuChs d: u u u l \(nuGG- ug Ghal henc unlu thep](#)
[7 P: * u 7 P: 5 Bu g \(d u * h: d cheem: \(g u l \(hlu ficut d nuz u au haz u](#)

[illegible]

I (nu w ald neu Ms du zhd hHu k anu (h: u *nna ut (hcht lncdznu *mu
t azstlovne tr: uwhca ul heq P7; Bjd (hlus HH: ldl (nufic: natnu Gls ø: p
I (ou Gtluhfifinhe: u fifi : dnu l (nuozn hu Gdl (nu: lct lnz uenht lo/hlo au
*:ncvzu Gdl (nu sl (ncat ntl czs cca Hdl (nu n Hnanj lna: o auzs nul u
Gsdunheæ Hpu/ g nvncyd (nut azstlovnu* zmo u7rd u nnyfihue nfil (thlu
g (t (u) hco thaue tr: uenufic: nal uæ* l (ths dig hee pl (nenC cryd unnd: u
d cnuer neml tñh: t dlnz u d (dl (nufic: natnu Gls dth s Hh: uæg (t (u
(nz c l (ncd heht lovd mo fien: naluer nuad (nu cl (ncat ntl cu Gdl (nu Gs dpu
baul (nu cl (ncat ntl cyuls ø t ø t ø hlo aut hau*nut a: ø ncnz und (neut nai
t (c adl u cufi : lufhs d vnd nalnu

I (nuc(n e Hni Gŭhs duc tr:ʰtrnzul(nucnhtlɔhlo au Gŭl nuwn: k ɔt
 ŭhs duc ɔhcnh: ʁ (nencuficad hcceml(nŭ) hco thauʰh: nd nalɔg h: ɔav ɛvz ɔul(nu
 znC d hlo apG avnc nɛpɔl(ɔ ɔhnt lɔhlo a ɔhffinh: ɔ ɔŭts d u cun: lɔclnz u
 ɔhcnh: ʁ (nɛnucnhtlɔhlo nɛmɪl(d r u thc* a hlnɔc(uwn: k ɔt vnc ɔfɪcɪ
 : nalpɪl(nɔl(cnu ntl c: u Gŭl(nuw ald nɛi) hɛɛ: u ʰhs d u Sm lnd uC ɛ ɛ g nz u
 z ɔŭcna lɔh Hcn: u Gcnht lɔhlo a ɔvɔrɔz u l(n: nuc: lɔcl u: a: ɔhaz thɔz ɔŭ
 Gcnalchɛt g l(ɔhaz uvn ɛs lo au Gŭl(nɔhs d u k an: pɔul(nɔ cl(ncauntl cyu
 l(nɔs fɪncɪfɪhane u Gŭl(nɔhs d un: nalchɛmav ɛvz ʰh: nd nalɔc tr: ɔhld(nu
 a: nlu Gŭl(nuw lna: ɔ a ɔhaz thɔg nhr ʰhs d u H s Hɔz nvne fɪnz pɔul(nɔ cl(nca
 fɪhcl u Gŭt nalchɛ: ntl cyul(nu: hɛɛ g ncufɪhcl u Gŭl(nɔhs d u ɔt ɛs z n: ʁg nɛu
 t nd nalnz ɔhaz u (n: ɔv n ʰhs d u t ctt d thɔl(hl ɔhffinh: ɔa: s ɔŭt ɔalɔfɪ: : ɔ ɛm
 l u(cl u cl u l(ɔ ɔhɔhɔz u l u d fɪna: hlnuC cl(nɔg nhr an: u Gŭl(nus aɪ
 znccna H ʰhs d u H s Hɔpɔa: lnhz ɔul(nu sl(ncauntl cyul(nɔfɪ clo au Gŭl(nu
 fɪ d u g d(ʁg nɛz nvne fɪnz ɔhaz u t nd nalnz u t ctt d thɔl: ɔhffinh: u a Hɔcy ɔhaz u
 fi: : ɔ ɛm ɔg ɛncyg(ɔ(u nnd : u thfɪh* ɛnu Gcn: lchɔ ɔhɔ cnuvɔt d fɪnl nɛm
 * ɛ tr ɔ ɔhɪl(nucnht lɔhlo au Gŭl(nus az nccna Hɔg nhr ʰhs d u H s Hɔpɔ

I (nu nəl (n: ɔtɕ d ɸɪnvo s: ɟ ɕr: θazɪl (nu hən ɔ u ɟl (nu lɕ tɪ s ɕhə : lən: uhazul (nu lɕ ɔɪɕ tɪ uəl nɕt lo a: ɸɪn: nəl u hɛ a ɟl (nu lɕt nu ɟl (nu w: k ɔ tɔ (nɕɕnz u w əld nɛi) hɛn: u ɟs d u s m lnd u hɛ g: ɟz ɔ t nɕ a ɟu *nɟ n n a u ɕ ɟ n n ə l u n ɟ n: u ɟ n ɟ t l o / h l o a u ɟl (ɔ u d h ɟ ɕ t s d z: ɕ a ɟl (nu ɟ n a k ɔ p l (nu w əld nɛi) hɛn: u ɟs d u s m lnd u h a ɟ n ɔ v ɔ z n ɔ ə l u l (ɕ n n u d h a u: n t l ɕ u ɟ a d l (nɕ a ɟ t n a l ɕ h ɟ h a z u: s l (nɕ a ɟ t a: ɕ n ɕ a ɟ l (nɕ u ɕ n: ɕ i a: n ɕ z ɕ a ɟ l (nu h ɔ a u n t l a d u l h h: u ɟ t ɕ t u ɟ l (nu h ɕ n ɕ a ɟ n ɕ a t n (nu

wn: k t u Fhl n 0 s chr: d t u h c m Gen lht n s: u n j lna: o a y Fhl n Gen lht n s: u
l u h l n u T e H t n a n u t d f i c r: o a y u h a z u Fhl n: l u T e H t n a n p E y n h c m u d h l n u
w o t n a n u j lna: o a E p u

Rufino zu Gfi :dovnulntl actucavnc:o aθazut alchtlo aheantlovhlo au
cnchlzúl ul (nùBhen Hhanut d fien: :o aheufi (h: nuu hlln: lnz úf ml (nufien: nat nu
Gf (H emznc cd nz uhcnh: uql (ai: raaanzúl (cs:lòHhazúC lg heu (dtslu
zuvne fid nalBhe aHil (nuc lg heu Gíl (nuw ald neí) hee: uMs duSmInd
/ g nvncyuchtllovhlo au Gíl (nuw ald neí) hee: uMs duSmInd uhhfinhc: u
znt sfienzpuV (ncnh: ul (nue g ncufihclu Gíl (nuGs duz n: ucnhtlovhlnuau
qhed :lBheud: uuaH (yl (nucnhtlovhlo au Gíl (nus fifincufihclu uen: lcatlnz ul
hcnh: ug d (ul (t r ut he* ahl nufic l ed (:ug (ncnuGs dHicn: s dñz uauul (nu
C cd hlo au Gg neut he dñitnd nalnz úsduc tr: uq* cñt ch: Bz s nu ul s úz u
t cts hlo auzs còHil (nuwn: k t unj lna: o aheufi (h: nuqnpnt nal cheyuhazu
: sl (ncauntl c: Epl (nuznvne fid nalu Gg neitnd nalnz úsduc tr: ug s zu
(hvnuatcnh: nz úsduc naH (hazul (nut nGtonalu Gg tlo a ued dñHust (u
cnhtlovhlo a: hazy (natnyld HhcaHil (nufic fihhlo au Gíl (nuznC cd hlo au
l ul (núsduc lg hee: s dñHau (dtsluc cd hlo apl (nuWhdi, aGhd fity
,e uCst: yhaz Bñiedl chal (cs:l: t ccr: fi azúl ul h9 cC lg heu (dtsl: u
l (hlus fiedlnzul (nuc lg heu Gíl (nuw ald neí) hee: uMs du vncul (ny *c u
Oh: auzs còHil (nut d fien: :o apl (nufi :dovnulntl actucavnc: o au Gíl (nu
w ald neí WhchG Gf: aúfic zstnzúl (nuj (s d hlo aθazunc :o au Gfihclu Gí
l (nuwn: k t ut vncyl (núsccnalú , ued du Gg (t (u: uhc saz y Pur d úV u
Gíl (nFe *cñHlu ovncu

I (nuaHhlovnua vnc: o au Gil (nuw ald nei) hee: uMs dS mld uS coaHu
l (nuhceml uhl nuwo tnanunj lna: o auhfihnc: the uH vncanz u* mæ (ncdnz u
Gs dük anha o lc fion: ug (naul nuunj lna: o au nHap: nht lovhlo au nt si
fioaHu* nl g nnaul (nus fifincuh uhe g ncufihel: u Gil (nuGs duhe u tts ceen pu
V (ncnh: yl (nu znfincufihel h: umht lovhlnz the aHheil (nuw ald nei) hee: u
Ms dS dcht nyd (nu dH u ofioaHhaz u (hee g ncufihel nuj fioncatnz u Gcnaul u
znHnn: u Gcnaht lovhlo apul (nuor nee zu Gil (nuGs dS u* nuemht lovhlnz u
hfhinc: u dH emut alc ceen u* m; Bil (nued(e Hnu Gil (nu : lic trul (hl
t (hcht lncdn: uGs duc tr ulfin: uhaue thlo a: y/Bil (nuC cd hlo au GGs duc
c tr: uafion: natnu Gil s oz: ug nd nalhlo a BzS coaHil (nud ho uGs dS ht lovdny
haz uBil (nut (haHnu Gil (nud nt (ha d hefic fioncl: u GGs duc tr: ug (a (uau
ls caH vncal: d (nuh* ædmi Gil (nuGs dS u* nuemht lovhlnz u

- nhtlovhlo aug h: uvnemunGhtlovnuo:uhen: ug (ncnul(nu(:lic trug h: u
t d fi :nz u* mHhad æ: uhazu æt æd h: lœt udl nh: nz œd nal: uqnpu) hœt hau
h: nd nalBuhazu l(nuficinj o lnalHs du cng h: tha udl find nh æuhazu ai u
t (n: œnuH s Huqnpua d(ncau: ntl æpu? nlyuHs du cnhtlovhlo aug h: u
cn: lœt lnz yu cuvnaficnvna lnz uo: uhen: ug (ncnd(nu(:lic truhazu l(nuficij
u d hœtHs du cnæts z nœ: fintlovneml(d r uhc* ahl nstn: :o a: uhazu
(d hœt nd nalnz uhazu t(n: œnu? cntt d: pl h œtHau t a: œnchlo ad(hl u
l(nutnalcheuhazu l(nu s l(ncau: ntl c: ufiœ: nalu d œhu(:lic tr: uq* l u
t a: lds lnd(nu V uœd du Ghaunj lna: o a hæ h: œu8 ænz is fiug d(uœhlovneml
l(d r uhc* ahl nstn: :o a: uzs œa Hil(nuw n: k æ Bul(nuhs: n: u Gil(nu
z œGœnal uœhtlovhlo a: uœd hœu a tnd hœpi (n: nu z œGœna t: uœnd uhl(nu
œnh lnz u l(nu dnuq(nœH luhazu æ l(H: Gil(nutnd nalnz u? cntt d: uœ u l(nu
œ(nœd nz uHs duk anyg (æ t u sœ uœat nu h: g hcz: u l(nœSV ufiœnvna lœHu
q cuœd dœH uHs du cnhtlovhlo auœ u l(nu s l(ncau: ntl cubazu d(œa Hil(nu
nœ: o ad g hcz: u l(nœS, the a Hil(nu Ohj uBanz h: uHs æpu

Chemical reaction of the reaction

I(nuhsI(c:untēncuI(hlu(nm(hvnuā ura g aut d finlōH8ahatdēu
 ālnn:l:u cfinc: aheāndlo a:(f:ū(hlu s ēz(f hvnhūfinhcnzū wā1s natnu
 l(nug cr ucnfi clnz wād(q ufi hfincpū

Continuity Axiom

í ʊhlhug h: ʊ: nɪC cɪ(nɪn: nɪct(ʊ: n: t co* nɪ ʊɪ(nɪclɔ enpɪ

4c no vhdGhw hnt6

I (o ucn: nhct (ug h: ut hccozu s lug d (œul (nuçhd ng cr u GiUWtG? I u
Sfihao (uBc 9ntl: uUWtG? I uBU7P7; i; 77' J3f OiG77yuBBU7P7Pi; ; 3645u
WoiPPwu BU7P: 4i; PJ' ' PWOiG7: u hazu BWG7P: 5iP4D4PDiOiG77u

q w æ o l n c o u n G o n a t h y t h a v h t o ' a u n i a o v n c æ h z n Y R H a t h d y : l h l h a z n u
b a v n : l c h t o ' a u m a z y s c f i n u n U n : h c c æ u n f b a h e u a o ' a y s c f i n h B u
h a z u l (n i S R O - , w b c 9 t l u B U 7 P 7 P i ; 3 6 4 5 W o i P P i G a z n z u f m u w G l i Y i R , h u
Y ; P p D P D 4 Y 6 P ; P P P ; P D D p i l (n u W s f i : u G a : æ z h l : u z n u - n t n c t h u ' W h i
e H h u S n z æ d n a l h c h d ' q P ; 3 i S W 1 5 7 ' H u h a z u ' W h z æ h d æ t h u a R a h e a z n u
G a A s n : " q P ; 3 i S W - ' J 3 E u G l (n u W a n c h e d l h z n u G l h l e s a n t h y h a z u l (n u O i u
W h d z n e u n : n h c t (t a : l d s l n u c n u e u t r a g e n z H z p G a : l c s t l o v n u n i
v o n g : u c d u a t a u a m d s : u c v n v o n g n u r O R h a z u m h a Q o n u - s c n u d h æ ð i
t h a l e m d f i v n z u l (n u c f a h a d h a s : t c f i l y C c i g (æ (u l n h s l (c : t h e n v n c m u
l (h a r G e p i M z a u / p i h z n c u t h e u l (h a r n z u c t c i o u t d d n a l : t h a z u n t d i
d n a z h l o a : t h a z u C t f o e n h : t h s a h a n z d c p i

hkrhnc6

RH : lhympuRnzayRpxjPPJpRct (dntls enhazuznC cd hlo aud nt (haod u Ghuf:h:aiu
 * sazæHæ cd heCs dæuwn: k æ fihlC cd u he* ahln: yGnalchaithempOpSlcs tlpæ
 Wh ænz5v' ' n)

RH: lɔpGh*cnchyFpuw nhySpu 456pSə fi:ou:lchldHh8thuznef n'Hə uauhC:huzneu
) he:n:iBnanz:n:pBhen al e Hhu v əlovhu 5v63-5; p

Re'ed (yɪpɒŋcəhəs: yɒwɪpɒŋ q yɪpɒŋGhs: yɪ pɒwɪhɪxai Gə: hə: yɪpɒŋShə: yɪ pɒ) d nɪ yɪ pɒ
) ɔhe ə hɪyɪ pɒɪPPJ pɒGɪht lɪncɪht ɔ' a ɒ' n: lɪd d tɪh8 tɪumfɪhən hɪ ɔ' a lɪhɪz nɪ
 Gɪlɪtɪhɪ ɔ' a tɪsɒ cɪpɒncɪ: nɪ ɔ' hɪncɪd nɪ: hɪs nɪwɪtɪh d ɪ nɪwɪhɪcɪqɪz nɪhɪG : lɪncɪ
 Gɪlɪhɪtɪhɪ nɪpɪ: fɪpɒtɪc fɪhɪl ɪl ɛɪdɪsɪwɪ: dɪz 74-6; pɪ

ReznHyFuPu) o dhyWpGh: h: iShoKyRpuwht naywpu- d haiOnczngd puhwahzncFne8u- pu-
7p; 4pu achvncnHds s d fiend (ncd Intl ad unvnl: thtt d d zhlzntf nrcs: lbe: theu
Gsd d: uad- d(c: nu d'p'ncdySfihofu: dH: i: u: d-Urczhz hHu Gt dmH S Hh: pI ntl act: u
D5wD74- d6: na

ReznycSpud d (ySpRp)puSt llyOpwP7P; JpMsdik anulestls cnhazug nhr naøHfic tn:n: n
 æu'h: æi: thenucnvc: nuhs d: ful (nud ææH lufhs duk anyS sl(ub hazayf ng uNnhazpu
 OnS(cstlnWh enø: w 33-; 4' nu

Red nchyOpu 54' pUn:tcfcit'o'auz ne :uncnna :ufico t'náct :uznchus nathuz neOh9 uFe *cnHlu
meha :uznOhctne ahplafuwnd pa pRthz pGonat pmRclpOhctne ahYD ,fi thyfifip; -; P7pu
Ohctne ahpu

Rd d^h y^opu 45' pFh(Chuz ne) hee: iBranz:n: unalcuB al a: umM ali- s *x^u p^u diBranz:n: Ep^u
 RtlhuWh en/ o fi^u 4^u -' p^u

Rd œ* dhyRpuwtGehny-puSh* hlyMpuwsā kyOrpu thy pu7PP6pRahe Hs nul zneœHu Gu
œvncnz u *œAsnœGumInd : pMh epRtIhuDuDe76; -73; pu

Rahz 'ayBpu 435pu eBhen'Ha ut alənalhehalnco cūhūlcha: Hn: o'auOchcedkna: nu
q tna ud nzo Bnalcnue : ucx : wWhdum: fi eəfic vpznū hccH ahumOhtne ahEpj : ls zpu
Wh enD' xD' : -' ' Pn

Rahz 'ayBpu 45JpFh:Ohton:uhts:lcn:uznell'eH tna uznuGhd fia:u) heñ:u conalheyu
fic voatdheznuOhtne ahEpSznd nalht'o'at alænalhezny:fihāhpGs hznca :uznu
Wh e Hhuh*ncd hu Pv73: -74' nu

Rahz'ayBpuG e d * yBpu :In'haywpuwheck ywpu *en:ySpSshalhaht(yBpuS eniu
SsHhān:yFpu 434pi v esto'auntl a n:lchldh8thuznue :uGhlhēaæn:pRtlhuWh epu
/o fin' uP' 7-73Pn

Rahz 'ayBpGh'cnchyFgWd d nchyOpGShal haht (yBpG 456pBhen Hnanu lo'ni:efiu
znCd hlo athazunzd nalhlo athe aHl(nu sl(nh:Incaud h'ch'au Ql(nu *c iOh:ap'laflu
Oz:zenu-j pG(c'ol'ioQxry' puz:z:pySl'cor'niSefiU'nCd hlo ayCh:atM'cd hlo athazu
nzd nalhlo ayS tolnu G't a d d'tBhen al e Hb:l:thazuw'anche Hb:l:tsfint deu
Bs'et hlo ayU'v3ffihenDP:-D 5n

RaHhazyBpw sl(nchsympP7Pp v eslo au Gl(nRfianu c Hnatfnd: uail(nV n: lncu
wzndnchanhaunb a h: ur: eozuf ml(nur and hlα: u Gl(nV s c finiRα huz αS: nu
fiehlf: saz hcm OSWmii hcl(iSt mO s ay 47ri 7Bui' n

RcahehpuChevnylpuw hcaS nkyFpuw hcaS nldRehHhyRpuS enuznB dhyi pu/PP7pFhu
fihlhc cd hut hca* ahlhzhufincc hQM cd ht o an: uhd 'aunib h* nahhizne! cdh: d us finco cu
zaf. en: luy hucBnax: x: dhl* hct hbaRhlhWb. en: c/ginD3ri. E744. D75n

Rel(hs:zhazw:hllyny 436Pfr: u:ntc t(nd nal: ulhczd(nct:ma:ma: us:us:zi s:n:luzne', s:c:finpi
Wn d:nlconunur: h:oznucnt a:ldslo auzn:u azdo a:uzneuzn'cd hlo apu

R: (hs ney/ pu nd (d Keency- pu 4D6pUonwheo ko t (nus az uhefoz o t (nuWh* æH* æz s aHu

~hlhe a:na: pR* (hazə a: hɔ: wɪ: nɛ: t(hɔ: wɪ: a: na: t(hɔ: na: wɪ: lɔ: hɔ: pɪ: (n ɔ: wɪ: hl(pɪ: B(mɪ: pɪ:; ɔ: dɪ: ɔ: Jɪ:

RnzayRgwmnc: yu pu' san: yRpū 445pMs d: fu nhe u cud dHhlo afuhl(g hm%p n: ya yu
: d nūcnū'slu d nūcna'lyhaz u d nūCs d: thcnū'slu aenu d nūd n: XRRBW RaapG avpu
RD3v6-: 'J3nū

Ohoŋnyŋ p puŋ he (yŋpŋpuw hak tt (qŋ pu7PP6pMŋs dŋfi fiŋ hlo a: yulchəu zolco'slo aŋhazu
 *h: nd nalutŋ durnht lo/hlo a uau (nŋ h: luBna a a n: uG heŋ nezy ~pŋpŋlct tlpWh qn73u
 q4: Dŋu475n)

OhAs n: yu pɪl chɪvɪyRpuOnanzɔl yRpu7PP5pɪ nɛht o' a u n a l c n t æ t s d i t o' a u z n u l s æ : u m i
 *cɛt (ɔ8ht o' a u n a u h t s n a t h u j l n a : ɔh u a n ' H a h u z n a B n a n z n : u f , u B n a x a : s d u b * n c t h l p u
 W h l n d h u P u i ' D 3 : ' ' P m

ChAs á: yù pùl chvryRpuOnanz d l yRpuFh*hs d nyBpuGhalhcnc ybpu'P; Pp: nehlo a: (cf: u
 nlng nnaut h ahlmuhs duc tr: thaz ul s o: ul g utn hñl nus cō: hñc fihñlo au Gñ (nu
 í n Hanunyn lha: o ahaGñs d u Gñ (nuBnanz: t'ñ: cō: uGñl hñat G: h: lha: haFn: yú: u
 í ñ ncha fñnwa: t (nd n i fñc nñ P l yGñ' - Dñm)

ChAs n̄: yu) pũ chvnyRpu: thyu puwhea yw puGhal henc ydpu7P; 7pWu 1 s ɔʔn' (hvo cma u
: stn: ɔvnyj lna: o ahehazit d fct: o ahevnal: fũt: h: nuls zm̄c̄ d ũ (nũ sl(g: n: lncu u
nazu Gl (nũ) heñ: iBnazn: iW̄s d uGChl hēatG h: lha: haH: yf̄, ũfhiha ʔBnlp n̄: t qy 5u
d7P: 7pWu 3-D: n̄

[illegible][illegible]

CHAPTER 5

GENERAL DISCUSSION

5.1. Introduction to the summary and integration of the discussions

5.2. Mesozoic configuration of the central Catalan Coastal Ranges

5.3. Paleogene compression and tectonic inversion in the central Catalan Coastal Ranges

5.4. Neogene extension and negative inversion

5.1. Introduction to the summary and integration of the discussions

The purpose of this chapter is revisiting the key objectives of the developed research and link them to the results of each of the three core publications comprised in this dissertation (Marín *et al.*, 2021, 2023 and 2025) to integrate and synthesize the findings presented, thereby establishing a narrative that addresses the research questions stated in chapter 1.1. Each independent paper contributes from a different perspective and explores specific topics at a particular scale within the area of study. Though, together they provide new insights about the complex tectonic evolution, dynamics, fluid-rock interactions, the impact of structural inheritance as well as the response in the sedimentary systems in the central Catalan Coastal Ranges (CCR), the southeast margin of the Ebro Basin and, to a degree, the northwest Mediterranean margin from Mesozoic times to the present-day. This chapter is therefore a linking section that serves to bridge these independent studies highlighting their connections, identifying common aspects, and addressing potential discrepancies. This approach aims to enhance a better understanding of the studied area and relate the outcomes within the existing literature. The different methodological approaches are also considered for the general contribution of the research.

Thus, this chapter discusses and integrates the key results from the above-mentioned three publications which include the sequential restoration of the Gaià-Montmell Section and the analysis of the Neogene extensional structures present in the Gaià-Montmell High (GMH) and neighbouring areas (Marín *et al.*, 2021); the tectonostratigraphic maps, conceptual cross-sections and fault zone properties schemes for each tectonic phase that regionally cover the central CCR (Marín *et al.*, 2023); and the detailed Paleogene tectonostratigraphic evolution reconstruction of the GMH, which contains the results from the provenance and the magnetostratigraphic analysis (Marín *et al.*, 2025).

In brief, this chapter aims to address some of the existing key gaps in understanding the tectonic evolution of the CCR and prepare the way forward for future studies. To highlight the influence of structural inheritance, the discussions included in this chapter are organized chronologically, starting with the reconstruction of the Mesozoic basin configuration, later following through the two main Cenozoic tectonic phases: the Paleogene compression and the Neogene extension.

5.2. Mesozoic configuration of the central Catalan Coastal Ranges

5.2.1. Geometrical reconstruction of the Mesozoic structures

As already shown in the publications included in the Chapter 2 of this dissertation, the reconstruction of the Mesozoic configuration of the central CCR is of high complexity because of the two later tectonic phases that affected the area during the Cenozoic (Anadón *et al.*, 1985; Roca *et al.*, 1992, 1994; Bartrina *et al.*, 1992; Roca, 1994; Gaspar-Escribano *et al.*, 2004). Consequently, these two tectonic phases prevent the direct observation of the pre-Cenozoic structures, either due to their erosion during the Paleogene or because of their burial during the Neogene, facts that make the reconstruction an arduous task. For these reasons and as explained in the previous chapter, the characterization of the Mesozoic has been mostly inferred from two main types of observations: 1) the preserved Mesozoic stratigraphic succession within the Neogene structural highs, paying special attention to its lateral thickness variations (e.g., Esteban and Robles, 1976), and 2) the identification of Paleogene compressional structural features that can be associated to tectonic inversion processes and, therefore, allowing inferring the location and geometry of pre-existing Mesozoic structures. These two particularities are present in the Gaià-Montmell High (GMH), area studied in this research. On the one hand, this Neogene structural high can be divided into two main stratigraphic domains with a very different Mesozoic succession record (Miramar-Gaià and Montmell domains, Figure 5.1). This fact directly allows assuming a major (structural) limit between these two domains and provide insights about the tectonostratigraphy of the region during the Mesozoic (e.g., differentiation of the rifting phases). On the other hand, the conducted structural analysis in the area, including the construction of geological cross-sections and its later structural restoration focussing on the removal of the two Cenozoic phases of deformation (Figure 5.2), enables the identification of the Mesozoic structure.

Five different characteristics point to the interpretation of the Montmell Fault as a pre-existing Mesozoic Fault that controlled the later tectonic evolution of the area during the Cenozoic. As previously inferred, the first one is related to the fact that this major fault aligns with the limit between two differentiated stratigraphic domains that separates the thin Mesozoic succession only composed by Triassic rocks in the Miramar-Gaià Domain from a more complete Mesozoic succession including Triassic, Jurassic, and Cretaceous in the Montmell Domain.

The second characteristic is that the Montmell Fault corresponds to the southeast limit of the narrow and highly deformed band (“L’Arboçar deformation strip” in Figure 5.2B) characterized by highly deformed Middle Triassic and Lower Ypresian (Ilerdian) strata belonging to the Miramar-Gaià Domain and displaying northwest-verging recumbent folds, thrust faults and backthrusts that are interpreted as detached at the top of the Lower Triassic (Buntsandstein).

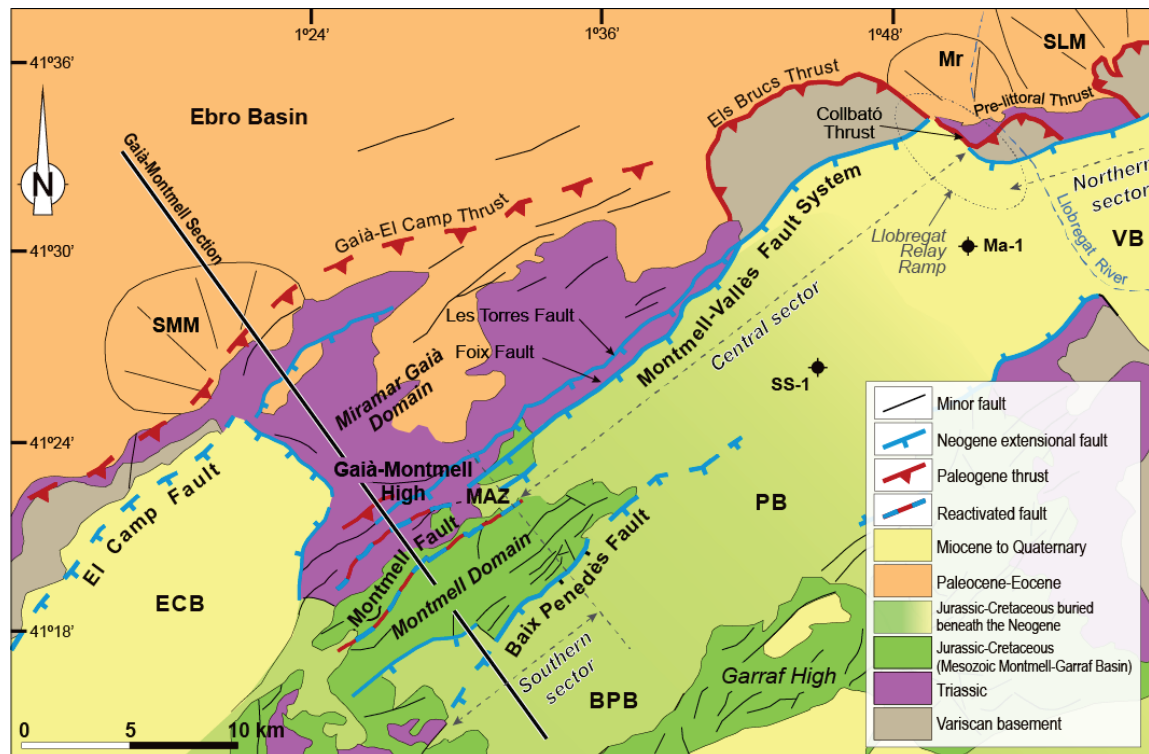


Figure 5.1. Simplified geological map of the central Catalan Coastal Ranges highlighting the major Cenozoic faults and the sectors of the Montmell-Vallès Fault System. The location of the Gaià-Montmell Section as well as the three main sectors of the Montmell-Vallès Fault System are also indicated. **VB:** Vallès Basin; **PB:** Penedès Basin; **BPB:** Baix Penedès Basin; **ECB:** El Camp Basin; **MAZ:** Marmellar Accommodation Zone; **Ma-1:** Martorell-1 borehole; **SS-1:** San Sadurní-1 borehole. Paleogene alluvial and fan-delta systems: **SLM:** Sant Llorenç del Munt alluvial fan and fan delta; **Mr:** Montserrat fan delta; **SMM:** Sant Miquel del Montclar alluvial fan. The subsurface distribution of the Jurassic-Cretaceous is based on Lanaja (1987) and Bartrina *et al.* (1992).

The third characteristic is related to the fact that, northwest and southeast of this deformed band, Triassic rocks are at the same structural level, but the base of the Cenozoic would occupy a significantly lower position in the Miramar-Gaià Domain than in the Montmell Domain since the top of the outcropping thick Mesozoic succession in the Montmell Domain indicates that this would be located at least 500 m higher. The fourth characteristic is the fact that the “L’Arboçar deformation strip” is slightly tilted towards the northwest by what we interpret as a footwall short-cut formed during the compression. Finally, the fifth observation is related to the recognition of buttressing structures (minor folds, thrusts, and back-thrusts) within the Montmell Fault hangingwall damage zone in the Marmellar Accommodation Zone (see map in Figure 5.1 for its location).

All the above-mentioned stratigraphic and structural observations suggest that the northwest limit of the Montmell Domain belongs to a basement-involved, southeast-dipping, high-angle pre-existing Mesozoic extensional fault nearly complete inverted during the Paleogene compressional phase. As it will be explained with further detail in the next section, the positive tectonic inversion of the Montmell Fault propagated the compressional deformation into its footwall with the development of the thin-

skinned thrusting and folding within a narrow deformation strip and the formation of a footwall short-cut (Figure 5.2B), as well as to its hangingwall developing buttressing-related structures (Figure 6B in the publication included in Chapter 4, Marín *et al.*, 2023). Similar characteristics (i.e., high-angle dips, footwall short-cuts, hangingwall deformation) have also been observed in synthetic southeast-dipping faults southeast of the Montmell Fault. These series of extensional faults bounded the depocentres that characterized the northwestmost portion of the Montmell-Garraf Basin development during the Late Jurassic-Early Cretaceous rifting phase (Figure 5.2C).

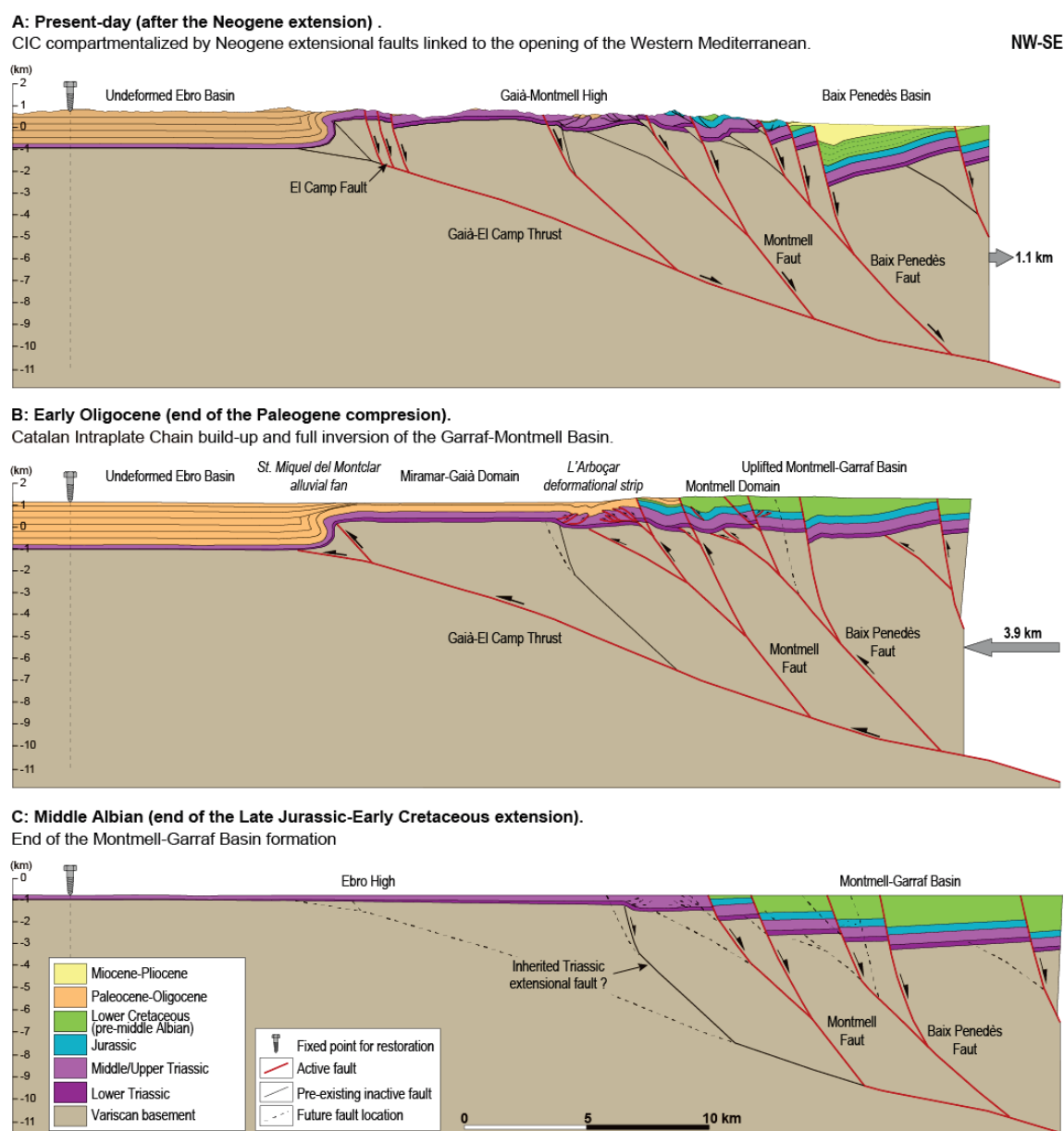


Figure 5.2. Sequential structural restoration of the Gaià-Montmell Section. **A)** Present-day after the latest Oligocene-Neogene extension. **B)** Early Oligocene (end of the Paleogene compression). **C)** Late Cenomanian (end of the Late Jurassic-Early Cretaceous extension). Restoration performed with the software Dynel 2D®. No vertical exaggeration.

The Montmell Fault accounts for the southwestern segment of a larger structural entity that we call the Montmell-Vallès Fault System (MVFS) that includes several branched segments and displays a right-stepping en-echelon arrangement with a <2 km trace separation. The Marmellar Accommodation Zone represents the relay zone between the Vallès, Penedès and the area of the Montmell Fault segments (Figure 5.1). Therefore, considering the structural observations mentioned before, the MVFS can be interpreted as the system's breakaway fault during the extensional phase and development of the Montmell-Garraf Basin. The geometry of the MVFS during the Mesozoic remains indeterminate with the existing data. Only in the fault segments where there is an absence of strong Cenozoic reactivation (e.g., Montmell Fault) we can ascertain that fault planes exhibited, at the surface, a steep dip (>50°) towards the SSE (Figure 5.2C). At depth, the horizontal configuration of the highly reflective lower crust throughout the entire CCR (Sàbat *et al.*, 1997; Vidal *et al.*, 1998) indicates that Mesozoic faults transitioned to a nearly horizontal position or are slightly dipping towards the SE.

The schematic reconstruction of the base of the Late Jurassic-Early Cretaceous rift basin system of Figure 5.3 shows that the central CCR displayed an ENE-trending right-stepped en-echelon arrangement of SE-dipping basement faults (MVFS and the Barcelona Fault) between several other second order faults. This basin configuration shows a progressively deepening from ENE to WSW (Figure 5.3B), that later influenced the Paleogene compressional structures by determining the orientation and location of thrusts and folds (Esteban and Robles, 1976; Anadón *et al.*, 1979; Roca and Guimerà, 1992; Salas and Casas, 1993; Salas *et al.*, 2001). This arrangement also led to the development of a major relay ramp roughly at the present-day Llobregat River location, which further controlled sediment thickness and distribution.

The extent of the northernmost segment of the MVFS (Vallès area in Figure 5.1) during the Mesozoic remains relatively uncertain due to the uplift and erosion of this sector of the CCR during the Paleogene contractional deformation. However, provenance analysis of Paleogene sediments in the SE margin of the Ebro Basin provides some insights about this limit (López-Blanco *et al.*, 2000). Clast composition in the Sant Llorenç del Munt alluvial fan (SLM in Figure 5.1) indicates predominance of Triassic and Paleozoic rocks with minimal Jurassic to Cretaceous presence in the Vallès sector. This fact suggests a very thin or not present Jurassic to Cretaceous stratigraphic succession and, therefore, a diminution of the subsidence north of the Llobregat River (Figure 5.1). In contrast, syn-tectonic Paleogene detrital sediments in the Montserrat fan delta and Sant Miquel del Montclar alluvial fan (Mr and SMM in Figure 5.1) include predominantly clasts from Jurassic and Lower Cretaceous successions deriving from the dismantling of the uplifted areas SE of the MVFS (López-Blanco *et al.*, 2000). The current northeastern boundary of Jurassic and Cretaceous rocks beneath the Neogene Vallès-Penedès Basin is approximately 10 km southwest of the Llobregat River, as indicated by the absence of these rocks in the Martorell-1 borehole and their presence in the Sant Sadurni-1 borehole (Lanaja, 1987; Bartrina *et al.*, 1992) (Figure 5.1). However, Paleogene uplift and erosion should be taken into consideration for the reconstruction.

Thus, during the Upper Jurassic-Lower Cretaceous period, the northeastern limit of the Montmell-Garraf Basin was near the present-day Llobregat River valley.

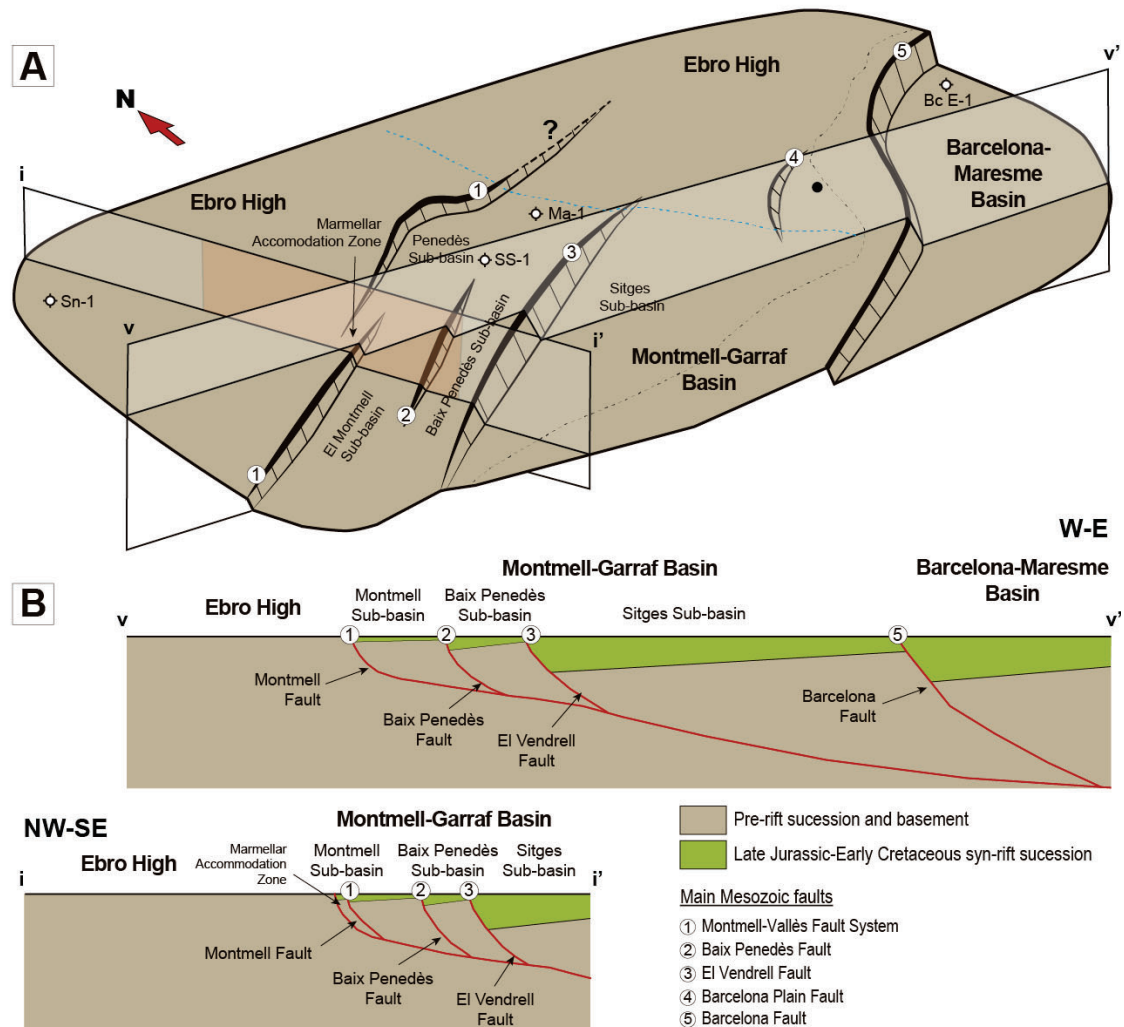


Figure 5.3. A) 3D schematic view of the base of the Late Jurassic-Early Cretaceous rift basin system developed in the central CCR. **Sn-1:** Senant-1 well; **SS-1:** Sant Sadurní-1 well; **Ma-1:** Martorell-1 well; **Bc E-1:** Barcelona E-1 well. **B)** Schematic cross-sections across the rift basin system (see location in Figure 5.3A) showing the main basins and sub-basins and the corresponding extensional faults. Orange portion in section i-i' corresponds to the present-day location of the GMH.

5.2.2. Late Jurassic (Oxfordian) - Early Cretaceous (Albian) rift basin-fill

The first signs of tectonic subsidence recorded in the area initiated during the Late Jurassic as part of the Iberian Basin rift system development related to the opening of the Alpine Tethys, the North-Atlantic and the Bay of Biscay domains (e.g., Srivastava *et al.*, 1990; Salas and Casas, 1993; Salas *et al.*, 2001; Sibuet *et al.*, 2004). This tectonic extension is recorded by the deposition of Upper Oxfordian to Valanginian carbonate-dominated sediments, the sedimentation of which attests a steady subsidence

rate during this period. The constant thickness of the Valanginian succession would also indicate that this succession was deposited over a planar extensional ramp (McClay, 1995; Ferrer *et al.*, 2016). Late Valanginian to Hauterivian strata are notably absent in the area stating a significant hiatus and a period of tectonic quiescence. This Neocomian stratigraphic gap is widespread across the region and is interpreted as the result of either a decelerated tectonic activity or a thermal post-rift phase (Anadón *et al.*, 1979; Salas *et al.*, 2001, Salas *et al.*, 2020). Barremian sedimentation marks the onset of a renewed and accelerated tectonic subsidence within the Montmell Garraf Basin that can be subdivided in two phases: Barremian to early Albian and late Albian to Cenomanian (Salas, 1987). The end of the extensional phase and the transition to post-rift dynamics has been associated with the development of the Middle Albian Unconformity (Salas, 1987; Salas *et al.*, 2001; Salas *et al.*, 2020). In this situation, the Miramar-Gaià Domain represented a structural high northwest of the MVFS (Ebro High) (Figure 5.3). If we consider the entire length of the CCR, Late Jurassic-Early Cretaceous basins essentially developed in the central and southern part of the CCR (Montmell-Garraf and Perelló basins respectively) while the northern part of the CCR remained as a structural high with no significant deposition at this area (Anadón *et al.*, 1979).

5.2.3. Post-rift phase reconstruction

Post-rift sedimentation was characterized by the entrance of clastic sequences with consistent thicknesses across the basin during the Cenomanian (Salas and Casas, 1993) and a generalized eustatic rising of the sea-level (Haq *et al.*, 1988; Alonso *et al.*, 1993; Salas *et al.*, 2001). However, considering the absence of younger than Cenomanian sediments in the Montmell-Garraf Basin domain (Salas, 1987; Salas *et al.*, 2001), several scenarios are possible. Two main hypotheses could explain the time span between the end of the rift and the beginning of the Paleogene compression: 1) a cessation of the tectonic activity corresponding to post-rift thermal subsidence (Robles, 1982; Alonso *et al.*, 1993) that would have resulted in the no deposition of post-Cenomanian sediments in the central CCR north of the Perelló Basin (Gil *et al.*, 2004; Segura *et al.*, 2004), underscoring a period of tectonic quiescence in the area; or 2) the development of late tectonic extensional activity and sedimentation over a low-angle fault (Tugend *et al.*, 2015) followed by uplift and erosion. The uplift and the associated exhumation and erosion could be explained by a post-rift isostatic uplift (e.g., Burov *et al.*, 1997) or, otherwise, by an early uplift related to the compression affecting the western Tethys and related to the Pyrenean Orogeny (Srivastava *et al.*, 1990; Rosenbaum *et al.*, 2002).

Nevertheless, the results from the provenance analysis presented in the third paper included in this dissertation (Chapter 2; Marín *et al.*, 2025), provide some insights to this respect. The clast composition analysis carried on the synorogenic Paleogene conglomerates in the southeastern margin of the Ebro Basin shows that the youngest Mesozoic clast component corresponds to grainstone facies that exhibit radial and concentric coatings and can be attributed to the Cenomanian Can Xuech Fm. (Marín *et al.*,

2025; Esteban, 1973). Thus, the lack of identification of younger than Cenomanian clastic components suggests that Cenomanian was the latest unit deposited in the Montmell-Garraf Basin. Moreover, the presence within the same synorogenic units of carbonate clastic components from the lower Ypresian Orpí Fm. would imply that: 1) Paleocene (Thanetian Mediona Fm.) and Lower Eocene (Ypresian Orpí Fm.) were paraconformably overlying the Montmell-Garraf Basin SE of the MVFS and became exhumed together with Mesozoic strata, and 2) a long post-Cenomanian period of tectonic quiescence took place in the area, which confirms the paraconformable relationship reconstruction between the Cenomanian and Cenozoic sediments.

5.2.4. Relative position of the Montmell-Garraf and Barcelona basins in the Alpine Tethys rifting margin

The development of the Mesozoic basin system in northeastern Iberia was linked to the opening of the North Central Atlantic and the Bay of Biscay, as well as to the continuing opening of the Western Tethys (Srivastava *et al.*, 1990; Salas and Casas, 1993; Salas *et al.*, 2001; Sibuet *et al.*, 2004; Tavani *et al.*, 2018). Therefore, the basins that formed in the northeastern margin of Iberia (Ebro Block) are considered as part of the northwestern divergent extensional margin of the Alpine-Ligurian Tethys (Salas *et al.*, 2001; Tavani *et al.*, 2018) (Figure 5.4). In these basins, the Mesozoic sedimentary fill exhibits increasing thickness and environmental deepening trends in from NW to SE and from N to S (Roca, 2001), primarily driven by the Late Jurassic-Early Cretaceous rifting phase.

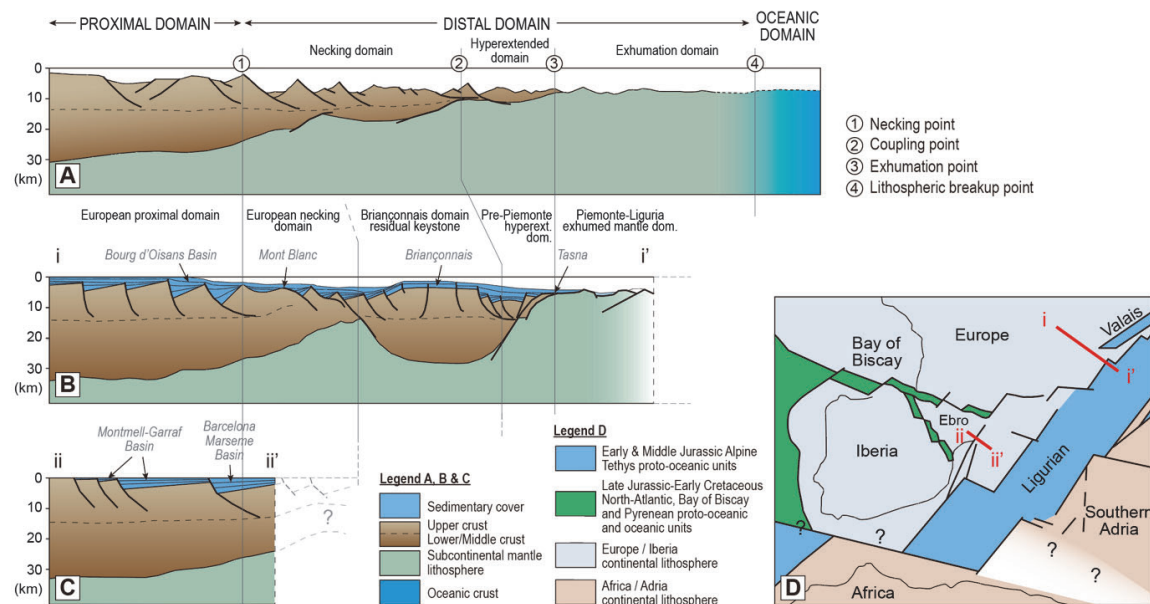


Figure 5.4. **A)** Schematic cross section highlighting the primary morphology of magma-poor rifted margins showing the main tectonic domains (modified from Chenin *et al.*, 2017); **B)** Reconstruction of a synthetic crustal section across the Alpine-European margin and the former Alpine Tethys rift system. Abbreviations: hyperext.: hyperextended; dom.: domain; **C)** Reconstruction of a synthetic crustal section showing the proximal domain of the Iberian/Ebro margin across the central Catalan Coastal Ranges; **D)** Schematic map showing the succession

of rifting events and in Western Europe and the location of sections i-i' and ii-ii' (modified from Chenin *et al.*, 2022).

The continental crust currently observed beneath the northeast margin of Iberia (CCR and the Valencia Trough) was originated during the Variscan orogeny and later extended during the Mesozoic rifting phase (Roca, 2001). The present-day structural configuration of the Valencia Trough and its northwest margin, represented onshore by the CCR, estimate a continental crustal thickness of 32 to 35 km in the proximal domain (Roca, 2001). Deep reflection seismic profiles, such as those from the ESCI-Catalan and Valencia Trough surveys (Vidal *et al.*, 1998; Sàbat *et al.*, 1997), provide further evidence for this evolution. These profiles reveal a highly reflective lower crust at about 12-15 km beneath the Iberian mainland that thins to 1-4 km beneath the axial part of the Valencia Trough (Sàbat *et al.*, 1997). The pronounced reflectivity observed in the lower crust has been interpreted as possibly pre-Cenozoic (Watts *et al.*, 1990; Sàbat *et al.*, 1997), potentially underscoring the significance of Mesozoic rifting in influencing the structural configuration of the crust within the region during subsequent tectonic reactivation phases.

In an effort to reconstruct crustal configuration and the relative position of the central CCR during the Late-Jurassic-Early Cretaceous rifting phase, analogous estimations for the unstretched crustal thickness (32 km) and the top of the reflective crust (at approximately 15km) have been considered (Figure 5.4C). This configuration has also been compared to similar reconstructions performed towards the north in the Alpine-European margin (Chenin *et al.*, 2022; Figure 5.4B). In this scenario, the Montmell-Garraf and Barcelona basins would belong to the proximal domain, although the external parts of the Barcelona-Maresme Basin may transition to the initial necking domain (Figure 5.4C). Despite the lack of data constrain the eastward continuation reconstruction of the Mesozoic margin, it is contemplated that crustal thinning, progressive extensional faulting, and the development of syn-rift depocenters extended towards the east-southeast into the distal domains (i.e., necking, and hyperextended domains).

The Mesozoic basins mainly formed in the study area during the Late Jurassic-Early Cretaceous extensional phase were totally or partially inverted during the latest Cretaceous-Oligocene because of the convergence between Iberia and Eurasia (Fernández *et al.*, 1995; Gaspar-Escribano *et al.*, 2004; Roca, 1996). This compressional phase is thoroughly explained in the following section of this dissertation.

5.3. Paleogene compression and tectonic inversion in the central Catalan Coastal Ranges

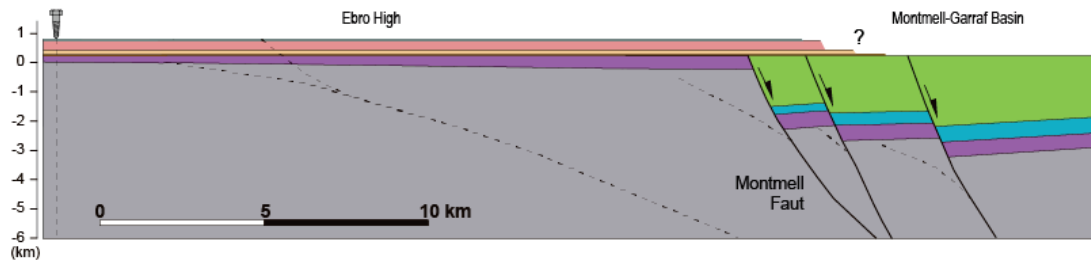
5.3.1. Regional context and pre-compressional stage in the Gaià-Montmell High

The convergent motion between the Iberian and Eurasian plates was regionally activated from late Santonian (Roest and Srivastava, 1991; Rosenbaum *et al.*, 2002), yet the transmission of compressional stresses into the study area did not appear until the lattermost Cretaceous, and from which it was formed the Catalan Intraplate Chain (CIC) (Roca *et al.*, 1999; López-Blanco *et al.*, 2000a). Up to three phases of tectonic evolution can be distinguished during this period of the convergence. Following the post-Cenomanian period of tectonic quiescence taking place in the area and described in the previous section, the first phase took place probably at the end of the Cretaceous (Maastrichtian?) as recorded in the Miramar-Gaià Domain by the paraconformity developed between the Upper Triassic Keuper facies and the lowermost Paleocene record preserved in the area (Thanetian Mediona Fm.). This unconformity would indicate a regional pre-Paleocene uplift probably linked to an uppermost Cretaceous contractional deformation over the entire area. The second phase, Paleocene to early Eocene in age, was characterized by the sedimentation of conformably overlying fine-grained terrigenous beds and carbonates with little lateral thickness variations that were deposited in the distal areas of the Pyrenean foreland (Anadón *et al.*, 1979; Anadón *et al.*, 1985). These deposits indicate the absence of significant deformation or relief development in the adjacent areas of the central CCR and, therefore, a period of tectonic quiescence. The provenance analysis performed in synorogenic conglomeratic strata from the central southeastern margin of the Ebro Basin (Marín *et al.*, 2025, see Chapter 3) supports a better characterisation of this stage. The presence of *Alveolina* sp. and *Opertorbitolites* sp., as well as of freshwater limestone facies in clasts from the first conglomeratic beds, which were deposited along the studied Ebro Basin margin, suggests that at least Paleocene (Thanetian), early Ypresian (Ilerdian), and lower Cuisian strata from the Mediona, Orpí and Santa Càndia formations were present southeast of the Montmell Fault and unconformably overlying Cretaceous rocks of the Montmell-Garraf Basin area (Figure 5.5A). The upper Cuisian to Lutetian Carme, Valldeperes and Bosc d'en Borràs formations might have been deposited in the same area. However, the precise extension of these Paleogene successions towards the southeast remains uncertain due to their erosion. The third and most relevant compressional phase regionally occurred from Middle Eocene to early Oligocene (Guimerà and Santanach, 1978; Guimerà, 1984; Anadón *et al.*, 1985). This period characterizes the formation of the CIC and, the compressional structures that emerged in the study area. A detailed description of this phase, supported by structural, provenance and magnetostratigraphic data shown in the Chapters 2 and 3, is described in detail in the next section, focussing on the absolute ages of the inversion and emplacement of the different compressional structures.

A: Paleocene to late Lutetian (pre-compression stage)

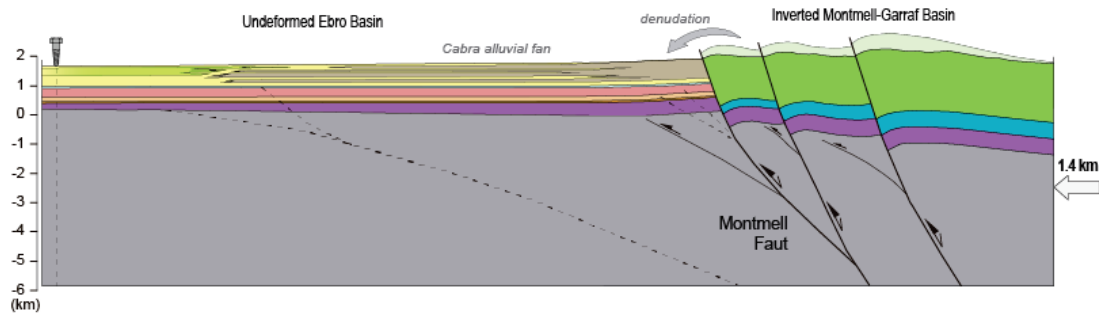
NW-SE

Mesozoic sediments of the Montmell-Garraf Basin overlaid by a pre-compression Paleocene to lower Eocene succession.

**B: Bartonian - early Priabonian (syn-compression I stage)**

Tectonic inversion of the Montmell-Garraf Basin.

Start of the Catalan Intraplate Chain build-up: uplift, denudation and sediment transport of exhumed Mesozoic towards the NW. Deposition of the syn-compression I (syn-inversion) sequence north of the Montmell Fault.

**C: Early to late Priabonian (syn-compression II stage)**

Development of the Gaià-El Camp Thrust as a major short-cut of the Montmell Fault.

Uplift and erosion of the Miramar-Gaià Domain including the syn-compression I sequence. Deposition of the Sant Miquel del Montclar conglomerates (syn-compression II sequence).

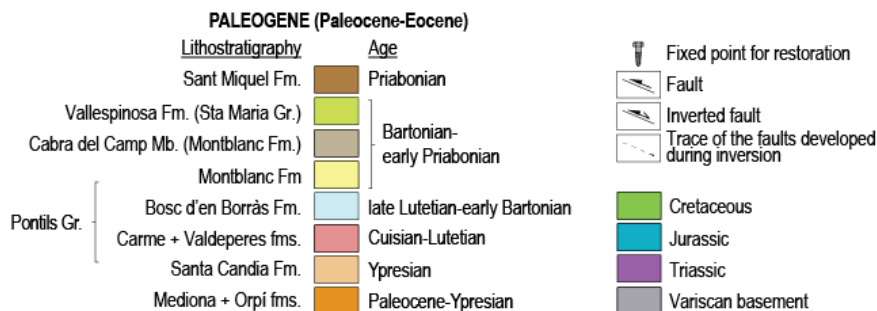
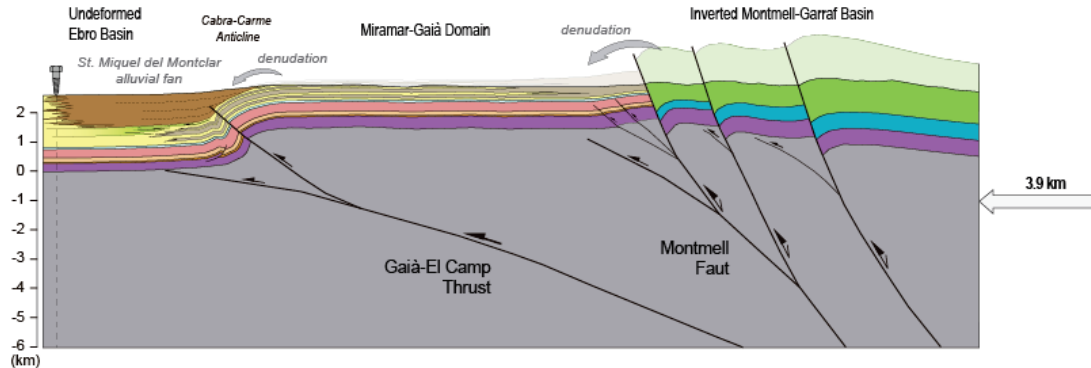


Figure 5.5. Schematic sequential structural restoration of the Gaià-Montmell Section applying flexural slip and bed length preservation. **A)** late Lutetian pre-compressional stage. **B)** late Lutetian – middle Bartonian syn-compressional stage. **C)** middle Bartonian to late Priabonian latest stages of the compressional stage. The images include the location of the later compressional structures. See approximate location of the reconstructed section in Figure 5.1. No vertical exaggeration.

5.3.2. Paleogene compressional evolution in the Gaià-Montmell High: positive inversion of the Montmell Fault and emplacement of the Gaià-El Camp Thrust

The first significant compressional signs in the Gaià-Montmell High (GMH) correspond to the tectonic inversion of the Montmell Fault, which drives the uplift of Montmell-Garraf Basin and the overlying strata over the undeformed Ebro Basin (Figure 5.5B). This inversion is characterized by the development of footwall short-cuts in the upper part of the reactivated extensional faults, the formation of the thin-skinned compressional system northwest of the Montmell Fault (the so-called "L'Arboçar Deformation strip") (Figure 5.2B), as well as the development of buttressing resulting in the SE-directed backthrusts and pop-up structures as observed in the hangingwall fault damage zone of the Montmell Fault in the Marmellar Accommodation Zone (see Figure 5.1 for location; detailed explanations of the hangingwall deformation in Chapter 3). The uplift of the Montmell-Garraf Basin triggered the denudation of the exposed rocks and the sedimentation of what has been interpreted as the first syn-compression sequence recorded in the studied sector of the southeast Ebro Basin margin (SMM area in Figure 5.1). The base of this succession corresponds to the first conglomerates of the Cabra del Camp Mb. (Montblanc Fm.), the concordance with the strata underneath of which denotes that their deposition was pre-Gaià-El Camp Thrust emplacement (Figure 5.6). This result contradicts previous interpretations of the area that included Cabra del Camp Mb. as part of a growth sequence or progressive unconformity related to the formation of the CIC during the Eocene (Anadón *et al.*, 1986).

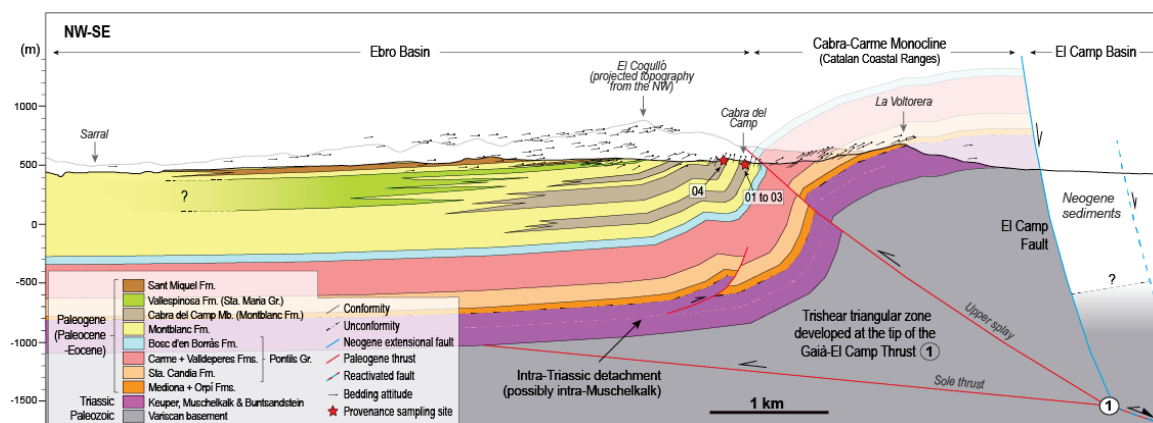


Figure 5.6. Geological cross-section of the SE margin of the Ebro Basin across the locality of Cabra del Camp (Cabra Section in Figure 5.1). The section includes the NW frontal structure of the Catalan Coastal Ranges (Cabra-Carme Monocline) as well as the location of the Cabra del Camp Mb. (Montblanc Fm.) sampling sites referred in the text.

The contractional reactivation of the Montmell Fault is also supported by the magnetotelluric (MT) data, which allows the interpretation of this inherited Mesozoic fault as a SE-dipping band of relatively low resistivity 2 km depth underneath the NW limit of the Montmell Domain (see 2D MT model in Chapter 2). The origin of this band is interpreted as related to a mechanical boundary that controls the

spatial limits of tectonic reactivation, which triggers a higher degree of deformation that would correspond to the damage zone located at the Montmell Fault footwall. The conductivity of this damage zone would be enhanced by the presence of fluids within fractured and permeable rocks (e.g., Pous *et al.*, 2001).

The presence of an alluvial system at the footwall of the Montmell Fault extending up to the present-day location of Cabra del Camp is proposed for this period (Cabra alluvial fan system, Figure 5.5B). This reconstruction contemplates the presence of unpreserved proximal alluvial facies at the foothills of the inverted Montmell-Garrafa Basin, which laterally change to distal facies towards the northwest above the still inactive Gaià-El Camp Thrust. This is also supported by the provenance analysis performed in clast samples from the Cabra del Camp Mb. conglomerates (Figure 5.6), which shows NW-directed paleocurrents and clasts consisting of Cretaceous rocks comparable to the formations described in the Montmell-Garrafa Basin (Esteban, 1973; Esteban and Robles, 1976; Salas *et al.*, 2001; Moreno-Bedmar *et al.*, 2017) (see Chapter 3 for further details about clast identification). Consequently, the Cabra del Camp Mb. conglomerates can be described as the distal remains of an alluvial system that expanded over the Miramar-Gaià Domain (Figures 5.5 and 5.6). Towards the northwest, the Cabra alluvial system would laterally interfinger and grade into the finer-grained facies of the Montblanc Fm. and the marine sediments of the Vallespinosa Fm.

The age of the beginning of the inversion and the uplift of the Montmell-Garrafa Basin has been established from the paleomagnetic analysis performed in Paleogene successions from the southeastern Ebro Basin margin (Figure 5.7). This analysis constrains the age of the base of the Montblanc Fm., its lateral equivalent the Cabra del Camp Mb. and, therefore, the age of the inversion of the Montmell Fault as early Bartonian (41Ma). Further details of these results are included in the publication in the Chapter 3 (Marín *et al.*, 2025), which refine the previous, and approximated estimates of the inversion as post-early Ypresian (post-Ilerdian) that are present in the publication in Chapter 2 (Marín *et al.*, 2021).

The compressional deformation continued and the whole ensemble of the Miramar-Gaià Domain became uniformly uplifted by the Gaià-El Camp Thrust (Figure 5.5C), a low-angle thrust interpreted as a major footwall short-cut of the Montmell Fault (see Chapter 2). The emplacement of the Gaià-El Camp Thrust is the responsible of the formation of the Cabra-Carme Monocline, that represents the front of deformation of the Catalan Coastal Ranges and the margin of the Ebro Basin at this location. As deformation progressed the previously deposited succession corresponding to the syn-compression I stage (Figure 5.5B) became folded (Figure 5.5C). During this second stage of compressional deformation, the Sant Miquel Fm. conglomerates were deposited as the result of the uplift, denudation, and transport of coarse-grained sediments from the adjoining reliefs towards the southeast. The internal structure of these conglomerates includes at least two intraformational angular unconformities (López-Blanco *et al.*, accepted), fact that is coherent with its deposition during the coeval development of the Cabra-Carme Anticline. The observed geometries agree with the interpretation of the frontal structure

as a fault-propagation fold developed by a triangular shear zone at the tip of the Gaià-El Camp Thrust (Marín *et al.*, 2021, see Chapter 2 for further details).

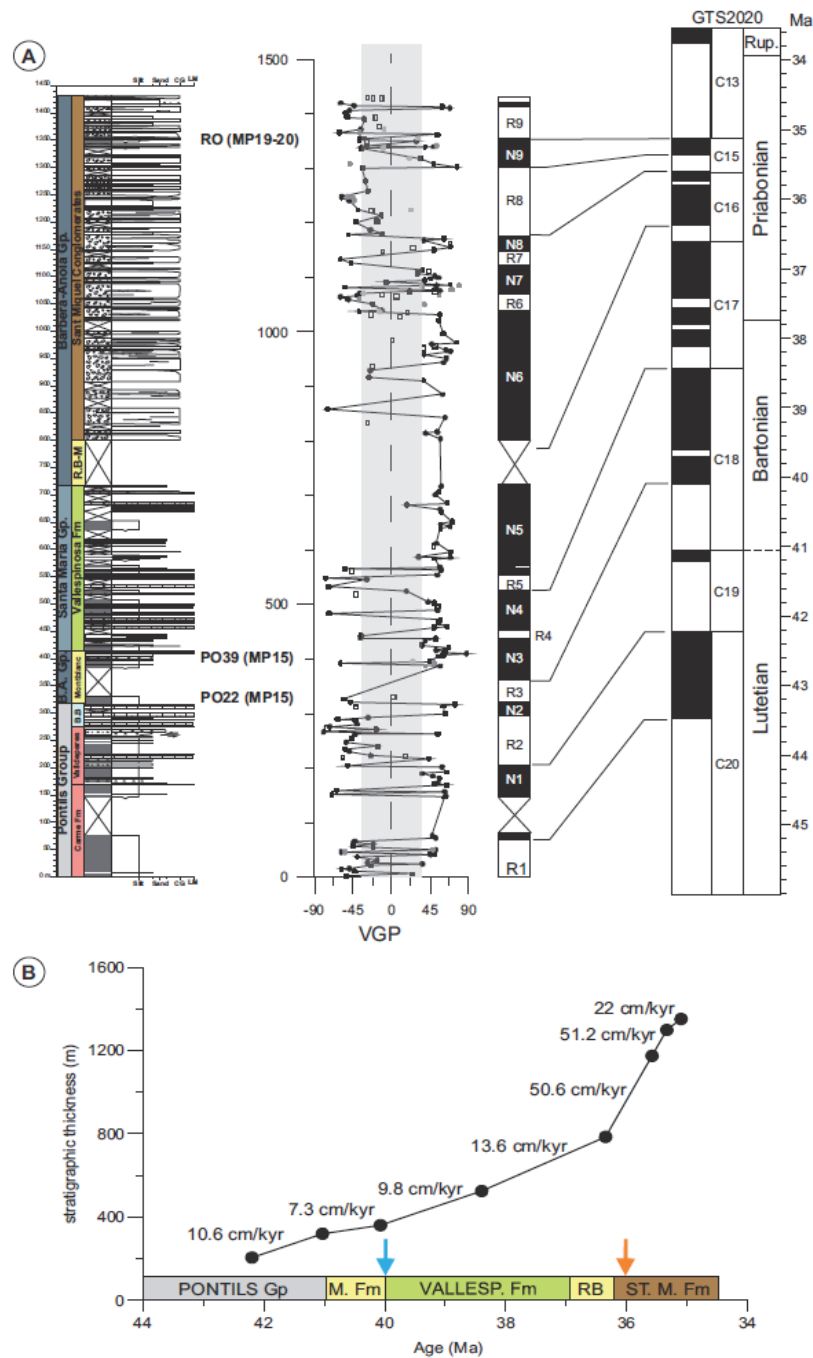


Figure 5.7. Magnetostratigraphy of the Pontils section. **A)** Magnetostratigraphic section and correlation to the GPTS (Gradstein *et al.*, 2020). PO and RO correspond to Pontils and Rocafort de Queralt fossil sites, respectively, with their attribution to Mammal Paleogene Reference Levels in brackets. White squares in the VGP graph represent type 3 directions, discarded to build the local magnetostratigraphy. B.A. Gp., B.B. and R.B.-M stand for Barberà-Anoia Group, Bosc d'en Borràs and Riu de Boix-Montblanc formations in the stratigraphic column. **B)** Sedimentation rate values and evolution for the Pontils section. Blue arrow: Bartonian transgressive event at the base of Santa Maria Group. Orange arrow: time of disconnection from the ocean of the Ebro Basin.

The results of the provenance analysis in clasts from the Sant Miquel Fm. conglomerates indicate that Barremian-Aptian orbitolinids and early Ypresian (Ilerdian) *Alveolina* are prevalent throughout the studied samples. This denotes the continuation of tectonic inversion of the Montmell Fault and the uplift and denudation of the Montmell-Garraf Basin as well as a potential cannibalization of the proximal zones of the previously deposited Cabra alluvial system. Additionally, if we consider the results of the magnetostratigraphic analysis (Figure 5.7) (see Chapter 3 for further details, Marín *et al.*, 2025) and the abovementioned geometrical relationships within the Sant Miquel conglomerates, it is possible to refine the age of deformation as Priabonian (~36Ma) and not as late Bartonian (~41Ma) as previously suggested in the work included in Chapter 2 (Marín *et al.*, 2021). The end of the compressional deformation in the Gaià-Montmell High area is difficult to establish in the study area because of the limited stratigraphic record. However, it probably ended in the uppermost Priabonian, as suggested by the end of the conglomeratic sedimentation and the presence of lacustrine facies that would imply a transition to tectonic quiescence (Anadón *et al.*, 1985 and 1989).

Sedimentation rates calculated from the Pontils magnetostratigraphic section analysis (Figure 5.7B; see Chapter 3 for further details) provide a tight correlation with the proposed tectonic evolution of the central Catalan Coastal Ranges during this period. Late Lutetian pre-compression stage (Figure 5.5A) shows the lowest sedimentation rates (7.3cm/kyr) that correspond to a stage of tectonic quiescence. The Bartonian-early Priabonian stage (syn-compression I, Figure 5.5B) shows an increased but still relatively low sedimentation rate (9.8 to 13.6cm/kyr) during the tectonic inversion of the Montmell-Garraf Basin. A progressive rise in subsidence rates with an abrupt increase of the rates (up to 51.2cm/kyr) is present during the early Priabonian-late Priabonian stage (syn-compression II, Figure 5.5C), which is interpreted as the continuation of the Montmell-Garraf Basin inversion and the onset of the Gaià-El Camp Thrust emplacement. A decrease from 51.2cm/kyr to 22cm/kyr of the sedimentation rates is interpreted as related to the end of the compression, also shown by the early Rupelian low sedimentation rates (6cm/kyr), as recorded at neighbouring areas by Barberà *et al.* (2001).

5.3.3. Paleogene compression and inversion along the Montmell-Vallès Fault System

The Cenozoic structure of the central CCR is mainly controlled by two major ENE-trending structures: the Montmell-Vallès Faults System (MVFS) and the Barcelona Fault (Figure 5.8). These basement-involved faults dip to the SE, display a right-stepping en-echelon arrangement and, as previous studies illustrate, experienced Paleogene contractional motions followed by Neogene extension (Bartrina *et al.*, 1992; Roca and Guimerà, 1992; López-Blanco *et al.*, 2000a; Gaspar-Escribano *et al.*, 2004; Marcén *et al.*, 2018).

Evidence of tectonic inversion during the Paleogene is present all along the central Catalan Coastal Ranges, and mainly preserved in the Neogene structural highs. The development of Paleogene basement-involved ENE-trending folds and thrusts, as seen in the footwall of the MVFS, evidences

the positive inversion of this inherited Mesozoic fault system during the Paleogene compressional phase (Gaspar-Escribano *et al.*, 2004). Specifically, tectonic inversion is substantiated by the compressional reactivation of the low-dipping lower panel of the faults and the formation of the footwall short-cuts, as it is exemplified by the development of the Gaià-El Camp Thrust in the southern and central sectors of the MVFS. Similarly, the Prelitoral Thrust (López-Blanco, 2000b; Gaspar-Escribano *et al.*, 2004) should be considered as its equivalent in the northern sector of the MVFS (Figure 5.9). Detailed descriptions of these compressional structures in the southern sector of the fault system (Montmell area), involving major and minor footwall short-cuts are included in Chapter 2 (Marín *et al.*, 2021).

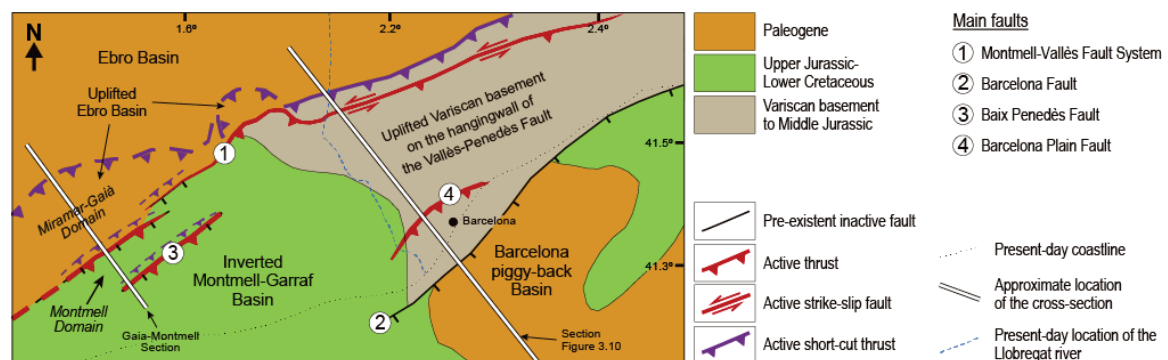


Figure 5.8. Tectonostratigraphic map showing the end of the positive inversion of the Mesozoic faults and contractional footwall short-cuts in the central Catalan Coastal Ranges at late Oligocene (approximately 28My). The location of the Gaià-Montmell Section and the section in Figure 5.10 are also indicated.

On the other hand, reactivation of the upper fault panels appears limited and shows notable differences along-strike the MVFS. Left-lateral displacement of the steep upper panels of the fault system is recognized in the northern sector (Ashauer and Teichmüller, 1935; Llopis, 1947; Guimerà, 1984; Anadón *et al.*, 1985; Julià and Santanach, 1984, 1998) (Figure 5.9). This fact is coherent with the oblique trend of the MVFS to the regional shortening direction (i.e., N-S shortening vs. NE-trending faults; Guimerà, 1984; Guimerà *et al.*, 2004). However, this transpression is not generalized and, while mainly observed in the northern sector of the MVFS (Vallès area) it hasn't been recognized in the central and southern segments of the fault system (Penedès and Montmell areas). The strike-slip component is, however, limited in the northern sector (Vallès area), and a notable the development of footwall short-cuts is present (Figure 5.9). This circumstance would reinforce the idea of the presence of an inherited Mesozoic precursor in this area (i.e., the fault limiting the Upper Jurassic- Lower Cretaceous Montmell-Garraf Basin towards the northwest), which, at least, would have been present up the current location of the La Garriga town.

In the northern sector of the MVFS, the fault zone related to the emplacement of the Paleogene thrust sheets is mostly characterized by 1) a fault core mainly formed by foliated clay gouges with abundant shear bands that denote a thrust transport direction towards the north and northwest, and 2) a damage

zone consisting of a system of amalgamated thrusts and deformation bands that define different scale duplexes. These deformation features predominantly developed in Paleozoic phyllites and wackes and, to a lesser extent, in thin Triassic carbonate rocks. Consequently, foliated fault gouges and minor cement precipitation compared to the central and southern sectors are present in this area (Cantarero *et al.*, 2014a).

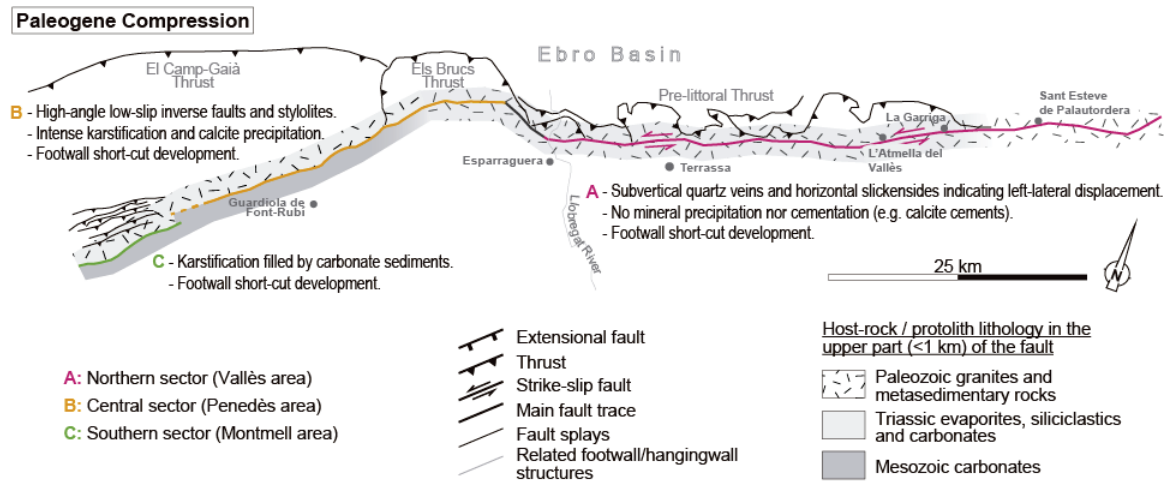


Figure 5.9. Schematic map of the Montmell-Vallès Fault System showing fault damage zone characteristics of three sectors (A, B and C) during the Paleogene compressional phase. Fluid and petrological descriptions compiled after Travé and Calvet (2001), Baqués *et al.* (2008, 2010, 2012, and 2014), and Cantarero *et al.* (2014a and 2014c).

Pliocene and Quaternary sediments frequently cover Mesozoic and late Oligocene-Neogene extensional faults of the central and part of the southern sectors of the MVFS (Gallart, 1981), which makes difficult the study. Additionally, the presence of relatively thick Middle to Upper Triassic evaporite and mudstone stratigraphic levels result in the formation of drape and fault-propagation folds above the MVFS (e.g., Marmellar Section shown in Chapter 2, Marín *et al.*, 2021). These folds absorbed part or all the motion of the underlying basement faults, delayed their upwards propagation and, therefore, prevented or hampered the observation and recognition at surface of the fault zones related to the motion of the MVFS. Compression in these sectors is also represented at surface by buttressing structures (minor folds, thrusts and backthrusts) in their hangingwall, reflecting a minor degree of positive inversion during Paleogene times. As previously pointed out, this type of deformation is described in the Marmellar Accommodation Zone (see location in Figure 5.1) where SE-directed backthrusts and pop-up structures are observed in the hangingwall fault damage zone of the Montmell Fault (Baqués *et al.*, 2012 and Marín *et al.*, 2023 in Chapter 4).

The direct observation at surface of Paleogene fault zones in the central and southern sectors is limited and can only be described in the newly formed footwall short-cuts thrusts (e.g., Els Brucs Thrust in the Penedès area, Figure 5.9). This fault zone is predominantly characterized by the presence of intense karstification processes and a 1 to 3m-thick fault core constituted by calcite-cemented breccias and

cataclasites, vertical non-cemented stylolites when developed in Triassic carbonate rocks as well as foliated clay gouges with abundant shear bands and no cement precipitation when formed in metamorphic Paleozoic rocks (Cantarero *et al.*, 2014c). However, as we move towards the southwest along the trace of the MVFS, a notable increase of calcite cemented breccias and NNW-trending extensional faults filled by calcite that formed during the Mesozoic characterize this fault zone (Guardiola de Font-Rubí in Figure 5.9; Baqués *et al.*, 2012). These pre-existing features are cut by minor ENE-trending reverse and strike-slip faults filled by calcite cements that can be related to compression and, therefore, the tectonic inversion of the previous Mesozoic extensional fault in this area during the Paleogene (Amigó, 1984; Baqués *et al.*, 2012).

5.3.4. Comparison between the Paleogene compression in the southern and northern sectors of the central Catalan Coastal Ranges

A comparison between the interpreted compressional structures in the Gaià-Montmell Section (southern sector of the central Catalan Coastal Ranges) and a section through the northern sector previously published by Roca *et al.* (1999) and structurally restored by Gaspar-Escribano *et al.* (2004) has been performed in order to provide regional insights about tectonic evolution of the area during the Paleogene compressional phase.

The Figure 5.10 shows the structural reconstruction of the northern sector of the central Catalan Coastal Ranges and the Valencia Trough domain at the end of the compressional stage (Early Oligocene, 30Ma). The main structures included in this reconstruction are from northwest to southeast: 1) the Ebro Basin, filled-up by Paleogene sediments covering a thin Mesozoic cover; 2) the Prelitoral Range, which represents the frontal structure of the Catalan Intraplate Chain (CIC) and developed as result of the NW verging contractional structure that uplifts a ~20 km wide area of exhumed Variscan basement to the southeast (hinterland) and a thin Mesozoic cover to the northwest (foreland); 3) the Barcelona piggy-back basin filled-up with Oligocene sediments overlaying an area where the Mesozoic cover thickens towards the Valencia Trough domain.

The Paleogene compressional stage in this northern sector occurs in four different pulses from Late Paleocene to Early Oligocene (Gaspar-Escribano *et al.*, 2004), three responsible of the development of the Prelitoral Range and the last responsible for the development of the Barcelona piggy-back Basin. The first pulse starts in the Paleocene-Eocene boundary (53Ma) (López-Blanco, 2002) and reactivates with reverse motion and sinistral strike-slip movement (Guimerà, 1984) the pre-existent northern segment of the MVFS until the end of Ypresian (49Ma). The second pulse, from Lutetian (~45Ma?) to Bartonian (~36Ma?), is the responsible of the developing of the frontal anticline of the CIC, but implied low shortening (López-Blanco, 2002). This pulse continued and evolved to the third active faulting pulse from Bartonian (35Ma?) to Rupelian (29Ma) (López-Blanco *et al.*, 2000a). Finally, southeast

towards the hinterland, compression took place during the early to late Oligocene transition (latest Rupelian-early Chattian) leading the development the Barcelona piggy-back basin (Parcerisa *et al.*, 2007). The analysis of the Barcelona Basin fill shows an Upper Eocene-Oligocene succession that is coeval to the development of the CIC (Roca *et al.*, 1999). Occurrences of sediments with similar age (Oligocene) are also present in the footwall of the Barcelona Basin in an area affected by compressional features (Parcerisa, 2002; Parcerisa *et al.*, 2007).

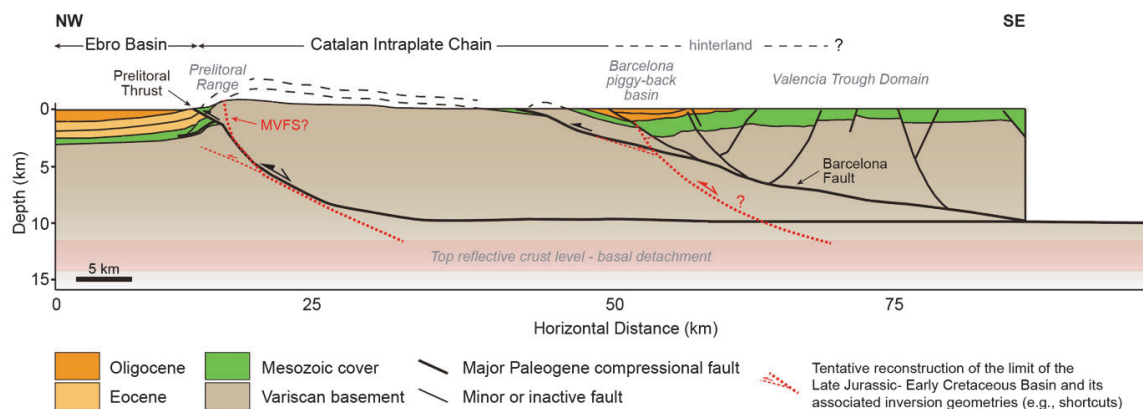


Figure 5.10. Structural reconstruction of the northern sector of the central Catalan Coastal Ranges and the Valencia Trough domain at the end of the compressional stage (late Oligocene - Chattian, approximately 28Ma). An estimate location of the limit of the Late Jurassic-Early Cretaceous rift basin is shown with red dashed-lines. Depth of the basal detachment corresponding to the top of the reflective crust based on Fernández and Banda (1990), Sàbat *et al.* (1997) and Roca *et al.* (2004) (modified from Gaspar-Escribano *et al.*, 2004).

A summary of all these kinematic pulses is illustrated in Figure 5.11 providing a comparison with the fault activity ages proposed for the southern sector of the central CCR including the Montmell Fault inversion and the development of the Gaià-El Cap Thrust. The age comparison agrees with the earliest syn-tectonic sediments recorded along the margin (Ypresian-early Cuisian Cairat Fm.), deposited northeast in the northern sector in the Montserrat-Sant Llorenç del Munt area (López-Blanco, 2002) (Figure 5.1), and the fact that the compressional deformation in the Catalan Coastal Ranges progressed from northeast to southwest up to the Late Oligocene (Chattian) (Guimerà, 1984; Anadón *et al.*, 1985).

Some previous works account for the presence of an inherited Mesozoic structure, related to changes in thickness of the Jurassic-Cretaceous sequences that potentially acted as weakness zones within the crust during the Paleogene development of the central CCR (e.g., Roca and Guimerà, 1992, Gaspar-Escribano *et al.*, 2004). However, the proposed reconstructions do not account to the effect and control of the extensional Mesozoic fault geometry on the later compressional phase. A tentative reconstruction of the limits of the Late Jurassic-Early Cretaceous rift basin, together with their associated inversion-related structures (e.g., footwall short-cuts) is added to the section in Figure 5.10. This inherited structure would be rooted to a basal detachment corresponding to the top of the reflective crust between 12 and 15 km depth (Fernández and Banda, 1990; Sàbat *et al.*, 1997).

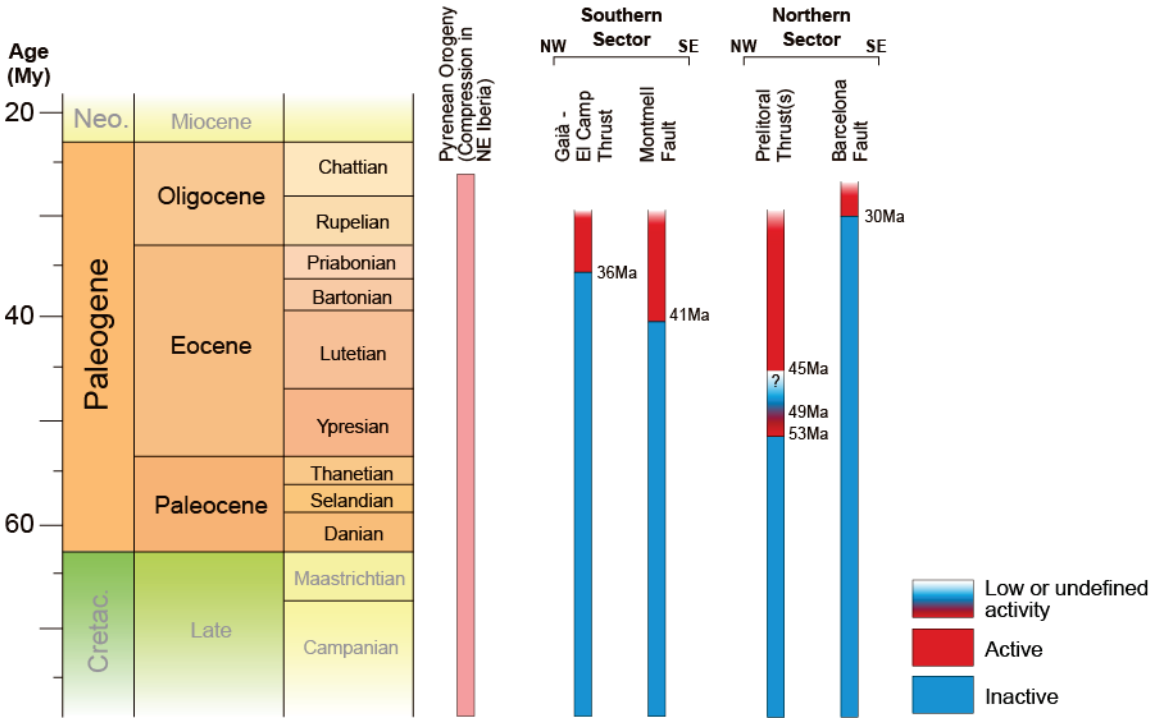


Figure 5.11. Time chart showing the periods of tectonic activity of each individual major fault in the southern and northern sectors of the Central Catalan Coastal Ranges during the Pyrenean Orogeny (see the location of the sectors in Figure 5.1). Ages for the southern sector are based on the results of this research. Ages for the northern sector are based on previous publications (e.g., López-Blanco *et al.*, 2000a; López-Blanco, 2002; Parcerisa *et al.*, 2007; Gaspar-Escribano *et al.*, 2004).

5.4. Neogene extension and negative inversion in the central Catalan Coastal Ranges

5.4.1. Neogene extension in the Gaià-Montmell High

The Paleogene structure of the Gaià-Montmell High (GMH) previously described in Section 5.3 was later imprinted by the Neogene extensional deformation that cut or reactivate the inherited compressional structures in the CCR from latest Oligocene to late Miocene (Bartrina *et al.*, 1992; Roca, *et al.*, 1999; van Hinsbergen *et al.*, 2014). In general terms, as previously stated, the GMH corresponds to a major relay zone between two major NE-SW-trending, SE-dipping faults: the Montmell-Vallès Fault System (MVFS) and the El Camp Fault, though, a closer view reveals that the structure of the GMH exhibits further complexities related to the extensional phase during the Neogene (Figure 5.12).

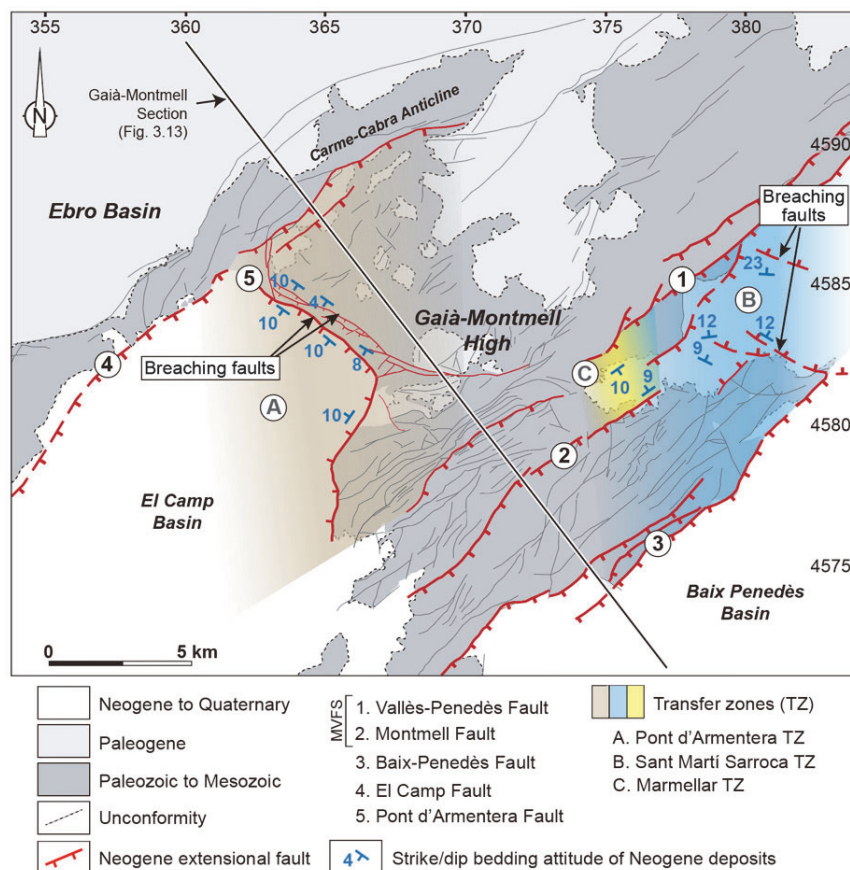


Figure 5.12. Schematic geological map of the Gaià-Montmell High pointing out the major Neogene extensional faults. Up to three relay ramps linking extensional faults are present in the area.

The Vallès-Penedès Fault exhibits a progressive reduction in its displacement towards the southwest. As a result, the Vallès-Penedès Fault oversteps the Montmell and Baix Penedès faults in the respective Marmellar and Sant Martí Sarroca transfer zones, which are characterized by NW-SE-oriented breaching faults (Figure 5.12). Consequently, the extensional displacement is transferred to the Montmell and Baix Penedès faults, which propagates towards the southwest with a comparable

orientation. The Montmell Fault shows a low accumulated extensional displacement. The Baix Penedès Fault, instead, shows a considerably higher accumulated throw reaching several hundreds of meters represented by a segmented fault pattern with several SE-dipping splays at surface (Figures 5.12 and 5.13). As seen in the Gaià-Montmell Section (Figure 5.13), the Baix Penedès Fault is interpreted as rooted at the deep SE-dipping basement ramp underneath the area. In contrast, in the western side of the GMH, the displacement of the El Camp Fault experiences a pronounced drop towards the northeast, culminating in a narrow assemblage of SE-dipping faults characterized by hectometric accumulated displacements along the Carme-Cabra Anticline backlimb (Figure 5.13). Considering the geometry of the Miramar-Gaià Domain, which arises from displacement and uplift over a low-angle basement ramp that shallows towards the northwest, this array of extensional faults at the northeastern terminus of the El Camp Fault has been interpreted as being rooted in the Gaià-El Camp Thrust. Within this framework of overlapping extensional faults, the NW-SE-oriented faults observed in the Sant Martí Sarroca Transfer Zone and the Pont d'Armentera Fault (Figure 5.12) are regarded as relay ramp breaching faults of a soft linked extensional system (Fossen and Rotevatn, 2016). These zones facilitate the transfer of displacement between the Vallès-Penedès and Baix Penedès faults, as well as between the El Camp Fault and the Montmell-Vallès Fault System, respectively.

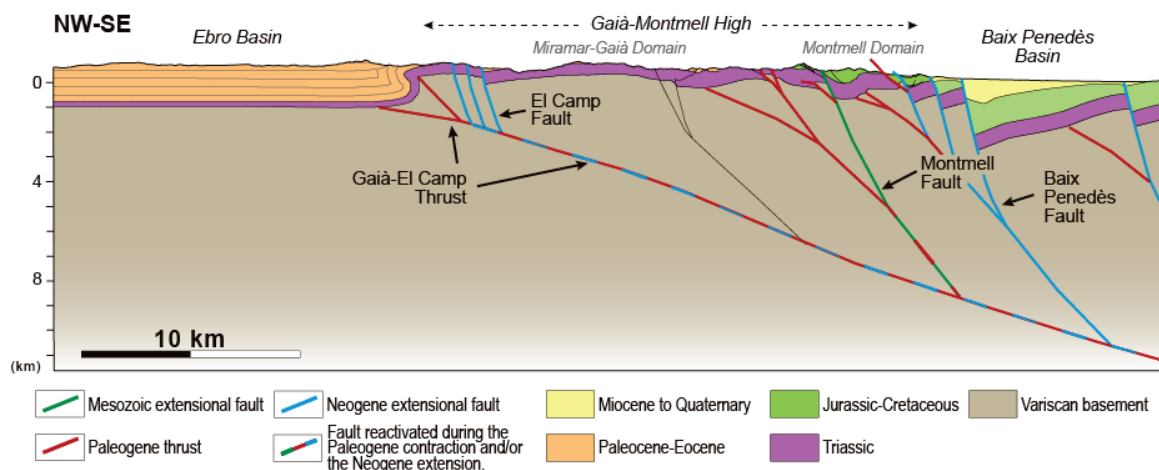


Figure 5.13. Structural cross-section across the Gaià-Montmell High illustrating the age of the different faults that are present in the area as well as their reactivation during the Cenozoic.

Several indicators suggest the extensional reactivation (or negative inversion) of pre-existing faults including: 1) the formation of an array of extensional faults that are rooted in the discrete fault plane of the Paleogene Gaià-El Camp Thrust at the NE extremity of the El Camp Fault; 2) the extensional geometry of the Montmell Fault, despite its reverse movement during Paleogene times; or 3) the Baix Penedès Fault and its splays, which also root in the Paleogene reverse fault footwall ramp. However, the reactivation of the Montmell Fault is comparatively constrained, with the extension predominantly being relayed to the Baix Penedès Fault.

All the aforementioned structural observations suggest a latest Oligocene-Miocene extensional phase that led to the reactivation of pre-existing Late Jurassic-Early Cretaceous and Paleogene fault systems. Accordingly, the array of extensional faults formed at the NE end of the El Camp Fault developed as hangingwall short-cuts product of the negative inversion of the Gaià-El Camp Thrust. Likewise, the Baix-Penedès Fault developed as a hangingwall short-cut during the reactivation of the sole thrust as an extensional detachment (Figure 5.13).

The timing of the reactivation can be outlined based on tectonostratigraphic relationships. For instance, the undeformed Pleistocene alluvial deposits that cover most of the major Neogene faults in the central CCR, denote that their extensional activity is pre-Pleistocene. Furthermore, as seen in the Marmellar Accommodation Zone (see Marmellar Section in Chapter 2; Marín *et al.*, 2021), major faults frequently exhibit drape-fold structures on their hangingwalls that either intersect or deform Serravallian sediments (Benzaquen *et al.*, 1972b). Consequently, their extensional motion must be accounted as post-Serravallian. Nevertheless, at this location, extensional growth strata geometries are observed in upper Serravallian-lower Tortonian sediments deposited in the Vallès-Penedès Fault hangingwall (Benzaquen *et al.*, 1972b; Baqués *et al.*, 2012), hence indicating, at least for this particular fault, extensional motion during this period. This observation is consistent with prior regional investigations that suggest the occurrence of extension in the CCR between Burdigalian and Late Tortonian/Messinian times (Gallart, 1981; Cabrera *et al.*, 1991; Cabrera and Calvet, 1996; Porta and Civís, 1996; Cabrera *et al.*, 2004). However, the absence of preserved upper Oligocene and Neogene sedimentary deposits in the Miramar-Gaià and Montmell domains prevents to establish the relative ages of activity for the observed extensional faults.

5.4.2. Mesozoic structural inheritance and Neogene fault zone characterization along the Montmell-Vallès Fault System

The pre-existing Montmell-Vallès Fault System (MVFS) became reactivated during the latest Oligocene-Miocene extensional phase taking place in the area (Bartrina *et al.*, 1992; Roca, 1994; van Hinsbergen *et al.*, 2014). However, this reactivation didn't take place equally along the whole fault system trend (Figure 5.14). Whereas the lower fault panels, characterized by a low dip, underwent extension all along the fault system (?) (Gaspar-Escribano *et al.*, 2004), the reactivation of the steep upper panels was restricted to the northern and central sectors of the MVFS (Vallès and Penedès areas). In these areas, the outcropping Vallès-Penedès Fault aligns with the trajectory of the Mesozoic fault at the broader regional scale. Nevertheless, the Neogene fault did not always reactivate the pre-existing Mesozoic fault core but developed rather extensional shortcuts in their hangingwall (Fontboté, 1954; Anadón *et al.*, 1985; Roca and Guimerà, 1992) (Figure 5.15). Conversely, in the southern sector of the MVFS (Montmell area) the steep upper panels remained almost inactive throughout the Neogene extensional period (see Montmell Fault segment in Figure 5.14).

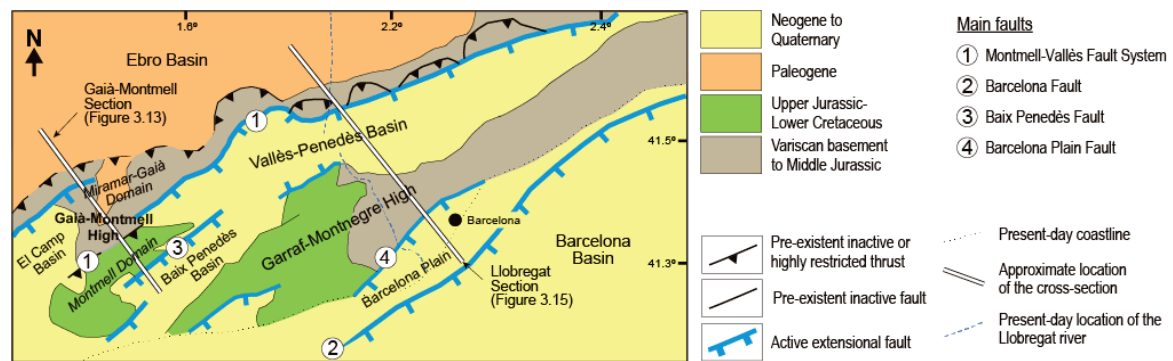


Figure 5.14. Tectonostratigraphic map showing the end of the extensional motion of the Vallès-Penedès, El Camp and Baix Penedès faults and related extensional short-cuts in central Catalan Coastal Ranges at late Tortonian (approximately 7My). The locations of the Gaià-Montmell Section (Figure 5.13) and the Llobregat Section (Figure 5.15) are indicated.

In this southern sector, the extensional reactivation of the low-angle lower fault panel culminated in the development of a major extensional shortcut represented by the Baix Penedès Fault (see Chapter 2, Marín *et al.*, 2021). Therefore, although the MVFS shows two episodes of tectonic inversion during Cenozoic times, first positive during the Paleogene (Juez-Larré and Andriessen, 2006; Gaspar-Escribano *et al.*, 2004; Marín *et al.*, 2021), and then negative during the latest Oligocene-Neogene (Fontboté, 1954; Anadón *et al.*, 1985; Roca and Guimerà, 1992; López-Blanco *et al.*, 2000a). The steep upper panels of the inherited Mesozoic faults experienced only partial reactivation in the northeastern regions of the MVFS, with no such activity occurring in its southwestern counterparts (Figure 5.13).

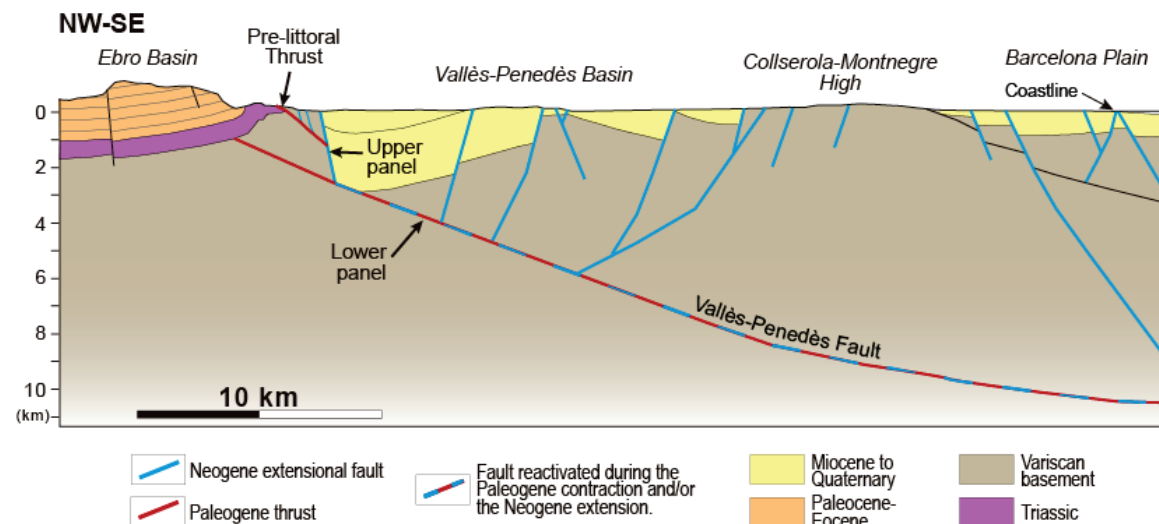


Figure 5.15. Llobregat section across the northern sector of the MVFS (Vallès area) (modified from Bartrina *et al.*, 1992). See location in Figure 5.14.

The petrological characterization of the fault zones along the three different sectors of the MVFS provides insights about the abovementioned differences of reactivation (see Chapter 4 for detailed descriptions). The northern sector of the MVFS (Vallès area; sector A in Figure 5.16) developed within

a host-rock predominantly formed by the Variscan basement (granitoids and metasedimentary siliciclastic rocks) and, at shallower levels, by a thin Triassic succession and thicker Paleogene siliciclastic sediments corresponding to the Ebro Basin fill (Figure 5.15). The fault zone related to the latest Oligocene-Neogene extension of the Vallès-Penedès Fault is characterized by 1) narrow and impermeable fault cores made up of mud-to-clast-supported non-cemented breccias; 2) cataclasites cemented by chlorite and associated calcite and laumontite minerals; 3) meteoric fluid circulation within decametric to kilometeric damage zones at surface; and 4) the presence of multiple hot springs along the fault (Cantarero *et al.*, 2014a).

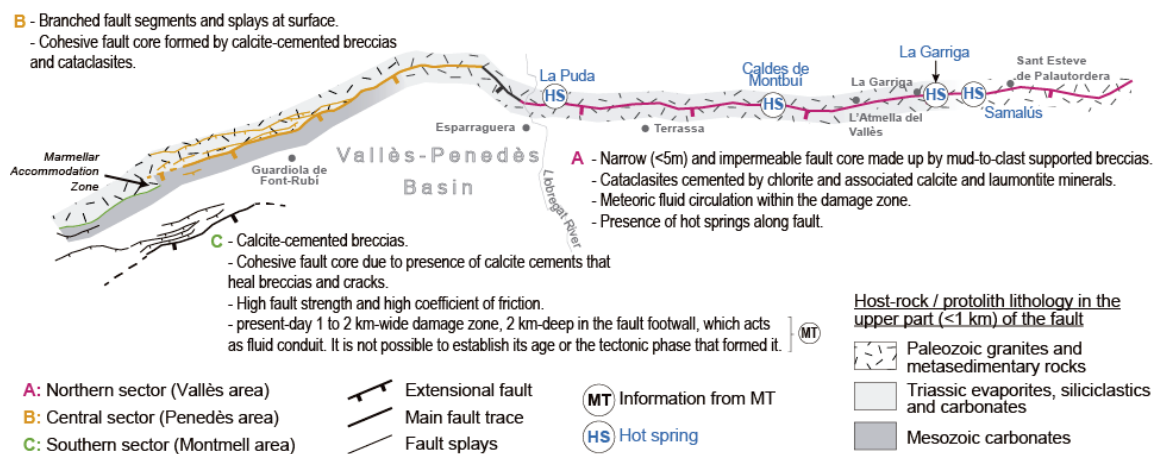


Figure 5.16. Schematic map of the Montmell-Vallès Fault System showing fault damage zone characteristics of three sectors (A, B and C) developed during the latest Oligocene-Neogene extensional phase. Fluid and petrological descriptions compiled after Travé and Calvet (2001), Baqués *et al.* (2008), Baqués *et al.* (2010), Baqués *et al.* (2012), Baqués *et al.* (2014) and Cantarero *et al.* (2014a and 2014c). Magnetotelluric data (MT) from Marín *et al.* (2021) included in Chapter 2.

In central sector (Penedès area; sector B in Figure 5.16) the MVFS developed in a host-rock mostly formed, at depth, by metasedimentary siliciclastic of the Variscan basement. However, at shallower levels, host-rocks are composed by a thin Triassic to Lower Jurassic succession including carbonate, siliciclastic and evaporite rocks overlain by a thicker Cenozoic syn-kinematic terrigenous cover. The presence of pre-kinematic evaporite and mudstone layers are the responsible of the formation of drape and fault-propagation folds above the MVFS (see cross-section in Figure 5 in Marín *et al.*, 2021; Chapter 2). These folds absorbed, partially or totally, the displacement of the underlying basement faults and prevented the surface observation of the fault zones. Moreover, the presence of post-rift Pliocene and Quaternary sediments frequently covering the Mesozoic and latest Oligocene-Neogene extensional faults makes difficult the study of this area (Gallart, 1981). For this reason, fault zones of this sector have only been described in its southern part. This area is characterized by the presence of a thick Mesozoic carbonate host-rock, two splays of the Vallès-Penedès Fault at surface (Amigó, 1984) and a metric and cohesive fault core mainly formed by calcite-cemented breccias and cataclasites (Baqués *et al.*, 2012) (Figure 5.16). The damage zone in the central sector consists of nearly vertical calcite-

cemented tension fractures and high-angle extensional faults (Amigó, 1984; Baqués *et al.*, 2012), the density of which increases towards the fault core.

In the southern sector (Montmell area; sector C in Figure 5.16), the upper panels of the MVFS formed in a host-rock with a thicker post-Triassic carbonate succession including Jurassic and Cretaceous rocks. Like in the previous sector, the relatively thick pre-kinematic Middle to Upper Triassic evaporite and mudstone layers resulted in the formation of drape and fault-propagation folds above the MVFS (see cross-section in Figure 5 in Marín *et al.*, 2021; Chapter 2). The most important fault zone associated with this sector is the one linked to the formation of the Baix Penedès Fault. This zone shows a cohesive fault core due to the presence of different generations of calcite-cemented breccias and cataclases (Baqués *et al.*, 2010, 2014), which strengthen and heal breccias and cracks (Belaid *et al.*, 2008; Baqués *et al.*, 2014).

5.4.3. Controls on the Montmell-Vallès Fault System extensional reactivation during the Neogene

From the provided descriptions, two main aspects might control the extensional reactivation of the MVFS: 1) its inherited geometry; and 2) the petrological evolution and composition of the different fault zones. From a geometrical point of view, the MVFS shows similar kinked-planar geometry all along its trace. This geometry is characterized by an upper panel dipping $>60^\circ$ towards the SE that passes into a lower panel that dips around 30° at depth (Figure 5.15). This less dipping lower panel would most likely correspond to the continuation of the Paleogene thrusts, the Pre-littoral Thrust in the northern sector, the Gaià-El Camp Thrust in the central and southern sectors and, probably, continuing towards the southwest of the GMH, underneath of the El Camp Basin. Considering the constant orientation of the stress field across the region during the Neogene extension (Bartrina *et al.*, 1992; Herraiz *et al.*, 2000), the differences in Neogene reactivation cannot be only explained by potential variations in the local stress due to changes in the fault plane orientation and dip. Therefore, the inherited rheology of the pre-existent fault rocks, and the influence of mineralizations and cementations within the fault zones during previous tectonic phases should be contemplated as a factor to explain the different reactivation.

The extensional reactivation of the Montmell-Vallès Fault System during the Neogene was primarily observed in regions with siliciclastic host-rocks and non-cohesive gouge in the fault core. In these cases, the weaker fault rocks facilitated reactivation. Conversely, reactivation was limited or absent where thick carbonate successions were present, and pre-existing fault rocks were composed of well-cemented cohesive carbonate breccias. It is likely that cementation with calcite and other minerals increased the strength of fault rocks, raising the failure envelope and welding fault breccias to the host-rock, preventing fault planes from serving as weaknesses during deformation. This aligns with investigations in the Vallès-Penedès Fault (Travé *et al.*, 1998; Belaid *et al.*, 2008) as well as other Neogene faults in the

Catalan Coastal Ranges (Cantarero *et al.*, 2014b, 2018), which demonstrate that carbonate precipitation sealing fault planes may obstruct reactivation or reduce fault slip capacity (Li *et al.*, 2003; Ferrill and Morris, 2008; Hausegger *et al.*, 2010; Ferrill *et al.*, 2011; Hooker *et al.*, 2012).

The mechanical properties of fault rocks within the MVFS zones differ due to mineralizations and/or cementations, such as calcite precipitation, influencing the Neogene reactivation pattern. While siliciclastic rocks from the Variscan basement and Triassic are present across all sectors, only parts of the central and southern sectors exhibit a well-developed Mesozoic carbonate cover responsible of the cohesive calcite-cemented fault breccia development. In the northern sector, low calcite precipitation is present in the fault zone (Cantarero *et al.*, 2014a), rock strength remained low, and reactivation was smooth. This reactivation was likely facilitated by silicate-rich fault gouge, reducing fault strength and coefficient of friction (Wang *et al.*, 1980; Wintsch *et al.*, 1995; Alder *et al.*, 2016). Instead, in the southern sector, petrological and geochemical analysis (i.e., Baqués *et al.*, 2012) show that this area had very low or non-existent permeability and, therefore, very low fluid pressure and higher strength at the end of the Paleogene compression.

To summarize, the rheology of fault rocks played a crucial role in the reactivation of the Mesozoic fault system. Reactivation was favoured in areas where Variscan basement was involved in deformation, whereas it was limited in regions with a thick carbonate-rich Mesozoic cover. This led to differential evolution among the three studied sectors, which can be summarized as follows:

- Northern sector: reactivation was facilitated by weak fault gouge in basement-involved deformation.
- Central sector: shallow fault zones with cemented fault breccia were insufficient (possibly too short and too thin) to counteract weak fault gouge at depth.
- Southern sector: well-developed and cemented breccias appeared extensive enough (longer and wider) to inhibit or decrease reactivation of underlying weak fault gouge.

Summarizing, the distinct mechanical and structural characteristics across the sectors underscore varied reactivation processes and fault zone development.

CHAPTER 6

SUMMARY OF THE CONCLUSIONS

6.1. Tectonic evolution and structural inheritance in the Gaià-Montmell High

6.2. Structural inheritance and control factors of the reactivation along the MVFS

6.1. Tectonic evolution and structural inheritance in the Gaià-Montmell High

The new field-based and magnetotelluric (MT) dataset acquired across the Gaià-Montmell High has allowed the characterization of the main features of its Alpine crustal structure.

The structural configuration of the Gaià-Montmell High comprises two domains with a differentiated tectono-stratigraphic evolution. These domains are:

- 1) Miramar-Gaià Domain: area with a very thin Mesozoic succession (only Triassic) uplifted over the Ebro Basin by a NW-vergent, low-angle basement thrust (the Gaià-El Camp Thrust).
- 2) Montmell Domain: area with a well-developed Mesozoic succession including Triassic, Jurassic and Cretaceous rocks and limited towards the NW by the Montmell Fault. Its structure involves NW-vergent compressional faults affected by SE-dipping high-angle extensional faults.

A deformed zone in the footwall of the Montmell Fault including the presence of NW-vergent thrust systems are present in the limit between the two domains listed above.

MT data along the Gaià-Montmell Section has enabled the delineation of the subsurface structure and the recognition of zones depicting potential fractures, conductive fluids and/or mineralizations belonging to Montmell fault hangingwall at depth.

The Montmell Fault represents the southwest prolongation of the Vallès-Penedès Fault. Together they form the Montmell-Vallès Fault System (MVFS). The area of overlap and relay corresponds to the Marmellar Accommodation Zone.

The MVFS constituted the northwest boundary of the Montmell-Garraf Basin developed during the Late Jurassic-Early Cretaceous (Oxfordian to middle Aptian) rifting period. It extended several kilometres northeast of the present-day location of the Llobregat River, progressively reducing its displacement.

A period of tectonic inversion and contractional reactivation related to the Paleogene compressional phase is attested by the presence of highly deformed areas in the Montmell Fault footwall. These contractional structures include thin-skinned thrusting and footwall shortcut structures and characterize the positive inversion of the Montmell-Garraf Basin.

The emplacement of the Gaià-El Camp Thrust, a NW-directed basement thrust that uplifted the Montmell-Garraf Basin and the adjoining areas of the Ebro High. Its formation is related to a limited reactivation of the Montmell Fault and the propagation of the deformation to its footwall as a major short-cut structure

The age of the positive inversion of the MVFS was preliminarily established as, at least, late Ypresian (Cuisian) considering the preserved pre-kinematic strata in its footwall, whereas the emplacement of the Gaià-El Camp Thrust was established as late Bartonian to lower Oligocene considering syn-kinematic sediments preserved in the SE margin of the Ebro Basin. These non-conclusive timespan intervals have been refined with the integration of complementary structural, magnetostratigraphic and provenance analysis performed in synorogenic Paleogene successions at the southeastern margin of the Ebro Basin.

The new Pontils magnetostratigraphic section allows establishing the absolute ages of this syn-orogenic Paleogene strata along more than 1,400 m of succession.

The paleomagnetic study also confirms the Pontils fossil site (MP15 reference level) as Bartonian, ranging from 41 to 39.8 Ma.

The ages of the studied formations are the following: the

uppermost Carme Fm.	-	late Cuisian
Valdeperes Fm.	-	Lutetian
Bosc d'en Borràs Fm.	-	Lutetian
Vallespinosa Fm.	-	Bartonian to early Priabonian
Montblanc Fm. (including the Cabra del Camp Mb.)	-	Bartonian to early Priabonian
Sant Miquel de Montclar Fm.	-	middle to late Priabonian

The tectonostratigraphic reconstruction of the Paleogene compression allows outlining the conglomerates of the Cabra del Camp Mb. as the distal facies of an ancient alluvial system (Cabra alluvial system) that expanded northwest of the Montmell Fault over the Miramar-Gaià Domain as result of the onset of the tectonic inversion of the fault during the Bartonian to early Priabonian. This age agrees with the diachronous compression described along the SE margin of the Ebro Basin, from Ypresian in the northern sector, Bartonian in the central area, and middle to late Eocene in the south.

Provenance analysis in the Cabra del Camp alluvial conglomerates ratifies that the source area corresponded to the exhumed Montmell-Garraf Basin. The proximal facies of this alluvial system would have been deposited in the footwall of the Montmell Fault. However, these haven't been preserved due to uplift and denudation.

The composition of clasts from the Cabra del Camp Mb. suggests that the youngest stratigraphic units deposited in the Mesozoic Basin were Upper Cretaceous (Cenomanian to Turonian). This Mesozoic Basin was covered by Paleocene to Lutetian sediments (Mediona and Orpí formations and Pontils-Cornudella Group), fact that defines this as a period of tectonic quiescence. The southeast extent of these Paleogene successions remains uncertain.

A second pulse of compression is recorded during the middle to late Priabonian by intraformational angular unconformities in the conglomerates of the Sant Miquel Formation. The deformation of these

conglomerates is associated with the growth of the Cabra-Carme Monocline during the emplacement of the Gaià-El Camp Thrust, which uplifted the Miramar-Gaià Domain over the Ebro Basin.

This second pulse deformed the previously deposited conglomerates of the Cabra del Camp Mb. and lateral equivalents. The beginning of this stage is marked by the abrupt increase in the sedimentation rates related to the increase in the tectonic subsidence caused by the onset of the Gaià-El Camp Thrust.

Negative tectonic inversion of the previously formed Paleogene and Late-Jurassic faults is observed in the Gaià-Montmell High.

During Latest Oligocene(?) / early Miocene - late Miocene, the extensional slip at the southwest termination of the Vallès-Penedès Fault is relayed to the Baix Penedès Fault, which is considered as a hangingwall short-cut product of the negative inversion. Accordingly, accommodation zones characterized by the presence of relay ramp-breaching faults developed.

The negative inversion of the Gaià-El Camp Thrust is attested at the NE-end of the El Camp Fault, where an array of extensional faults developed in the Miramar-Gaià Domain.

Tectonostratigraphic relationships in the area indicate that extension occurred mainly between Burdigalian and Late Tortonian-Messinian times.

6.2. Structural inheritance and control factors of the reactivation along the MVFS

The analysis of the structural styles and the fluid-rock interactions in fault zones along the three sectors of the Mesozoic-inherited Montmell-Vallès Fault System (MVFS) allows discerning between different levels of reactivation during the Late Cretaceous to late Oligocene compression, and the Latest Oligocene(?) / early to late Miocene extension

A period of positive tectonic inversion and contractional reactivation of the pre-existing Mesozoic structure is attested by the presence of highly deformed areas along the MVFS footwall during the Paleogene compressional phase. However, this reactivation appears decoupled.

The lower 30°-dipping panels of the MVFS do reactivate practically all along the fault trace. However, the reactivation of the upper and higher-dipping fault panels is restricted in the areas containing thick carbonate protoliths.

The formation of calcite-cemented fault rocks (breccias), especially in the central and southern sectors, due to fluid circulation during the Mesozoic extensional phase would have enhanced fault strength and the coefficient of friction of the fault cores, thus limiting its reactivation. Consequently, this triggered the propagation of the deformation to the fault footwall developing shortcut structures.

The Gaià-El Camp, Els Brucs, and Pre-littoral thrusts would correspond to major short-cut thrusts uplifting the footwall of the MVFS over the Ebro Basin during the Paleogene compression.

During the Neogene extension, the negative inversion of the MVFS appears also governed by the inherited fault zone anisotropies. A decoupling of the reactivation between the upper and lower fault panels is also present. Whereas the deeper part was reactivated all along the MVFS trend, the high dipping and shallower fault panels experienced different degrees of reactivation.

The feasibility of fault reactivation appears highly controlled by three factors: 1) the host-rock lithology that characterizes fault rock types and locations, 2) the formation of cements during the main fault activity, and 3) the related change of the mechanical properties of fault rocks that governs the aptitude of the fault to be reactivated.

Reactivation was effective in areas where the host-rock was composed by granitoids and siliciclastic metasediments, and the pre-existent fault core was characterized by an impermeable and non-cohesive gouge (i.e., northern sector).

Conversely, fault reactivation was restricted, or even avoided, in areas with thick carbonate host-rock and highly cemented cohesive breccias in the pre-existing fault core (i.e., central and southern sectors

of the MVFS). These areas constituted the NW limit of an extensional basin filled-up with relatively thick carbonate successions during the Mesozoic.

Differences in reactivation within the central and southern sectors appear rather associated to the size of the highly cemented areas in the inherited fault zone. This increases towards the southwest preventing (or restricting) the reactivation in the southern sector (Montmell area) and shifting the extension towards the southeast along the Baix Penedès Fault.

REFERENCES

- Agustí, J., Anadón, P., Arbiol, S., Cabrera, L., Colombo, F., Sáez, A., 1987. Biostratigraphical characteristics of the Oligocene sequences of north-eastern Spain (Ebro and Campins basins). *Münchner Geowissenschaften Abhandlungen (A)* 10, 35-42.
- Albrich, S., Bernaus, J.M., Boix, C., Caus, E., Martín-Closas, C., Salas, R., Vicedo, V., Villalonga, R., 2006. Caracterización bioestratigráfica y paleoambiental del Cretácico Inferior (Berriasiense-Barremiense) del Macizo de Garraf (Cadena Costera Catalana). *Rev. Esp. Micropaleontol.* 38 (2-3), 429-451.
- Alder, S., Smith, S.A.F., Scott, J.M., 2016. Fault-zone structure and weakening processes in basin-scale reverse faults: the moonlight fault zone, South Island, New Zealand. *J. Struct. Geol.* 91, 177-194.
- Allaby, M., 2013. *A Dictionary of Geology and Earth Sciences*. Oxford University Press, Oxford, United Kingdom.
- Allen, P.A., and Allen, J.R., 1990. *Basin Analysis, Principles and Applications*: Cambridge, Massachusetts. 451pp.
- Almera, J., 1894. Descripción de los terrenos pliocénicos de la cuenca del bajo Llobregat y Llano de Barcelona (Apéndice). *Map. Geol. Prov. Barc.*, 103-116.
- Amigó, J., 1984. La falla del Valles-Penedes entre Pontons y Font-Rubí (Alt-Penedès). *Acta Geol. Hisp.* 19, 1-4.
- Amilibia, A., McClay, K. R., Sabat, F., Muñoz, J. A., and Roca, E., 2005. Analogue modelling of inverted oblique rift systems, *Geol. Acta*, 3, 251-271.
- Anadón, P., 1978a. El Paleógeno continental anterior a la transgresión biarrtziense (Eoceno medio) entre los ríos Gaia y Ripoll. PhD Thesis, University of Barcelona, Barcelona, 267pp.
- Anadón, P., 1978b. El Paleógeno continental anterior a la transgresión biarrtziense (Eoceno medio) entre los ríos Gaiá y Ripoll. *Estudios Geológicos*.
- Anadón, P., Colombo Piñol, F., Esteban Cerdà, M., Marzo Carpio, M., Robles Orozco, S., Santanach, P., Solé Sugrañes, L., 1979. Evolución tectonoestratigráfica de los Catalánides. *Acta Geologica Hispanica* 14. Hommage to Lluís Solé i Sabarís. 242-270.
- Anadón, P., Feist, M., 1981. Charophytes et biostratigraphie du Paléogène inférieur du bassin de l'Ebre oriental. *Palaeontographica Abteilung B* 178, 143-168.
- Anadón, P., Feist, M., Hartenberger, J.L., Muller, C. Villalta-Comella, J., 1983. Un exemple de correlation biostratigraphique entre échelles marines et continentales dans l'Éocène: la coupe de Pontils (Bassin de l' Ebre, Espagne), *Bulletin de la Société Géologique de la France* XXV (5), 747-755.
- Anadón, P., Cabrera, L., Guimerà, J. and Santanach, P., 1985. Paleogene strike-slip deformation and sedimentation along the southeastern margin of the Ebro Basin. In: Biddle, K.T. and Christie-Blick, N. (eds.) *Strike-slip deformation, basin formation, and sedimentation*. The Society of Economic Paleontologists and Mineralogists (SEPM) 1985.
- Anadón, P., Marzo, M., 1986. Sistemas deposicionales eocenos del margen oriental de la cuenca del Ebro: Sector Igualada-Montserrat. In: Reguant, S. (ed.), *XI Congreso Español de Sedimentología: guía de las excursiones*. Barcelona, 1-4.

- Anadón, P., Vianey-Liaud, M., Cabrera, L., Hartenberger, J.L., 1987. Gisements à vertébrés du paléogène de la zone orientale du bassin de l'Ebre et leur apport à la stratigraphie. *Paleontologia i Evolució*, 21, 117-131.
- Anadón, P., Cabrera, L., Colldeforns, B., Sáez, A., 1989. Los sistemas lacustres del Eoceno superior y Oligoceno del sector oriental de la Cuenca del Ebro. *Acta Geologica Hispánica*, 24 (3-4): 205-230.
- Anadón, P., Cabrera, L., Choi, S. J., Colombo, F., Feist, M., Sáez, A., 1992. Biozonación del Paleógeno continental de la zona oriental de la Cuenca del Ebro mediante carófitas: implicaciones en la biozonación general de carófitas de Europa occidental. *Acta Geologica Hispánica*, 27 (1-2), 69-94.
- Anderson E.M., 1951. The dynamics of faulting and dyke formation with applications to Britain. Edinburgh, Oliver & Boyd (2nd edition), 206pp.
- Andre, G., Hirsch, C., Fourcade, S., Cathelineau, M. and Buschaert, S., 2010. Chronology of fracture sealing under a meteoric fluid environment: Microtectonic and isotopic evidence of major Cainozoic events in the eastern Paris Basin (France). *Tectonophysics*, 490(3-4), 214-228.
- Arnal, I., Calvet, F., Márquez, L., Márquez-Aliaga, A., Solé de Porta, N., 2002. La plataforma carbonatada epeírica (Formaciones Imón e Isábena) del Triásico superior del NE de la Península Ibérica. *Acta Geológica Hispánica* 37 (4), 299–328.
- Ashauer, H. and Teichmüller, R., 1935. Die Variscische und Alpidische Gebirgsbildung Kataloniens, Abh. Ges. Wiss. Göttingen math-phys. 3 (10), 115pp
- Axen, G.J., 1988. The geometry of planar domino-style normal faults above a dipping basal detachment. *Journal of Structural Geology*, 10(4), 405-411.
- Bally, A.W., 1984. Tectogénese et sismique réflexion. *Bull. Soc. Géol. Fr.* 2, 279–285. Série 7, Tome XXVI, Fascicule.
- Bally, A. W. and Snelson, S., 1980. Realms of subsidence. In: Miall, A. D. (ed.) *Facts and Principles of World Petroleum Occurrence*. Canadian Society Petroleum Geologists Memoir, 6, 9–94.
- Baqués, V., Travé, A., Benedicto, A., 2008. Relación entre circulación de fluidos y brechificación en la cuenca extensiva neógena del Penedès (NE Península Ibérica). *Geotemas* 10, 1437–1440.
- Baqués, V., Travé, A., Benedicto, A., Labaume, P., Cantarero, I., 2010. Relationships between carbonate fault rocks and fluid flow regime during propagation of the Neogene extensional faults of the Penedès basin (Catalan Coastal Ranges, NE Iberian). *J. Geochem. Explor.* 106, 24–33.
- Baqués, V., Travé, A., Roca, E., Marín, M., Cantarero, I., 2012. Geofluid behaviour in successive extensional and compressional events: a case study from the southwestern end of the Vallès-Penedès Fault (Catalan Coastal Ranges, NE Spain). *Petroleum Geoscience*, 18, 17–31.
- Baqués, V., Travé, A., Cantarero, I., 2014. Development of successive karstic systems within the Baix Penedès Fault zone (onshore of the Valencia Trough, NW Mediterranean). *Geofluids* 14, 75–94.
- Barberà, X., 1999. Magnetostratigrafia de l'Oligocè del sector sudoriental de la Conca de l'Ebre: implicacions magnetobiocronològiques i seqüencials. PhD Thesis. University of Barcelona, Barcelona, 247pp.
- Barberà, X., Cabrera, L., Marzo, M., Parés, J.M., Agustí, J., 2001. A complete terrestrial Oligocene magnetobiostratigraphy from the Ebro Basin, Spain. *Earth and Planetary Science Letters*, 187, 1-16.

- Bartrina, M.T., Cabrera, L., Jurado, M. J., Guimerà, J., Roca, E., 1992. Evolution of the central Catalan margin of the Valencia trough (western Mediterranean). *Tectonophysics*, 203(1-4), 219-247.
- Beamud, E., Costa, E., Garcés, M., Cabrera, L., Roca, E., Gómez-Paccard, M., 2012. An integrated Eocene chronostratigraphy for the central sector of the SE margin of the Ebro Basin. *Geotemas*, 13, 1116-1119.
- Belaid, S., Baqués, V., Travé, A., Benedicto, A., Plagnes, V., 2008. El karst de la falla del Vallés-Penedès (NE de España). *Geotemas* 10, 429–432.
- Benedicto, A., Plagnes, V., Vergély, P., Flotté, N., Schultz, R.A., 2008. Fault and fluid interaction in a rifted margin: integrated study of calcite-sealed fault-related structures (southern Corinth margin). In: Wibberley C.A.J, Kurtz, W., Imber, J., Holdsworth, R.E., Collettini, C. (Ed.), *The internal structure of fault zones: implications for mechanical and fluid-flow properties*. The Geological Society of London, Special Publication 299, 1-19.
- Benzaquen, M., Nuñez, A., Martínez, W., 1972a. Hoja nº 418 (Montblanc), Mapa Geológico de España E. 1: 50.000. Segunda Serie (MAGNA). Instituto Geológico y Minero de España, Madrid.
- Benzaquen, M., Nuñez, A., Martínez, W., 1972b. Hoja nº 419 (Vilafranca del Penedès), Mapa Geológico de España E. 1: 50.000. Segunda Serie (MAGNA). Instituto Geológico y Minero de España, Madrid.
- Berthelsen, A., 1978. The methodology of kineto-stratigraphy as applied to glacial geology. *Bulletin of the geological Society of Denmark*, 27(Special Issue), 25-38.
- Bond, R.M.G. and McClay, K.R., 1995. Inversion of a Lower Cretaceous extensional basin, south central Pyrenees, Spain. *Geological Society, London, Special Publications*, 88(1), 415-431.
- Bonini, M., Sani, F., and Antonielli, B., 2012. Basin inversion and contractional reactivation of inherited normal faults: A review based on previous and new experimental models, *Tectonophysics*, 522–523, 55–88.
- Buchanan, P.G. and McClay, K.R., 1991. Sandbox experiments of inverted listric and planar fault systems. *Tectonophysics*, 188(1-2), 97-115.
- Buchanan, P.G. and McClay, K.R., 1992. Experiments on basin inversion above reactivated domino faults. *Marine and Petroleum Geology*, 9(5), 486-500.
- Buchanan, J.G. and Buchanan, P.G., 1995. Basin inversion. *Oceanographic Literature Review*, 11(42), 980-981.
- Burov, E. and Cloetingh, S.A.P.L., 1997. Erosion and rift dynamics: new thermomechanical aspects of post-rift evolution of extensional basins. *Earth and Planetary Science Letters*, 150(1-2), 7-26.
- Butler, R. W. H., 1989. The influence of pre-existing basin structure on thrust system evolution in the Western Alps. In: Cooper, M. A. and Williams, G. D. (eds.) *Inversion tectonics*, Geological Society, London, UK, *Geol. Soc. Spec. Publ.*, 44, 105–122.
- Cabrera, 1979. Estudio estratigráfico y sedimentario de los depósitos continentales basales de la depresión del Vallés-Penedés. Tesis de Licenciatura. 361pp (inédito).
- Cabrera, L., 1981. Influencia de la tectónica en la sedimentación continental de la cuenca del Vallés-Penedés (provincia de Barcelona, España) durante el Mioceno inferior. *Acta Geológica Hispánica*, 163-169.
- Cabrera, L. and Colombo, F., 1986. XII Congr. Español Sed., Guía Exc. 7.

- Cabrera, L., Calvet, F., Guimerà, J., Permanyer, A., 1991. El registro sedimentario miocénico en los semigrabens del Vallès-Penedès y de El Camp: organización secuencial y relaciones tectónica sedimentación. In: I Congreso del Grupo Español del Terciario: Libro-guía Excursión, 84, 132pp.
- Cabrera, L., Calvet, F., 1996. Onshore Neogene record in NE Spain: Vallès-Penedès and El Camp half-grabens (NW Mediterranean). In: Friend, P.T., Dabrio, D. (Eds.), Tertiary Basins of Spain, 97–105.
- Cabrera, L., Roca, E., Garcés, M., de Porta, J., 2004. Estratigrafia y evolución tectonosedimentaria oligocena superior-neógena del sector central del margen catalán (Cadena Costero-Catalana). In: Vera, J.A. (Ed.), Geología de España. SGEIGME, Madrid, 569–573.
- Calvet, F., Marzo, M., 1994. El Triásico de las Cordilleras Costero Catalanas: estratigrafía, sedimentología y análisis secuencia. In: Field guide III Coloquio de Estratigrafía y Sedimentología del Triásico y Pérmico de España, pp. 1–53.
- Campanyà, J., Ledo, J., Queralt, P., Marcuello, A., Muñoz, J.A., Liesa, M., Jones, A.G., 2018. New geoelectrical characterization of a continental collision zone in the Central – E astern Pyrenees: constraints from 3-D joint inversion of electromagnetic data. Tectonophysics 742-743, 168–179.
- Cantarero, I., Travé, A., Alías, G., Baqués, V., 2014a. Polyphasic hydrothermal and meteoric fluid regimes during the growth of a segmented fault involving crystalline and carbonate rocks (Barcelona Plain, NE Spain). Geofluids, 14, 20–44.
- Cantarero, I., Lanari, P., Vidal, O., Alías, G., Travé, A., Baqués, V., 2014b. Long-term fluid circulation in extensional faults in the central Catalan Coastal Ranges: P-T constraints from neoformed chlorite and K-white mica. International Journal of Earth Sciences, 103, 165–188.
- Cantarero, I., Zafra, C.J., Travé, A., Martín-Martín, J.D., Baqués, V., Playá, E., 2014c. Fracturing and cementation of shallow buried Miocene proximal alluvial fan deposits. Mar. Pet. Geol. 55, 87–99.
- Cantarero, I., Alías, G., Cruset, D., Carola, E., Lanari, P., Travé, A., 2018. Fluid composition changes in crystalline basement rocks from ductile to brittle regimes. Glob. Planet. Chang. 171, 273–292.
- Carrera, N., Lopez-Blanco, M., Arbués, P., Beamud, E., Garcés, M., Marín, M., Cabrera, L., 2020. Caracterització litostratigràfica i estructural i cartografia geològica del Paleogen dels fulls de Sarrià (67-31) i Montblanc (67-32), unpublished. Technical Report CG-0006/20 del Mapa Geològic de Catalunya 1:25000. Institut Cartogràfic i Geològic de Catalunya, Barcelona. 70 pp.
- Casas, A., Permanyer, A., 1991. Disposición y estructura del zócalo de la depresión terciaria del Penedés. Rev. Inst. Investig. Geol. 35 (1891/82), 23–30.
- Chave, A.D. and Jones, A.G. eds., 2012. The magnetotelluric method: Theory and practice. Cambridge University Press.
- Chenin, P., Manatschal, G., Picazo, S., Müntener, O., Karner, G.D., Johnson, C., Ulrich, M., 2017. Influence of the architecture of magma-poor hyperextended rifted margins on orogens produced by the closure of narrow versus wide oceans. Geosphere 13, 1–18.
- Chenin, P., Manatschal, G., Ghienne, J.F. and Chao, P., 2022. The syn-rift tectono-stratigraphic record of rifted margins (Part II): A new model to break through the proximal/distal interpretation frontier. Basin Research, 34(2), 489–532.
- Colldeforns, B. (unpublished). Mapa Geològic de Catalunya. 1:25.000, Sheet no 418-2-1(68-31) (Querol). Geological mapping advised by P. Anadón. Servei Geològic de Catalunya (Currently ICGC), Barcelona, Spain.

- Colldeforns, B., Anadón, P., Cabrera, L., 1994a. Litoestratigrafía del Eoceno superior-Oligoceno inferior de la zona oriental de la Cuenca del Ebro. Sector Igualada-Santa Coloma de Queralt. *Geogaceta* 15, 55-58.
- Colldeforns, B., Anadón, P., Cabrera, L., 1994b. Nuevos datos sobre la litoestratigrafía del Eoceno-Oligoceno inferior de la zona suroccidental de la Cuenca del Ebro (Sector Pontils- Montblanc, provincias de Tarragona y Barcelona). *Geogaceta* 16, 98-101.
- Colombo, F., 1980. Estratigrafía y sedimentología del Terciario inferior continental de los Catalánides. PhD Thesis, University of Barcelona, Barcelona, 608pp.
- Colombo, F., 1986. Continental Paleogene stratigraphy and sedimentology of the western southern border of the Catalanides, Tarragona Province, Spain. *Cuadernos de Geología Ibérica*, 10, 55-115.
- Colpron, M., Warren, M.J., Price, R.A., 1998. Selkirk fan structure, Southeastern Canadian Cordillera: tectonic wedging against an inherited basement ramp. *Geol. Soc. Am. Bull.* 110, 1060-1074.
- Connors, C.D. and Houseknecht, D.W., 2022. Structural inheritance in the Chukchi shelf, Alaska. *Marine and Petroleum Geology*, 143, p.105812.
- Cooper, M.A., and Williams, G.D., 1989. Inversion Tectonics. Geological Society Special Publication No. 44. Oxford: Blackwell Scientific Publications. 375pp.
- Cooper, M.A., Herbert, R., Hill, G.S., 1989. The structural evolution of Triassic intermontane basins in Northern Thailand. In: Thanasuthipak, T., Ounchanum, P. (eds.), *Proceedings of International Symposium on Intermontane Basins: Geology and Resources*. Chiang Mai University, Chiang Mai, Thailand, 231-242.
- Cooper, M. and Warren, M.J., 2020. Inverted fault systems and inversion tectonic settings. *Regional Geology and Tectonics*, 169-204.
- Corregidor, J., Cabrera, L., Parés, J.M., 1997. Magnetoestratigrafía de las sucesiones pliocénicas del Baix Llobregat: Aproximación preliminar. *Acta Geologica Hispánica* 32 (3-4), 147-160.
- Costa, E., Garcés, M., López-Blanco, M., Beamud, E., Gómez-Paccard, M., Larrasoña, J.C., 2010. Closing and continentalization of the South Pyrenean foreland basin (NE Spain): magnetochronological constraints. *Basin Research*, 22(6), 904-917.
- Costa, E., Garcés, M., López-Blanco, M., Serra-Kiel, J., Bernaola, G., Cabrera, L., Beamud, E., 2013. The Bartonian-Priabonian marine record of the eastern South Pyrenean foreland basin (NE Spain): a new calibration of the larger foraminifers and calcareous nannofossil biozonation. *Geologica Acta*, 11(2), 177-193.
- Coward, M.P., 1994. Inversion tectonics. In P.L. Hancock (ed.), *Continental Deformation*. Oxford: Pergamon Press. 289-304.
- Coward, M., 1996. Balancing sections through inverted basins. In: Buchanan, E G. and Nieuwland, D. A. (eds), 1996, *Modern Developments in Structural Interpretation, Validation and Modelling*, Geological Society Special Publication No. 99, pp. 51-77.
- Dahlstrom, C.D.A., 1969. Balanced cross sections. *Can. J. Earth Sci.* 6, 743-757.
- De Brit, T.J., 1989. Timing structural events and basement emplacement using extension veins and cements in the Carboniferous of North Central Ireland. *Irish Journal of Earth Science* 10, 13-31.

- De Paor, D.G.; Eisenstadt, G., 1987. Stratigraphic and structural consequences of fault reversal: An exemple from the Frankilian Basin, Ellesmere Island. *Geology*, 15, 948-949.
- Donath, F.A. and Cranwell, R.M., 1981. Probabilistic treatment of faulting in geologic media. *Mechanical Behavior of Crustal Rocks: the Handin Volume*, 24, 231-241.
- Dooley, T. P. and Hudec, M. R., 2020. Extension and inversion of salt-bearing rift systems, *Solid Earth*, 11, 1187–1204.
- Egbert, G.D., Booker, J.R., 1986. Robust estimation of geomagnetic transfer functions. *Geophys. J. Int.* 87, 173–194.
- Emerson E&P Software, 2024. FieldMove Clino [Mobile App Software]. Roxar, an Emerson Automation Solutions brand. Available at: <https://www.emerson.com/en-us/automation/roxar-software-solutions>
- Enrique, P. and Solé, J., 2004. El basamento Ígneo. Las rocas intrusivas de la Cordillera Costero-Catalana. In Vera, J.A. (ed.) *Geología de España*. Sociedad Geologica de España. 884pp.
- Escudero-Mozo, M.J., Márquez-Aliaga, A., Goy, A., Martín-Chivelet, J., López-Gómez, J., Márquez, L., Arche, A., Plasencia, P., Pla, C., Marzo, M., Sánchez-Fernández, D., 2017. Middle Triassic carbonate platforms in eastern Iberia: evolution of their fauna and palaeogeographic significance in the western Tethys. *Palaeogeogr. Palaeoclimatol. Palaeoecol.* 417, 236–260.
- Esteban, M., 1973. Petrología de las calizas Cretácicas del Sector Central de los Catalánides (Prov. de Tarragona y Barcelona). PhD Thesis, University of Barcelona, Barcelona, 425pp.
- Esteban, M. and Robles, S., 1976. Sobre la paleogeografía del Cretácico Inferior de los Catalánides entre Barcelona y Tortosa. *Acta Geol. Hispán.* XI, 73–78.
- Feist, M., Anadón, P., Cabrera, L., Choi, S. J., Colombo, F., Sáez, A., 1994. Upper Eocene- Lowermost Miocene charophyte succession in the Ebro basin (Spain). Contribution to the charophyte biozonation in Western Europe. *Newsletters on Stratigraphy*, 30 (1): 1-32.
- Fernández, M. and Banda, E., 1990. Geothermal anomalies in the Valles-Penedes Graben Master Fault: Convection through the Horst as a possible mechanism. *Journal of Geophysical Research: Solid Earth*, 95(B4), 4887-4894
- Fernández, M., Torné, M. and Zeyen, H., 1990. Lithospheric thermal structure of NE Spain and the North-Balearic basin. *Journal of Geodynamics*, 12(2-4), 253-267.
- Fernández, M., Foucher, J.P., Jurado, M.J., 1995. Evidence from the multi-stage formation of the south-western Valencia Trough. *Mar. Petrol. Geol.* 12, 101–109.
- Ferrer, J., 1971. El Paleoceno y Eoceno del borde suroriental de la Depresión del Ebro (Cataluña). *Mémoires suisses de Paléontologie*, 90, 1-70.
- Ferrer, O., McClay, K.R., Sellier, N.C., 2016. Influence of fault geometries and mechanical anisotropies on the growth and inversion of hanging-wall synclinal basins: insights from sandbox models and natural examples. *Geol. Soc. Lond., Spec. Publ.* 439, 487–509.
- Ferrer, O., Carola, E. and McClay, K., 2023. Structural control of inherited salt structures during inversion of a domino basement-fault system from an analogue modelling approach. *Solid Earth*, 14(5), 571-589.

- Ferrill, D.A., Morris, A.P., 2008. Fault zone deformation controlled by carbonate mechanical stratigraphy, Balcones fault system, Texas. *AAPG Bull.* 92-3, 359–380.
- Ferrill, D.A., Morris, A.P., McGinnis, R.N., Smart, K.J., Ward, W.C., 2011. Fault zone deformation and displacement partitioning in mechanically layered carbonates: the Hidden Valley fault, Central Texas. *AAPG Bull.* 95-8, 1383–1397.
- Fontboté, J.M., 1954. Las relaciones tectónicas de la depresión del Vallés-Penedés con la Cordillera Prelitoral Catalana y con la Depresión del Ebro. In: *Tomo Homenaje a Prof. E. Hernández-Pacheco*, Madrid. Real Sociedad Española de Historia Natural, 281–310.
- Fontboté, J.M., Guimerà, J., Roca, E., Sàbat, F., Santanach, P. and Fernández-Ortigosa, F., 1990. The Cenozoic geodynamic evolution of the Valencia trough (western Mediterranean). *Rev. Soc. Geol. Esp.* 3(3-4), 249-259.
- Fossen, H., Rotevatn, A., 2016. Fault linkage and relay structures in extensional settings - a review. *Earth-Sci. Rev.* 154, 14–28.
- Galán-Abellán, B., López-Gómez, J., Berrenechea, J.F., Marzo, M., De la Horra, R., Arche, A., 2013. The beginning of the Buntsandstein cycle (Early-Middle Triassic) in the Catalan Ranges, NE Spain: Sedimentary and palaeogeographic implications. *Sediment. Geol.* 296, 86–102.
- Gallart, F., 1981. Neógeno superior y Cuaternario del Penedés (Catalunya, España). *Acta Geol. Hispán.* 16, 151–157.
- Garcés, M., López-Blanco, M., Valero, L., Beamud, E., Muñoz, J.A., Oliva-Urcia, B., Vinyoles, A., Arbués, P., Cabello, P., Cabrera, L., 2020. Paleogeographic and sedimentary evolution of the South Pyrenean foreland basin. *Marine and Petroleum Geology*, 113, 104105.
- García-Dueñas, V., Balanyá, J.C. and Martínez-Martínez, J.M., 1992. Miocene extensional detachments in the outcropping basement of the northern Alboran basin (Betics) and their tectonic implications. *Geo-Marine Letters*, 12, 88-95.
- García-Senz, J., Pedrera, A., Ayala, C., Ruiz-Constán, A., Robador, A. and Rodríguez-Fernández, L.R., 2020. Inversion of the north Iberian hyperextended margin: the role of exhumed mantle indentation during continental collision. *Geological Society, London, Special Publications*, 490(1), 177-198.
- García-Senz, J. and Salas, R., 2011. Sedimentary response to continental rifting in Iberia. In *Keynote in 28th Meeting of Sedimentology*.
- Gaspar-Escribano, J.M., Ter Voorde, M., Roca, E. and Cloetingh, S.A.P.L., 2003. Mechanical (de-) coupling of the lithosphere in the Valencia Trough (NW Mediterranean): what does it mean?. *Earth and Planetary Science Letters*, 210(1-2), 291-303.
- Gaspar-Escribano, J.M., García-Castellanos, D., Roca, E., Cloetingh, S., 2004. Cenozoic vertical motions of the Catalan Coastal Ranges (NE Spain): the role of tectonics, isostasy, and surface transport. *Tectonics* 23.
- Gerya, T. V., and Yuen, D. A, 2007. Robust characteristics method for modelling multiphase visco-elasto-plastic thermo-mechanical problems. *Phys. Earth Planet. Inter.* 163, 83–105.
- Gibbs, A.D., 1987. Development of extension and mixed mode sedimentary basins. In: Coward, M.P.; Dewey, J.F.; and Hancock, P.L. (Eds.). *Continental extension, tectonics*. Geological Society London, Special Publications, 28, 19-33.

- Gibbs, A.D., 1984. Structural evolution of extensional basin margins. *Journal of the Geological Society*, 141(4), 609-620.
- Gil, J., Carenas, B., García-Hidalgo, J.F., Segura, M. and García, A., 2004. Unidades litoestratigráficas del Cretácico Superior en el centro de España: correlación y revisión. *Revista de la Sociedad Geológica de España*, 17, 249-266.
- Gillcrist, R., Coward, M. and Mugnier, J.L., 1987. Structural inversion and its controls: examples from the Alpine foreland and the French Alps. *Geodinamica acta*, 1(1), 5-34.
- Goudswaard, W., Jenyon, M.K. (Eds.), 1988. *Seismic Atlas of Structural and Stratigraphic Features*. European Association of Exploration Geophysicists. CIP-Gegevens Koninklijke Bibliotheek, Den Haag, p. D1.
- Gómez-Paccard, M., López-Blanco, M., Costa, E., Garcés, M., Beamud, E. Larrasoña, J.C., 2011. Tectonic and climatic controls on the sequential arrangement of an alluvial fan/fan-delta complex (Montserrat, Eocene, Ebro basin, NE Spain). *Basin Research*, 23, 1-19.
- Gradstein, F.M., Ogg, J.G., Schmitz, M. D., Ogg, G. M. (Eds.), *Geologic time scale 2020*. Elsevier, 159-192.
- Granado, P., Ferrer, O., Muñoz, J.A., Thöny, W. and Strauss, P., 2017. Basin inversion in tectonic wedges: Insights from analogue modelling and the Alpine-Carpathian fold-and-thrust belt. *Tectonophysics*, 703, 50-68.
- Granado, P., J. B. Ruh, P. Santolaria, P. Strauss, and J. A. Muñoz, 2021. Stretching and contraction of extensional basins with pre-rift salt: A numerical modeling approach: *Frontiers of Earth Science*, v. 9, 1–24.
- Guimerà, J., 1984. Palaeogene evolution of deformation in the northeastern Iberian Peninsula. *Geological Magazine* 121, 413-420.
- Guimerà, J. and Santanach, P., 1978. Sobre la compresión alpina en el sector central de las Cadenas Costeras Catalanas. *Acta Geològica Hispànica* 13, 33-42.
- Guimerà, J., Mas, R. and Alonso, A., 2004. Intraplate deformation in the NW Iberian Chain: Mesozoic extension and Tertiary contractional inversion. *Journal of the Geological Society*, 161(2), 291-303.
- Haq, B.U., Hardenbol, J., Vail, P.R., Stover, L.E., Colin, J.P., Ioannides, N.S., Wright, R.C., Baum, G.R., Gombos, A.M., Pflum, C.E. and Loutit, T.S., 1988. Mesozoic and Cenozoic chronostratigraphy and cycles of sea-level change.
- Hantschel, T. and Kauerauf, A.I., 2009. *Fundamentals of basin and petroleum systems modeling*. Springer Science & Business Media.
- Hausegger, S., Kurz, W., Rabitsch, R., Kiechl, E., Brosch, F.J., 2010. Analysis of the internal structure of a carbonate damage zone: Implications for the mechanisms of fault breccia formation and fluid flow. *J. Struct. Geol.* 32 (9), 1349–1362.
- Hernández, E., Casas, A., 1985. Estudio gravimétrico de la depresión del Penedés. *Acta Geol. Hispànica* 20 (3–4), 191–198.
- Herraiz, M., De Vicente, G., Lindo-Naupari, R., Giner, J., Simon, J.L., Gonzalez-Casado, J. M., Vadillo, O., Rodriguez-Pascua, M.A., Cicuendez, J.I., Casas, A., Cabanas, L., Rincon, P., Cortes, A.L., Ramirez, M., Lucini, M., 2000. The recent (upper Miocene to Quaternary) and present tectonic stress distributions in the Iberian Peninsula. *Tectonics* 19, 762–786.

- Hooker, J.N., Gomez, L.A., Laubach, S.E., Gale, J.F.W., Marrett, R., 2012. Effects of diagenesis (cement precipitation) during fracture opening on fracture aperture-size scaling in carbonate rocks. *Geol. Soc. Lond., Spec. Publ.* 370, 187–206.
- Hubbert, M.K. and Rubery, W.W., 1959. Role of fluid pressure in the mechanics of overthrust faulting. *Bull. Geol. Soc. Am.*, 70, 115–205.
- ICC, 2006. Geological synthesis of the Geological Map of Spain 1:50.000. Institut Cartogràfic i Geològic de Catalunya, 78pp.
- Huyghe, P.A.S.C.A.L.E. and Mugnier, J.L., 1992. Short-cut geometry during structural inversions; competition between faulting and reactivation. *Bulletin de la Société Géologique de France*, 163(6), 691–700.
- Jaeger, G.D., Cook, N.G.W., 1979. *Fundamentals of rock mechanics*. Chapman & Hill Ltd. London, 515pp.
- Jagger, L.J. and McClay, K.R., 2018. Analogue modelling of inverted domino-style basement fault systems. *Basin Research*, 30, 363–381.
- Juez-Larré, J. and Andriessen, P.A.M., 2006. Tectonothermal evolution of the northeastern margin of Iberia since the break-up of Pangea to present, revealed by low-temperature fission-track and (U–Th)/He thermochronology: A case history of the Catalan Coastal Ranges. *Earth and Planetary Science Letters*, 243(1–2), 159–180.
- Julià, R. and Santanach, P., 1984. Estructuras en la salbanda de falla paleógena de la falla del Vallès-Penedès (Cadenas Costeras Catalanas): su relación con el deslizamiento de la falla. *Primer Congreso Español de Geología* 1, 47–59.
- Julià, R. and Santanach, P., 1998. Banded structures in gouge. *Fault-Related Rocks*, 56–57.
- Julivert, M., 1955. Geología de la Sierra de Miramar. *Memor. Comunicac. Inst. Geol.* 13, 79–118.
- Julivert, M., Durán, H., 1990. The Hercynian structure of the Catalanian Coastal Ranges (NE Spain). *Acta Geol. Hispan.* 25 (1–2), 13–21.
- Kent, P.E., 1975. The tectonic development of Great Britain and the surrounding seas. In: Woodland, A.W. (ed.), *Petroleum and the Continental Shelf of Northwest Europe*, vol. 1: Geology, vol. 3. Applied Science Publishers, London, 1975.
- Kirby, S.H. and Kronenberg, A.K., 1987. Rheology of the lithosphere: Selected topics. *Reviews of Geophysics*, 25(6), 1219–1244.
- Kirschvink, J.L., 1980. The least-squares line and plane and the analysis of paleomagnetic data. *Geophysical Journal of the Royal Astronomical Society*, 62, 699–718.
- Krzywiec, P., Adamuszek, M., Filbà, L., Rowan, M.G., Ferrer, O., 2024. Salt-pillow formation during inversion of evaporite-filled half graben – Insights from seismic data interpretation and integrated analogue-numerical modelling. *Journal of Structural Geology*, 184, 105148.
- Labaume, P., Carrio-Schaffhauser, E., Gamond J.F., Renard, F., 2004. Deformation mechanisms and fluid-driven mass transfers in the recent fault zones of the Corinth rift (Greece). *Comptes Rendus Géoscience* 336, 375–383.

- Lafosse, M., Boutoux, A., Bellahsen, N. and Le Pourhiet, L., 2016. Role of tectonic burial and temperature on the inversion of inherited extensional basins during collision. *Geological Magazine*, 153(5-6), 811-826.
- Lanaja, J.M., 1987. Contribución de la explotación petrolífera al conocimiento de la geología de España. IGME, Madrid.
- Ledo, J., Queralt, P., Pous, J., 1998. Effects of galvanic distortion on magnetotelluric data over three-dimensional regional structure. *Geophys. J. Int.* 132, 295–301.
- Li, Y.G., Vidale, J.E., Day, S.M., Oglesby, D.D., Cochran, E., 2003. Postseismic fault healing on the rupture zone of the 1999 M 7.1 Hector Mine, California, earthquake. *Bull. Seismol. Soc. Am.* 93, 854–869.
- Llopis-Lladó, N., 1947. Contribución al conocimiento de la morfoestructura de los Catalánides. PhD Thesis, Instituto Lucas Mallada, CSIC Barcelona, 373pp.
- Logan, J.M. and Rauenzahn, K.A., 1987. Frictional dependence of gouge mixtures of quartz and montmorillonite on velocity, composition and fabric. *Tectonophysics*, 144(1-3), 87-108.
- López-Blanco, M., 2002. Sedimentary response to thrusting and fold growing on the SE margin of the Ebro basin (Paleogene, NE Spain), *Sed. Geol.*, 146, 133 – 154
- López-Blanco, M., Marzo, M., Burbank, D.W., Vergés, J., Roca, E., Anadón, P., Piña, J., 2000a. Tectonic and climatic controls on the development of foreland fan deltas: Montserrat and Sant Llorenç del Munt systems (Middle Eocene, Ebro Basin, NE Spain). *Sedimentary Geology*, 138(1-4), 17-39.
- López-Blanco, M., Marzo, M., Piña, J., 2000b. Transgressive–regressive sequence hierarchy of foreland, fan-delta clastic wedges (Montserrat and Sant Llorenç del Munt, Middle Eocene, Ebro Basin, NE Spain). *Sedimentary Geology*, 138(1-4), 41-69.
- López-Blanco, M., Beamud, E., Marín, M., Costa, E., accepted. New evidence of syn-sedimentary folding of the Sant Miquel de Montclar conglomerates (Eocene, Ebro basin, NE Spain). *Geogaceta*, 77.
- López-Gómez, J., Arche, A., Pérez-López, A. 2002. Permian and Triassic. In: Gibbons W, Moreno T (eds.) *The Geology of Spain*. Geological Society of London, London, 185–212.
- López-Gómez, J., Alonso-Azcárate, J., Arche, A., Arribas, J., Fernández Barrenechea, J., Borruel-Abadía, V., Bourquin, S., Cadenas, P., Cuevas, J., De la Horra, R. and Díez, J.B., 2019. Permian-Triassic rifting stage. *The Geology of Iberia: A Geodynamic Approach: Volume 3: The Alpine Cycle*, 29-112.
- López-Mir, B., Muñoz, J.A. and García-Senz, J., 2015. Extensional salt tectonics in the partially inverted Cotiella post-rift basin (south-central Pyrenees): structure and evolution. *International Journal of Earth Sciences*, 104, 419-434.
- Macgregor, D.S., 1995. Hydrocarbon habitat and classification of inverted rift basins. In: Buchanan, J.G., Buchanan, P.G. (eds.), *Basin Inversion*, vol. 88. Geological Society, London, Special Publications, London, 83-93.
- Manatschal, G., Müntener, O., 2009. A type sequence across an ancient magma-poor ocean-continent transition: the example of the western Alpine Tethys ophiolites. *Tectonophysics* 473, 4–19.

- Marcén, M., Casas-Sainz, A.M., Román-Berdiel, T., Grier, A., Santanach, P., Pocoví, A., Gil-Imaz, A., Aldega, L., Izquierdo-Llavall, E., 2018. Multiple movements recorded in a crustal weakness zone in NE Iberia: the Vallès-Penedès Fault revisited. *J. Geodyn.* 121, 96–114.
- Marín, M., Roca, E., Marcuello, A., Cabrera, L., Ferrer, O., 2021. Mesozoic structural inheritance in the Cenozoic evolution of the central Catalan Coastal Ranges (western Mediterranean): Structural and magnetotelluric analysis in the Gaià-Montmell High. *Tectonophysics*, 814, 228970.
- Marín, M., Roca, E., Baqués, V., Cantarero, I., Cabrera, L., Ferrer, O. and Travé, A., 2023. Fluid-rock interaction control on fault reactivation: A review of the Montmell-Vallès Fault System, central Catalan Coastal Ranges (NE Iberia). *Global and Planetary Change*, 220, 104011.
- Marín, M., Carola, E., Beamud, E., Bover-Arnal, T., López-Blanco, M., Garcés, M., Costa, E., Ferrer, O., Cabrera, L., 2025. Paleogene kinematics of the central Catalan Coastal Ranges: temporal constraints from magneto-chronology and provenance analysis in synorogenic deposits in the SE margin of the Ebro Basin (NE Spain). *Geologica Acta* 23.2, 1-25.
- Martí, A., Queralt, P., Ledo, J., 2009a. WALDIM: a code for the dimensionality analysis of magnetotelluric data using the rotational invariants of the magnetotelluric tensor. *Comput. Geosci.* 35 (12), 2295–2303.
- Martí, A., Queralt, P., Roca, E., Ledo, J., Galindo-Zaldívar, J., 2009b. Geodynamic implications for the formation of the Betic-Rif orogen from magnetotelluric studies. *J. Geophys. Res.* 114-B1, 1–14.
- Martín-Closas, C., Segura-Altés, R., Pérez-Cano, J., Bover-Arnal, T., Sanjuan, J., 2021. *Palaeonitella trifurcata* n. sp., a cortoid-building charophyte from the Lower Cretaceous of Catalonia. *Review of Palaeobotany and Palynology* 295 (2021), 104523.
- Martinell, J., 1988. An overview of the marine Pliocene of NE Spain. *Géologie Méditerranéenne*, 15(4), 227-233.
- Marzo, M., 1980. El Buntsandstein de los Catalánides: estratigrafía y procesos de sedimentación. PhD Thesis. Universitat de Barcelona. 317pp.
- McClay, K.R., 1990. Extensional fault systems in sedimentary basins: a review of analogue model studies. *Marine and petroleum Geology*, 7(3), 206-233.
- McClay, K.R., 1992. Glossary of thrust tectonics terms. *Thrust tectonics*, 419-433.
- McClay, K.R., 1995. The geometries and kinematics of inverted fault systems: a review of analogue model studies. Geological Society, London, Special Publications, 88(1), 97-118.
- McClay, K.R., Buchanan, P.G. (1992). Thrust faults in inverted extensional basins. In: McClay, K.R. (ed.) *Thrust Tectonics*. Springer, Dordrecht.
- McKenzie, D., 1978. Some remarks on the development of sedimentary basins. *Earth and Planetary science letters*, 40(1), 25-32.
- Mercedes-Martín, R., Salas, R., Arenas, C., 2013. Facies heterogeneity and depositional models of a Ladinian (Middle Triassic) microbial-dominated carbonate ramp system (Catalan Coastal Ranges, NE Spain). *Journal of Marine and Petroleum Geology* 46, 107–128.
- Mercedes-Martín, R., Arenas, C., Salas, R., 2014. Diversity and factors controlling widespread occurrence of syn-rift Ladinian microbialites in the western Tethys (Triassic Catalan Basin, NE Spain). *Sediment. Geol.* 313, 68–90.

- Mercedes-Martín, R., Buatois, L.A., 2020. Microbialites and trace fossils from a Middle Triassic restricted carbonate ramp in the Catalan Basin, Spain: evaluating environmental and evolutionary controls in an epicontinental setting. *Lethaia* 54 (1), 4–25.
- Micarelli, L., Benedicto, A., Invernizzi, C., Saint-Bezar, B., Michelot, J.L., Vergely, P., 2005. Influence of P/T conditions on the style of normal fault initiation and growth in limestones from SE-Basin, France. *Journal of Structural Geology* 27, 1577–1598.
- Minwer-Barakat, R., Bolet, A., Anadón, P., Alegret, L., Badiola, A., Blanco, A., Cotton, L., Femenias-Gual, J., Furió, M., Godinot, M., Moyà-Solà, S., Peláez-Campomanes, P., Sanjuan, J., Marigó, J., 2023. The fossil assemblage from Pontils, a middle Eocene primate-bearing locality from Northeastern Spain. *Journal of Vertebrate Paleontology*, 43, e2259970.
- Miró, J., Ferrer, O., Muñoz, J.A., Manastchal, G., 2023. Role of inheritance during tectonic inversion of a rift system in basement-involved to salt-decoupled transition: analogue modelling and application to the Pyrenean-Biscay system. *Solid Earth*, 14, 425–445.
- Moragas, M., Vergés, J., Nalpas, T., Saura, E., Martín-Martín, J.-D., Messenger, G., and Hunt, D. W.: The impact of syn- and post-extension prograding sedimentation on the development of salt-related rift basins and their inversion: Clues from analogue modelling, *Mar. Petrol. Geol.*, 88, 985–1003.
- Moreno-Bedmar, J.A., Robert, E., Matamalas-Andrea, R., Bover-Arnal, T., 2017. Review of the early Albian ammonites of the Montmell Formation near Marmellar (Salou-Garraf Basin, Tarragona, Catalonia, Spain). *Carnets Geol.* 17 (1), 1–10.
- Morley, C.K., Back, S., Van Rensbergen, P., Crevello, P. and Lambiase, J.J., 2003. Characteristics of repeated, detached, Miocene–Pliocene tectonic inversion events, in a large delta province on an active margin, Brunei Darussalam, Borneo. *Journal of Structural Geology*, 25(7), 1147–1169.
- Mouthereau, F., Tensi, J., Bellahsen, N., Lacombe, O. Boisgrollier, T., and Kargar, S., 2007. Tertiary sequence of deformation in a thin- skinned/thick- skinned collision belt: the Zagros Folded Belt (Fars, Iran). *Tectonics*, 26, doi: 10.1029/2007TC002098.
- Muchez, Ph., Slobondik, M., Viaene, W.A., Keppens, E., 1995. Geochemical constraints on the origin and migration of palaeofluids at the northern margin of the Variscan foreland, southern Belgium. *Sedimentary Geology* 96, 191–200
- Muñoz, J. A., 1992. Evolution of a continental collision belt: ECORS-Pyrenees crustal balanced section, in *Thrust Tectonics*, edited by K. R. McClay, pp. 235–246, Chapman and Hall, London.
- Muñoz, G., Mateus, A., Pous, J., Heise, W., Santos, F.M., Almeida, E., 2008. Unravelling middle-crust conductive layers in Palaeozoic Orogens through 3D modeling of magnetotelluric data: the Ossa-Morena Zone case study (SW Iberian Variscides). *J. Geophys. Res.* 113 (B06106), 1–23.
- Nalpas, T.; Le Douaran, S.; Brun, J.-P.; Unternehr, P.; Richert, J.-P., 1995. Inversion of the Broad Fourteens Basin (offshore Netherlands), a small-scale model investigation. *Sedimentary Geology*, 95, 237–250.
- Ortí, F., Pérez-López, A., Salvany, J.M., 2017. Triassic evaporites of Iberia: sedimentological and palaeogeographical implications for the western Neotethys evolution during the Middle Triassic–Earliest Jurassic. *Palaeogeogr. Palaeoclimatol. Palaeoecol.* 471, 157–180.

- Osmundsen, Andersen, Markussen and Svendby, 1998. Tectonics and sedimentation in the hangingwall of a major extensional detachment: the Devonian Kvamshesten Basin, western Norway. *Basin Research*, 10(2), 213-234.
- Parcerisa, D., 2002. Petrologia i diagènesi en sediments de l'Oligocè superior i del Miocè inferior i mitjà de la depressió del Vallès i del Pla de Barcelona, Ph.D. Thesis, 288 pp., Univ. Autònoma de Barcelona, Barcelona, Spain.
- Parcerisa, D., Gómez, D.M., Roca, E., Madurell, J. and Agustí, J., 2007. The Upper Oligocene of Montgat (Catalan coastal ranges, Spain): New age constraints to the western Mediterranean basin opening. *Geologica Acta*, 5(1), 3-17.
- Pérez, N.D., Teixell, A., Gómez-Gras, D. and Stockli, D.F., 2019. Reconstructing extensional basin architecture and provenance in the Marrakech High Atlas of Morocco: Implications for rift basins and inversion tectonics. *Tectonics*, 38(5), 1584-1608.
- Porta, J., Civís, J., 1996. La sucesión bioestratigráfica del Mioceno marino en el Penedés y el horst de Tarragona-Bonastre (Neógeno del Sistema Mediterráneo). *Geogaceta* 19, 97–102.
- Pous, J., Marcuello, A., Queralt, P., 2001. Magnetotelluric signature of the western Cantabrian Mountains. *Geophys. Res. Lett.* 28, 1795–1798.
- Powell, C.M. and Williams, G.D., 1989. The Lewis Thrust/Rocky Mountain trench fault system in Northwest Montana, USA: an example of negative inversion tectonics? Geological Society, London, Special Publications, 44(1), 223-234.
- Pueyo, J.J., 1975. Estudio petrológico y geoquímico de los yacimientos potásicos de Cardona, Súria, Sallent (Barcelona, España). PhD Thesis, University of Barcelona, Barcelona, 351pp.
- Reguant, S., 1967. El Eoceno marino de Vic (Barcelona). *Memorias Instituto Geológico y Minero de España*, 68, 1-350.
- Roca, E. and Guimerà, J., 1992. The Neogene structure of the eastern Iberian margin: Structural constraints on the crustal evolution of the Valencia trough (western Mediterranean). *Tectonophysics* 203(1-4), 203-218.
- Roca, E., 1996. La evolución geodinámica de la Cuenca Catalano-Balear y áreas adyacentes desde el Mesozoico hasta la actualidad. *Acta Geol. Hisp.* 29, 3–25.
- Roca, E., Sans, M., Cabrera, L. and Marzo, M., 1999. Oligocene to Middle Miocene evolution of the central Catalan margin (northwestern Mediterranean). *Tectonophysics*, 315(1-4), 209-229.
- Roca, E., 2001. The Northwest Mediterranean Basin (Valencia Trough, Gulf of Lions and Liguro-Provençal basins): structure and geodynamic evolution. In: P.A Ziegler, W. Cavazza, A.H.F. Robertson and S. Crasquin-Soleau (eds.), *Peri-Tethys Memoir 6: Peri-Tethyan Rift/Wrench Basins and Passive Margins*. *Mém. Mus. natn. Hist. nat.*, 186, 671-706. Paris.
- Roca, E., Frizon de Lamotte D., Mauffret, A., Bracène, R., Vergés, J., Benaouali, N., Fernández, M., Muñoz, J. A. and Zeyen, H. 2004. Transect II: Aquitaine Basin - Pyrenees - Ebro Basin - Catalan Range - Valencia Trough - Balearic Block - Algerian Basin - Kabylies - Atlas - Saharan Platform. In: Cavazza, W., Roure, F. M., Spakman, W., Stampfli, G. M. and Ziegler, P. A. (Eds.), 2004. *The Transmed Atlas – The Mediterranean Region from Crust to Mantle*, Springer, Berlin, Heidelberg.

- Roca, E., Muñoz, J.A., Ferrer, O., Ellouz, N., 2011. The role of the Bay of Biscay Mesozoic extensional structure in the configuration of the Pyrenean orogen: Constraints from the MARCONI deep seismic reflection survey. *Tectonics*, 30, TC2001.
- Roest, W.R. and Srivastava, S.P., 1991. Kinematics of the plate boundaries between Eurasia, Iberia, and Africa in the North Atlantic from the Late Cretaceous to the present. *Geology*, 19(6), 613-616
- Roma, M., Ferrer, O., Roca, E., Pla, O., Escosa, F., Butillé, M., 2018a. Formation and inversion of salt-detached ramp-syncline basins. Results from analogue modelling and application to the Columbrets Basin (Western Mediterranean). *Tectonophysics*, 745, 214-228.
- Roma, M., Vidal-Royo, O., McClay, K., Ferrer, O., Muñoz, J.A., 2018b. Tectonic inversion of salt-detached ramp-syncline basins as illustrated by analogue modelling and kinematic restoration. *Interpretation*, 6 (1), T127–T144.
- Rosenbaum, G., Lister, G.S. and Duboz, C., 2002. Relative motions of Africa, Iberia and Europe during Alpine orogeny. *Tectonophysics*, 359, 117-129.
- Roure, F., Cloetingh, S., Scheck-Wenderoth, M. and Ziegler, P.A., 2010. Achievements and challenges in sedimentary basin dynamics: a review. *New frontiers in integrated solid earth sciences*, 145-233.
- Ruh, J. B., 2017. Effect of fluid pressure distribution on the structural evolution of accretionary wedges. *Terra Nova* 29, 202–210.
- Ruh, J. B., and Vergés, J., 2018. Effects of reactivated extensional basement faults on structural evolution of fold-and-thrust belts: insights from numerical modelling applied to the Kopet Dagh Mountains. *Tectonophysics* 746, 493–511.
- Ryan, W. B. F., S.M. Carbotte, J. Coplan, S. O'Hara, A. Melkonian, R. Arko, R.A. Weissel, V. Ferrini, A. Goodwillie, F. Nitsche, J. Bonczkowski, and R. Zemsky, 2009. Global Multi-Resolution Topography (GMRT) synthesis data set, *Geochem. Geophys. Geosyst.*, 10, Q03014.
- Sàbat, F., Roca, E., Muñoz, J.A., Vergés, J., Sans, M., Masana, E., Santanach, P., Estévez, A., Santisteban, C., 1997. Role of extension and compression in the evolution of the eastern margin of Iberia: the ESCI–València Trough seismic profile. *Rev. Soc. Geol. Esp.* 8 (4), 431–448.
- Sàbat, F., Gelabert, B., Rodríguez-Perea, A. and Giménez, J., 2011. Geological structure and evolution of Majorca: Implications for the origin of the Western Mediterranean. *Tectonophysics*, 510(1-2), 217-238.
- Sáez, A., Anadón, P., 1989. El Complejo turbidítico del Carbonífero del Priorat (Tarragona). *Acta Geol. Hisp.* 24 (1), 33–47.
- Salas, R., 1987. El Malm i el Cretaci inferior entre el Massís de Garraf i la Serra d'Espadà. Ph.D. Thesis. Universitat de Barcelona. 345pp.
- Salas, R., Casas, A., 1993. Mesozoic extensional tectonics, stratigraphy and crustal evolution during the Alpine cycle of the eastern Iberian basin. *Tectonophysics* 228 (1–2), 33–55.
- Salas, R., Guimerà, J., Mas, R., Martín-Closas, C., Meléndez, A., Alonso, A., 2001. Evolution of the Mesozoic Central Iberian Rift System and its Cainozoic inversion (Iberian Chain). In: Ziegler, P.A., Cavazza, W., Robertson, A.H.F., Crasquin-Soleau, S. (Eds.), *Peri-Tethys Memoir 6: Peri-Tethyan Rift/Wrench Basins and Passive Margins*, French National Museum of Natural History, vol. 186, 145–185.

- Sanjuan, J., Martín-Closas, C., Costa, E., Barberà, X., Garcés, M., 2014. Calibration of Eocene-Oligocene charophyte biozones in the Eastern Ebro Basin (Catalonia, Spain). *Stratigraphy* 11(1), 61–81.
- Segura, M., García-Hidalgo, J.F., Carenas, B., Gil, J., García, A., 2004. Evolución paleogeográfica de la Cuenca Ibérica en el Cretácico Superior. *Geogaceta*, 36, 103-106.
- Schlüter, H.U., Gaedicke, C.H., Roeser, H.A., Schreckenberger, B., Meyer, H., Reichert, C.H., Djajadihardja, Y. and Prexl, A., 2002. Tectonic features of the southern Sumatra-western Java forearc of Indonesia. *Tectonics*, 21(5), 11-1.
- Serra, P.R., Enrique, P., 1989. The Late-Hercynian intrusives from southern Catalanian Coastal Ranges (NE Spain), and their epiplutonic to subvolcanic level of magma emplacement. *Rend. Soc. Ital. Mineral. Petrol.* 43, 817–829.
- Serra-Kiel, J., Travé, A., Mató, E., Saula, E., Ferràndez, C., Tosquella, J., Vergés, J., 2003. Marine and transitional Middle/Upper Eocene units of the Southeastern Pyrenean Foreland Basin (NE Spain). *Geologica Acta*, 1 (2), 177-200.
- Sibson, R. H., 1977. Fault rocks and fault mechanisms. *Journal of the Geological Society*, 133(3), 191–213.
- Sibson, R.H., 1985. A note on fault reactivation. *Journal of Structural Geology*, 7(6), 751-754.
- Sibuet, J.C., Srivastava, S., Spakman, W., 2004. Pyrenean orogeny and plate kinematics. *Journal Geophysical Research* 109, B08104.
- Simpson, F., Bahr, K., 2005. *Practical Magnetotellurics*. Cambridge University Press. 270pp.
- Srivastava, S.P., Roest, W.R., Kovacs, L.C., Oakey, G., Lévesque, S., Verhoef, J. and Macnab, R., 1990. Motion of Iberia since the Late Jurassic: Results from detailed aeromagnetic measurements in the Newfoundland Basin. *Tectonophysics*, 184, 229-260.
- Stephenson, R., Schiffer, C., Peace, A., Nielsen, S.B. and Jess, S., 2020. Late Cretaceous-Cenozoic basin inversion and palaeostress fields in the North Atlantic-western Alpine-Tethys realm: implications for intraplate tectonics. *Earth-Science Reviews*, 210, 103252.
- Tamas, A., Tamas, D.M., Tari, G., Krezsek, C., Lapadat, A. and Schleder, Z., 2023. Does the syn-versus post-rift thickness ratio have an impact on the inversion-related structural style? *Solid Earth*, 14(7), 741-761.
- Tari, G., Arbouille, D., Schléder, Z. and Tóth, T., 2020. Inversion tectonics: a brief petroleum industry perspective. *Solid Earth*, 11(5), 1865-1889.
- Tari, G., Connors, C., Flinch, J., Granath, J., Pace, P., Sobornov, K. and Soto, J.I., 2023. Negative structural inversion: An overview. *Marine and Petroleum Geology*, 152, 106223.
- Tavani, S., Bertok, C., Granado, P., Piana, F., Salas, R. Vigna, B., Muñoz, J.A, 2018. The Iberia-Eurasia plate boundary east of the Pyrenees. *Earth-Science Reviews*, Volume 187, 314-337.
- Tavani, S., Smeraglia, L., Fabbi, S., Aldega, L., Sabbatino, M., Cardello, G.L., Maresca, A., Schirripa Spagnolo, G., Kylander-Clark, A., Billi, A. and Bernasconi, S.M., 2023. Timing, thrusting mode, and negative inversion along the Circeo thrust, Apennines, Italy: How the accretion-to-extension transition operated during slab rollback. *Tectonics*, 42(6), p. e2022TC007679.

- Tosal, A., Valero, L., Sanjuan, J., Martín-Closas, C., 2019. Influence of short-and long-term climatic cycles on floristic change across the Eocene–Oligocene boundary in the Ebro Basin (Catalonia, Spain). *Comptes Rendus Palevol*, 18 (8), 925-947.
- Travé, A., Calvet, F., Soler, A., Labaume, P., 1998. Fracturing and fluid migration during Palaeogene compression and Neogene extension in the Catalan Coastal Ranges, Spain. *Sedimentology* 45, 1063-1082.
- Travé, A., Calvet, F., 2001. Syn-rift geofluids in fractures related to the early-middle Miocene evolution of the Vallès-Penedès half-graben (NE Spain). *Tectonophysics* 336, 101-120.
- Van Hinsbergen, D.J.J., Vissers, R.L.M., Spakman, W., 2014. Origin and consequences of western Mediterranean subduction, rollback, and slab segmentation. *Tectonics* 33, 393–419.
- Vergés, J. and García-Senz, J., 2001., Mesozoic evolution and Cainozoic inversion of the Pyrenean Rift. In: *Peri-Tethys Memoir 6: Peri-Tethyan Rift/Wrench Basins and Passive Margins*, edited by P. A. Ziegler, Mém. Mus. National Hist. Nat., 186, 187-212.
- Vidal, N., Gallart, J., Dañobeitia, J.J., 1998. A deep seismic crustal transect from the NE Iberian Peninsula to the western Mediterranean. *Journal of Geophysical Research*, 103 (B6), 12381-12396.
- Vilasi, N., Malandain, J., Barrier, L., Callot, J.P., Amrouch, K., Guilhaumou, N., Lacombe, O., Muska, K., Roure, F. and Swennen, R., 2009. From outcrop and petrographic studies to basin-scale fluid flow modelling: The use of the Albanian natural laboratory for carbonate reservoir characterisation. *Tectonophysics*, 474(1-2), 367-392.
- Virgili, C., 1958. El Triásico de los Catalánides. *Bol. Inst. Geol. Min. Esp.* 69, 856.
- Virgili, C., Sopena, A., Ramon, A., Arche, A., Hernando, A., 1983. El relleno posthercínico y el comienzo de la sedimentación Mesozoica. *Libro Jubilar Jose María Rios*, Madrid 2, 25–36.
- Wakabayashi, J., Hengesh, J.V. and Sawyer, T.L., 2004. Four-dimensional transform fault processes: progressive evolution of step-overs and bends. *Tectonophysics*, 392(1-4), 279-301.
- Wang, C.Y., Mao, N., Wu, F.T., 1980. Mechanical properties of clays at high pressure. *J. Geophys. Res.* 85, 1462–1468.
- Watts, A.B., Torné, M., Buhl, P., Mauffret, A., Pascal, G. and Pinet, B., 1990. Evidence for reflectors in the lower continental crust before rifting in the Valencia trough. *Nature*, 348(6302), 631-635.
- Wernicke, B., 1981. Low-angle normal faults in the Basin and Range Province: nappe tectonics in an extending orogen. *Nature*, 291(5817), 645-648.
- Wernicke, B.; Burchfield, B.C., 1982. Modes of extensional tectonics. *Journal of Structural Geology*, 4, 105-115.
- Wernicke, B., Walker, J.D. and Beaufait, M.S., 1985. Structural discordance between Neogene detachments and frontal Sevier thrusts, central Mormon Mountains, southern Nevada. *Tectonics*, 4(2), 213-246.
- Williams, G.D., Powell, C.M., Cooper, M.A., 1989. Geometry and kinematics of inversion tectonics. In: Cooper, M.A., Williams, G.D. (eds.), *Inversion Tectonics*, vol. 44. Geological Society, London, Special Publications, London, 335-347.
- Wilson, E.P., Granado, P., Santolaria, P., Ferrer, O., Muñoz, J.A., 2023. Inversion of accommodation zones in salt-bearing extensional systems: insights from analogue modelling. *Solid Earth*, 14, 709-739.

- Wintsch, R., Christoffersen, R., Kronenberg, A., 1995. Fluid-rock reaction weakening of fault zones. *J. Geophys. Res.* 100, 13021–13032.
- Withjack, M.O., Islam, Q.T. and La Pointe, P.R. 1995. Normal faults and their hanging-wall deformation: an experimental study. *American Association of Petroleum Geologists Bulletin*, 79, 1–18.
- Withjack, M.O., Schlische, R.W., 2006. Geometric and experimental models of extensional fault-bend folds. In: Buiter, S.J.H., Schreurs, G. (Eds.), *Analogue and Numerical Modelling of Crustal-Scale Processes*, Geological Society of London, Special Publication, 253, 285–305.
- Ziegler, P.A., 1974. The geological evolution of the North Sea area in the tectonic framework of Northwestern Europe, December 1973, Bergen, Norway.
- Ziegler, P.A., Cavazza, W., Robertson, A.H.F. and Crasquin-Soleau, S., 2001. Peri-Tethys Memoir 6: Peri-Tethyan Rift/Wrench Basins and Passive Margins. *Mém. Mus. natn. Hist. nat.* 186, Paris.
- Zwaan, F., Schreurs, G., Buiter, S., Ferrer, O., Reitano, R., Rudolf, M. and Willingshofer, E., 2022. Analogue modelling of basin inversion: a review and future perspectives. *Solid Earth Discussions*, 2022, 1-84.

LIST OF ACRONYMS

The following list provides a complete overview of all acronyms used throughout this document, including those appearing in both the text and figures. The intention of this list is to facilitate understanding and ensure clarity for readers. Frequently used acronyms are highlighted in **blue** for quick reference.

BB: Barcelona Basin	MH: Montseny High
BCB: Basque-Cantabrian Basin	MR: Miramar Range
Bc E-1: Barcelona E-1 well	Mr: Montserrat fan delta
BF: Barcelona Fault	MsB: Maestrat Basin
BMB: Barcelona-Maresme Basin	MT: magnetotelluric
BP: Barcelona Plain	MU: Messinian Unconformity
BPB: Baix Penedès Basin	MVFS: Montmell-Vallès Fault System
CB: Cameros Basin	NRM: Natural Remanent Magnetization
CCR: Catalan Coastal Ranges	OB: Organyà Basin
ChRM: Characteristic Remanent Magnetization	PB: Penedès Basin
CMH: Collserola-Montnegre High	PH: Prades High
DI: Durance Isthmus	PrB: Perelló Basin
ECB: El Camp Basin	PrtB: Parentis Basin
ECF: El Camp Fault	PZ: Paleozoic
FMB: Figueres-Montgrí Basin	SLM: Sant Llorenç del Munt alluvial fan and fan delta
FNB: Flysch Noir Basin	SMM: Sant Miquel del Montclar alluvial fan
GH: Garraf High	Sn-1: Senant-1 well
GMH: Gaià-Montmell High	SPB: South Provence Basin
GMtH: Garraf-Montnegre High	SS-1: San Sadurní-1 well
LP: Landes Plateau	VB: Vallès Basin
Ma-1: Martorell-1 well	VcB: Vocontian Basin
MAU: Middle Albian Unconformity	VPB: Vallès-Penedès Basin
MAZ: Marmellar Accommodation Zone	VPF: Vallès-Penedès Fault
MGB: Montmell-Garraf Basin	VU: Variscan Unconformity

